Oscillatory sequences of firing in the locust olfactory system: mechanisms and functional significance

Thesis by

Michael S. Wehr

In partial fulfillment of the requirements for the degree of doctor of philosophy

California Institute of Technology
Pasadena, California

1999
(Submitted 24 September, 1998)

Acknowledgements

Thanks Lisa, Kev, Carol, Tim, Grandmama, Grandada, Wim, Kay, Dan, Shaun, Kate, Mark, Leslie, Alex, Ari, Pz, Maneesh, Sylvie, Erin, and Gilles!

This work was supported by the Office of Naval Research, the National Science Foundation, the Sloan Foundation, and the National Institute of Health.

Abstract

What neural codes does the brain use to represent and process sensory information? Stimulus-evoked oscillatory synchronization of neuronal activity has been observed in many systems, yet the possible functions of such rhythmic synchronization in neural coding remain largely speculative. In the locust, odors appear to be represented by dynamic ensembles of transiently synchronized neurons. The experiments described here explored the design and function of the locust olfactory system, focusing on projection neurons in the antennal lobe. The first goal was to characterize, by means of intracellular and multiple extracellular recordings, the oscillatory synchronization and slow temporal patterns in PN odor responses *in vivo*. After the system had been characterized, specific coding hypotheses were tested. The results demonstrated that the cycle-by-cycle firing patterns across ensembles of PNs encode odor identity information, but that other response features (such as phase or frequency) do not. Finally the mechanisms for the generation of these dynamics were addressed. Odors do not evoke oscillatory synchronization in the population activity of olfactory receptor afferents, and non-specific, temporally unpatterned electrical stimulation of receptor axons can evoke both oscillatory synchronization and slow temporal patterns in PNs, similar to those evoked by natural stimulation with odors. Oscillatory synchronization of olfactory neurons therefore originates in the antennal lobe, and slow temporal patterns in projection neurons can arise in the absence of temporal patterning of the afferent input.

Contents

The work in this thesis appeared in the following publications:

Chapter 2: Laurent G, Wehr M, Davidowitz H (1996) Temporal representations of odors in an olfactory network. J Neurosci 16:3837-3847.

Chapter 3: Wehr M, Laurent G (1996) Odor encoding by temporal sequences of firing in oscillating neural assemblies. Nature 384:162-166.

Chapter 4: Wehr M, Laurent G (1998) Relationship between afferent and central temporal patterns in the locust olfactory system. Submitted.

Appendix A: Ryckebusch S, Wehr M, Laurent G (1993) Distinct rhythmic locomotor patterns can be generated by a simple adaptive neural circuit: biology, simulation, and VLSI implementation. J Comput Neurosci 1:339-358.

Appendix B: Wehr M, Pezariz J, Sahani M (1998) Simultaneous Paired Intracellular and Tetrode Recordings for Evaluating the Performance of Spike Sorting Algorithms. In preparation.

Chapter 1: Background and significance

The experiments described in this thesis explore the design and function of the locust olfactory system. I chose a twofold approach to investigating odor-evoked oscillatory synchronization in this neural system. First, I sought to understand the functional significance of these dynamics—in other words, I wished to know what the system was doing, and what use it could be for information processing (Chapters 2 and 3). Second, I sought to understand the mechanisms underlying the generation of these dynamics—in other words, how the system works (Chapter 4). The backdrop for these explorations can be broadly divided into two areas. The first issue is how information is encoded into spike trains in nervous systems—neural coding. This area is relatively theoretical and benefits from comparison of different sensory systems, animals, and theoretical models. The second issue is olfactory information processing, which has been extensively studied in a variety of animals over the last 50 years. This review begins with an overview of olfaction, and then covers neural coding.

Olfaction

The nature of olfaction

The detection and analysis of an animal's chemical environment is so crucial to its survival that almost all animals, from nematodes to bloodhounds, have olfactory systems. The molecules floating though the air or water in which animals live provide a large amount of often very specific information about food, danger, and conspecifics interested in mating or defending their territory. Odorants are small,

generally volatile, organic compounds with molecular weights less than 300 Daltons. The number of different odorant molecules has been estimated at 400,000 (Mori and Yoshihara, 1995); yet most odors in the natural world are complex blends of these compounds, leading to an astronomical number of possible smells. Still, each odor, whether monomolecular or a blend, generally evokes a singular percept. The ability of the olfactory system to memorize, recognize, and discriminate such a vast array of molecules is rivaled only by the immune system, which recognizes peptides, carbohydrates, or other antigen molecules or epitopes. Animals can detect odorants at extremely low concentrations, yet still discriminate between different odors. Slight alterations in the structure of an odorant molecule can have profound effects on its perceived odor quality.

Odors can evoke powerful emotions and behavioral reactions, and form associative memories that last a lifetime. Odor-evoked memories are well described anecdotally and in literature, with Proust's madeleine being perhaps the most famous example. Experimental efforts to characterize odor-evoked associative memories in humans have demonstrated that they tend to be highly emotional, vivid, specific, rare, and relatively old (Herz and Cupchik, 1992). For example, after associative pairing of a painting with either an odor or a verbal label, memories elicited by an odor cue were more emotional than those cued with verbal cues on a variety of measures (Herz and Cupchik, 1995). While the designs of these experiments leave much to be desired from the perspective of a neurophysiologist, it appears that cognitive psychology has at least partly confirmed the conventional wisdom of folk psychology.

Olfactory bulbectomy has been proposed as a working model for depression, which may be related to the extensive coupling of the olfactory system to the limbic

system in vertebrates. Many of the behavioral effects of bulbectomy in rats are similar to those observed in depressed patients, and many of these behavioral changes are ameliorated by chronic treatments with antidepressants such as the tricyclics and selective serotonin reuptake inhibitors (Kelly et al., 1997).

Odor-mediated behavior

Odor-evoked and odor-mediated behavior has been studied in a wide variety of species. Detection of food odors elicits stereotyped antennal scanning behavior in the cockroach (*Periplaneta americana*), a nocturnal scavenger. This olfactory scanning, observed in total darkness with an infrared camera, consisted of circular antennal movements at ~1.5-7 Hz , after which both antennae point in the direction of the odor source for 1-2 seconds. The animal then orients toward and approaches the source (Chee-Ruiter and Laurent, 1995).

Detection of female sex pheromone by a male sphinx moth (*Manduca sexta*) elicits stereotypical mate-seeking behavior. Male moths zigzag upwind through the pheromonal odor plume, approach and contact the source, and attempt to copulate with it (Willis and Arbas, 1991). The structure of an odor plume several cm from the source consists of packets of odor interspersed with regions of clean air, which create corresponding temporal fluctuations in concentration for the moth as it flies upwind (Murlis et al., 1992). Controlled presentation of temporal fluctuations in pheromone concentration elicit orientation and counterturning behavior in moths (Mafro-Neto and Cardé, 1994).

Olfactory guided behavior has been studied in numerous other species. Olfactory tracking by dogs has long been of practical use to humans. Characteriza-

tion of olfactory tracking behavior in dogs has demonstrated their remarkable ability to correctly determine the heading direction of a trail of 20-minute-old footsteps within 3-5 seconds after encountering it (Thesen et al., 1993). Sockeye salmon use a combination of visual and olfactory cues to return straight to their natal area from open water (Ueda et al., 1998). Adult toads (*Bufo japonicus*) migrate to their home pond for breeding up to three years after metamorphosis, and can exclusively use olfactory cues to do so (Ishii et al., 1995).

Convergent evolution?

There are striking parallels between the olfactory neural circuits of animals, across several phyla. The olfactory systems of insects, crustaceans, and most vertebrates feature glomeruli, discrete structures of neuropil which have been described as one of the most distinctive structures in the brain (Shipley and Ennis, 1996). In addition, mollusks, arthropods, and chordates exhibit odor-evoked oscillations, whose functions have remained enigmatic for over half a century. These anatomical and physiological parallels, to be described in detail below, suggest fundamental principles underlying the circuit design and processing function of olfactory systems in general. These parallels in design and function are thought to be the result of convergent evolution. The divergence of mollusks, arthropods, and chordates occurred in the mid-Precambrian (roughly 1,000 million years ago), before animals had evolved hard parts (such as shells or bones), and the fossil record is therefore impoverished. Conclusions about Precambrian paleontology are based on trace fossils (body impressions in the mud) and are thus speculative and subject to much debate (Glaessner, 1984). It is generally agreed that mollusks and arthropods diverged from an acoelomate (no body cavity) metazoan ancestor, probably Platyhelminthes (flatworms, the first bilaterally symmetric organisms and also the

first organisms with a central nervous system [Gustafsson and Reuter, 1990]). Arthropods and deuterostomes, which later split into echinoderms (e.g., starfish, urchins) and hemichordates, likely shared a coelomate, archiannelid wormlike common metazoan ancestor (Clark, 1979). Very little is known about those metazoan animals, and the synaptic organization of modern Platyhelminthes nervous systems has not been studied in detail (Reuter, 1990). Ultrastructural analysis has demonstrated that at least one species of flatworm (*Stenostomum leucops*) contains a neuropilar region with conventional synapses (Reuter and Palmberg, 1990), in contrast to previous reports that Platyhelminthes neurons were capable only of nonsynaptic release into extracellular space (i.e., neuroendocrine), and communicated by means of electrotonic junctions (Moraczewski et al., 1977). They have ciliated sensory receptor neurons, some of which are presumably chemosensory, but no reported glomerular organization (Reuter and Palmberg, 1990). They do, however, possess a structure reminiscent of the insect mushroom body (N Strausfeld, unpublished observations). The nervous system of modern nematodes, a pseudocoelomate phylum also likely to have appeared in the acoelomate radiation, is well-studied and may shed light on the metazoan nervous system. The nervous system of the hermaphrodite nematode *Caenorhabditis elegans* contains only 302 neurons, and a single sensorimotor neuropilar region called the nerve ring. The chemosensory system of this animal contains only 4 olfactory neurons and 2 interneurons, with limited synaptic processing and certainly no glomerular organization (White et al., 1986; Bargmann, 1993). Taken together, these observations from paleontology and modern comparative neurology suggests that the similarity in olfactory circuitry across phyla are the result of convergence, rather than conservation from a common ancestor, although these conclusions should not be seen as set in stone.

Olfactory information processing

Perireceptor events

Before odorant molecules are recognized by olfactory receptors, they must first cross an aqueous interface. In vertebrates, the olfactory epithelium is covered by the nasal mucosa, which is about 5-30 μm deep depending on the species and living environment (Menco, 1980). In insects, the sensillar lymph is situated between olfactory receptor neuron (ORN) dendrites and the cuticular walls of the sensilla. The functions of this aqueous environment between ORNs and the external environment are largely speculative at this point, but there are a few readily apparent functions, and others which are the subject of ongoing investigation. First, the aqueous layer certainly protects the delicate ORNs. It also provides the aqueous environment required for the biochemistry of ligand binding. However, olfactory mucosa are present in fish, and even bacteria have a periplasmatic space, while neither of these organisms require such a layer to provide an aqueous environment. The function of this layer may therefore be more complex.

Olfactory binding proteins (OBPs)

The presence of a large variety of proteins in both olfactory mucosa and sensillar lymph suggests that they may have biochemical functions. Proteins have been described in both vertebrates and insects that interact directly with odorant molecules. These can be divided into olfactory binding proteins (OBPs), and odorant degrading enzymes (ODEs). OBPs have been described in numerous vertebrate and insect species (bovine: Pelosi et al., 1982; Bignetti et al., 1985; Pevsner et al., 1985; rat: Pevsner et al., 1986, 1988; rabbit: Dal Monte et al., 1991, mouse:

Pes et al., 1992; Pes and Pelosi, 1995; pig: Dal Monte et al., 1991; boar: Marchese et al., 1998; porcupine: Felicioli et al., 1993; insect (Lepidoptera): Vogt and Riddiford, 1981; Gyorgyi et al., 1988; Krieger et al., 1991, 1993; Raming et al., 1990; Vogt et al., 1991; Pelosi and Maida, 1995). OBPs are soluble, low molecular weight proteins which reversibly bind to odorant molecules. On the basis of amino acid sequence, OBPs can be assigned to the superfamily of soluble proteins called lipocalins (Sansom et al., 1994), which typically function as carrier proteins for hydrophobic ligands in aqueous media. A single species can contain several types of OBP (Pelosi, 1994). These are not isoforms, because their amino acid sequences have low similarity. In fact, OBPs from different species can be more closely related than OBPs from the same species (Pelosi, 1994).

In insects, OBPs and pheromone-binding proteins (PBPs) are highly concentrated in the sensillar lymph, constituting almost the entire lymph protein content. Their amino acid sequences bear no homology to vertebrate OBPs (Pelosi and Maida, 1995). Although there is no direct evidence that PBPs bind to pheromones, immunocytochemical methods have localized them in trichodeal sensilla (known to sense pheromones) in Lepidoptera, whereas general OBPs were localized to the generalist basiconic sensilla (Kaissling, 1986; Steinbrecht et al., 1992; Maida et al., 1993; Laue et al., 1994).

Interestingly, the expression of a protein significantly similar to Lepidoptera and *Drosophila* OBPs has been reported in the antenna, tarsi, and labella of the fly *Phormia regina* (Ozaki et al., 1995). This suggests that a single protein may serve the same function in both transduction of volatile airborne compounds and contact chemoreception of aqueous compounds.

Olfactory degrading enzymes (ODEs)

Degrading enzymes distinct from OBPs are also present in olfactory mucosa and sensillar lymph, with very high activity. Olfactory forms of cytochrome P-450, a degrading enzyme of broad specificity first described in the liver, have been identified and cloned (Dahl, 1988; Ding and Coon, 1988; Ding et al., 1991; Nef et al., 1989). Enzymes which further detoxify the products of cytochrome P-450 have also been reported in the olfactory system, such as UDP-glucuronosyl transferase and glutathion S-transferase (Longo et al., 1988; Lazard et al., 1990; Rama-Krishna et al., 1992). The activity of these olfactory degrading enzymes (ODEs) is as high or even higher than in the liver. Clearly, one function of these enzymes is to protect against toxic odorants. After all, the olfactory system is the only part of the nervous system directly exposed to the external environment. A further potential function of ODEs is the termination of the sensory message. The temporal fluctuations of odor concentration in an odorant plume contain important information about the source. The search strategy used by male moths, for example, strongly depends on the intermittency of pulsed female sex pheromones. Persisting compounds in the perireceptor space could reduce the temporal fidelity of olfactory transduction. ODEs may therefore remove odorant molecules in order to prevent reactivation of the receptors. A similar function has also been proposed for OBPs.

Functional roles of olfactory binding proteins

Although the functions of the olfactory mucosa and sensillar lymph are poorly understood, some of their effects are evident from first principles. Because odorants are typically hydrophobic, an aqueous layer would hinder their access to receptors, thereby reducing the sensitivity and speed of ORN response (Getchell et

al., 1984). While hydrophobic compounds might be presumed to reach lower concentrations in an aqueous layer than in air, calculation of partition coefficients shows that concentrations are actually higher in the aqueous layer by two orders of magnitude (Amoore and Buttery, 1978).

Despite their ubiquity in olfactory systems, the function of OBPs remains largely speculative. For most odorants, the concentrations of OBPs in vertebrates are too low by an order of magnitude to affect odorant concentrations around receptors. In insects, however, because OBP concentrations are much higher and sex pheromones typically have low solubility in water, the presence of OBP in the sensillar lymph does increase the concentration of pheromone around receptor dendrites. Apart from this concentrating effect, which is only potentially relevant in some species and for certain specific odorants, the possible functional roles of OBPs are only conjectural (Pelosi, 1996).

OBPs could act as passive, nonspecific odorant carriers through the aqueous layer, although the presence of several classes of OBPs, even in the same animal, suggests that their functions may be more complex and specific. They may be involved in recognition, analogous to chemoreception mechanisms used by bacteria (Koshland, 1981; Mowbray and Cole, 1992). There, soluble proteins in the periplasmatic space bind to sugars, and the complex is then recognized by receptors in the plasma membrane. In this way receptors need not be directly exposed to potentially hazardous compounds. Pelosi (1994) has even proposed that multiple, broadly tuned OBPs could support a role in discrimination. Kim and Smith (1997) showed that *Drosophila* mutants lacking LUSH, an OBP expressed in trichoid sensilla, display normal olfactory behavioral responses to a wide range of odorants (including a range of alcohols), but exhibit a defect in avoidance of high

ethanol environments. In addition, expression of a moth pheromone binding protein (not normally present in *Drosophila*) in the same sensilla, under control of the LUSH promoter, causes transgenic flies to be repelled by even minute amounts of moth pheromone. These remarkable, though preliminary, results suggest first of all that trichoid sensilla contain ORNS specific for avoidance behavior. The implication for odorant binding protein function is that OBPs alone are sufficient to determine the chemical specificity of olfactory neurons within a sensillum. In contrast, as discussed below in greater detail, olfactory receptors are known to be seven transmembrane domain, G-protein coupled receptors, which typically recognize small organic ligands rather than proteins. This suggests that recognition interactions between OBPs and receptors are unlikely (Pelosi, 1996).

The high concentration of OBPs in the perireceptor space of all olfactory systems, combined with their rapid turnover—complete replacement within two days in the sensillar lymph (Vogt et al., 1989)—represents a huge expenditure of energy. Despite this cost, which must be balanced by some great benefit to animal species, the functional role of OBPs in olfaction remain an open question.

Olfactory receptors

The vertebrate olfactory epithelium contains three types of cells: supporting cells, basal cells, and olfactory receptor neurons (Retzius, 1892). Basal cells are precursors of olfactory receptor neurons. ORNs continually turn over and have a lifetime of about 2 weeks in humans (Graziadei and Monti-Graziadei, 1979). ORNs are small, bipolar neurons with apical cilia which protrude into the nasal mucosa (Retzius, 1892). Olfactory receptor proteins and the associated transduction machinery are located in these cilia (Menco, 1980). The binding of odorant molecules

to these receptors is the first step in the process of olfactory perception.

In insects, ORNs are located in sensilla, cuticular structures on the antennal flagellum which can take a variety of forms. Each sensillum type contains a characteristic set of receptor cells, typically including ORNs along with mechanosensory receptor neurons, and often other receptors such as contact chemoreceptors, thermoreceptors, and hygroreceptors (Boeckh et al., 1984). Typically a group of 4-6 (up to 20) of these receptor neurons are closely associated with 3 non-neural auxiliary cells. The cuticular structure of sensilla vary widely and form the basis for their classification. For example, the sensilla trichodea in moths have hairlike extensions which can reach 500 μm in length (Kaissling, 1986). Odorant molecules penetrate the cuticular walls of the sensilla via pore tubules, and then must pass through the sensillar lymph before reaching the olfactory receptors presumably located on the outer dendrites of ORNs.

Mammalian olfactory receptors are members of a superfamily of G-protein coupled receptors with seven transmembrane domains which includes rhodopsin, dopaminergic, adrenergic, muscarinic, and other receptor types (Dohlman et al., 1991)—which is in fact the basis for the strategy by which they were discovered (Buck and Axel, 1991). These proteins are expressed in ORNs () and are therefore olfactory receptors, but have yet to be conclusively demonstrated to function as odorant receptors— and so should properly be termed ‘putative’ odorant receptors. However, much evidence suggests their role as odorant receptors— in the words of Firestein (1991), “After all, it is hard to imagine what else they might do.” Indirect evidence that these proteins are in fact odorant receptors comes from the great number and diversity of olfactory receptor genes—by far the largest gene family in

the genome! Although they could in principle subserve axonal guidance roles without functioning as odorant receptors, this seems unlikely given the amount of 'real estate' they occupy in the genome. The cost of this genetic investment must be balanced by a great benefit, perhaps the same adaptive value for which all animal species have had chemoreceptory systems since before the Cambrian.

More direct evidence for a role of these genes as functional odorant receptors is given by their expression in the sensory epithelium, as shown by in situ hybridization with probes for multiple subfamilies (Ressler et al., 1993; Vassar et al., 1993). Furthermore, use of a recombinant adenovirus vector to drive expression of a particular receptor gene in an increased number of sensory neurons led to greater EOG response to a very small subset of the 74 odorants tested (namely, to 7-,8-, and 9- carbon aldehydes!) in the rat (Zhoa et al., 1998). Other evidence that these gene products function as odorant receptors comes from the study of Raming et al. (1993), who demonstrated odor responses in a heterologous expression system. Olfactory receptor genes with expression localized to rat ORNs were introduced into an insect cell line using recombinant baculovirus. Odors stimulated the production of the second messenger inositol trisphosphate (IP_3) in membrane preparations from these transfected cells, presumably by activating the host phosphatidylinositol system, but no IP_3 increase was seen if a wild-type baculovirus control was used. No increase in the second messenger cyclic adenosine monophosphate (cAMP) was seen for any odor. This demonstrates that olfactory receptor genes can be functionally expressed, at least in the insect cells used, and that the receptors interact with odor ligands to generate second messenger responses. The fact that odors increased IP_3 but not cAMP in this heterologous expression system reveals nothing about the second messenger pathways that these receptors utilize in rat ORNs. Other groups have so far failed to replicate these findings, which may

be due to the speed of IP_3 responses and the rapid quenching technique required to measure them. IP_3 increases were seen to varying extents for 5 of 13 odor mixtures tested, suggesting that olfactory receptors are broadly tuned yet have some selectivity. The combination of broad tuning and selectivity also characterizes the response profiles of ORNs, as discussed in greater detail below. Although the results of Raming et al. (1993) suggest that this broad tuning could originate at the level of the receptor protein, an alternative hypothesis is that receptors are narrowly tuned, and that ORNs express multiple receptors. The latter hypothesis has not yet been disproven, but the number of different receptors expressed by an individual ORN has been estimated, using statistical arguments, to be one or at most a few (Ressler et al., 1993; Chess et al., 1994).

The mammalian olfactory receptor gene family probably has 500-1000 members, which could account for the remarkable ability of mammals to recognize and discriminate a vast number of different odorants with great specificity and sensitivity. The highest degree of diversity is in the transmembrane domains, which may be involved in ligand binding (Buck and Axel, 1991). Putative olfactory receptor genes have now been identified in rat (Buck and Axel, 1991), mouse (Ressler et al., 1993), catfish (Ngai et al., 1993), salamander (Zhao et al., 1995), and human (Parmentier et al., 1992). Seven-transmembrane-domain gene families that are expressed in chemosensory neurons have been identified in *C. elegans* (Troemel et al., 1995). These receptors are not homologous to mammalian olfactory receptors. One receptor, Odr-10 (Sergupta et al., 1994) has been directly shown to be an odorant receptor using heterologous expression in human cells. Odr-10 binds to diacetyl (2,3 butadione), and produces IP_3 elevation via activation of a human G-protein (Zhang et al., 1997). In mouse, receptor genes have been located at multiple loci in the genome (on at least seven different chromosomes), which suggests

that their diversification may have occurred largely through duplication and modification (Sullivan et al., 1996). In mammals, finally, two other families of vomeronasal (pheromonal) olfactory receptor genes (with no homology between them, or with general olfactory receptor genes) have recently been identified (Dulac and Axel, 1995; Herrada and Dulac, 1997; Matsunami and Buck, 1997; Ryba and Tirindelli, 1997).

Second messenger cascades in olfactory receptor neurons

Binding of odorant molecules to receptors in the cilia of ORNs is thought to activate G-proteins, which are likely coupled to the receptors and in turn activate adenylyl cyclase or phospholipase C, to produce cAMP or IP_3. The G-protein mediating cAMP production is likely to be G_{olf} (Bakalyar and Reed, 1990), which is localized to the olfactory cilia (Jones and Reed, 1989), but the G-protein involved in IP_3 production in ORNs remains unknown (Restrepo et al., 1996). In rat, catfish, and insect, odorant stimulation has been shown to rapidly and transiently stimulate the formation of either cAMP or IP_3 in isolated cilia (Boekhoff et al., 1990; Breer et al., 1990; Breer and Boekhoff, 1991; Restrepo et al., 1993a). While cAMP is widely agreed to be involved in odor transduction, the role of IP_3 is controversial. Knockout of the cyclic nucleotide-gated channel or G_{olf} produces totally anosmic mice, which is inconsistent with a role for IP_3 as a primary mediator of excitatory olfactory signal transduction (Brunet et al., 1996; Belluscio et al., 1998). IP_3 may instead modulate cAMP-mediated odorant responses. However, some odors lead to production of IP_3 without measurable production of cAMP (Boekhoff et al., 1990; Breer and Boekhoff, 1991; Restrepo et al., 1993a), which is inconsistent with a modulatory role for IP_3. In addition, IP_3 signalling has been implicated in pheromone transduction in rat vomeronasal neurons (Inamura et al., 1997). Despite this contro-

versy, the fact that both second messenger systems are seen across phyla suggests that dual pathways, like the many other phylogenetically conserved features in olfactory systems, play a fundamental role in olfaction (Boekhoff et al., 1994). The fact that both messengers are activated within 50 ms of odor stimulation suggests that these pathways work in parallel rather than sequentially (Boekhoff et al., 1994). Second messenger formation is known to be guanine nucleotide dependent (Boekhoff et al., 1990; Restrepo et al., 1993a). Production of cAMP or IP_3 is differentially sensitive to toxins which affect G-proteins, suggesting that different G-proteins are responsible for the two pathways (Boekhoff et al., 1990). In lobster ORNs, IP_3 and cAMP have been demonstrated electrophysiologically to activate opposing ionic conductances (Fadool and Ache, 1992; Michel and Ache, 1992). Similarly, different odors have been shown to have excitatory or inhibitory effects on a given ORN in mudpuppy (Dionne, 1992), toad (Morales et al., 1995), catfish (Ivanova and Caprio, 1992), and squid (Lucero et al., 1992). Cyclic AMP activates a cyclic nucleotide gated (CNG) nonspecific cation channel, which allows Ca^{++} entry (Nakamura and Gold, 1987). This in turn activates a Ca^{++}-dependent Cl^- channel (Zhainazarov and Ache, 1995; not the same channel as in vertebrates) which is probably depolarizing because of reversed $[Cl^-]$ gradients across the ciliar membrane, at least in vertebrate ORNs (Zhainazarov and Ache, 1995). Conflicting reports from different investigators may stem from the sensitive dependence of these conductances on $[Cl^-]$ and $[Ca^{++}]$. IP_3 also activates a nonspecific cation channel (Restrepo et al., 1990), and leads to Ca^{++} entry, either through this channel or possibly an independent Ca^{++} channel. Intracellular Ca^{++} opens an outward Ca^{++}-dependent K^+ conductance in the cilia (Morales et al., 1995; Restrepo et al., 1993a).

In rat, different odors (at 1μM concentration) exclusively stimulated either cAMP or IP_3 formation (Boekhoff et al., 1990; Breer et al., 1990). In lobster, 1μM odorant

concentrations also stimulate the formation of either one or the other second messenger, whereas at high concentrations (1mM), both pathways are stimulated (Boekhoff et al., 1994). It is possible that similar results would have been obtained in rat, had higher odorant concentrations been presented, although it is difficult to compare concentrations between terrestrial (airborne) and aqueous odorants. In both species, peak second messenger concentrations are reached within 50 ms, which is certainly fast enough to account for odor response latencies of ORN axonal recordings, which are approximately 100 ms (Schmitt and Ache, 1979). In lobster, furthermore, whole-cell recordings demonstrate that ORNs vary in their pattern of sensitivity to odors. ORNs tested with two amino acids (which are relevant odorants for lobster) were either excited by one odor, inhibited by one odor, or excited by one and inhibited by the other (Boekhoff et al., 1994). This suggests that, at least in lobster, the dual stimulation of second messengers by a given odor can occur within a single ORN. This possibility is particularly relevant to the work described in this thesis, because if multiple second messengers can be activated within a given ORN, and if these second messengers can activate opposing (i.e., inward and outward) membrane conductances, then odors could evoke complex temporal response patterns in ORNs. The complex slow temporal patterns seen downstream, in projections neurons or mitral cells, might therefore be driven by ORN response dynamics. An alternative hypothesis is that the slow temporal patterns seen in projection neurons (which will be examined in detail throughout this dissertation) are generated by the intrinsic circuitry of the antennal lobe.

Gaseous second messengers, such as nitric oxide (NO) and carbon monoxide (CO), are likely to be involved in olfactory transduction, although their precise roles are not yet clear (Broillet and Firestein, 1996a). NO has the highest diffusion coefficient of any biological molecule, and is estimated to diffuse 500 μm in tissue

(Dawson and Snyder, 1994). NO may not be the only active form; other redox states such as nitrosothiols (R-SNO) are comparatively stable compounds (with up to 40 minute half-lives) and are known to occur under physiological conditions (Stamler et al., 1992, Pryor et al., 1982). Staining for neuronal nitric oxide synthase (nNOS) is widely distributed throughout the mammalian brain, and is particularly high in the olfactory epithelium and olfactory bulb (Bredt et al., 1991; Bredt and Snyder, 1994). Both NO and CO can directly activate guanylyl cyclase, probably by binding to the iron moiety in the heme group. Odor-evoked cGMP formation is increased upon application of CO or the NO donor nitroprusside, and abolished by hemoglobin or the NOS inhibitor L-N-nitroarginine (Breer et al., 1992, Leinder-Zufall et al., 1995). Cyclic GMP can activate the same cyclic nucleotide gated channel normally thought to be activated by cAMP, leading to Ca++ entry and depolarization. NO donors can also directly activate this CNG channel, through a different pathway not involving guanylyl cyclase or cyclic nucleotides (Broillet and Firestein, 1996b). This activation appears to result from the binding of NO (or R-SNO) to an intracellular cysteine residue of the CNG channel known to be involved in channel gating (Gordon and Zagotta, 1995). CO effectively depolarizes ORNs through tonic activation of the CNG channel, leading to a delayed and sustained modulation of neuronal excitability (Leinder-Zufall et al., 1995). Thus the physiological role of NO and CO could be modulatory. For example, NO could rapidly diffuse through a volume of tissue, and then produce a long-lived nitrosothiol which might have a general effect on the gain of olfactory transduction (e.g., olfactory adaptation). NO and CO may also play a role in development and regeneration, especially in the olfactory epithelium, where NOS is expressed transiently by newly developing ORNs and is absent by postnatal day 7 (Roskams et al., 1994).

Odor responses in olfactory receptor neurons

Electrophysiological studies of ORN odor responses in a number of species (both vertebrate and arthropod) indicate that in general, ORNs respond to more than one odorant, but with different (overlapping) response profiles. Thus each odor tends to activate a unique, though overlapping, set of ORNs. Selectivity is greater at lower concentrations; as concentration is increased, ORNs respond to additional odorants, although some odorants cannot evoke responses in some ORNs at any concentration (Gesteland et al., 1965; O'Connell and Mozell, 1969; Getchell, 1974; Revial et al., 1978; Sass, 1978, 1980; Selzer, 1981; Sicard and Holley, 1984; Sicard, 1985; Firestein and Werblin, 1987, 1989; Dionne, 1992; Firestein et al., 1993; Kang and Caprio, 1995; Hansson et al., 1996). Odors can either excite or inhibit ORNs (Dionne, 1992; Michel and Ache, 1992; Fadool and Ache, 1992; Kang and Caprio, 1995; Hansson et al., 1996). In newt ORNs, odors can also cause suppression of odorant responses by an unknown mechanism which is neither excitation, inhibition, nor adaptation (Kurahashi et al., 1994).

A unifying concept for ORN function is that they serve as high-gain detectors (Trotier and Døving, 1996a). Second messenger cascades impart much of this gain, such that an activated receptor protein can generate about 10^6 second messenger molecules (Lancet, 1986). The high surface area of olfactory cilia increase the probability that odorant molecules are captured, and their small volume allows rapid increases in second messenger concentration to activate the nucleotide-gated cation channels, which in turn leads to the opening of calcium-activated chloride channels (Breer et al., 1990; Trotier and Døving, 1996a). ORNs have a high input resistance and are thus sensitive to small depolarizing currents (Trotier et al., 1993). ORNs have multiple voltage and calcium-activated conductances which shape their

firing properties; accordingly, their firing properties are strongly dependent on membrane potential (Trotier et al., 1993). In frogs, ORNs typically have resting membrane potentials more negative than -80 mV. They are unusual in that no potassium channels are open at rest, and the membrane potential appears to be set mainly by the sodium pump (which has a reversal potential of -140 mV) and an inward rectifier current, I_h (Trotier and Døving, 1996b).

Extracellular unit recordings show that the number of action potentials in an odor response does not encode concentration information (Holley and Døving, 1977). Similarly, in current clamp recordings, no clear relationship was seen between injected current and spike count (Firestein and Werblin, 1987). Typically, only a single spike was evoked at low currents, and repetitive firing was only evoked within a narrow range of current amplitudes, above which only a transient burst of spikes was evoked (Trotier and Døving, 1996a). If spike count is taken as the encoding scheme, then the very narrow dynamic range of these cells suggests that they function as high-gain detectors, signalling the presence of a suprathreshold concentration of odorant, rather than precisely encoding the actual concentration of the stimulus (Trotier and Døving, 1996a). However, more information about concentration could be extracted with decoding schemes other than simple spike counts. For example, by comparing different epochs of the response, the different firing properties seen at different intensities could be easily discriminated, providing a wider dynamic range than provided by spike count alone. The conclusion reached by Trotier and Døving (1996a) that ORNs are high-gain detectors, adapted to signal the presence or absence of a threshold concentration of odorant, is a classic example of a potentially misleading conclusion drawn about neural function when the implicit assumption of a spike count code is made.

Zonal epithelial topography

In other sensory systems, the physical location of receptor cells (neural space) imparts information about stimuli. In the eye, for example, the lens allows the visual field to be spatially sampled by the retina in a *topographic* manner; that is, neighborhood relations are preserved across the transformation from stimulus to initial neural representation. Objects near each other in the visual field are represented by neurons near each other in the retina. This topographic map is preserved and elaborated as visual information is processed at successive levels of the visual system. The question of the existence of topography in the olfactory system has a long history. In the olfactory epithelium, many studies have combined focal odorant application and electro-olfactograms (EOG, an extracellular field potential technique), demonstrating that some regions of the epithelium were reliably more sensitive to particular odorants than other regions (Mustaparta, 1971; Kauer and Moulton, 1974; Moulton, 1976; Thommesen and Dϕving, 1976; MacKay-Sim et al., 1982; Mozell et al., 1987; MacKay-Sim and Kesteven, 1994; Ezeh et al., 1995; Scott et al., 1996). Differential distribution of odor responses across the epithelium has also been shown by voltage-sensitive dye recordings (Kent et al., 1996; Youngentob et al., 1995). Both EOG and optical techniques show consistency across animals.

The discovery of a mammalian superfamily of putative odorant receptor genes by Buck and Axel in 1991 allowed a new approach to the question of topography in the olfactory system. In situ hybridization studies have revealed a spatial pattern of receptor expression in the rodent olfactory epithelium (Ressler et al., 1993; Vassar et al., 1993). ORNs expressing a given receptor are restricted to one of four zones in the epithelium. Within each zone, cells expressing a given receptor appear to be

randomly dispersed throughout the zone. These distinct spatial zones run longitudinally from anterior to posterior in the nose, are bilaterally symmetric, and are invariant across animals. Homologous genes appear to be expressed within the same zone. Naturally, the hybridizations have only been done with a subset of the superfamily of olfactory receptors, leaving open the possibility of future discovery of novel expression patterns. The significance of these expression zones for information processing is not clear. In catfish, in which only about 100 olfactory receptor genes have been identified, no distinct expression zones have been found (Ngai et al., 1993). One evolutionary interpretation of these results is that the adaptation to terrestrial existence included wholesale duplication and modification of the epithelium and the receptor gene family that existed then, which in mammals remain segregated both in the nose and in the genome (Ngai et al., 1993; Vassar et al., 1993).

How do these expression zones relate to the regions of differential sensitivity to odors previously investigated with EOGs? To address this question, Scott and coworkers (1997) reinvestigated the distribution of odor sensitivity in rat epithelium across the longitudinally oriented stripe-shaped expression zones described by Ressler et al. (1993) and Vassar et al. (1993). By placing an array of EOG electrodes across the four gene expression zones, they found regions of differential sensitivity to different odors which roughly corresponded to the zones. When they instead oriented the array parallel to the zones, sensitivity for a given odor was similar across all the electrodes. These results suggest that the expression zones may account for the regions of differential EOG response first reported twenty years before the discovery of the olfactory receptor gene superfamily.

Axonal convergence from olfactory receptor neurons to glomeruli

In vertebrates, ORN axons project to the olfactory bulb, where they ramify within discrete glomeruli. Mitral and tufted cell apical dendrites arborize within a single glomerulus in mammals and in one to several glomeruli in lower vertebrates. The massive convergence of ORNs to second order neurons is a common feature across phyla. The convergence ratio is about 1,000 to one in mammals (Allison and Warwick, 1949) and fish (Gemne and Døving, 1969). While many investigators searched for topography in the projections from epithelium to bulb, until recently essentially all that was known was that restricted regions of the bulb receive input from large regions of the epithelium, and conversely, a restricted region of the epithelium projects widely across the bulb (Le Gros Clark, 1951; Adrian, 1956; Land, 1973; Costanzo and O'Connell, 1978; Greer et al., 1981; Saucier and Astic, 1986; Schowba and Gottlieb, 1986; Stewart and Pedersen, 1987; Schwarting and Crandall, 1991; Schoenfeld et al., 1994).

With the revolution enabled by the cloning of odorant receptor genes (Buck and Axel, 1991), axonal convergence from ORNs to glomeruli was discovered to be precise and orderly. Axonal projections from ORNs expressing a given receptor converge on two glomeruli, one in the medial olfactory bulb, and one in the lateral bulb (Ressler et al., 1994; Vassar et al., 1994). While the *in situ* hybridization techniques used by Ressler, Vassar, and colleagues allowed the detection of sites of convergence in the bulb, the elegant tau-lacZ homologous recombination method of Mombaerts et al. (1996) allowed visualization of single axons as they course towards the bulb and finally converge onto individual glomeruli. The stunning images produced by this technique confirmed that ORNs expressing a given receptor project to a stereotypical pair of glomeruli, suggesting that the olfactory bulb con-

tains a topographic map of receptor activation in the epithelium. The glomeruli targeted by a given receptor type are invariant across animals, suggesting a wiring strategy which does not depend on environmental cues or the experience of the animal (Ressler et al., 1994; Vassar et al., 1994; Mombaerts et al. 1996). If ORNs expressing a given receptor are experimentally manipulated to express an anomalous substitute receptor protein, their axons project to a new pair of glomeruli distinct from those targeted by either the wild-type or substitute ORNs. These receptor swap experiments demonstrate that the receptor actually expressed by an ORN plays an instructive, but not determining, role in axon guidance.

In insects, the axons of ORNs terminate in glomeruli of the ipsilateral antennal lobe. The molecular biological techniques that elucidated glomerular convergence in vertebrate olfactory bulb have not yet been applied in insects, but certainly will be as soon as insect olfactory receptors are cloned. In the generalist olfactory system, attempts to label individual sensilla or receptor neurons have failed to reveal special projection areas for given types of sensilla or receptor neurons (Boeckh et al., 1984). In the pheromonal system, however, specific receptor neurons respond selectively to one or the other component of the pheromone blend (Kaissling et al, 1989). Each of these project to a distinct region of the specialized macroglomerular complex (Hansson, 1992; Christensen et al., 1995).

The glomerulus: a module?

The vertebrate olfactory bulb contains a highly ordered synaptic organization. The microcircuitry among the ORN axons, projection neurons, local interneurons, and centrifugal feedback is one of the best characterized in the brain, and has led to the concept of the “canonical microcircuit” (Shepherd, 1972, 1979; Mori, 1987;

Powell and Price, 1971; Pinching and Powell, 1971). The olfactory bulb is a layered structure, which is commonly divided into 5 layers. The outermost is the olfactory nerve layer, occupied by the converging receptor axons described above. The glomerular layer is composed (eponymously) of glomeruli, the sites of massive synaptic input from receptor axons onto dendrites of mitral, tufted, and periglomerular cells. Numbers of glomeruli range from roughly 2000 in rodents to 100 in fish (Baier and Korsching, 1994). Glomeruli are enclosed by a glial wrapping which give them the anatomical appearance of individual functional units, as noted by early anatomists (Golgi, 1875; Cajal, 1890; Retzius, 1892). With typical prescience, Adrian (1951) proposed that the glomerulus served as a functional unit, integrating information from its afferents. This idea has experimental support, as described below.

The projection neurons of the olfactory bulb are mitral and tufted cells. Mitral cell bodies form the mitral cell layer, while tufted cell bodies are located in the external plexiform layer. These cell types are similar in many ways, and thus are often lumped together as mitral/tufted cells. In mammals, both send their primary dendrite to a single glomerulus, whereas in amphibians, fish, and reptiles, mitral cells can have multiple apical dendrites that enter several glomeruli (Herrick, 1931). The basal dendrites of both mitral and tufted cells branch in the external plexiform layer, and both cell types are excitatory and project axons to the piriform cortex via the lateral olfactory tract. Periglomerular cells have their cell bodies in the glomerular layer, outside of the glomeruli. They send a primary dendrite into a glomerulus, where they receive direct inputs from receptor afferents. Their dendrites also make reciprocal dendrodendritic synapses with mitral/tufted cells in that glomerulus. Periglomerular cell axons ramify in other glomeruli and in the external plexiform layer. These cells are GABAergic and are therefore often presumed to be

inhibitory, providing feedforward as well as lateral inhibition. However, electrophysiological evidence using intracellular (Nowycky et al., 1981) as well as evoked potential and current-source density techniques (Gonzalez-Estrada and Freeman, 1980; Martinez and Freeman, 1984) suggest that periglomerular cells have an excitatory action on each other and on mitral/tufted cells. GABA-mediated excitation has been reported elsewhere in the CNS (e.g., in neonatal CA3 hippocampal neurons, Cherubini et al., 1991; in hilar neurons, Michelson and Wong, 1991) and is presumably due to reversed [Cl^-] gradients across postsynaptic cell membranes. Typically, [Cl-] is greater extracellularly, and ionotropic $GABA_A$ channels thus generate an outward (hyperpolarizing) current. Histochemical evidence that [Cl-] is high in some periglomerular cell bodies and dendrites, and is very low in certain parts of the glomerular neuropil including the intercellular clefts, suggests that reversed chloride gradients may be responsible for excitatory GABA effects on periglomerular and/or mitral cells (Siklos et al., 1995).

The deepest layer of the bulb is the granule cell layer, where granule cell somata lie. Granule cells are inhibitory, GABAergic cells whose dendrites arborize in the external plexiform layer. There, granule cells and mitral/tufted cells reciprocally inhibit and excite each other via dendrodendritic synapses (Jahr and Nicoll, 1982). These interactions take place on the basal dendrites of mitral/tufted cells, which can extend laterally for up to a millimeter in rat (Orona, 1984), thus providing both local and lateral inhibitory feedback of mitral/tufted cells. A small population of often overlooked short axon cells is distributed throughout the external plexiform, mitral, and granule cell layers.

The insect antennal lobe is remarkably similar to the vertebrate olfactory bulb (Boeckh et al., 1984; Flanagan and Mercer, 1989; Kanzaki et al., 1989; Laurent

and Davidowitz, 1994; MacLeod and Laurent, 1996). As in the bulb, the number of glomeruli varies 10-fold by species, ranging from roughly 1000 in the locust to 156 in the honeybee and even less in *Drosophila*. Cell bodies of projection neurons (PNs), the analogs of mitral/tufted cells, line the outer surface (cortex) as is the rule in invertebrate central nervous systems. In some species, such as moth, cockroach, and honeybee, projection neurons can project to one or multiple glomeruli, whereas in locust only the latter has been seen. As in the bulb, inhibitory GABAergic local neurons (LNs) provide feedforward and feedback inhibition via reciprocal dendrodendritic synapses in the glomeruli, but unlike vertebrate local neurons arborize globally throughout the lobe. In honeybee and cockroach, local neurons fire action potentials, but in locust they are strictly non-spiking. Locust LNs do, however, exhibit possibly regenerative TTX-resistant spikelets of variable amplitude which are most likely calcium-mediated (Laurent and Davidowitz, 1994). Projection neurons send axons via the antennoglomerular tract (AGT) to the mushroom body, where they make en passant synapses before terminating in the lateral protocerebral lobe, a region whose function is as yet not clearly determined.

Activity mapping of the vertebrate olfactory bulb and the insect antennal lobe has demonstrated that different odorants activate overlapping yet unique sets of glomeruli. Consistent results have been obtained with 2-deoxyglucose uptake in the shrew (Skeen, 1977), rat (Stewart et al., 1979; Sallaz and Jourdan, 1993; Jourdan et al., 1980; Guthrie et al., 1993), and guinea-pig (Astic and Saucier, 1983), voltage- and calcium-sensitive dyes in the salamander (Kauer and Cinelli, 1993; Cinelli et al., 1995), zebrafish (Friedrich and Korsching, 1997), and honeybee (Joerges et al., 1997), and immediate early gene (namely c-fos) induction in the rat (Onoda, 1992; Sallaz and Jourdan, 1993; Guthrie et al., 1993). Individual glomeruli typically respond to many odors, and each odorant typically activates many glomeruli. Yet

the pattern of activated glomeruli is unique and specific for a given odor and is thus capable of representing odor identity information.

Similar to results described above for ORNs, increased concentration increases the number of activated glomeruli, and thereby increase the degree of overlap between patterns evoked by different odors. Nonetheless, general properties of the response patterns for each odorant remain similar across concentrations and across animals. Concentration response functions of different glomeruli can have various shapes and thresholds. Thus odorant concentration as well as quality could be encoded combinatorially by patterns of activated glomeruli (Friedrich and Korsching, 1997; Cinelli et al., 1995; Joerges et al., 1997).

These demonstrations that odorants activate overlapping but unique sets of glomeruli support the hypothesis that the glomerulus serves as a functional unit for processing or even coding of olfactory information. In moths, however, Willis et al. (1995) have shown that normal glomerular organization of the antennal lobes is not necessary for odor-modulated flight. Glomerular development in Manduca sexta females was altered by partial deafferentation during development. Adult moths with mostly aglomerular antennal lobes (including a few abnormal, glomerulus-like structures) were nevertheless able to fly upwind to the source of a host-plant odor in a wind tunnel, showing flight behavior similar to normal moths. This suggest either that even a few abnormal glomeruli are sufficient to mediate this behavior, or that glomerular organization per se is not necessary for this behavior.

Response profiles of projection neurons in the vertebrate olfactory bulb and insect antennal lobe

In general, both vertebrate mitral/tufted cells and arthropod PNs respond to multiple odors, and a given odor can activate multiple neurons (Kauer, 1974; Hamilton and Kauer, 1989; Macrides and Chorover, 1972; Mathews, 1972; Tanabe et al., 1975; Mair, 1982; Harrison and Scott, 1986; Wilson and Leon, 1988; Wellis et al., 1989; Waldow 1977; Wachowiak and Ache, 1998; Laurent and Davidowitz, 1994; Laurent et al., 1996, Wehr and Laurent, 1996). This broad tuning seen in output cells agrees with the glomerular activity mapping results discussed above, suggesting that odor quality information is processed in a parallel, distributed fashion (Hildebrand, 1996). The degree to which neighboring mitral/tufted cells respond similarly to a given odor depends on the distance between the cells, with those further apart displaying opposite responses (Buonviso and Chaput, 1990, Meredith, 1986; Wilson and Leon, 1987). Potentially, cells very near each have similar odor response profiles because they innervate the same glomerulus, and cells further apart show complementary responses because they reciprocally inhibit each other via interneurons (Scott et al., 1993). Mitral cells can have non-monotonic intensity response functions (Meredith, 1986, Harrison and Scott, 1986). For example, a cell might be excited at intensities just above threshold, then inhibited at intermediate concentrations, and excited by higher concentrations. One explanation for such a result is that cells in a neighboring glomerulus, with a higher threshold for the given odorant, mediate lateral inhibition at intermediate intensities, but are dominated by local excitatory afferent input at higher concentrations (Meredith, 1986).

In addition to broad tuning that can include excitatory or inhibitory responses, both mitral/tufted cells and PNs display complex temporal patterns which can con-

tain multiple epochs of excitation, inhibition, and periods of silence in a single odor-evoked response (Kauer, 1974; Meredith, 1986; Hamilton and Kauer, 1989; Wellis et al., 1989; Christensen and Hildebrand, 1987, 1988; Waldrop et al., 1987; Waldrow, 1977; Sun et al., 1993; Wachowiak and Ache, 1998; Laurent and Davidowitz, 1994; Laurent et al., 1996, Wehr and Laurent, 1996; MacLeod and Laurent, 1996). The functional significance of these slow temporal response patterns is, in part, the subject of this thesis. Because temporal patterns differ for different odors and neurons, they contain odor information (Harrisson and Scott, 1986; Scott, 1990; Laurent and Davidowitz, 1994; Wehr and Laurent, 1996). It remains unknown, however, whether this information is involved in odor coding by the olfactory system. The role of such temporal coding in vision, for example, remains controversial (McClurkin et al., 1991; Shadlen and Newsome, 1998). The slow temporal patterns in the locust olfactory system are odor- and neuron-specific, and thereby shape the population of activated, rhythmically synchronized projection neurons into an evolving sequence of synchronized oscillatory assemblies which contains information about the odor presented (discussed below, Laurent and Davidowitz, 1994; Laurent et al., 1996; Wehr and Laurent, 1996). Odors thus appear to be encoded by dynamic neural ensembles, whose components and update are both stimulus-specific (Laurent, 1996).

The mechanisms by which odor-evoked slow temporal patterns are generated in projection neurons and mitral/tufted cells are poorly understood. Although they are thought to involve lateral synaptic interactions (Christensen et al., 1993; White et al., 1992; Meredith, 1986, 1992) the details of these interactions are unknown and only rarely have been the subject of speculation. Interestingly, the slow temporal patterns evoked by odors in locust PNs persist in the presence of picrotoxin, an antagonist of vertebrate $GABA_A$ and insect ionotropic GABA receptors (MacLeod

and Laurent, 1996). This suggests that the mechanisms which generate them are distinct from those which generate synchronous oscillations (discussed in detail elsewhere in this and other chapters). One hypothesis is that the slow temporal patterns seen in PNs are driven by slow temporal patterns in the afferent input. For example, olfactory receptor neurons could respond with different time courses to different ligands due to perireceptor events (Pelosi, 1996), competitive binding interactions at receptors, combinations of multiple odor-activated membrane conductances (Restrepo et al., 1996), or differential activation of (possibly interacting) second messenger cascades (Restrepo et al., 1996). Alternatively, these temporal patterns could be generated by complex dynamics resulting from intrinsic antennal lobe circuitry. These (nonexclusive) hypotheses are addressed directly by the experiments described in Chapter 4.

Mori and coworkers have for a number of years investigated the relationship between chemical structure of odorant molecules and mitral/tufted cell responses. Many studies that address this question are difficult to interpret, because mitral cells respond to multiple odors, and the relationship between those odors is not always evident. A unifying concept introduced by Mori is the “molecular receptive range” of a bulbar neuron (Mori et al., 1992; Imamura et al., 1992). The molecular receptive range of a neuron is its “olfactory tuning,” defined as the range of odor molecules that excite or inhibit it, and is analogous to the spatial receptive field of a visual neuron or the frequency tuning curve of an auditory neuron. When tested with a large panel of molecules which systematically vary in structure, the receptive ranges of mitral/tufted cells appears to consist of odor molecules with similar conformations. All compounds that activate a given mitral/tufted cell contain at least one common structural feature. With aliphatic (open chain) hydrocarbons, for example, at least three systematic variables are well correlated with response speci-

ficity: chain length, functional group (e.g., -COOH, -CHO, -OH, or -H), and the position of the functional group within the molecule (Mori et al., 1992; Imamura et al., 1992). For example, a mitral cell might respond to 3-, 4-, and 5-carbon aldehydes and carboxylic acids, but not to any alcohols or alkanes. For aromatic (ring-containing) hydrocarbons, additional features such as isomer configurations (ortho, meta, or para) play a systematic role in response selectivity (Katoh et al., 1993). This successful demonstration of systematic molecular receptive ranges is all the more remarkable in that Mori and his colleagues analyzed odor responses solely with spike counts (from anaesthetized rabbits). While there is no consensus for how to extract odor information from temporal response patterns, that information would likely make the molecular receptive ranges of bulbar and projection neurons more complex.

Systematic differences are seen in the molecular receptive ranges of mitral/tufted cells from different regions of the bulb (Katoh et al., 1993; Mori and Yoshihara, 1995). Mitral/tufted cells sensitive to aliphatic acids are mostly concentrated in the dorsomedial bulb, whereas cells responsive to alkanes are exclusively located in the ventral bulb. Cells responsive to aliphatic alcohols tended to be concentrated in the ventromedial region, and cells sensitive to aliphatic aldehydes were distributed throughout the bulb.

Mitral/tufted cells can also be inhibited by odors, as might be expected from their reciprocal circuitry with granule and periglomerular cells. The molecules that inhibit a neuron tend to share conformational features. Moreover, conformations of molecules that inhibit a cell can be slightly different from, but relatively similar to, conformations of excitatory molecules (Yokoi et al., 1995). With the above example of a cell that was excited by 3-, 4-, and 5-carbon aldehydes, 2- and 6-carbon

aldehydes might inhibit it. This suggests to Yokoi et al. (1995) that the local circuitry in the bulb may serve to enhance contrast in the response specificity of bulbar neurons, much as lateral inhibition enhances spatial contrast in the retina (Yokoi et al., 1995). Neighboring glomeruli may even participate in 'odor opponency', analogous to color opponency in the visual system. Enhanced contrast is only meaningful if molecules can be related in some systematic way. Ideally those relations would be metric, so that tuning curves could be constructed along a coding dimension. Conformational similarity, while not a metric space, can at least support a rank ordering of relative distances between molecules. It is this approach which renders the data of Mori and coworkers interpretable, and allows conclusions to be drawn about both the molecular receptive range of mitral cells and information processing in the olfactory bulb. Further advances will depend on a deeper understanding of the stimulus space; with knowledge of the specificity of interactions between odorant molecules and olfactory receptors, olfactory stimuli may someday move out of the organic chemistry stockroom and into a true metric space.

An alternative approach to introduce order into the olfactory stimulus space is to appeal to the behavioral significance of an odorant molecule—what it means to the animal. For general odors, this approach entails conditioning an animal to associate an odor with a positive or negative reinforcement. The odor thereby becomes meaningful to the animal. While some interesting results have been obtained with this approach, the difficulty of recording from awake behaving animals has largely limited investigators to techniques such as the EEG. In rabbits trained to discriminate between two odors, odor-specific spatial patterns of oscillatory EEG amplitude across the bulb were seen using electrode arrays. Odor-specific information was not localizable to subsets of array locations, suggesting that the output of the bulb involved the entire structure (Freeman and Baird, 1987). Factor analy-

sis of spatial EEG patterns could be used to correctly classify the odor 75-90% of the time. These patterns persisted across recording sessions, yet changed when the stimulus-response contingencies change. These results suggest that stable spatial patterns of bulbar activity can be recorded for as long as odors are meaningful to the animal (Freeman and Viana Di Prisco, 1986; Freeman and Grajski, 1987).

While the behavioral significance of general odors is difficult to assess without recording in a behaving animal, a class of odorants exists with precise and well understood meaning to the animal. Pheromones are used by most if not all species as a means of chemical communication. In some insects, the use of sex pheromones as behaviorally relevant olfactory stimuli has helped elucidate the functional organization of this specialist olfactory subsystem (Hildebrand, 1996). These studies, primarily using the moth, take advantage of the olfactory control of behavior by specific molecules. Female sex pheromone (a specific blend of known composition), when detected by male moths, triggers and sustains a complex yet stereotyped mate-seeking behavior: zigzagging upwind, approaching and contacting the source, and attempting to copulate with it (Willis and Arbas, 1991). Specific olfactory receptor neurons on the antenna selectively respond to one or the other component of the pheromonal blend (Kaissling et al., 1989), and they each project their axons exclusively to a distinct region of the specialized macroglomerular complex (MGC, Hansson et al., 1992; Christensen et al., 1995). Projection neurons that respond selectively to one or the other pheromone component arborize exclusively in the corresponding MGC compartment, while PNs that respond to the blend arborize throughout the MGC. These latter PNs can respond similarly or oppositely to each component, so that their response to the blend can be excitatory or a mixed inhibitory-excitatory (-+-) response. These neurons have a precise and narrow

molecular receptive range, and the connectivity in this pathway therefore represents a classical ‘labeled line.’ The macroglomerular complex therefore appears to be a functionally significant unit (Hildebrand, 1996). Although generalist PNs are more broadly tuned and use combinatorial coding, study of the pheromone system may reveal common principles of organization and function used by the olfactory system in general, which are exaggerated in the specialist subsystem to ensure reproductive success (Hildebrand, 1996).

The mushroom body and piriform cortex

Mammalian mitral/tufted cells project to pyramidal cells in piriform (olfactory) cortex via the lateral olfactory tract. Piriform cortex is thus unique among sensory cortical areas; sensory information from all other modalities is first relayed through the thalamus before reaching cortex. Piriform (also termed prepyriform, prepiriform, or anterior piriform) cortex is a three layered structure similar to reptilian cortex and described as paleocortex (because of its presumed phylogenetic age), in contrast to the six layered neocortex forming all other primary sensory cortices in mammals. The superficial layer, or layer 1, consists of apical dendrites of pyramidal cells, afferent fibers from the lateral olfactory tract, and intrinsic associative cortico-cortical collaterals. The afferents and association fibers are segregated, with the afferents superficial to the association fibers. Layer 2 contains pyramidal cell bodies, and layer 3 contains basal dendrites of pyramidal cells, deep pyramidal cell bodies, and multipolar neurons. The association fiber pathway has been likened to the recurrent feedback characteristic of artificial neural network models (Haberly, 1985; Ketchum and Haberly, 1991).

Projection neurons in insects project to Kenyon cells in the mushroom body

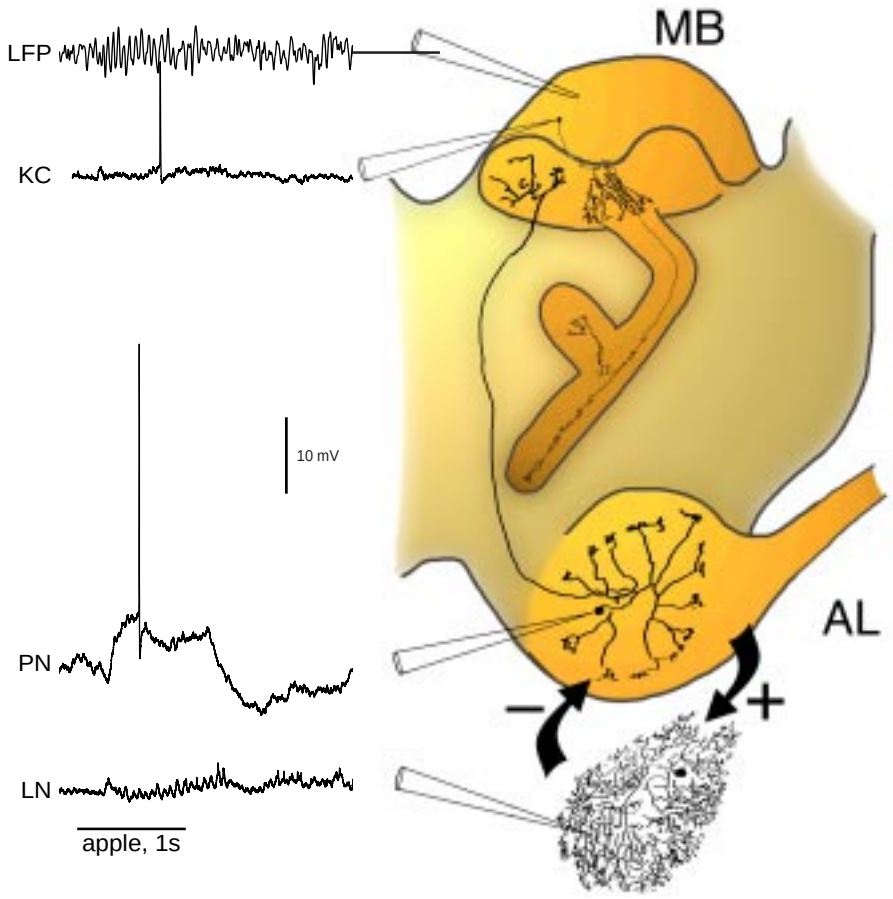

Figure 1. The locust olfactory system. Receptor afferents project from the antenna (not shown) to the antennal lobe (AL). The AL consists of projection neurons (PNs) which are spiking, excitatory cells with discrete glomerular arborization patterns, and local neurons (LNs) which are nonspiking, inhibitory cells with global arborization patterns. Both cell types, as well as Kenyon cells (KC), experience odor-evoked membrane potential oscillations as shown in representative intracellular recordings at left in response to apple odor (each cell recorded separately in different animals and aligned to the 1s odor pulse, indicated by solid bar). Projection neurons project to the mushroom body, where odors evoke oscillations in the local field potential (LFP, here low-pass filtered at 50 Hz). Cobalt fills courtesy of G. Laurent.

---

via the antennoglomerular tract (AGT). There they make en passant synapses in the neuropil of the calyx before continuing to the lateral protocerebral lobe, where they ramify and make terminal synapses. The mushroom body, like piriform cortex,

has an orderly, repeating structure. Extrinsic mushroom body neurons form potential recurrent feedback pathways (Mobbs, 1982; Gronenberg, 1987; MacLeod and Laurent, 1997). Kenyon cells, like pyramidal neurons, have dendritic spines, and the mushroom body has been implicated in learning and memory in a variety of insect species. In flies, the genes responsible for several olfactory learning mutants encode enzymes in the cAMP pathway, and are preferentially expressed in the mushroom body (Davis, 1993). Chemical ablation of the mushroom body leads to a total loss of olfactory learning (de Belle and Heisenberg, 1994). The honeybee displays a robust olfactory learning known as proboscis extension response (PER) conditioning. Cooling the brain induces retrograde amnesia for this olfactory memory trace, and cooling the mushroom body calyx induces a similar amnesia, while cooling other brain regions (e.g., the lateral protocerebral lobe) do not (Menzel and Muller, 1996).

Concise overview of locust olfactory system anatomy

Although details of the locust olfactory are provided in numerous locations elsewhere in this chapter, below is a self-contained and concise overview of locust olfactory system anatomy (shown in Figure 1), chiefly for those not familiar with it. Olfactory receptor neurons (ORNs) are found in small groups in sensilla on the antenna. They project to the ipsilateral antennal lobe, where they synapse onto both local neurons (LNs) and projection neurons (PNs) (Leitch and Laurent, 1996). LNs are local, axonless, non-spiking inhibitory neurons which make graded, dendrodendritic GABAergic synapses onto PNs. They arborize globally throughout the antennal lobe and number about 300. PNs are excitatory, spiking neurons, which number about 830, and each arborizes discreetly in 10-20 glomeruli. They send their axons via the antennoglomerular tract (AGT) to the mushroom body, where

they make en passant synapses onto Kenyon cells before continuing on to terminate in the lateral protocerebral lobe. The mushroom body is so named because of its shape; the cap or calyx contains the 50,000 Kenyon cell bodies, which send dendrites down into the neuropilar region of the calyx where they receive synapses from PNs. Kenyon cells project axons down the stalk, or pedunculus, of the mushroom body, where they are coupled by axo-axonic synapses (Schürmann, 1974; Leitch and Laurent, 1996). Each axons bifurcates and sends a branch to both the alpha- and beta-lobe, where each contacts extrinsic mushroom body neurons. These extrinsic neurons can have discreet arborization patterns in the lobes, pedunculus, or both, often branching densely within a 'slab' across the entire axon tract (Mobbs, 1982; Gronenberg, 1987; MacLeod et al., 1998). They can also send processes to the lateral protocerebal lobe, forming additional pathways for recurrent feedback.

Odor-evoked oscillations in the vertebrate olfactory system

Fast oscillations were first reported in the hedgehog olfactory bulb by Lord Adrian (1942), and have since been described in a large number of vertebrate species, from fish to humans. These oscillations range widely in frequency: 50-60 Hz in small mammals, ~40 Hz in large mammals, 5-15 Hz in fish, and 5-30 Hz in amphibians and reptiles. Odor-evoked oscillations have been reported in the olfactory bulbs of fish, including rainbow trout (Hara et al., 1973), himé salmon (Satou 1974), chum salmon (Kaji et al., 1975), and char (Dϕving and Belgaugh, 1977); in amphibians, including frog (Otoson, 1959; Takagi and Shibuya, 1960; Hobson, 1967), and toad (Takagi and Shibuya, 1960; Segura and De Juan 1966; Graystone et al., 1970); in reptiles, including iguana (Graystone et al., 1970), caiman (Verlander and Huggins, 1977), coachwhip snake (Graystone et al., 1970), bullsnake (Graystone et al., 1970), and turtle (Boudreau and Freeman, 1962; Lam et al., 1998), in birds,

including albatross (Wenzel and Sieck, 1972), duck (Wenzel and Sieck, 1972), shearwater (Wenzel and Sieck, 1972), vulture (Wenzel and Sieck, 1972), and pigeon (Sieck and Wenzel, 1969), in mammals, including rat (Bressler and Freeman 1980), rabbit (Hughes and Hendrix, 1967; Moulton, 1963; Bressler and Freeman 1980; Bressler, 1984), hedgehog (Adrian 1942, 1950), cat (Gault and Leaton, 1963; Bressler and Freeman 1980), dog (Domino and Ueki, 1960), monkey (Domino and Ueki, 1960, Hughes and Mazurowski, 1962), and human (Hughes et al., 1969).

Fast oscillations have also been reported in piriform cortex in rat (Woolley and Timiras, 1965; Bressler and Freeman, 1980), cat (Freeman, 1959, 1968; Boudreau, 1964; Bressler and Freeman, 1980), and rabbit (Bressler and Freeman, 1980). Fast odor-evoked oscillations in the olfactory epithelium, as measured by the EOG, have been reported in frog (Ottoson, 1956; Delaney and Hall, 1996) and salamander (Hamilton and Kauer, 1989; K Dorries and J Kauer, unpublished observations).

Odor-evoked oscillatory activity originates in the olfactory bulb and propagates to olfactory cortex via the lateral olfactory tract (Adrian, 1942, Boudreau, 1964). EEG oscillations are primarily generated by granule cells (Rall and Shepherd, 1968). The firing of mitral/tufted cells is oscillatory and phase-locked to the EEG oscillations, with a 90° phase lead (Eeckman and Freeman, 1990). This is consistent with a model in which bulbar oscillations are generated by negative feedback interactions between granule cells and mitral/tufted cells (Freeman, 1975). Inspiration evokes EEG oscillations in the olfactory bulb even when isolated from the CNS. Reversible isolation of the bulb by cryogenic blockade increases the amplitude and decreases the frequency and variance of these oscillations, and increases the coherence of mitral/tufted cell firing with the EEG (Gray and Skinner, 1988). However, oscillations can also be generated independently in piriform cortex even after

ablation of the olfactory bulb (Freeman, 1968; Bressler and Freeman, 1980). Oscillations at the same frequency as those evoked by odors can also be evoked by electrical stimulation, in both olfactory bulb and piriform cortex, in response to shock of either the olfactory nerves or lateral olfactory tract (Freeman, 1968, 1972, 1974). Shock-evoked oscillations last only a few cycles, and have been described as a damped sinusoid. Thus the vertebrate olfactory epithelium, olfactory bulb, and piriform cortex are each capable of generating oscillations in isolation, suggesting that these structures share a matched resonant capability, rather than any one driving the other (Freeman, 1962, 1968; Ottoson, 1956; Delaney and Hall, 1996; K Dorries and J Kauer, unpublished observations).

The oscillatory response of the piriform cortex to a volley of action potentials in the lateral olfactory tract is not synchronous, but rather consists of waves that spread across the cortex from ventroanterior to dorsoposterior cortex (Scott, 1981). These waves are due to the tangential distribution of lateral olfactory tract axons and their collaterals, such that the afferent action potentials reach ventroanterior cortex before dorsoposterior cortex. This is in contrast to thalamocortical afferents in other cortical areas, from which action potentials arrive at all regions of the cortical area simultaneously.

The spatial and temporal ordering of synaptic events in piriform cortex has a well-defined relationship to the oscillatory waves of activity. Shock stimulation of the LOT evokes a sequence of synaptic events in pyramidal cells, consisting of an initial monosynaptic EPSP from the afferents, closely followed by a disynaptic EPSP from association fibers (Haberly and Bower, 1984; Haberly and Shepherd, 1973; Satou et al., 1983), and finally a long lasting IPSP with an early chloride-mediated phase and a late potassium mediated phase (Satou et al., 1983; Tseng and Haberly,

1988). Because the conduction velocities of LOT collaterals and association fibers are similar, the interval between these events is constant across central and posterior piriform cortex. Oscillatory responses to weak shock stimuli consist of repeated cycles of this sequence of synaptic events (Ketchum and Haberly, 1988).

Current-source density analysis has been used to show that the early monosynaptic afferent EPSP occurs on the distal apical dendrites of pyramidal cells, and the later disynaptic association EPSP occurs on deeper dendrites (Rodriquez and Haberly, 1989). These results suggest that the afferent and association fiber EPSPs converge in adjacent dendritic segments during each cycle of the oscillation. Following this excitatory pairing, IPSPs in the cell body region reset the membrane potential before the start of the next cycle. In addition to this juxtaposition of EPSPs within each cycle, the possibility exists that afferent volleys of action potentials could overtake association fiber volleys from the previous cycle in the posterior piriform cortex, allowing the juxtaposition of EPSPs between cycles (Ketchum and Haberly, 1991). This pairing of recurrent feedback with the spatially distributed inputs evoked by odors forms the basic architecture of a recurrent neural network. Because models of recurrent neural networks with modifiable synapses demonstrate features such as content-addressable memory and pattern recognition and completion (e.g., Anderson, 1972; Hopfield, 1982), the piriform cortex has been postulated to possess these properties as well. NMDA-dependent long term potentiation (LTP) has been demonstrated in piriform cortical slices, in both the afferent and associative pathways (Kanter and Haberly, 1990), which demonstrates that these synapses are modifiable. Incorporation of time delays (Fukushima, 1973; Hopfield and Tank, 1987) or asymmetrical connections combined with fast and slow feedback systems (Kleinfeld, 1986; Sompolinsky and Kantor, 1986) can imbue recurrent networks with the capability to store and recognize spatiotemporal patterns.

Thus the oscillatory dynamics in piriform cortex have been proposed to subserve the storage and recall of spatiotemporal patterns of inputs from the olfactory bulb. Using the framework of Sompolinksy and Kantor (1986), Ketchum and Haberly (1991) have argued that the functional significance of within- and between-cycle pairings of afferent and associative inputs are to store and recall sequences of spatial patterns using the interplay of fast and slow feedback systems. The pairing of afferent inputs and recurrent signals within each cycle would serve as a fast feedback system, causing the piriform cortex to converge to a stable, recognized spatial pattern on each cycle. The slower pairing of afferent and recurrent associative inputs between cycles would serve as the slow feedback system, causing a transition from one spatial pattern to the next, as a stored sequence is recalled.

Odor evoked oscillations in the insect olfactory system

Odor-evoked oscillations in insects are best understood in the locust, where they were first described, but have also been reported in the moth (Wu et al., 1995; Heinbockel et al., 1998), honeybee (Stopfer et al., 1997, 1998), wasp, and cockroach (Stopfer et al., 1998). Odors evoke 20-30 Hz oscillations in the local field potential (LFP) recorded with a blunt extracellular electrode inserted into the calyx of the locust mushroom body. The frequency and envelope of these oscillations can vary slightly from odor to odor, but one cannot discern from the LFP response which odor was presented (Laurent and Naraghi, 1994). The LFP oscillations are thought to be generated by the synaptic current loops of Kenyon cell dendrites, which summate constructively in the extracellular space due to the orderly dendritic orientation in the calyx. Since these synaptic currents are due to incoming EPSPs from antennal lobe PNs, Laurent recorded odor responses intracellularly from PNs and LNs (Laurent and Davidowitz, 1994). The results showed that odors evoke 20-

30 Hz membrane potential oscillations in both PNs and LNs, which consist of sequences of alternating EPSPs and IPSPs out of phase with each other. Paired intracellular recordings showed that these membrane potential oscillations in PNs and LNs are phased locked to each other and to the LFP oscillations. When PNs fired action potentials during an odor response, they were often phase-locked to the oscillation. These findings have been replicated by paired recordings from antennal lobe neurons in the honeybee (Stopfer et al., 1997). Because of the broad tuning of PNs, an odor will activate an ensemble of them. Many of these will display oscillations, thus synchronizing their action potentials and generating volleys of synchronous spikes travelling up the AGT. These in turn will generate volleys of synchronous EPSPs in Kenyon cell dendrites, and the resulting extracellular currents produce the field potential oscillations recorded in the calyx.

The slow temporal patterns evoked in PNs by odors add an additional layer of complexity to antennal lobe dynamics. These slow temporal patterns, which consist of epochs of excitation, inhibition, and periods of silence, continually change the oscillatory ensemble of PNs. As PNs are excited or inhibited, they join or drop out of the synchronous ensemble at each cycle. Thus the membership of the ensemble changes over time, such that the odor response consists of a sequence of synchronized, oscillatory ensembles. These results are examined in depth in Chapters 2 and 3.

The LNs are known to be GABAergic and to synapse directly onto PNs (Leitch and Laurent, 1996), and are responsible for the fast IPSPs seen in odor-evoked membrane potential oscillations (Laurent and Davidowitz, 1994; MacLeod and Laurent, 1996). Injection of picrotoxin (PCT), a vertebrate $GABA_A$ receptor antagonist and invertebrate ionotropic GABA receptor antagonist, into the antennal lobe abol-

ished odor-evoked LFP and PN membrane potential oscillations in locust (MacLeod and Laurent, 1996) and honeybee (Stopfer et al., 1997). This indicates that the inhibitory synapses of LNs onto PNs are necessary for their odor-evoked oscillatory synchronization. Interestingly, the slow temporal patterns persisted after PCT injection, suggesting that they arise by a distinct mechanism. This result provided a unique tool with which to investigate the functional significance of oscillatory synchronization for encoding of odors, because PNs could be selectively desynchronized without altering their slow temporal patterns or the spatial pattern of activated PNs. This investigation was then carried out in honeybees (Stopfer et al., 1997).

Honeybees were taught to discriminate between three odors using the PER conditioning paradigm. Bees could easily discriminate between molecularly dissimilar odorants such as an aliphatic alcohol and the monoterpene geraniol. They discriminated nearly as well between molecularly similar odorants (hexanol and octanol), but generalized somewhat more than between the structurally different molecules. After PCT injection, which desynchronizes the odor responses of antennal lobe neurons, bees could still discriminate between dissimilar odors but could no longer discriminate between two similar odors. These results demonstrate that desynchronization selectively impairs fine odor discrimination, namely that between structurally similar molecules (Stopfer et al., 1997). One interpretation of these results is that the spatial pattern of activated glomeruli is different for molecularly different odors, and is thereby sufficient to support discrimination between them. For similar odors, i.e., hexanol and octanol, the spatial pattern of activated glomeruli may be highly overlapping, as suggested by the results of Mori and colleagues discussed above. With such a highly overlapping spatial representation, the additional information carried by oscillatory synchronization of PNs appears to be necessary for discrimination. These results demonstrate that the oscillatory synchroni-

zation seen in the insect olfactory system is no artifact nor epiphenomenon, but rather participates in odor encoding. That is, the odor-specific information contained in oscillatory synchronization is available not just to the experimenter, but is used by the animal for olfactory discrimination. It seems likely that oscillatory synchronization in other olfactory systems may similarly be involved in information processing.

Odor evoked oscillations in the molluscan olfactory system

Oscillations in the olfactory system of the terrestrial mollusc, *Limax maximus*, have been investigated by Gelperin and colleagues. As with arthropods and vertebrates, oscillatory activity can be recorded in the second order neuropil (namely antennal lobe in insects, olfactory bulb in vertebrates) which in the molluscan brain is the procerebral (PC) lobe. The PC lobe in *Limax* contains about 10^5 local interneurons and receives direct input from olfactory receptors (Chase, 1985; Chase and Tolloczko, 1993; Gelperin et al., 1996), although the existence of a parallel pathway through the tentacle ganglion (a glomerular synaptic region with ultrastructural similarity to mammalian olfactory bulb) suggests that the PC lobe may be more akin to the mushroom body than to the antennal lobe in insects (Chase and Tolloczko, 1993). At rest, the PC lobe is continuously traversed by spontaneous travelling field potential waves (Gelperin and Tank, 1990). These waves originate at the distal tip of the PC lobe and propagate to its base, with a frequency of about 0.7 Hz, as determined by multiple simultaneous field potential recordings both *in vitro* and *in vivo* (in awake behaving animals), and by imaging studies *in vitro* using voltage-sensitive dyes (Delaney et al., 1994; Kleinfeld et al., 1994). Odor stimulation causes a transient collapse of this phase gradient, so that for a few cycles the entire lobe oscillates coherently. No difference in the evoked response was seen

for different odors, whether appetitive or aversive. These results are similar to those seen in vertebrates and insects, in that all odors evoke similar field potential oscillations which are spatially coherent. However, the presence of the spontaneous travelling wave is apparently unique to the molluscan olfactory system. In addition to *L. maximus*, these oscillations have also been seen in *Helix* (Schütt and Basar, 1994) and *L. flavus* (Kimura et al., 1993). Furthermore, no odor-specific spatial patterns were seen in the oscillatory PC responses, in contrast to the spatial patterns of oscillatory EEG amplitude seen by Freeman and Viana Di Prisco (1986) and the spatial patterns seen in voltage-sensitive dye recordings from honeybee antennal lobe (Joerges et al., 1997) and salamander olfactory bulb (Cinelli et al., 1995). However, the spatiotemporal resolution of the optical recording techniques may not have been sufficient to resolve spatial patterns, and this issue will thus require further investigation (Gelperin et al., 1996).

The involvement of the gaseous neurotransmitter nitric oxide (NO) in molluscan olfaction was suggested by intense diaphorase staining in the olfactory pathway of the snail *Helix* (Cooke et al., 1994; Sánchez-Alverez et al., 1994). Reduction of NO production in *Limax*, by either quenching with oxyhemoglobin or inhibiting nitric oxide synthase with the false substrate L-N-nitroarginine methyl ester (L-NAME), causes a transient and reversible decrease in oscillation frequency. This decrease is dose-dependent; at high concentrations of L-NAME the oscillations are reversibly abolished. Application of NO, by either photorelease of caged NO or evolution by diethylamine/NO, increases oscillation frequency by up to 20% (Gelperin, 1994). Photorelease of caged carbon monoxide similarly increases oscillation frequency (Gelperin et al., 1996). Nitric oxide could play a role in synaptic plasticity in the PC lobe, as has been shown in mammalian brain structures (Schuman and Madison, 1994, Kantor et al., 1996). The fact that NO is necessary for odor-evoked

oscillations may provide a link between oscillatory activity and synaptic plasticity in an animal whose olfactory learning capabilities are well-established (Sahley et al., 1992).

Neural coding

The issues of neural coding, information transmission, and neural computation are central to an understanding of sensory information processing. Sensory systems evolved to extract relevant information from the environment, and process it for appropriate behavioral decisions to be made. Thus one characterization of sensory information processing is the transmission of information from the environment centrally towards sensorimotor areas. Our everyday conception of information is often influenced by implicit assumptions about how this information is, or should be, represented. The revolution that Shannon (1948) brought to communications theory was the mathematical framework for quantifying information in a *representation-independent* way, by expressing it in terms of entropy. Thus the information which a neuronal spike train can transmit to postsynaptic neurons can be quantified, in bits/second, without having to worry about the neural code. This approach has been enormously useful in demonstrating that many sensory neurons operate near the physical limits of signal detection imposed by Brownian motion or spontaneous rhodopsin isomerization in photoreceptors (e.g., Bialek and Owen, 1990). However, neural function has ends other than the faithful transmission of information centrally. Computation is the transformation of information from one representation to another, and is thus fundamentally *representation-dependent*. Computation is essentially a coordinate transformation, from one frame of

reference to another, and necessarily includes a loss (or preservation at best) of information. 'Reading-out' a code is precisely this transformation, from one representation into another. Quantification of representation-independent information transmission by a neuron reveals nothing about the computation performed by that neuron, which depends on how that information is encoded. Similarly, the demonstration that a given code conveys information about a stimulus does not establish that the code is used by that system for neural computation. Some representations may make certain computations easy, as illustrated by the question 'is 3630225 divisible by 7?' The answer requires long division, unless the number is in base 7, in which case the answer merely requires inspection of the last digit (Hopfield, 1995). One might expect that the nervous system has evolved to encode information in representations that allow useful computations to be effortlessly performed by the biophysical mechanisms available to neurons. In the words of van de Grind (1988), "If one chooses to do so, it is hard to see why an old-fashioned balance or a windmill should not be called an 'algorithm' or why the bending of a tree in the wind should not be called a computation."

As a case in point, the demonstration of spatial maps in the vertebrate olfactory bulb does not establish that neural space encodes odor quality information (except to the investigator). How such a code could be read is unclear; in other words, the neural space representation (map) may not provide any advantage for the computation of odor identity. Odor identity discrimination is likely a holographic, pattern recognition computation, which in principle could function equally well if the map were scrambled. For example, heading direction can be determined by pooling the activity of hippocampal place cells in rats, despite a lack of topography and the scrambling of the map for each different spatial environment. Other computations, however, clearly benefit from the existence of a map. Contrast enhance-

ment, for example, can be achieved by lateral inhibition of neurons with similar stimulus selectivity. Within a topographic map, lateral inhibition is easily implemented by simple local connectivity rules. Synaptic integration to enhance signal-to-noise can also be easily and locally implemented within a map representation. Thus a map (i.e., a neural space code) may aid some computations but not others; which representations are used for which computations is an empirical question.

The code used by a neural system like the locust olfactory system may therefore reveal much about the computations it is designed to perform, and conversely, an understanding of and appreciation for the relevant computations and ethological role of olfaction may help us understand the purpose of an otherwise arcane neural code. The oscillatory synchronization seen in PN odor responses, from the perspective of information theory, is redundant and decreases the efficiency with which PNs transmit odor-related information. In other words, the same information could be transmitted with fewer neurons if a different (less correlated) code was used. Why, then, did the locust olfactory system evolve to use an inefficient representation? It is tempting to speculate that this oscillatory synchronization reflects a neural code optimized for relevant olfactory computations, such as discrimination, memorization, or recognition, and that the adaptive value of easily performing such computations outweighs the cost of a redundant code. This assumes, however, an evolutionary pressure for coding efficiency. If the evolutionary cost of simply adding more PNs was low, a redundant code might persist without adaptive value. This seems unlikely given the metabolic cost of neurons, and the penalty for increased mass in a flying insect. Moreover, the antennal lobe is an information-processing bottleneck in the insect olfactory system, and this pattern of convergence and divergence is common across phyla. A bottleneck suggests a pressure for coding efficiency, which underscores the redundancy in rhythmic odor responses

and the speculation that this representation is optimized for some neural computation.

Rate coding versus temporal coding

Fifteen years before his pioneering recordings from the hedgehog olfactory bulb, Adrian (1926) first demonstrated that changes in the firing rate of a neuron encoded information about the stimuli he presented to the animal. Those results, made possible by the recent invention of the vacuum tube, showed that the firing rate of a stretch receptor in a frog leg muscle was proportional to the force applied to the leg. This idea that neurons use a rate code to transmit information was a powerful one, and was soon generalized to other sensory systems, and eventually to the entire nervous system. The estimation of firing rate by counting spikes during a response period has been enormously successful in advancing our understanding of sensory information processing. From the functional mapping of the visual system by Hubel and Weisel to the demonstration of systematic molecular receptive ranges in mitral/tufted cells by Mori, spike counts have revealed meaning in the brain. However, this approach is not without its problems.

The use of a spike count measure to explore brain function entails the assumption that what is being measured reflects the neural code. Few would argue that postsynaptic neurons construct peristimulus time histograms, or count spikes for 1 second following a stimulus. Many do assume, however, that postsynaptic neurons integrate inputs over some window of time, and that the spike count or firing rate code reflects this to some degree. If this is true, then an animal must be able to estimate firing rates of its own neurons in real time in order to function in the environment. In many cases, the speed with which real nervous systems process

information precludes the use of an integration window long enough to estimate firing rates. For example, the courtship behavior of male flies (e.g., *Calliphora*) includes high speed aerial pursuit of the female. The ability of males to follow the maneuvers of the female place an upper limit of 30 ms on the total visual processing time required for course corrections (Land and Collet, 1974). Neurons in primate superior temporal sulcus can respond selectively to faces with latencies of 100 ms (Oram and Perrett, 1992). Moreover, event related potentials which correlate with high-level categorization decisions (i.e., “is there an animal in this image or not?”) occur within 150 ms in humans, suggesting that visual object recognition is *completed* within this time (Thorpe et al., 1996). Given the number of intervening synapses between retina and infratemporal cortex (at least ten), even at peak firing rates there would only be enough time for one or possibly two spikes to be integrated. This precludes a neural code which integrates spike rates over time (Thorpe and Imbert, 1989). If a rate code is used, then, it must integrate instead over a pool of neurons to encode an analog signal. Whether a spike count recorded from one neuron estimates in some way the instantaneous activity of such a pool is unknown. Evidence for integration over pools of neurons has come from the work of Georgopoulos (1982), who has shown that vector averaging over pools of sequentially recorded motor cortical neurons can accurately reconstruct movement trajectories in monkeys. These vector averages are from neuronal responses integrated over the entire duration of the movement (~500 ms), which does not demonstrate that population coding can obviate temporal integration. However, vector averages computed over much shorter integration windows (10-20 ms) can accurately predict the directional time course of dynamic movements such as spiral drawing (Schwartz, 1994). Whether this is also true for information processing in sensory systems remains to be seen. A more sophisticated way in which spikes might be integrated over pools of neurons was proposed by Thorpe and Gautrais (1997).

This theoretical neural code uses the temporal order of spikes in an ensemble to convey analog information. The temporal order (or relative pattern of latencies, in a related formulation) can be read out by the latency of a simple integrate-and-fire neuron, thus allowing an output ensemble to transform one pattern of spike orders into another.

Further skepticism about the use of a firing rate code arises from the response dynamics seen in many neural systems. Synchrony and oscillations were first reported by Berger (1929) and have since been recorded in many brain areas and species, for example those described above for olfactory systems. Oscillations in macroscopic recordings such as field potentials or the EEG indicate synchronized oscillatory activity in a large population of neurons—if desynchronized, the EEG signal would be relatively flat. The presence of such coherent activity is functionally inexplicable from a rate coding viewpoint. If information is only contained in mean firing rates, this widespread oscillatory synchronization could only be epiphenomenal.

If information is encoded not just in the mean number of spikes within a response window, but instead (or in addition) in the distribution of spikes within that window, then by definition the system is using a temporal encoding scheme (Theunissen and Miller, 1995). Several hypotheses have been put forward proposing such temporal encoding schemes. Many of these are inspired by experimentally observed oscillatory synchronization, and speculate how it might convey information. Some encoding schemes have been addressed experimentally, while others are purely theoretical. None have been thoroughly tested, and all are controversial. Here I review several of the foremost encoding schemes, as a prelude to Chapter 3, which experimentally tests alternative temporal encoding schemes in

the locust olfactory system.

The temporal correlation hypothesis

In the mammalian visual system, enormous progress has been made in understanding how an image is analyzed by single neurons with diverse feature selectivities. The mechanisms with which these visual features are integrated for global computations such as figure-ground segmentation and object recognition are essentially a mystery. Different aspects of a visual object may be represented as distributed activation patterns in different cortical areas, which must be identified as belonging to the same object and integrated without interfering with coexisting activity patterns corresponding to other visual objects. These problems of figure segmentation and feature binding cannot be flexibly solved using only a rate code, because relationships between features cannot be encoded along with the features themselves. The only way to integrate specific combinations of features using a rate code is with dedicated connections to a downstream neuron. This hardwired integration is unfeasible because of the combinatorial explosion of possible complex patterns of features which constitute any ordinary visual scene. That we effortlessly recognize objects anywhere in the visual field, whether behind a branch or rolling towards us, suggests that visual features are integrated with a dynamic, flexible mechanism. The temporal correlation hypothesis suggests that synchronization may provide this mechanism (Milner, 1974, von der Malsburg, 1981; von der Malsburg and Schneider, 1986; Gray, 1994; Singer and Gray, 1995).

According to the temporal correlation hypothesis, the firing patterns of neurons responding to features of the same object should be synchronized. Since objects have spatial extent, this coherent firing should extend within a cortical area, as well

as between extrastriate areas representing higher order features such as motion or color, and even between hemispheres. Synchronous oscillatory activity in the gamma (20-70 Hz) frequency range has been recorded at all of these spatial scales in the cat and monkey visual cortex (Gray and Singer, 1989; Gray et al., 1989; Eckhorn et al., 1988; Gray and DiPrisco, 1997; Livingstone, 1991). Moreover, the degree of synchronization depends on global stimulus properties. For example, separate bars swept through the non-overlapping receptive fields of neurons with similar preferred orientations elicited oscillatory synchronization, which was strengthened dramatically if a single long bar was used instead (Gray et al., 1992). The only difference in the two types of stimuli was the connecting region of the long bar, which lay outside of the classical receptive fields of the two cells. This suggests that long-range lateral connections are involved in generating this synchrony.

The tendency of oscillations to accompany synchronization is not directly relevant to the temporal correlation hypothesis. Rhythmicity may be a rapid and efficient means for synchronizing neurons. The mechanisms for oscillatory synchronization are not well understood in most systems, but recent reports of a novel class of fast rhythmic intrinsically bursting neurons in cat visual cortex may provide clues (Calvin and Sypert, 1976; Gray and McCormick, 1996; also reported in sensorimotor cortex by Steriade et al., 1998). These pyramidal cells, termed ‘chattering cells,’ fire short repetitive bursts at 20-70 Hz in response to current injection, and display membrane potential oscillations in response to visual stimulation. By bursting (a potentially effective way to drive postsynaptic cells), these neurons may be able to recruit large populations of cells into synchronously firing assemblies. This mechanism, if true, would contrast with the mechanism by which oscillatory synchronization is believed to be generated in the olfactory bulb, which relies on inhibitory feedback from granule cells (a network property) rather than intrinsically rhythmic

neurons. Brainstem modulation may play an important role in the mechanisms for oscillatory synchronization. Electrical stimulation of the brainstem reticular formation, which has an activating effect on the EEG characteristic of arousal (Moruzzi and Magoun, 1949), enhanced the stimulus-specific synchronization of neuronal spike responses in cat visual cortex (Munk et al., 1996).

Oscillatory synchronization in the gamma range has also been reported in retinal and thalamic neurons (Ghose and Freeman, 1972; Neuenschwander and Singer, 1996). This input is unlikely to drive synchronized oscillations in cortex, because its stimulus dependence differs from that in cortical neurons, and thalamocortical projections do not diverge enough to synchronize widely separated regions of cortex (Gray, 1994). The visual system thus resembles the olfactory system in that oscillatory synchronization is seen at many levels, from sense organs to cortex, and appears to be generated independently in each area, potentially allowing inter-area locking of activity by matched resonance properties.

Other examples of temporal coding

The introduction to neuroscience of the analytical technique of reverse correlation or stimulus reconstruction by Bialek (1991) has demonstrated the importance of the timing of single spikes for encoding dynamic stimulus information. The stimulus reconstruction paradigm quantifies the information about the stimulus (in the sense of Shannon, 1948) contained in a spike train by finding the optimal filter with which to reconstruct the stimulus from the spike train. This technique has most successfully been applied to motion-sensitive neurons in the fly optic lobe, wind-direction sensitive neurons in the cricket cercal system, as well as the electroreception system in weakly electric fish (Bialek et al., 1991; Theunissen et

al., 1996; Gabbiani et al., 1996). The amount of information transmitted by single action potentials is generally high. For example, the H1 neuron in the *Calliphora* visual system can transmit up to 90 bits/s, within a factor of 2 of the physical limit set by the entropy of the spike train itself (Strong et al., 1998). However, in most cases, the linear filter term recovered all significant information about the stimulus (Bialek, 1991; Bialek and Reike, 1992; Warland et al., 1991), indicating the operation of a rate code (Theunissen and Miller, 1995), albeit one with a relatively short integration window. Nevertheless, these results suggest that an organism could accomplish real-time stimulus estimation, if it were desirable to do so. In the context of olfaction, the application of the stimulus reconstruction technique is not straightforward. As yet the quantification of mutual information depends on it being contained in the time variations of a dynamic stimulus, such as horizontal motion of a bar. The mathematics for quantification of odor *quality* information have not been worked out, but in principle could be addressed within a broader interpretation of the stimulus reconstruction paradigm (W Bialek, personal communication). The essential difficulty lies in quantifying the entropy of the stimulus. A post hoc quantification of the entropy of the set of odors used in an experiment is certainly possibly—it is just $\log$ n, if n different odors were presented an equal number of times, and $\sum P(i)\log P(i)$, if P(i) is the probability of odor *i* being presented—but I find this approach unsatisfying given the virtually infinite number of odors that *could* have been applied. For the quantification of stimulus entropy, the set of stimuli presented ought to span the stimulus space—which is practically impossible in olfaction. The ability of olfactory neurons to transmit information about the temporal dynamics of an odor stimulus is a different question. Temporal fluctuations in pheromone concentration can be faithfully transmitted by some MGC projection neurons in *Manduca sexta* males (Christensen and Hildebrand, 1988), and have dramatic effects on their orientation and counterturning behavior as they zigzag through an

odor plume (Mafro-Neto and Cardé, 1994). How faithfully this information is transmitted has not yet been quantified.

Neurons in frontal cortex have been shown to dynamically modulate the coherence of their firing in a systematic relationship to behavioral events in awake behaving monkeys (Vaadia et al., 1995). This loosely correlated firing (within 70 ms) of neurons can evolve within a fraction of a second, and can emerge without modulation of firing rates. The suggestion is that synchronization enables neurons to rapidly and flexibly associate into functional groups, which are distinct from other concurrently active groups. More precise coincidences have also been seen among frontal cortical neurons (Abeles et al., 1993a, 1993b, 1994). Most interesting are repeating and precise ($\pm$1 ms) patterns of spikes at long intervals (up to several hundred ms) among a group of neurons. These patterns, which are found in the data by 'brute force' searching, occur more often than would be expected by chance (although estimates of 'chance' vary among investigators). Patterns can be preferentially associated with a certain behavioral event, and different patterns can be associated with different behavioral conditions (e.g., Go vs. No-Go). One interpretation of these results is that they reflect the operation of a neural code (or cortical processing mode) created by what Abeles (1991) terms the 'syn-fire chain'.

The syn-fire chain concept is based on the prediction that, given typical cortical connectivity, firing rates, and synaptic strengths, synchronous inputs are likely to drive postsynaptic cells more effectively than asynchronous inputs (Abeles 1991). One might imagine, then, a group of a hundred neurons which converge and diverge such that when they fire synchronously, a second group of neurons are all driven to fire synchronously. A chain of such groups would propagate synchronous activity, at intervals of about one synaptic delay: this is a syn-fire chain. Diverging,

converging, and reverberating syn-fire chains could be the basis for information processing and computation in the cerebral cortex. The recordings of accurate spatiotemporal patterns described above are taken as evidence of the syn-fire chain concept, although the analysis required to extract these patterns from the data, and the statistics used to provide significance values, have produced skepticism. Clearly more evidence is needed, from different laboratories and animals, to support this provocative view of cortical function.

Possible temporal encoding in the primate visual system has been demonstrated independent of oscillatory synchronization (McClurkin et al., 1991; Richmond et al., 1987; Richmond and Optican, 1987; Optican and Richmond, 1987). Ganglion cells, LGN neurons, V1 and IT cortical neurons convey stimulus-related information not just by the number of spikes they produce, but also by the distribution of those spikes within the response period. This conclusion is based on principal component analysis of spike trains to a complete set of black-and-white images based on Walsh functions. The first principal component (the mean spike count) contained information about the stimuli, but inclusion of the second, third, and fourth principal components conveyed more information. The relative gain in information due to higher order components increased in the higher visual areas. This temporal code could thus increase the efficiency of information transmission. Furthermore the higher principle components are independent and could thus keep separate information which a single component code would confound.

In the somatosensory and motor areas of thalamus and cortex, oscillatory synchronization appears to play a role in attentive behavior and movement planning. EEG oscillations in the 35-45 Hz range in cat and ~15 Hz in monkey can be recorded during periods of attentive immobility, for example as a cat watches a mouse

(Rougel et al., 1979; Bouyer et al., 1981, 1987). These oscillations are synchronized between sensorimotor regions of thalamus and cortex (Bouyer et al., 1981, 1987). Oscillations in monkey motor cortex performing a repetitive task are synchronized over 10 mm in cortex, and are present only during preparation of a planned motor act, vanishing upon initiation of movement (Murthy and Fetz, 1992; Sanes and Donoghue, 1993). Both the amplitudes of the oscillations and the probability of recording them were greater if the tasks were untrained exploratory movements, or extraction of raisins from a hiding place, tasks which engage the monkey's attention (Murthy and Fetz, 1992, 1996a, 1996b). While the functional significance of these oscillations is still unknown, they appear to be a correlate of attention and planning of movements, rather than being directly involved in the execution of movements.

In the vertebrate auditory system, the timing of action potentials conveys information about the phase of sound pressure waves arriving at the ear. Cochlear afferents can show phase-locking to frequencies far higher than those at which any individual neuron can respond; phase information must then be represented across the population of responding cells. This phase-locking is a clear example of a code in which the precise timing of spikes conveys information, and the mean firing rate is clearly an inadequate measure of stimulus-related information. Auditory phase locking is not strictly an example of temporal encoding, in the sense used by Theunissen and Miller (1995), in that the precise spike timing encodes temporal aspects of a dynamic stimulus—and are thus consistent with a rate code which uses a very short integration window. In contrast, temporal encoding as defined by Theunissen and Miller would require that the precise timing of spikes *within the encoding window* (which must be shorter than or equal to the integration window) convey information about the stimulus. This is true in auditory cortex, where syn-

chronization between neurons can convey information about features (e.g., the presence of a pure tone) even when the firing rates do not change (deCharms and Merzenich, 1996).

A novel encoding scheme proposed by Hopfield (1995) proposes that ensembles of neurons—e.g., mitral/tufted cells in the olfactory bulb—encode information by virtue of their pattern of spike times relative to the global odor-evoked oscillation. If the population exhibited synchronous subthreshold membrane potential oscillations, then exponential increases in stimulus strength would be encoded by a linear time advance in the spikes, while the relative pattern of spike times remained invariant with respect to intensity. This multiplexing of identity and intensity information could be transmitted quickly (within one cycle) and decoded easily by a recurrent network incorporating time delays (the same architecture discussed above in the context of decoding mitral cell temporal patterns by the piriform cortex: Tank and Hopfield, 1987). The applicability of this coding scheme to the locust olfactory system, given the presence of global synchronous membrane potential oscillations, is addressed directly in Chapter 3.

Specific aims

The following chapters describe a natural progression of experiments exploring the design and function of the locust olfactory system, focusing on projection neurons in the antennal lobe. The experiments in Chapter 2 attempt to characterize the responses of PNs to odors. These results (Laurent et al., 1996) build on previous results by Laurent and Davidowitz (1994). The goal of these experiments was to confirm and extend, by means of multiple simultaneous extracellular recordings, the oscillatory synchronization and slow temporal patterns in PN odor re-

sponses. A related goal was to quantify slow temporal patterns, which are in general only described anecdotally.

Only after the system had been characterized could specific coding hypotheses be tested. In Chapter 3, predictions of two alternative coding schemes were tested by paired extracellular recordings from PNs. These results (Wehr and Laurent, 1996) demonstrated that the cycle-by-cycle firing patterns across ensembles of PNs encode odor identity information, but that other response features (such as phase or frequency) do not. These results also showed that odor responses in PNs could be more precise than was previously thought. This observation refined our understanding of the relationship between oscillatory synchronization and slow temporal patterns, by demonstrating that these patterns can evolve on a cycle-by-cycle basis.

Finally, the experiments in Chapter 4 address the mechanisms underlying the generation of these dynamics. Previous work had shown that oscillatory synchronization in PNs and local neurons persists after ablation of the mushroom body, but is abolished after injection of picrotoxin (a $GABA_A$ receptor antagonist) into the antennal lobe (Laurent and Davidowitz, 1994; MacLeod and Laurent, 1996). This suggests that the antenna and antennal lobe are sufficient for generation of odor-evoked oscillatory synchronization. Slow temporal patterns in PNs persist after picrotoxin injection, suggesting that the mechanisms which generate them are distinct from those that generate synchronous oscillations. The goal of the experiments described in Chapter 4 was to investigate the role of temporal patterns in primary receptor afferents in the generation of both oscillatory synchronization and slow temporal patterns in PNs. These results (Wehr and Laurent, 1998) showed that odors do not evoke oscillatory synchronization in the population activity of olfactory receptor afferents, and that nonspecific, temporally unpatterned electrical stimulation of receptor axons can evoke both oscillatory synchronization and slow temporal patterns in PNs, similar to those evoked by natural stimulation with odors.

Chapter 2: Temporal representations of odors in an olfactory network

Abstract

The responses of projection neurons in the antennal lobe of the locust brain (the functional analog of mitral/tufted cells in the vertebrate olfactory bulb) to natural blends and simple odors were studied with intracellular and multiple extracellular recordings *in vivo*. Individual odors evoked complex temporal response patterns in many neurons. These patterns differed across odors for a given neuron, across neurons for a given odor, but were stable for each neuron over repeated presentations (separated by seconds to minutes) of the same odor. The response of individual neurons to an odor was superimposed on an odor-specific coherent oscillatory population activity. Each neuron usually participated in the coherent oscillations during one or more specific epochs of the ensemble activity. These epochs of phase-locking were reliable for each neuron over tens of repeated presentations of one odor. The timing of these epochs of synchronization differed across neurons and odors. Correlated activity of specific pairs of neurons hence generally occurred transiently during the population response, at times that were specific to these pairs and to the odor smelled. This progressive transformation of the synchronized ensemble over the course of the odor response is not revealed by the field potential oscillations. We propose that (1) odors are represented by spatially and temporally distributed ensembles of coherently firing neurons and (2) the field potential oscillations which characterize odor responses in the olfactory system occur, at least in this animal, in parallel with a slower dynamic odor representation.

Natural odors (such as plant fragrances for example) are usually complex blends of many volatile compounds. The percept that a natural fragrance evokes in us, however, is usually singular (e.g., jasmine, onion or a skunk). Our brains, therefore, most likely form a unique internal representation of each specific blend, from which individual components (such as amyl acetate or heptanone, for example) are difficult or impossible to segment. This specific odor representation must, in addition, be sufficiently inclusive to allow like-odors (e.g., roses of distinct varieties, or roses smelt in different climatic conditions) to be 'recognized' as the same. Finally, this representation must be stable over time— odor memories are generally very long lasting (Hildebrand, 1995).

A major challenge in the study of olfaction is to understand the computational rules or algorithms used by the brain to encode, store and retrieve these complex and multidimensional stimuli. Recent remarkable developments in the molecular biology of vertebrate olfaction have shed light on some crucial aspects of the 'mapping' of odor-signals in the olfactory bulb (Axel, 1995; Buck and Axel, 1991; Vassar et al., 1994; Sullivan et al., 1995). These results complement physiological and imaging studies of odor processing that indicate broad, distributed stimulus representation schemes (Kauer, 1991; Cinelli et al., 1995). Other recent results from physiological studies of molluscan and insect olfaction indicate that the olfactory nervous system of several invertebrates generates oscillations (Gelperin and Tank, 1990; Delaney et al., 1994; Laurent and Naraghi, 1994), a macroscopic feature similar to one described previously in the olfactory brain of vertebrates (Libet and Gerard, 1939; Adrian, 1942; Freeman, 1975; 1978; Satou, 1990; Gray, 1994; Gray and Skinner, 1988). These results, combined with anatomical evidence that arthro-

pod, molluscan and vertebrate olfactory circuits have very similar designs, suggest that the computational rules used by olfactory systems may be similar (or conserved) across animal phyla.

We focus here on odor processing in the olfactory nervous system of an insect, the locust *Schistocerca americana*, and examine the properties of individual and ensembles of neurons in response to odor presentation *in vivo*, continuing the studies of Laurent and Naraghi (1994) and Laurent and Davidowitz (1994). These neurons are the antennal (or olfactory) lobe projection neurons whose signals are sent to the mushroom body, a center for learning and memory (Davis, 1993; Hammer and Menzel, 1995). The projection neurons are thus the functional analog of the mitral/tufted cells in the vertebrate olfactory bulb. In this paper, we examine in detail the potential role of time as a variable in the combinatorial representation of sensory stimuli by this part of the brain. We focus on processing of odors to which the animal has been exposed, i.e., we do not consider here the responses evoked by the first 1 to 3 presentations of an unfamiliar odor. We find that the temporal firing patterns of individual neurons, as well as the synchronization of firing across groups of neurons, are stimulus-specific. In other words, each odor appears to be represented not simply by an ensemble of synchronized neurons but by a progressive and odor-specific transformation of that ensemble, so that each neuron synchronizes with several others only during one or more precise epochs of the ensemble response. We thus propose that oscillations in the olfactory nervous system occur, at least here, in parallel with a slower code which is distributed both in time and across many neurons.

Methods

The preparation. Adult locusts were immobilized and dissected as described in Laurent & Naraghi (1994) and Laurent & Davidowitz (1994). The following modifications were applied to the experimental protocol used for experiments in Figs. 1, 13-19. The gut was left intact, and the head was only intermittently (rather than continuously) superfused with locust physiological saline (mM: 140 NaCl, 5 KCl, 5 $CaCl_2$, 4 $NaHCO_3$, 1 $MgCl_2$, 6.3 Hepes, pH 7.0).

Olfactory stimulation. The open ends of a set of up to 24 glass capillaries or stainless steel tubes (0.5 mm inner diameter) were placed 2.5 to 5 cm from the antenna, angled so that they converged onto the antenna. The other end of each capillary was connected via polyethylene tubing to a 5 ml odorant-containing syringe body. Each chamber contained a 1 cm^2 piece of filter paper, on which was deposited 20 μl of one of the following odors: artificial cherry flavor (Bell Fragrances), iso-amyl acetate (iaa), citral, cineole, benzaldehyde, geraniol (Aldrich), pure spearmint oil (Flavco), apple blossom, strawberry, or vanilla potpourri oils (Gilbertie's Herb Gardens), lavender oil (Nuit Unlimited), eugenol, n-pentanol, n-hexanol, n-octanol, α-pinene (Sigma), crushed wheat grass, crumbled rat chow, or no odorant (air control). The chambers were connected to an air pressure injection system via a set of valves, so that electronically controlled gentle pressure pulses (insufficient to visibly bend the antenna) could be delivered to the animal. For three of the odor lines, pressure pulses were individually regulated. Pressure-actuated check valves were interposed between the odorant chamber and the animal, to prevent passive diffusion of odorant. For the other odor lines, a common pressure line was connected to each odor chamber in parallel. Odors were mixed by applying a simultaneous pressure pulse to each one of the selected odor lines. For these experi-

ments, pulses of variable duration were delivered at a minimum interval of 10 s. Although odor delivery to the antenna was always delayed relative to the command pulse to the air valves (due to the physical nature of the stimulus), the delay between command and delivery was constant from trial to trial. This could be demonstrated simply by averaging successive local field potential traces evoked by the delivery of an odorant and locked on the stimulus pulse. In all cases, this produced a clear average field potential signal (one to several oscillation cycles) at a time corresponding to the onset of the response of any one of the successive trials. (Because the field potential is not a pure and constant periodic signal, however, the average calculated from the oscillation cycles occurring after the first or second one was often flat.) The delay between command and delivery was also shown to be constant with the use of a particle velocity microphone.

Intracellular recordings (Figs. 3-12). 100-300 MΩ glass microelectrodes pulled with a horizontal puller (Sutter Instr.) and filled with 0.5 M K acetate were used to record from the somata of projection neurons in the antennal lobes, using established techniques (Laurent and Davidowitz, 1994). The antennal lobe contains two types of neurons: local and projection neurons. The antennal lobe local neurons in locust produce no conventional action potentials but rather TTX-resistant 'spikelets' of variable amplitudes, probably caused by voltage-dependent calcium currents (Laurent and Davidowitz, 1994; Laurent and Naraghi, 1994). Neurons could thus easily be identified as local or projection neurons from physiological recordings.

Extracellular recordings (Figs. 1, 13-19). Extracellular recordings were performed using 2-6 glass microelectrodes pulled with a horizontal puller (Sutter Instr.). Electrodes for local field potential (LFP) recordings had ~2 μm tips with a DC

resistance of <1 MΩ. Electrodes for single-unit extracellular recording had 0.5-1 μm tips with a DC resistance of 1-2 MΩ. Both types of electrodes were filled with locust physiological saline. LFP signals were differentially amplified, band-pass filtered (1 - 500 Hz), “notch-filtered” at 60 Hz (A-M Systems 1700), and stored to digital audio tape (DAT, Micro Data Instr.) (5.5 kHz cut off). The DAT recorder included an analog Nyquist frequency low-pass filtering stage before analog-to-digital conversion. Some single-unit extracellular signals were amplified and stored in this manner, with band-pass filtering at 10 Hz - 5 kHz. Other single-unit extracellular signals were amplified using an Axoclamp 2A amplifier (Axon Instr.) before storage to DAT. Each projection neuron (PN) recording was obtained with an individual extracellular electrode (up to five simultaneously), as was the LFP. No spike sorting was carried out with any of the extracellular single unit data presented here.

Off-line Analysis. The data analyzed and presented here were obtained from animals already exposed to the odors tested. In other words, we do not consider here the first one to three responses of neurons to unfamiliar odors. Data were redigitized from DAT at 5 kHz (National Instruments: LabVIEW software and NBMIO16L hardware) after AC amplification and low-pass filtering at 3 kHz (Brown Lee Precision 210A amplifier). LFPs were digitally band-pass filtered (5 - 50 Hz) using MATLAB (The MathWorks, Inc.) on a Macintosh (Power Computing Corp.). Single-unit extracellular signals were converted to lists of spike times (rounded to the nearest ms) using a threshold discriminator algorithm, and confirmed by visual inspection (LabVIEW). Peri-stimulus-time histograms (PSTHs) were constructed by averaging blocks of trials aligned on the odor pulse command, and using bins of 25-150 ms. All intracellular traces are displayed with action potentials clipped.

Phase analysis (Fig. 14). PN spike times were converted to a phase represen-

tation with respect to the odor-induced LFP oscillations. Raw LFP traces were band-pass filtered (10-50 Hz) using a digital noncausal (i.e., no phase distortion) 5-pole Butterworth filter. Peaks, troughs, and zero-crossings of the LFP signal were used as phase reference points as follows: peaks of the LFP were assigned a phase of 0 or 2π, troughs a phase of π, and zero-crossings a phase of $\frac{\pi}{2}$ or $\frac{3\pi}{2}$. The time of a PN spike ($t_{PNspike}$) was then compared to the nearest peak ($t_{LFPpeak}$), trough, and/or zero-crossing in the simultaneously recorded LFP, and assigned a phase by linear interpolation. The phase was calculated by interpolating either between peaks (whole cycle), between nearest peak and trough (half cycle), or between nearest zero-crossing and nearest peak or trough (quarter cycle). For example, using the whole-cycle method, the phase of a PN spike was given by

$$\phi_{PNspike} = 2\pi \cdot \left(\frac{t_{PNspike} - t_{lastLFPpeak}}{t_{nextLFPpeak} - t_{lastLFPpeak}} \right)$$

Phase histograms obtained using these three methods did not differ qualitatively from each other.

Sliding window cross-correlation analysis (Figs. 15-17, 19). Cross-correlation analysis was performed using MATLAB. After converting simultaneously recorded PN traces to rasters, pairwise cross-correlation analysis was performed on the rasters on 300 ms windows beginning 1 s before the onset of the odor pulse and ending 3 seconds after the end of the odor pulse (10 ms bins). The first 300 ms window was then slid forward by 100 ms, and a new cross-correlation analysis was performed on the new (overlapping) window. This procedure was carried out with the entire data set. The cross-correlation calculated on each window could thus be represented as a row in a matrix, in which each column represents a specific time-

lag of the cross-correlation and each row a successive time-window around the odor pulse. Odors were presented several times [at 10 s (or more) intervals], this analysis was performed for each trial, and the cross-correlation matrices calculated for all the trials were aligned to the odor pulse and added together. The magnitude of the cross-correlation was then represented using a cool-to-warm color scale, normalized over the entire data set. Thus, a dark blue region (Figs. 15,16,19) indicates that there were no spikes in either PN at that time and time-lag. A red region indicates that, over all the trials, spikes coincided often at that time-lag and time of the trial. The actual number of coincident spikes encoded by a red color is indicated in the figure legends. This number (e.g., 15) indicates that each PN fired, e.g., 15 spikes in the corresponding bin. In an initial attempt to test the significance of periodic patterns in the cross-correlograms, we divided the data for each experiment in several subsets (e.g., from an experiment containing 26 trials: odd trials 1, 3...25 in one subset and even trials 2, 4...26 in another, or 2 complementary subsets of 13 randomly selected trials in the entire set) and calculated the cross-correlation on each subset independently, as described above. Any spurious correlation between the two cells analyzed appeared as non-matching cross-correlations patterns in the different subsets. By contrast, any pair of cells with consistent cross-correlation patterns from subset to subset was considered to show a significant degree of stimulus-induced correlation. In all cases where this occurred, the cross-correlograms indicated a periodicity identical to that of the corresponding local field potential. Cells displaying such cross-correlations were considered synchronized (although it is clear that synchrony does not require periodic firing). In a second series of tests, synthetic data sets were produced to mimic the experimental data, except for periodicity and correlation. Trains of ‘spikes’ were synthesized, whose timing was described by Poisson statistics and whose average frequency (as a function of time) matched precisely the experimental data. These synthetic data

were then processed in a manner identical to the experimental data, and periodic cross-correlation patterns were sought. Never did any periodic pattern such as those described for the experimental data emerge from these synthetic data sets. The existence of periodic cross-correlations patterns in the data are thus not the result of coincident increase in the firing rates of the neuron pairs. A rigorous analysis of the statistics of the experimental data using spectral techniques (namely coherence analysis) is presented in Chapter 3.

Pairwise sliding window cross-correlation analysis was also performed between the rasters of each PN and the simultaneously recorded LFP in the mushroom body (Fig. 17). Raw LFP traces were band-pass filtered (10-50 Hz) using a 'noncausal' (no phase distortion) digital 5-pole Butterworth filter. The sliding window cross-correlation analysis was identical to that described above for pairs of PN rasters. A dark blue region (Fig. 17) indicates that, on average, there was, at that time of the trial, a trough in the LFP at that time-lag relative to a PN spike. Similarly, a red region indicates that, on average, there was, at that time of the trial, a peak in the LFP at that time-lag relative to a PN spike. A light blue region indicates that, on average, the LFP was in between peak and trough at that time-lag relative to a PN spike. A light blue band spanning all time-lags at a given time of the trial indicates that no PN spike occurred at that time of the trial. Note that the magnitude of the cross-correlation function assigned to a given color (e.g., red) is here a product of both the LFP amplitude and the coherence between PN spikes and the LFP oscillations. Note also that the magnitude of the cross-correlation between a PN raster and the LFP signal can be positive (red) or negative (dark blue), with zero correlation represented by light blue (Fig. 17). This is in contrast to the cross-correlation calculated between two PN rasters (Fig. 15,16,19), which was never negative.

Principal components analysis (Figs. 7-9). Principle components analysis was performed on intracellularly recorded responses of one PN to 134 presentations of 18 odors (including air). Each trace was digitally low-pass filtered at 50 Hz (as above) and the covariance matrix was computed from all resulting traces. The eigenvectors and eigenvalues of this matrix were extracted by standard linear algebra methods. The principle components (Fig. 7) are these eigenvectors ranked by the magnitude of their associated eigenvalues. Projections of the mean responses to each odor onto these components (i.e., inner products) were then calculated (Figs. 8-9) resulting in a set of coefficients for all components for each mean odor response. Euclidean distances between these sets of coefficients (truncated to the first 10) were calculated according to the distance formula, and used to rank the neighborhood relations of all mean odor responses (Fig. 9). These relations were displayed in similarity tree, built by starting with the closest pairs of responses, and iteratively adding a branch to each successively more distant response or group of responses.

Results

Temporal response patterns in projection neurons

The presentation of any odor to the antenna of an animal *in vivo* typically led to a change in the firing behavior of many projection neurons in the ipsilateral antennal lobe. The response of each neuron to a stimulus, however, differed from that of other neurons by its duration, its timing relative to the odor delivery and its temporal structure. Figure 1 shows simultaneous extracellular recordings from three different projection neurons and their responses to an apple+cherry mixture. While one neuron (PN 1) responded with a short burst of high frequency action potentials, PN 2 responded to the same odor by a period of suppression preceding delayed spik-

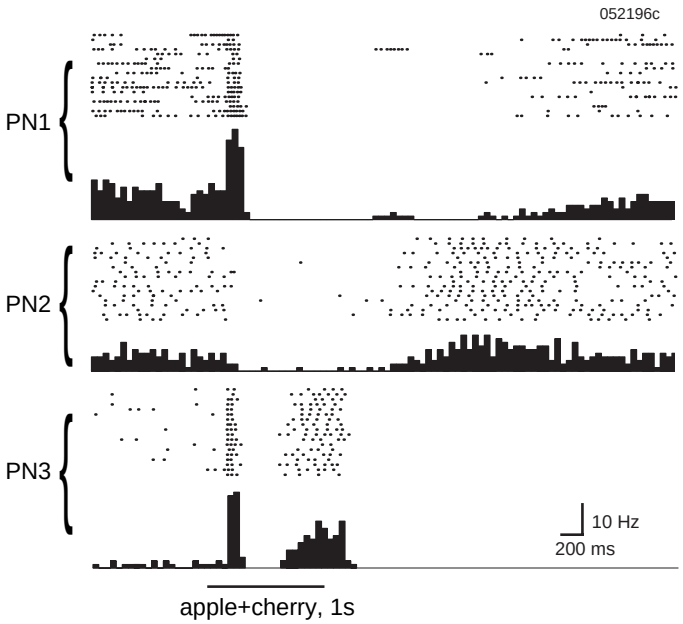

Figure 1. Range of temporal patterns of response to a single odor across neurons. Temporal response patterns of three simultaneously recorded antennal lobe projection neurons in response to the odor apple+cherry. Dot rasters (top) from the extracellular recordings were aligned to the odor pulse and averaged (50 ms bins) to form the PSTH (below). Note the distribution of response patterns, from short and brisk (PN1), to inhibitory (PN2), to multiphasic (PN3). Note also the consistency of the response patterns over time (see also Fig. 2). Not all neurons that responded to this odor, therefore, were active at the same time. Rather, the ensemble response was distributed in time. (Note: PN3 is the same neuron as PN2 in Chapter 3, Figures 5-6, although recorded earlier and with different simultaneously recorded PNs.)

---

ing. PN 3 displayed a complex mixed response containing successive epochs of high frequency firing, suppression, sustained excitation, and prolonged suppression. This indicates that, if individual odors are represented by an ensemble of neurons, this ensemble is dynamic and that all participating neurons do not participate simultaneously.

The temporal structure of the response of individual projection neurons to a given odor was consistent and reliable. Figure 2 shows the response of an intracellularly recorded neuron evoked by 1 second pulses of cherry and octanol. Recordings were obtained up to 15 min. apart and aligned on the odor pulse. For both cherry presentations, the PN's response consisted of a short initial burst of action

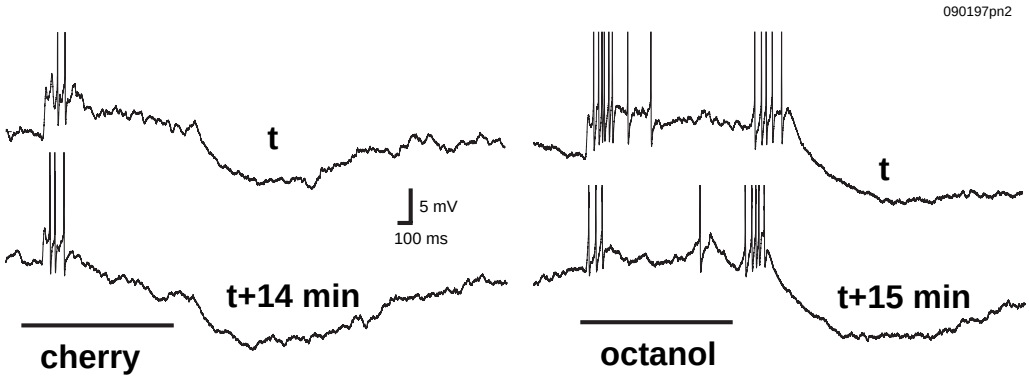

Figure 2. Consistency of response patterns and odor-specificity. Intracellular recording of a projection neuron. A pulse of artificial cherry odor was presented once (t), and presented again 14 minutes later (t + 14 min). The recordings obtained for these two responses have been aligned on the odor pulse. They demonstrate the consistency of the temporal response patterns over repeated presentations. The response to octanol was also consistent over repeated presentations (15 minutes later), but the temporal response pattern was clearly and reliably different than the response to cherry. (Note that these and other odors were presented during the 14/15 minute intervals). Projection neurons usually respond to multiple odors, generally with different (i.e., odor-specific) temporal patterns (see Figs. 3-6).

---

potentials (riding on a oscillatory subthreshold pattern), a ~1 s period of silence and a final period of inhibition. Similarly, the response to octanol, on both occasions, consisted of two bursts of action potentials separated by a period of silence.

Whereas the overall temporal structure of individual neurons' responses was consistent from trial to trial (in identical stimulus conditions), the very fine detail of the response was not. The response to cherry (Fig. 2), for example, consisted of an action potential at cycles 3 and 4 of the subthreshold oscillatory pattern during the first presentation, but at cycles 2, 3 and 4 of the next presentation, 14 minutes later. The same variability can be observed in the responses of simultaneously recorded neurons in Fig. 1. There, knowing the exact sequence of action potentials

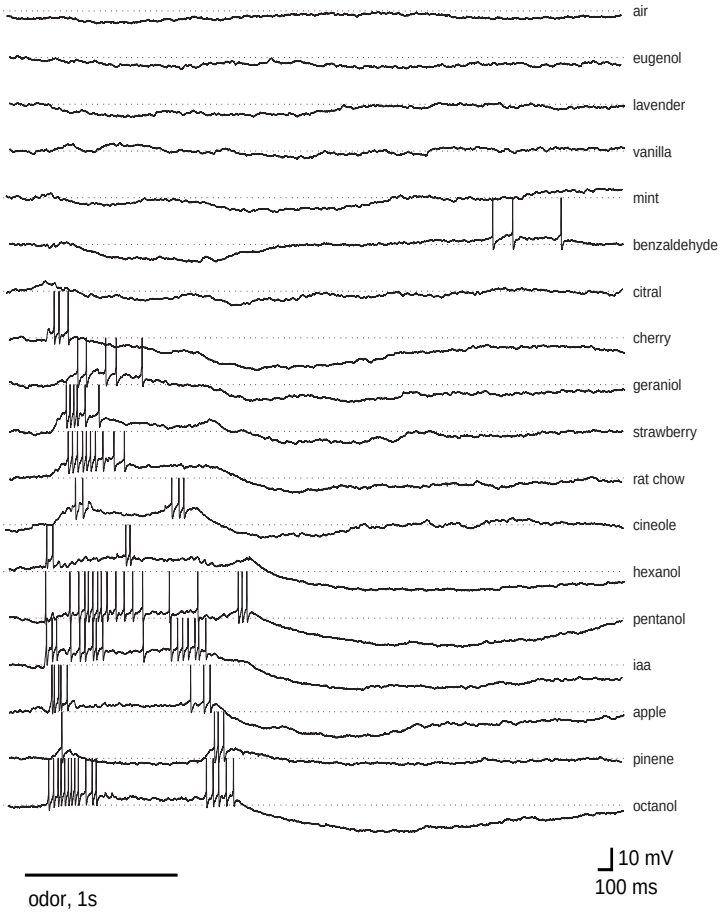

Figure 3. Odor specific slow temporal response patterns. PNs usually respond to multiple odors. The response patterns evoked by these multiple odors, however, are generally different. Here is shown an intracellular recording of a PN whose membrane potential was affected by 14 of 18 odors presented. The responses ranged from inhibition (e.g., benzaldehyde) to complex successions of excitation and inhibition (e.g., octanol). Excitatory "bursts" do not necessarily overlap in time, and are therefore not simple onset or offset reponses (e.g., compare cineole, hexanol). Membrane potential oscillations and/or rhythmic firing are evoked by several odors (e.g., cherry, cineole, hexanol) but the epochs of oscillations can vary.

---

in one neuron did not allow one to predict what the exact sequence of action potentials in the second neuron would be: The responses of PN 3 at the onset of the odor pulse were remarkably similar in all trials, while they were not for PNs 1 and 2. Two neurons can therefore be transiently 'synchronized' over episodes of fifty to several hundreds of ms, but the occurrence of spiking events during these episodes often remained probabilistic. (The fine structure of the synchronization will be further addressed below. The predictive value of one PN's firing about another PN's firing during the same trial will be explored in detail in Chapter 3.)

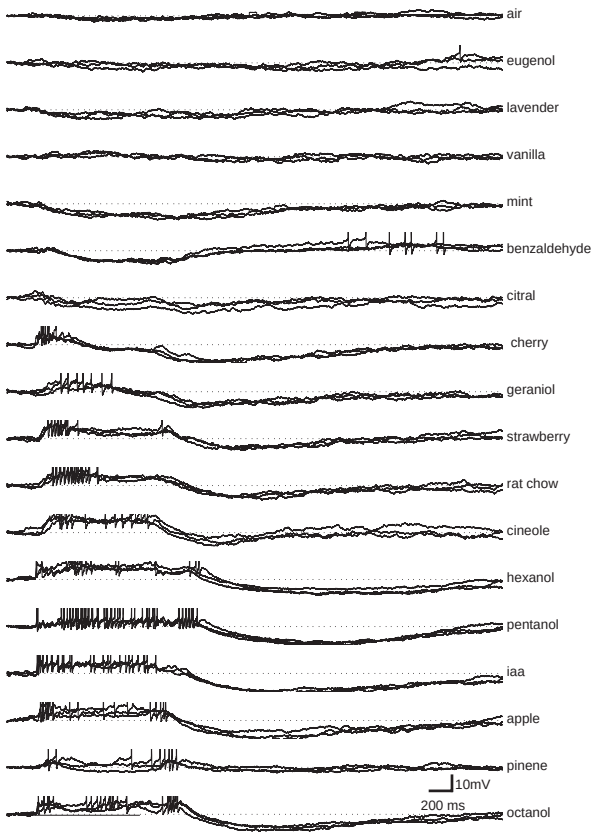

Figure 4. Consistency of odor specific slow temporal response patterns. Here three responses to each given odor are overlaid, for the same PN (responding to the same odors) as shown in Fig. 3. The periods of excitation and inhibition reliably overlap over repeated presentations. This indicates that the typical traces shown in Fig. 3 are representative of the PN's response profile.

The temporal activity patterns observed in a given neuron in response to an odor stimulus were odor-dependent. Individual neurons usually responded to many of the 20 test odors that could be presented to an animal. An example is given in Fig. 3 of a neuron that responded to 14 of 18 odors tested (including air). As can be seen, the response patterns were markedly different for the different odors. For example, while the neuron's response to strawberry consisted of an initial burst of activity, then a plateau period, followed by deep inhibition, the response to octanol contained two "bursts" of spikes separated by a plateau period. Note that bursts of spikes evoked by some odors occurred exactly at the time when the neuron would have been inhibited during its response to other odors (e.g., cineole vs. hexanol). The remarkable complexity, diversity, and reliability of these temporal patterns, even

Figure 5. Slow temporal patterns can be seen from the mean. The mean membrane potential across all responses to a given odor demonstrates the reliability of the epochs of excitation and inhibition across trials. This representation of the response profile, for the same PN (responding to the same odors) as shown in Fig. 3, has the advantage of clearly showing consistent periods of excitation and inhibition with a minimum of complexity. However, response variance is excluded, and firing patterns are obscured.

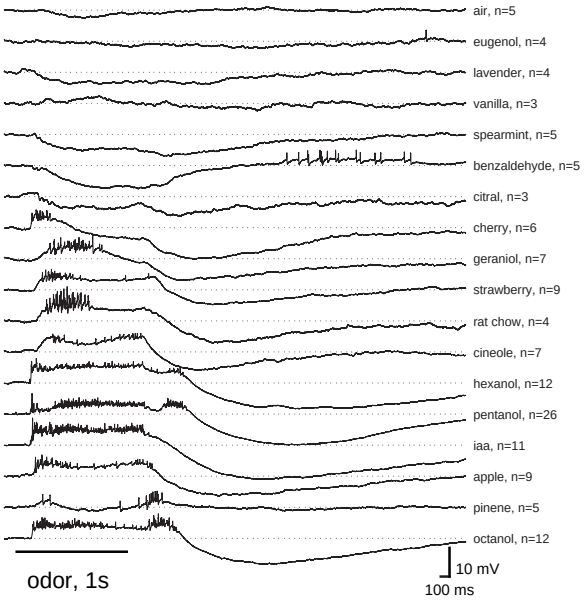

in a single PN, is impossible to convey in a single figure or with a single representation of neural activity. Figures 3-9 compare several approaches to displaying and quantifying different aspects of these complex responses. The typical trials shown in Fig. 3 demonstrate membrane potential and firing patterns, but cannot address trial-to-trial reliability. These different slow temporal response patterns were stable over repeated presentations of each odor, as can be seen in Fig. 4. Here three responses to each odor are plotted over each other, to demonstrate the reliable overlapping of the response features across trials. In Fig. 5, the membrane potential features (epochs of excitation and inhibition) which are stable across trials can be seen clearly in the mean membrane potential taken over all presentations of a given odor. This representation emphasizes reliable membrane potential features, but does not provide information about regions of variance across trials. The mean membrane potential also obscures firing patterns, which can be most clearly seen using dot rasters and peri-stimulus time histograms (PSTHs) as shown in Fig. 6.

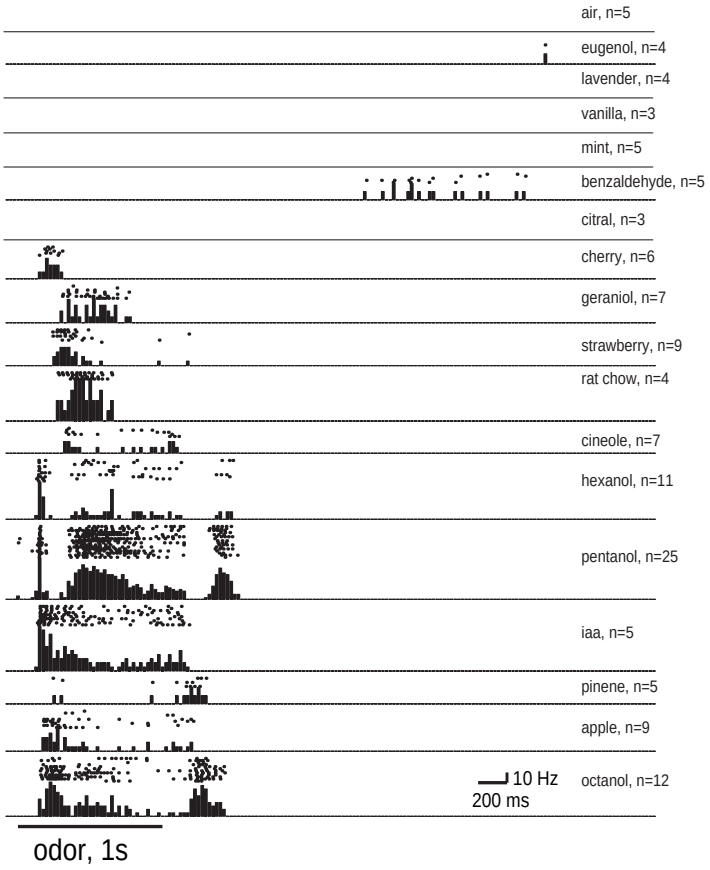

Figure 6. Odor specific firing patterns. The slow temporal response patterns can be seen in PN spike trains as well as the membrane potential. Here this is demonstrated by dot rasters and PSTHs from the same PN (responding to the same odors) as shown in Fig. 3. The consistency of these firing patterns over numerous repeated presentations indicates that the output of PNs to higher structures preserves much of the slow temporal structure seen in the membrane potential.

The diversity of these firing patterns, and their consistency across trials, are demonstrated by the tight vertical banding of the dot rasters. “Bursts” evoked by different odors do not necessarily overlap (e.g., cherry vs. strawberry, pentanol vs. iaa). The similarity of these firing patterns to the membrane potential patterns indicates that the output of PNs to higher structures preserves much of the slow temporal structure seen in the membrane potential.

How many different temporal patterns can be evoked in a given projection neuron? How similar or different are these patterns from each other? The high dimensionality of intracellularly recorded odor responses in these neurons greatly hinders any approach to exploring these important questions. In principle, intracellular recordings are continuous waveforms and are thus infinite-dimensional. Even

when sampled in practice (e.g., at 5 kHz), tens of 10 s trials generate an odor response profile of order 10^6 dimensions. Moreover, the features which are likely relevant to comparisons between responses (such as bursts of firing or epochs of inhibition) form a much smaller subspace and are not available by inspection in such a 10^6 dimensional vector. As discussed in Chapter 1, the right representation may make certain computations easy. For the computation in question (comparisons among odor responses), the representations presented in Figs. 3-6 differ in their suitability, but all remain high dimensional and thus hinder quantitative comparisons. Many dimensionality reduction techniques have been developed for such purposes, such as Fourier analysis, linear discriminant analysis, and principal component analysis. All of these are linear transforms of data onto a particular basis set, chosen to provide insight into the data structure. The ideal basis set (i.e., analytical technique chosen) corresponds to the underlying features one wishes to reveal in the data—in this case, epochs of excitation and inhibition. While many techniques would be suitable (e.g., wavelet transforms, linear discriminant analysis), principal components analysis offers a straightforward approach to quantifying neuronal temporal response patterns which has been successfully applied in the mammalian visual system (Richmond and Optican, 1987).

Principal components analysis uses an ordered set of basis vectors (the principal components) which represent decreasing proportions of the total variance across the data. These principal components are just the eigenvectors of the covariance matrix of the data, ranked by eigenvalue magnitude. This transform is optimal (in the least-squares sense) for representing data with a truncated set of basis vectors. Figure 7 shows the first 10 principal components of the odor responses of the same PN shown in Figs. 3-6. The first principal component (pc 1) closely resembled the mean of all responses to all odors, and had the largest magnitude.

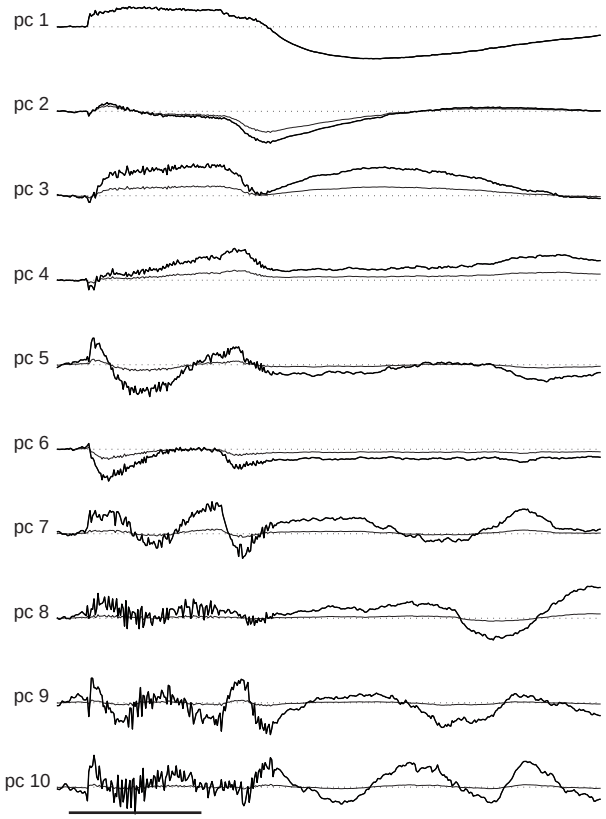

Figure 7. Principal components of slow temporal patterns. The first 10 principal components of the set of all 134 odor responses, for the same PN (responding to the same odors) as shown in Fig. 3-6, are plotted here as a function of time, aligned to the odor pulse (1s, indicated by horizontal bar). The components are plotted in absolute magnitude (fine line) and also normalized to the first principal component (heavy line). The absolute magnitude decreased for higher principal components. The first component (pc 1) was similar to the mean response across all odors, while higher components resembled the epochs of excitation or inhibition evoked by given odors. For example, pc 2 resembled the burst-plateau-inhibition response to cherry, whereas pc 7 resembled the early and late bursts evoked by cineole. The late burst evoked by octanol, which occurred later than that of cineole, resembled that of pc 9.

Higher principal components had decreasing amplitudes (fine lines show absolute magnitudes). To emphasize their features, higher principal components were also normalized in Fig. 7 (heavy lines). These vectors, plotted as a function of time and aligned to the odor pulse, contained features reminiscent of the epochs of excitation and inhibition seen in PN odor responses. For example, pc 2 resembled the burst-plateau-inhibition response to cherry, whereas pc 7 resembled the early and late bursts evoked by cineole. The late burst evoked by octanol, which occurs later than that of cineole, resembled that of pc 9. Spectral analysis of these principal

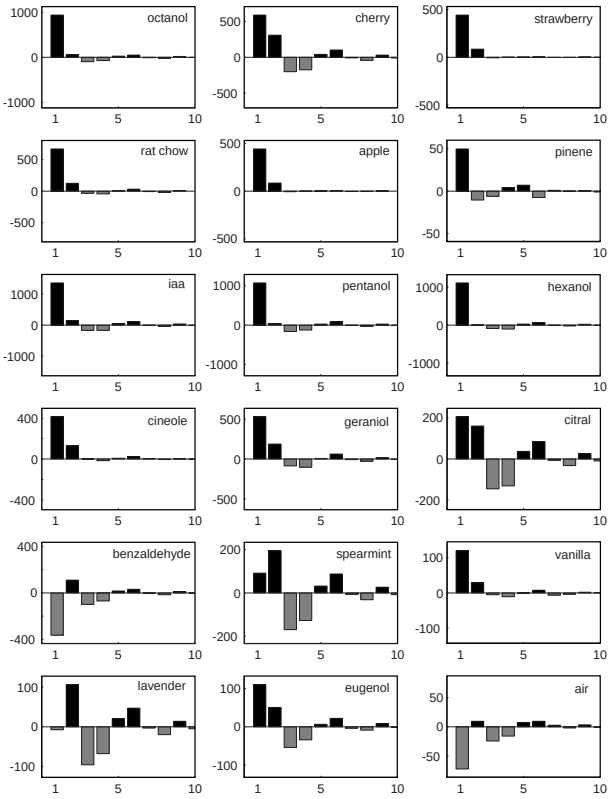

Figure 8. Coefficients of principal components. The coefficients of each principal component are plotted for each odor. These coefficients represent the degree to which a given principal component accounts for the variance in the responses to a given odor. Odors which evoked similar slow temporal response patterns had similar coefficients (e.g., pentanol, hexanol, octanol). Conversely, odors which evoked distinct slow temporal patterns had different coefficients (e.g., octanol, benzaldehyde, lavender). This compact representation (i.e., 10 numbers) can therefore capture similarities and differences between odor responses in a quantitative way (see text for details). Moreover, the patterns of coefficients illustrate how the principal components represent different features of the slow temporal patterns. For example, odors which evoked inhibition (e.g., lavender, benzaldehyde, spearmint) had high coefficients for principal components with inhibitory epochs (e.g., pc 2, 5, 6), and negative coefficents for principal components with only excitatory epochs (e.g., pc 3,4).

---

components revealed no prominent increase in power in the 20-30 Hz range (the frequency of odor-evoked oscillatory synchronization) compared to other frequencies (not shown).

Because the principal components form a basis set, each odor response can be represented as a weighted sum of these components. These weights, or coefficients, indicate how much variance in the response is accounted for by the re-

spective component. The coefficients are just the magnitude of the projection of an odor response onto the principal components. The coefficients of the first 10 principal components are plotted for each odor in Fig. 8. The patterns of coefficients illustrate how the principal components represent different features of the slow temporal patterns. For example, odors which evoke inhibition (e.g., lavender, benzaldehyde, spearmint) have high coefficients for principal components with inhibitory epochs (e.g., pc 2, 5, 6), and negative coefficients for principal components with only excitatory epochs (e.g., pc 3,4). Moreover, odors which evoke similar slow temporal response patterns have similar coefficients (e.g., pentanol, hexanol, octanol). Conversely, odors which evoke distinct slow temporal patterns have different coefficients (e.g., octanol, benzaldehyde, lavender). These observations can be quantified by computing the euclidean distance between these odor response representations. For example, pentanol and hexanol evoke similar response patterns and lie very near each other (at a distance of 96) in the space of the first 10 principal components. Benzaldehyde and iaa evoke strikingly different temporal response patterns, and are far apart (at a distance of 1,722) in this space. This compact representation (i.e., 10 numbers) can therefore capture similarities and differences between odor responses in a quantitative way, as illustrated in Figure 9. Each mean odor response, represented by the coefficients of its first three principal components, was plotted in the space of those three components in Fig. 9A. Points representing odor responses with similar slow temporal patterns were near each other in the space, while distinct odor responses were widely separated. The responses therefore appeared to be grouped into 3 or 4 clusters. For example, the responses to the three aliphatic alcohols (octanol, hexanol, and pentanol) had similar temporal patterns (cf. Figs. 3-6), and these responses clustered together in Fig. 9A. The response to benzaldehyde was quite different and was plotted correspondingly far away from the alcohols. Figure 9B shows the distances between the re-

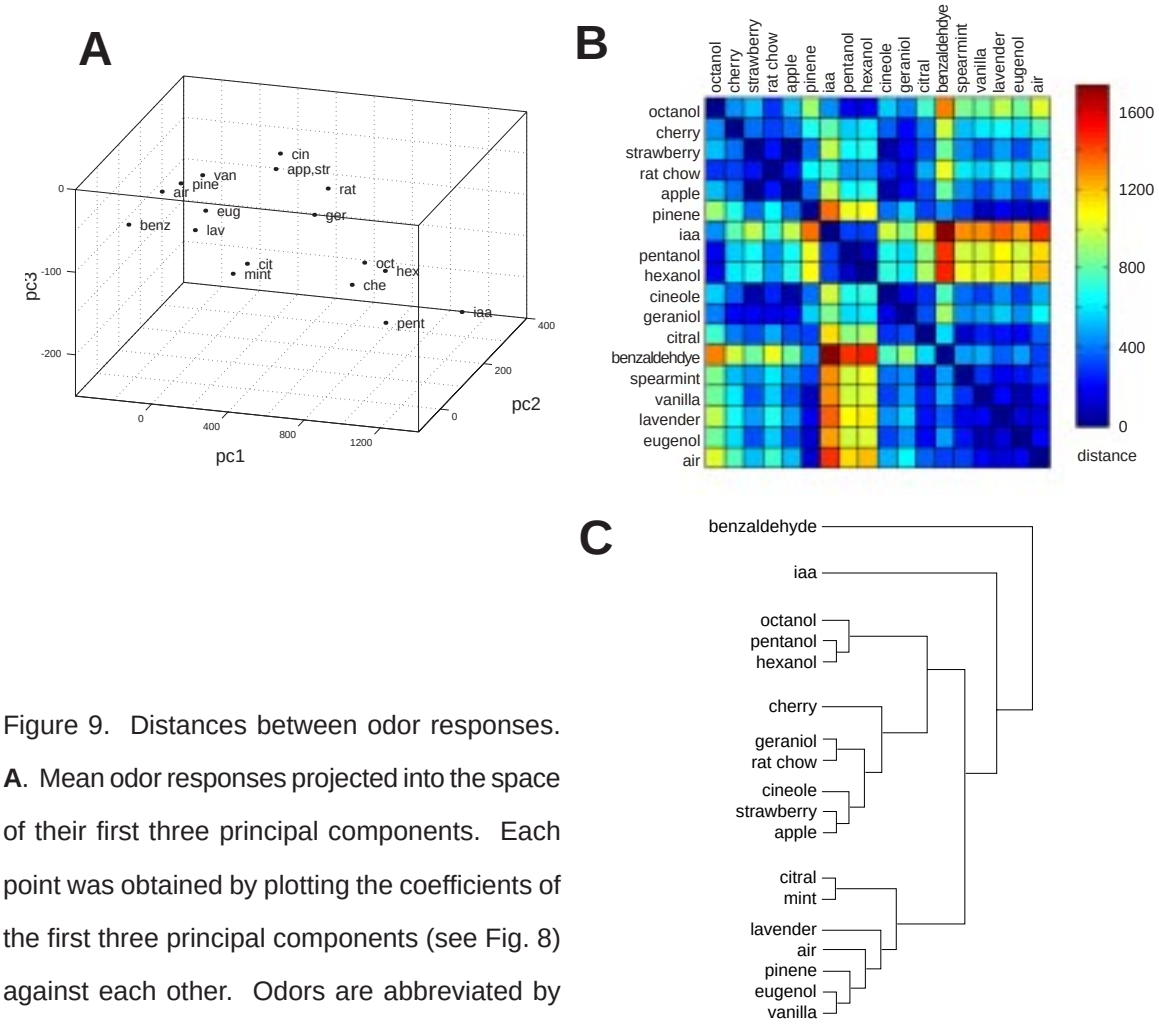

Figure 9. Distances between odor responses. **A**. Mean odor responses projected into the space of their first three principal components. Each point was obtained by plotting the coefficients of the first three principal components (see Fig. 8) against each other. Odors are abbreviated by their first 3-4 letters. Odor responses appear to be grouped into 3-4 clusters. Points for apple and strawberry are plotted over each other. **B**. Euclidean distance calculated between mean odor responses. Distances are plotted here using a cool-to-warm color scale. Odor responses were represented by their coefficients for the first 10 principal components. Odor pairs which evoked similar reponses (and thereby had small distances) are colored blue, while those which evoked very different responses (and thus large distances) are colored red. **C**. Odor response neighborhood tree calculated from the distances shown in B. Each branch represents a rank increase in distance. As in A, 3-4 clusters are evident.

sponses to different odors in the space of the first 10 principal components. Distance is represented as a cool-to-warm color scale, such that odor pairs which evoke similar responses (and thereby have small distances) are colored blue, while those which evoke very different responses (and thus large distances) are colored red. Because distance is commutative (i.e., distance from *a* to *b* equals distance from *b* to *a*), the comparison matrix is diagonally symmetric. Blue regions around the diagonal (e.g., upper left and lower right corners) indicate clusters of odors which evoked similar responses; red/yellow regions off the diagonals correspond to groups of odors which evoked distinct responses in this neuron. A distance histogram calculated from the values shown in Fig. 9B contained 3 or 4 peaks, depending on bin width (not shown). Figure 9C shows a dendrogram or neighborhood tree representation of rank distances between mean odor responses. The distances between odor responses shown in Fig. 9B were ranked, and successively connected by branches from closest to furthest. In agreement with the cluster plot in Fig. 9A (which used only principal components 1-3), the odor responses appeared to be grouped into 3 or 4 clusters.

Effect of pulse duration

To what extent are the odor-evoked slow temporal patterns in PNs dependent on the duration of the odor pulse? Do the different features or epochs of these responses depend uniformly on pulse duration, or does this dependence vary for different features? To address these questions, pulses ranging in duration from 10 ms to 60 s were delivered to the same PN as shown in Figures 3-9. The responses to cherry are shown in Figure 10. An initial oscillatory compound EPSP followed by inhibition was reliably evoked in this cell for pulse durations of 25 ms or greater, with longer pulses eliciting a rhythmic burst of action potentials riding on the excitation. The membrane potential oscillations during the initial excitation can be clearly

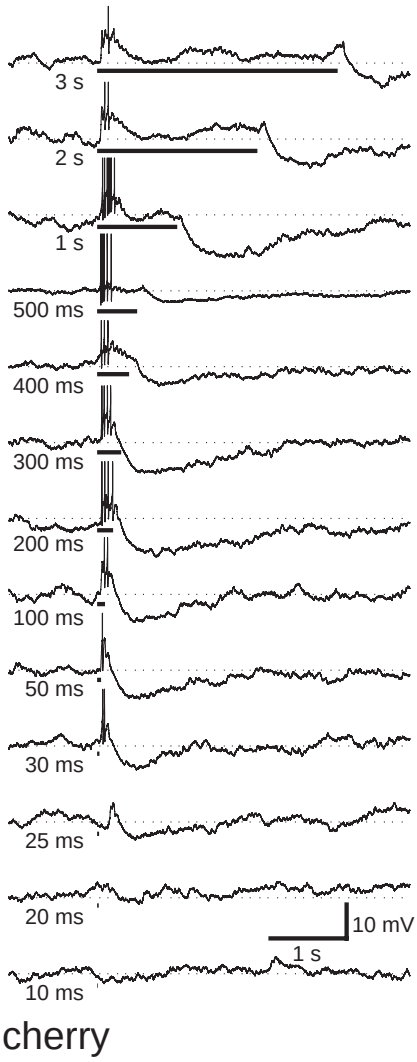

Figure 10. Effect of odor pulse duration. Pulses of artificial cherry flavor, ranging from 10 ms to 3 s in duration, were presented to the same PN as shown in Figs. 3-9. The different features of the slow temporal response pattern were differentially dependent on odor pulse duration. A 10 ms pulse evoked no response in this PN (this may exceed the speed of the solenoid valves in the odor delivery system). As duration increased, initial excitation was evoked (sub-threshold at first), followed by inhibition, and only at durations of 400 ms or greater was the plateau phase evident. The duration of the excitatory and inhibitory epochs appeared independent of pulse duration, unlike the duration of the plateau phase.

seen, for example, in the response to a 400 ms pulse in Fig. 10. Shorter pulses (i.e., 10 or 20 ms) could evoke small compound EPSPs, but these were not seen consistently across trials. These very fast pulse commands may have exceeded the speed of the solenoid valves in the odor delivery system. As the duration was increased beyond 400-500 ms, an additional plateau epoch emerged in the temporal response pattern. While the durations of the initial excitatory burst and the final deep inhibition remained invariant over a wide range of pulse durations, the plateau phase increased proportionally to the pulse duration, so that the deep inhibi-

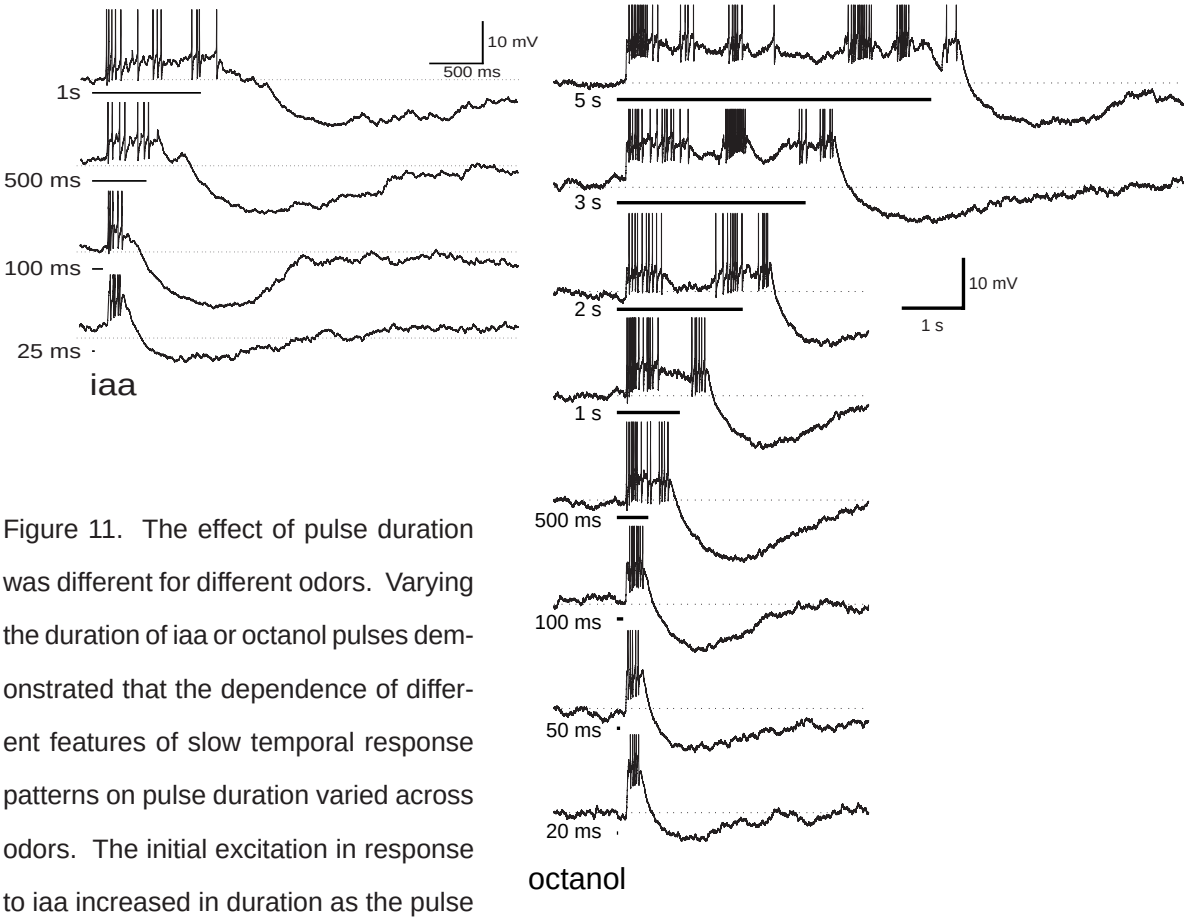

Figure 11. The effect of pulse duration was different for different odors. Varying the duration of iaa or octanol pulses demonstrated that the dependence of different features of slow temporal response patterns on pulse duration varied across odors. The initial excitation in response to iaa increased in duration as the pulse was lengthened, unlike the initial excitation in response to cherry (Fig. 9). For octanol, prolonging the pulse increased the duration of a complex response period, which contained mixed epochs of excitation and inhibition. The pattern of epochs within this period differed across pulse durations.

---

tion always followed the termination of the odor pulse. Thus these different features of the slow temporal responses depend in different ways on the duration of the odor pulse. Similarly, the response to iaa contained a (potentially) sustained excitatory epoch with increased duration as the odor pulse was lengthened, and a final inhibitory epoch of constant duration (Fig. 11). Octanol evoked a response with a similar initial excitatory burst and terminal inhibition, but the intervening period was composed of a complex succession of excitatory and inhibitory epochs.

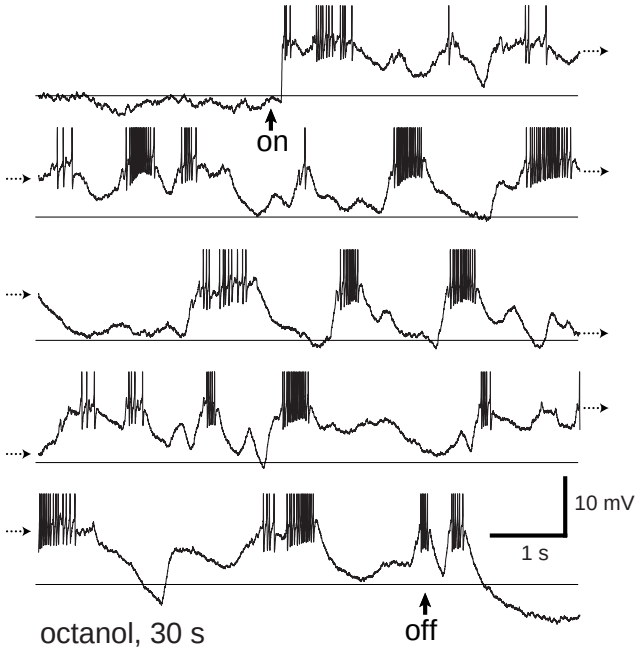

Figure 12. Indefinite temporal patterns in response to octanol. The complex mixed response was sustained for the duration of a 30 s octanol delivery. This is a continuous record; each trace is continued on the trace underneath it (dotted arrows). Resting membrane potential is indicated by the solid horizontal line. The succession of "bursts," plateaus, and inhibitory epochs continued for as long as the odor was delivered.

The order and durations of the epochs in this complex response period varied across pulse durations, and showed no discernible regularity. Indeed, the irregular succession of excitatory bursts, plateau phases, and inhibitory epochs were sustained for odor pulses of 30 s (as shown in Fig. 12) or even 60 s (not shown). Figure 12 shows a continuous record of this neuron's response to a 30 s presentation of octanol. It is not clear if the sustained complex temporal patterning in this response was generated intrinsically by the olfactory system; it could be due in part to fluctuations in the stimulus delivery caused by microturbulence at the antenna. Such long lasting responses were not observed with other odor stimuli. Octanol is a known gap junction uncoupling agent, thought to act nonspecifically by virtue of its lipophilic nature (Johnston et al., 1980). The significance of this fact for the stationarity of octanol-evoked responses in PNs has yet to be tested.

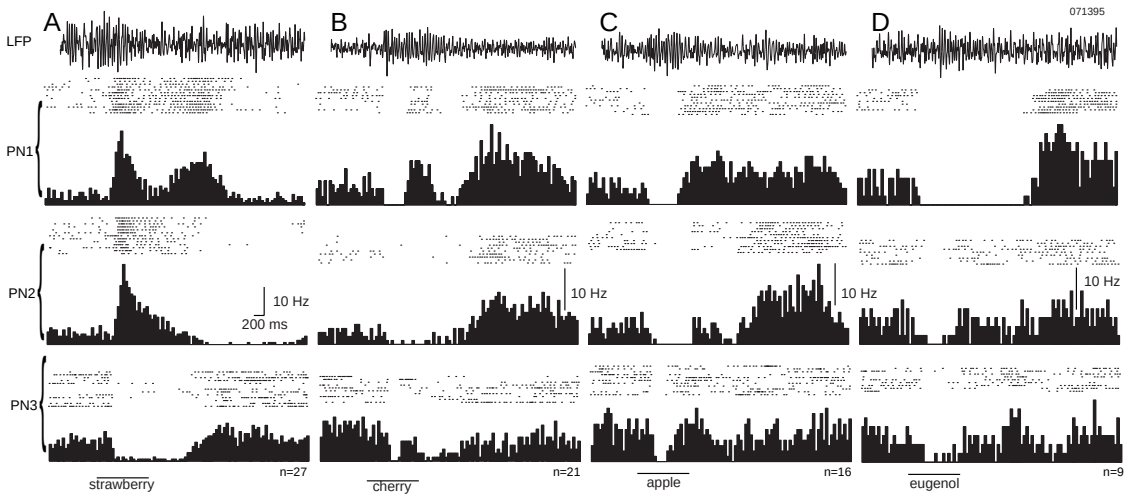

Figure 13. Simultaneous recordings of activity from 3 projection neurons and the ipsilateral mushroom body, showing directly the complex and odor-dependent temporal activity patterns. Top trace is the local field potential (LFP). For each PN (1-3), dot rasters are plotted above, and underneath is the PSTH created for each PN from n presentations of the same odor (n given on right-hand side of each bottom trace). Odor pulse (1 s) indicated by the horizontal bars at the bottom. A-D: Data recorded and analyzed in the same conditions and from the same 3 PNs in response to 4 different odors (of 11 sampled alone and 3 binary combinations). Note the differing temporal response patterns of the 3 neurons for each odor, and of each neuron for the 4 odors. Note also the long period of co-activity of PNs 1 and 2 (1.5 sec) in response to strawberry (A).

Transient odor-specific synchronization between projection neurons

Knowing that individual neurons show odor-specific firing patterns, we next examined the fine structure and timing of the action potentials evoked during each period of activity. We recorded the extracellular activity of up to 5 antennal projection neurons simultaneously, as well as the field potential in the mushroom body, and presented up to 11 odors to the animal. An example of the response patterns evoked in 3 projection neurons by 4 different odors is shown in Fig. 13. When an

odor is presented, the field potential (LFP, top trace) shows 20 Hz oscillations (indicating synchronization of a population of neurons, Laurent and Davidowitz, 1994) and the PNs display a pattern of action potentials, whose structure obeys the macroscopic features described above. The post-stimulus-time histograms reveal that each odor evoked different response patterns in the 3 neurons, as shown above for other neurons. Strawberry, for example, evoked an initial increase in the firing rate of PNs 1 and 2, and a decrease in that of PN3, while eugenol initially inhibited all three neurons. Note that, during the period of the odor response when no neuron fires (e.g., to eugenol), the LFP nevertheless displays oscillations, indicating the existence of other neurons (not recorded) that fired synchronously at that time.

We used the field potential recorded in the mushroom body as a time reference and studied the phase structure of each odor-evoked spike train, i.e., the variations in phase of each action potential (relative to the field potential) over the duration of the response. We then considered all the spikes present in each odor response and calculated their phase relative to their corresponding field potential oscillation cycle. Because the field potential is not a perfect sine wave, we calculated the phase relative to the entire period, or to the 1/2 period or 1/4 period and extrapolated linearly (see Methods). The different methods yielded essentially the same results and the phases plotted here are calculated relative to the corresponding 1/4 cycle of the oscillation.

Each action potential was thus represented by its phase (0 was arbitrarily defined as the peak of the LFP oscillation), and its time of occurrence, in phase vs. time raster plots (Fig. 14). Each trial was separated from the next by 10 s. All action potentials were used to generate a phase frequency histogram (at left, along each phase axis, Fig. 14) and a time histogram (at bottom, along the time axis).

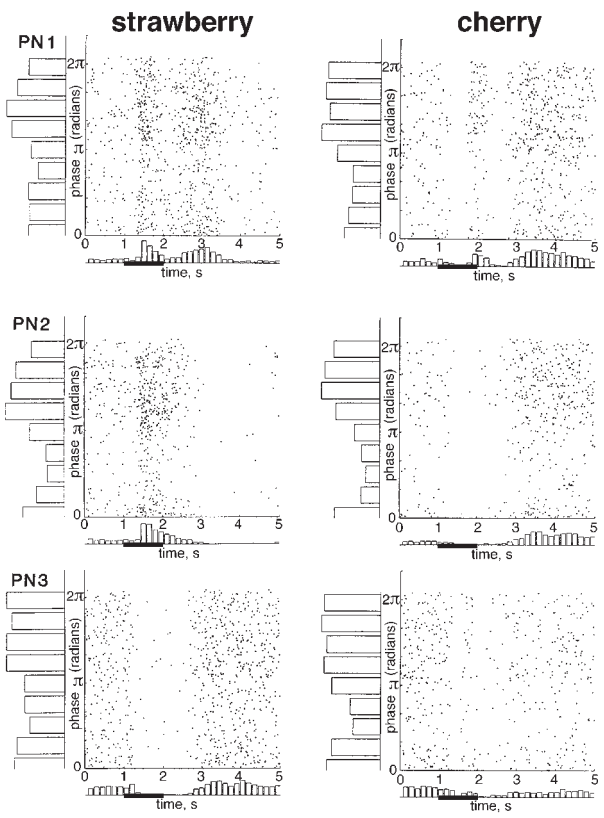

Figure 14. Phase vs. time plots representing the odor-evoked activity in 3 simultaneously recorded projection neurons (PN1-3), in response to two different odors. These plots show a phase representation, with respect to the simultaneously recorded local field potential (LFP) in the ipsilateral mushroom body, of two of the same odor responses from the same PNs shown in Figure 13. The phase of all the action potentials (relative to their respective LFP oscillation cycle) was measured (see methods) and plotted as a function of time. The positive peak of the oscillation was defined as 0. Each action potential is represented as a dot, with its time of occurrence during the trial represented on the x-axis (in s), and its phase represented on the y-axis (in radians, from 0 to 2π). All spikes are summed to form a peri-stimulus time histogram (PSTH) underneath the time axis (horizontal, cf. Fig. 13), and are also summed to form a phase histogram to the left of the phase axis (vertical). The phase-locking behavior of each PN can thus be followed as the population response unfolds throughout each trial. The peaked structure of the phase histograms indicates periodic firing of these PNs on average, with a single preferred phase of $3\pi/2$. This preferred phase is the same across PNs and odors. Thus when PNs phase-lock to the field potential, they do so at the same average phase. The preferred phase of firing can also be seen from the increased density of the dot rasters in the upper half of the plot. The increased density of the dot rasters also forms "columns," which reflect the slow temporal patterns of firing which can be seen clearly in the PSTHs. Thus any pair of PNs will phase-lock and oscillate at different times and for different durations over the ensemble response. The temporal structure of phase-locking of individual neurons is stable over repeated presentations of the odor. Therefore, not only do projection neurons display reliable temporal firing patterns in response to odors, but the periods of time during which they phase-lock with other projection neurons (or the field potential) are stable (for a given odor at a given concentration).

The time histograms (PSTHs) are identical to those in Fig. 13. The peaked structure of the phase histograms indicates that, on average, spikes from these neurons evoked by these odors were phase-locked to the field potential, with a single preferred phase of $3\pi/2$. This preferred phase can also be seen from the increased densities of the dot rasters in the upper half of the plots. “Clouds” of increased dot density are formed by the preferred phase (horizontally) and the temporal firing patterns (vertically) which can be seen in the respective histograms. Using this representation, we could study not only the times during which a given neuron was active in response to an odor, but those during which it was active and synchronized to the oscillating population (and thus to other neurons).

Spiking activity during the odor response did not necessarily imply synchronization. PN1 for example showed increased synchronization to the field during its first “burst” in response to strawberry (as can be seen by the clustering of the dot rasters during this epoch, at ~1.5 s), and less tightly synchronized during the second burst, although it continued firing (~3 s). Similarly, PN2 showed synchronization to the field potential during its excitatory epoch for this odor, while PN3 was relatively desynchronized during its epoch of delayed firing.

From these observations it follows that cross-correlation of any two spike trains should only reveal significant periodic synchronization during very specific epochs of the population response. One can see for example that a cross-correlation between PNs 1-2 should yield a significant periodic function if calculated at ~1.5 s, but that none would if it were calculated elsewhere, e.g., ~2 s after stimulus onset. The representation used here, however, does not indicate whether any pair of neurons actually oscillated in synchrony during any part of the responses evoked by each odor. We therefore demonstrated this prediction directly by using a sliding-window

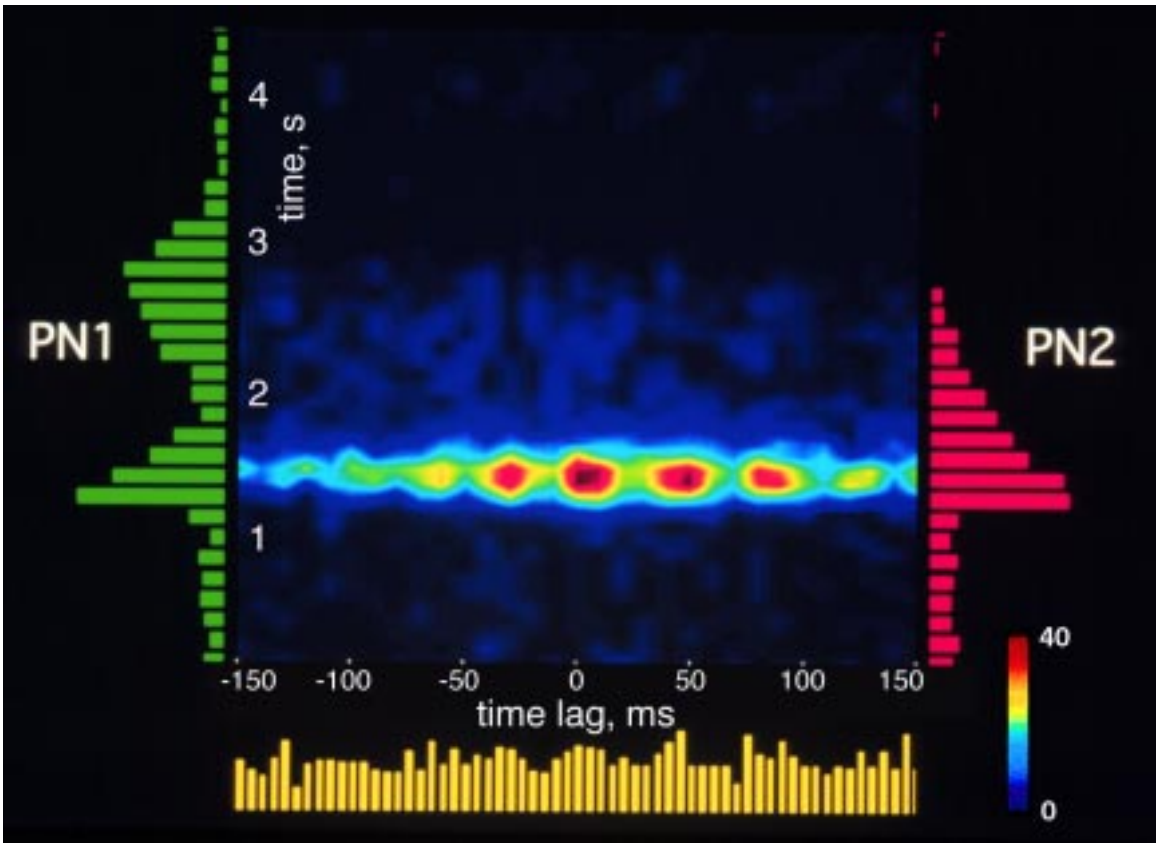

Figure 15. Synchronized oscillations in pairs of projection neurons are restricted to small temporal windows during the ensemble response. The cross-correlation was calculated, using a sliding window method (see Methods), between the spike trains of PN 1 and PN 2 in response to strawberry (same odor responses from two of the same PNs as shown in Figure 13). This cross-correlation is thus based on action potential data only, and not on intracellularly recorded subthreshold activity, as was shown in Laurent and Davidowitz (1994). It is thus based here on the true axonal output of the projection neurons during an odor response, but it is calculated using the data accumulated over 27 successive presentations (whereas cross-correlations calculated with intracellular data in Laurent and Davidowitz, 1994, were based on single odor presentations). Time lag of the cross-correlation function is along x-axis, and time along y-axis. The amplitude of the cross-correlation, which here represents the number of times spikes from each of the 2 PNs coincided in the same 10ms-wide bin, is color-coded such that a red area indicates that 40 spike pairs (accumulated from the 27 odor presentations) were found to coincide in this time bin, whereas dark blue indicates 0 coincidences. Post-stimulus time histograms for each PN in response to this odor (cf. Fig. 13) are plotted vertically, along the time axis, aligned to the sliding-window cross correlation. Odor delivered between 1 and

(continued on next page)

cross correlation technique. The cross-correlation functions so calculated for the responses evoked by strawberry are seen in Figure 15 (see Methods for details on sliding cross-correlation technique). In these diagrams the time lag of the cross-correlation function is on the x-axis and time is on the y-axis. The odor was presented between 1 and 2 s. Figure 15 reveals that PNs 1 and 2 briefly synchronized and oscillated together for ca. 250 ms about halfway through the odor pulse. This period of synchronization was considerably briefer than the period of co-activity revealed by the peri-stimulus time histograms (>1 s), which are plotted vertically along the time axis for reference. Two neurons are therefore not necessarily synchronized when they both fire in response to an odor. The conventional cross-correlation was also computed between the entire spike trains of PNs 1 and 2 (i.e., without sliding windows), and the cross-correlation histogram is plotted horizontally in yellow, underneath the time lag axis, aligned to the sliding-window cross correlation. The transient oscillatory synchronization seen so clearly in the sliding-window cross correlation is obscured in the conventional cross-correlation histogram, because unsynchronized spikes fired by these neurons outside of the transient epoch

---

Figure 15 (cont.):

2 sec. Note that odor presentation led to a short but clear period of synchronized oscillations in PNs 1 and 2, but that this period was shorter than the time during which both neurons were active (as seen from the PSTHs). Two neurons are therefore not necessarily synchronized when they both fire in response to an odor. The conventional cross-correlation was also computed between the entire spike trains of PNs 1 and 2 (i.e., without sliding windows), and the cross-correlation histogram is plotted horizontally in yellow, underneath the time lag axis, aligned to the sliding-window cross correlation. The transient oscillatory synchronization seen so clearly in the sliding-window cross correlation is obscured in the conventional cross-correlation histogram, because unsynchronized spikes fired by these neurons outside of the transient epoch of synchronization are included.

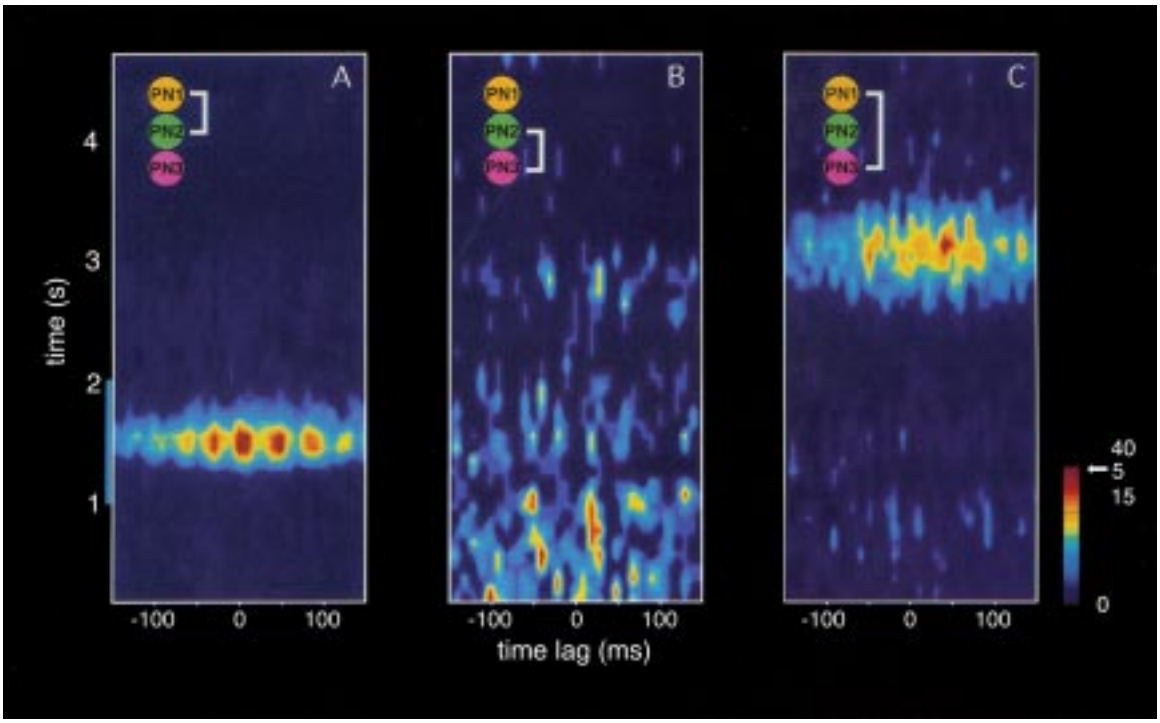

Figure 16. Transient ocillatory synchronization in pairs of projection neurons is pair- and odor-specific. Each panel (A-C) plots the sliding window cross-correlation calculated pairwise (PN 1x2 in A; 2x3 in B; 1x3 in C) as in Fig. 15. Panel A replots the same sliding window cross-correlation as in Fig. 15. Odor delivery (strawberry) between 1 and 2 s (light blue bar). The amplitude of the cross-correlation is color-coded following the scale given at bottom right. A red area means that 40, 5, 15 spike pairs (accumulated from the 27 odor presentations) were found to coincide in this time bin in A, B and C respectively. Note that while strawberry led to a short but clear period of synchronized oscillations in PNs 1 and 2, this odor led to no visible synchronized activity in neurons 2 and 3 (B). PNs 1 and 3 are co-active (though less tightly synchronized than neurons 1 and 2, A), 2 seconds after the odor pulse onset (C). A neuron can therefore synchronize with several others, but at different times during an odor response.

---

of synchronization are included.

In contrast to projection neurons 1 and 2, cross-correlation between spikes of PNs 2 and 3 revealed no odor-evoked synchronization, while cross-correlation between neurons 1 and 3 revealed partial synchronization and coupled periodic firing

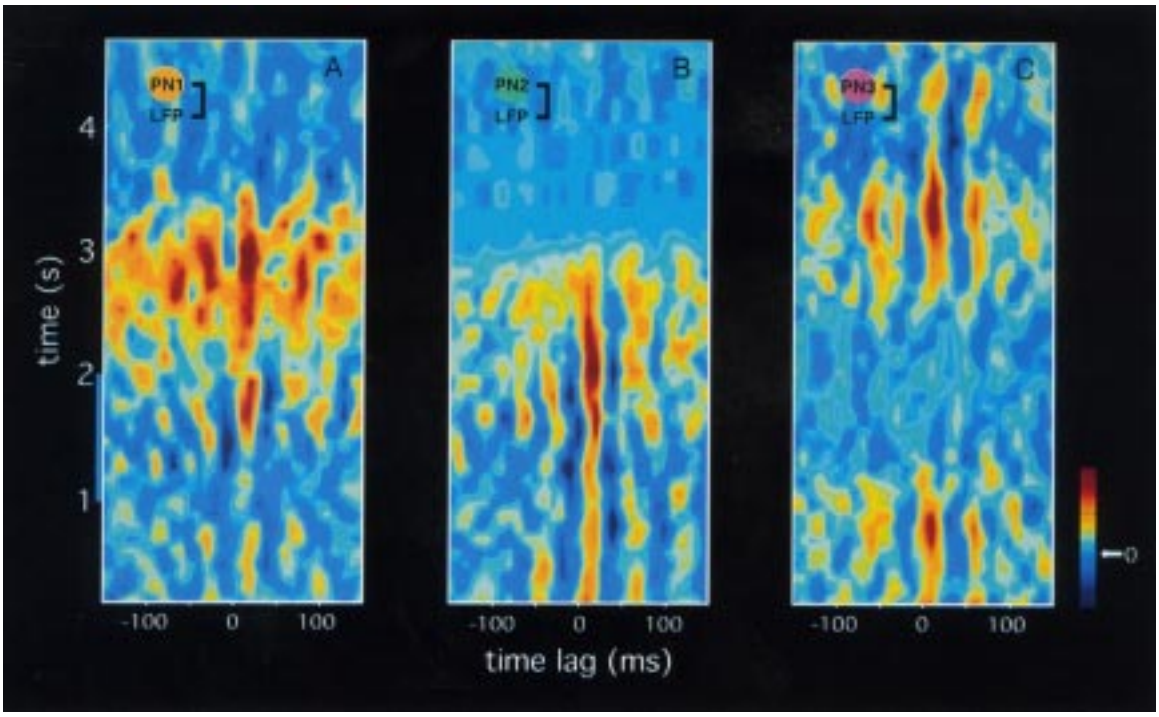

Figure 17. The timing of the synchronization between individual projection neurons and the field potential oscillations is neuron- and odor-specific. Cross-correlations calculated between the field potential and each of the 3 projection neurons recorded in Figure 13, for responses to strawberry odor (see Methods for details on color scales). Each panel is an average calculated over 27 presentations of the odor. The cross-correlation patterns displayed here are therefore consistent over repeated presentations of the same stimulus. Note that the time periods at which each of the 3 neurons synchronizes with the LFP differ and sometimes partially overlap (PN1-PN2: A,B; PN1-PN3: A,C), indicating that these neuron pairs probably synchronize during these periods (cf. Figure 16).

about 2 s after the onset of the odor pulse (Fig. 16). None of the 11 other odors tested with this animal and these neurons produced any significant oscillatory synchronization between any of the 3 pairs of neurons (PNs 1-2, 2-3, 1-3). This result directly demonstrates that an individual neuron can synchronize with different neurons at different times during an odor-evoked response, and that each temporal pattern of oscillatory synchronization is odor-specific. We then calculated the cross-correlation of the spike trains of each PN with the simultaneously recorded mush-

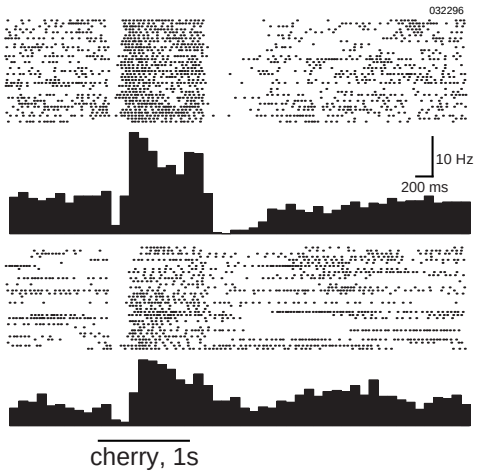

Figure 18. Simultaneous recordings of activity from two projection neurons, showing complex temporal activity patterns in response to cherry odor. For each PN, dot rasters are plotted above, with the PSTH below (as in Figs. 1,6,12). Odor pulse (1 s) indicated horizontal bar. Note the long period of co-activity during the odor response.

room body LFP. Figure 17 shows that each of the three simultaneously recorded neurons phase-locked to the oscillatory field potential at different times around the odor pulse (vertical stripes in cross-correlation displays). This confirms the observation that individual projection neurons necessarily synchronize to others only for limited durations during their responses to odors.

A further example of this transient oscillatory synchronization is shown in Figs. 18-19. The spike trains and histograms shown in Fig. 18 reveal distinct slow temporal patterns in two simultaneously recorded PNs in response to cherry odor. Despite the sustained period of co-activity (>1 s), the sliding-window cross correlation (Fig. 19 A) reveals that these neurons were strongly synchronized for only ~200 ms. The auto-correlations of each PN (i.e., cross-correlation with itself) are shown in Fig. 19 B-C. The presence of side band structure at $\pm$ 50 ms time lags in Fig. 19 B indicates that PN 1 fired rhythmically for the full duration of its odor response, although this rhythmicity is stronger during the initial burst. PN 2, however, fired rhythmically only during the initial ~200 ms epoch of its response (Fig. 19 C). Although it continued to fire for >1 s (as can be seen from the prolonged central band in Fig. 19 C or equivalently from Fig. 18), this latter firing was not periodic. Thus,

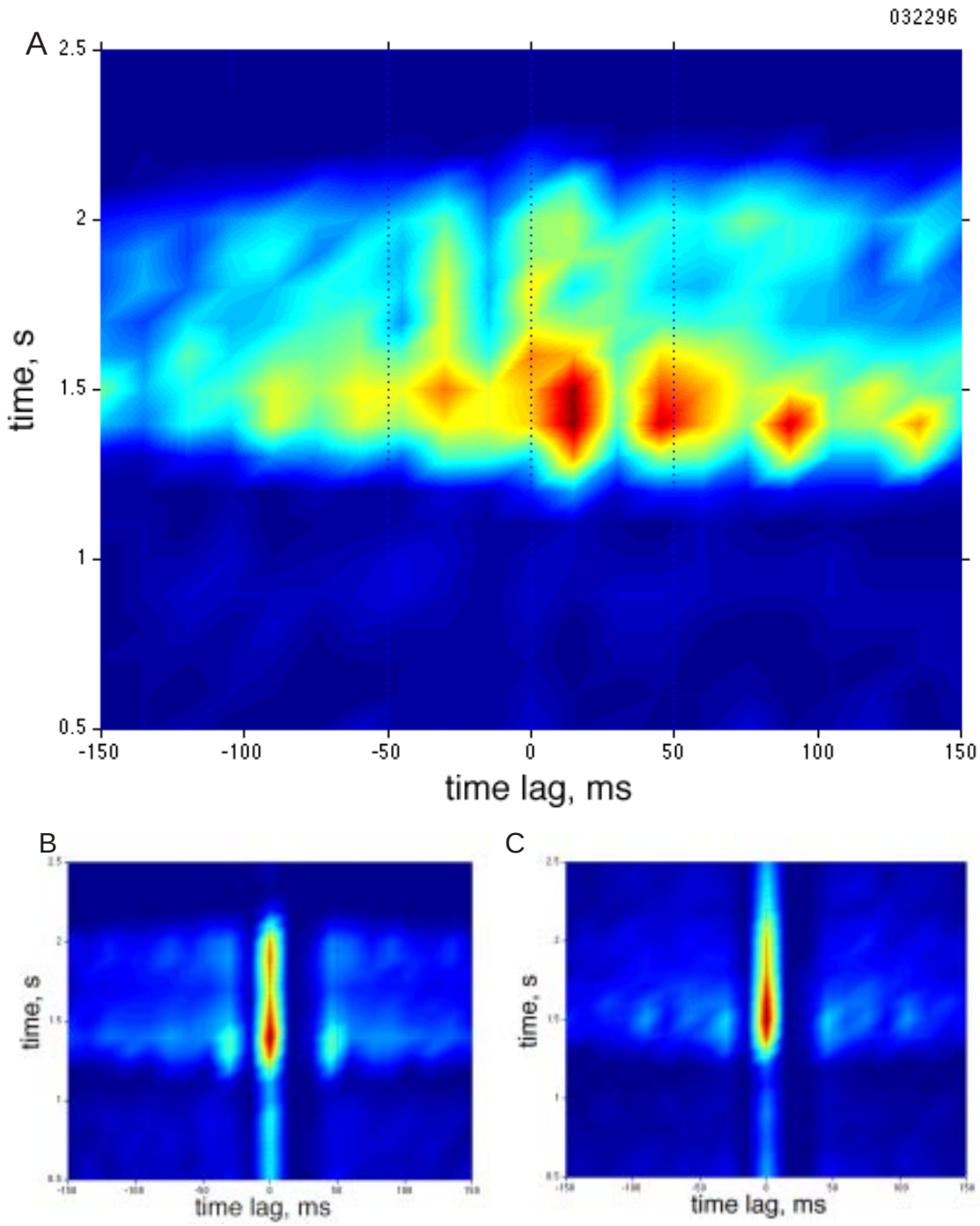

Figure 19. Sliding-window cross-correlations of the responses of the two PNs shown in Fig. 18 to cherry odor. A: Cross-correlation of PNs 1-2. Note the transient oscillatory synchronization around 1.5 s, corresponding to the intitial excitatory odor response in Fig. 18. During the second excitatory "burst" around 2 s these neurons were also synchronized, but much more weakly so despite the nearly similar firing rate. Thus degree of synchronization is independent of firing rates of co-active

(continued on next page)

while PNs 1-2 were tightly synchronized for the initial ~200 ms epoch, they were not later in the trial. Because PN 1 continued to fire rhythmically, it could potentially have been synchronized during that time with some other PN(s) which were not recorded.

Discussion

We demonstrated that odors evoke odor-specific temporal response patterns in projection neurons in the antennal lobe of the locust, the functional analog of the olfactory bulb of the vertebrate olfactory system. Different neurons responded with different temporal patterns to the same odor, and individual neurons responded with different temporal patterns to different odors. Distinct aspects of these temporal patterns (i.e., membrane potential fluctuations or firing patterns) are emphasized in different representations of neural responses. Complex slow temporal patterns can be quantitatively compared across odors in a given neuron, for example with principal components analysis. This and related analytical techniques will likely provide useful tools for comparing slow temporal response patterns across odors and neurons. (We do not consider in this paper the influence of the concentration of a single odor on the temporal patterns evoked in a single neuron.) In

---

Figure 19 (cont.):
neurons. B,C: Sliding window auto-correlations of PNs 1 and 2, respectively. The auto-correlation is the sliding window cross-correlation of a neuron with itself, and is therefore symmetrical about time lag 0. Both neurons showed periodicity in their spike trains around 1.5 s, corresponding to their epoch of transient oscillatory synchronization seen in A. PN 1, but not PN2, also showed rhythmic firing during the second burst at 2 s. Thus, whereas PNs 1 and 2 were only weakly synchronized during the second burst, PN 1 could potentially be strongly synchronized with another (unrecorded) neuron.

addition, the participation of individual neurons in a synchronized oscillatory ensemble was usually transitory, but occurred during one or several precise epochs of an odor response. Repeated presentations of the same odor in the same conditions seconds or minutes later led to the same temporal patterns, and each neuron oscillated in phase with the local field potential in the mushroom body during the same epoch of each response. The existence of action potentials in these epochs of synchronization, however, remained probabilistic: in other words, the knowledge of the exact sequence of spikes produced by a neuron in one trial did not allow one to predict the sequence of spikes in the same neuron on the next trial. Finally, our data are not consistent with a phase-encoding of sensory stimuli, i.e., a representation in which the delays between the spikes of two neurons, or the phase delays between individual neurons and an average potential (such as the field potential oscillation), vary in a stimulus-specific manner, as suggested in theoretical models of sensory processing (von der Malsburg and Schneider, 1986; Hopfield, 1995). In other words, a neuron was either phase-locked to the field potential during an epoch or it was not. If it was phase-locked, it always fired around a particular mean phase which was constant across neurons and stimuli (Laurent and Davidowitz, 1994). Repeatable and stimulus-specific phase sequences such as those observed in hippocampal place units of rats (O'Keefe and Recce, 1993) were not seen.

Our results are summarized in Figure 20. Here, the projection neurons are symbolized by an array of 4x4 units, which can be in 3 'states': silent (which can mean depolarized, but below threshold) or inhibited (dark), spiking but not phase-locked to the field potential (gray), or spiking and locked to the field potential (green). Before an odor is presented, a few neurons fire randomly and independently, and the field potential in the mushroom body shows no oscillations (Laurent and Naraghi,

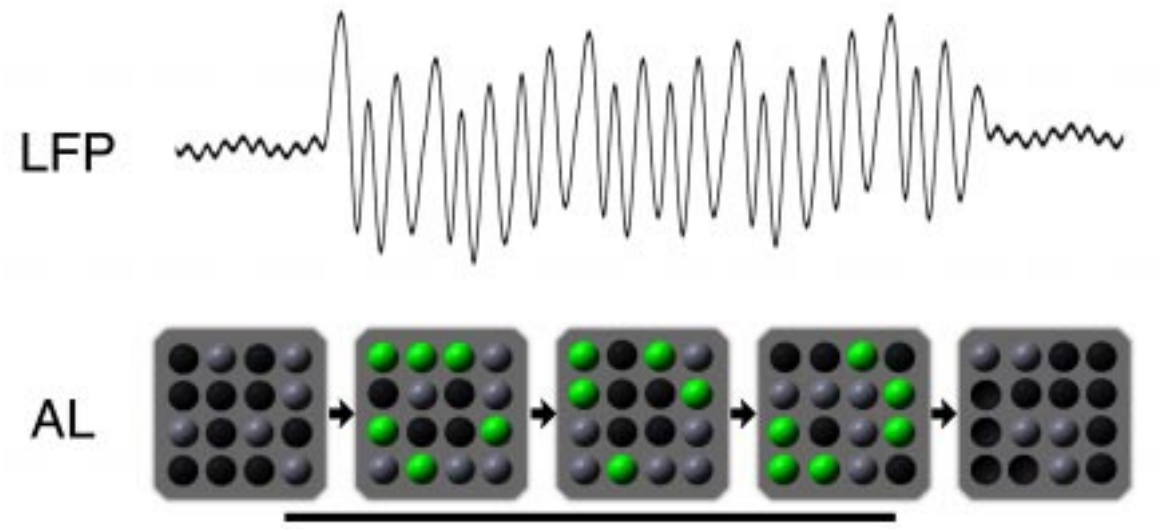

Figure 20. Schematic representation of our hypothesis of odor coding in this olfactory system. AL: antennal lobe; LFP: local field potential. Color code: Each small sphere symbolizes a projection neuron that can be in 1 of 3 states: silent or inhibited (black), active (spiking) but not synchronized with the LFP (gray), active and phase-locked with the LFP (green). The five successive squares represent the successive states of the system around and during an odor pulse (pulse indicated horizontal bar). The LFP oscillations in the mushroom body are therefore caused by successive and odor-specific ensembles of synchronized neurons. See discussion for details.

1994; Laurent and Davidowitz, 1994). At the onset of an odor pulse (indicated by the horizontal bar), a group of neurons is activated (green and gray), only some of which oscillate at 20 Hz and phase-lock to one another, thus giving rise to the field potential oscillation that can be recorded in their target area, the mushroom body. Several 100 ms later (arbitrary time step), however, the ensemble of active neurons differs from what it was earlier. Some neurons that were initially inactive become active, while some that were oscillating desynchronize and yet others only now phase-lock to the oscillating ensemble. The field potential recorded from the mushroom body, although indistinguishable from what it was earlier in its frequency characteristics, is therefore now caused by a new ensemble of synchronized neu-

rons, which overlaps with the starting ensemble. This progressive transformation of the oscillating ensemble occurs in an odor-specific manner, and the number of neurons participating in the oscillation and/or the tightness of their phase-locking can vary over the duration of the population response. This leads to variations in the envelope of the field potential, as observed experimentally (Laurent and Naraghi, 1994). When the odor stimulus ends, the ensemble progressively breaks up and the field potential oscillations disappear. We conclude that odor stimuli are represented in the antennal lobes as dynamical ensembles of synchronized and oscillating neurons. These ensembles often comprise about 10-20% of the total complement of neurons (Laurent and Davidowitz, 1994), although their size probably varies with odor concentration, as suggested in other animals by imaging experiments (Cinelli et al., 1995). We therefore propose that the macroscopic 20 Hz oscillations are caused by a stimulus-specific message that is distributed in space (the odor-specific sets of synchronized neurons) and in time (the time at which these neurons synchronize and desynchronize, in an odor-specific fashion).

Practical consequences for the analysis of distributed neuronal representations

The existence of oscillations in a local field potential is usually interpreted as implying correlated and phase-locked firing of ensembles of neurons (generally those which terminate and synapse into the area from which the field potential is recorded) (Singer and Gray, 1995). Nothing requires, however, that the oscillating neurons be synchronized over the entire duration of the field potential oscillations (i.e., the population activity). The methods usually employed to study inter-neuronal synchronization, however, often implicitly assume that this is the case. For example, cross-correlation analysis, which is the method of choice to assess whether two neurons are phase-locked and oscillating, is often carried out and averaged

over relatively long stretches of data. Hence, the existence of transient but reliable synchronization between two neurons could become masked in the time-averaged cross-correlation function (as demonstrated in Fig. 14). Our present results show that two neurons in an oscillating ensemble sometimes phase-lock only for a very brief period (e.g., only a few oscillation cycles), requiring the use of fine analysis techniques, such as dynamic cross-correlation (Laurent and Davidowitz, 1994; this paper; Vaadia et al., 1995). One should therefore be careful when concluding that phase-locking and oscillations do not exist between neurons in a large and distributed ensemble, especially if the stimulus representation (i.e., the response of a neuronal ensemble) is spread over a significant time period, as often happens in sensory systems.

Are such representations likely to be common to other olfactory systems?

The distributed representation described in this insect's olfactory system consists of three concurrent stimulus-evoked phenomena: (1) temporally structured neuronal responses (odor- and neuron-specific temporal patterns); (2) oscillatory mass activity, whose frequency characteristics are not odor-specific; (3) transient and dynamic synchronization of neuronal groups in an odor-specific manner. Are these phenomena observed elsewhere, and if so, are they also concurrent?

Temporally structured neuronal responses. All olfactory bulb responses examined to date provide evidence for odor-evoked temporal patterns consisting at least of sequential excitatory and 'suppressive' phases of neuronal activity. Such patterns have been observed in amphibians (salamander: Kauer, 1974; Kauer and Shepherd, 1977), in bony fish (goldfish: Meredith and Moulton, 1978; Meredith, 1981) and in mammals (rat, rabbit and hamster: Chaput and Holley, 1980; Mair, 1982; Meredith, 1986; 1992). Although suggestions were made that 'suppression'

patterns arise in certain olfactory bulb neurons of the salamander when odor concentrations are too high ('concentration tuning hypothesis'; Kauer, 1974), more recent data from mammals indicate that suppression patterns are not more frequent at higher odor concentration, and that certain neurons even go from an inhibitory to an excitatory response pattern as odor concentration is raised (Meredith, 1986). In insects, our results provide evidence that general odors evoke odor-specific response patterns in the antennal lobe projection neurons. Other investigators showed that pheromones evoke temporally structured responses in the cockroach *Periplaneta* and the moth *Manduca* (Burrows et al., 1982; Kanzaki et al., 1989). It appears, therefore, that such temporal features of responses to odors are common to neurons in the first olfactory relay of many animal phyla and classes.

Oscillatory mass activity. 'Induced waves', or oscillations in the EEG caused by olfactory stimulation have been demonstrated in the olfactory bulb of amphibians (frog: Libet and Gerard, 1939), fish (Salmonidae: Thommesen, 1978; carp: Satou, 1990) and mammals (hedgehog: Adrian, 1942; rat, rabbit, cat: Freeman, 1975; Bressler and Freeman, 1980), including humans (Hughes et al., 1969). More recently, oscillations were also discovered in the olfactory systems of a terrestrial mollusk (*Limax maximus*: Gelperin and Tank, 1990; Delaney et al., 1994; Kleinfeld et al., 1994) and an insect (locust: Laurent and Naraghi, 1994; Laurent and Davidowitz, 1994). These observations have now been repeated in other insect species, such as cockroaches and honeybees (Stopfer et al., 1998) and moths (Heinbockel et al., 1998). In all cases but that of *Limax*, oscillatory activity appears to be triggered (or dramatically enhanced) by odor stimulation. In *Limax*, oscillations are present 'at rest', i.e., even in the absence of odors, but odor stimuli cause a collapse of the phase gradient that exists across the procerebral lobe (Delaney et al., 1994). In all cases, the oscillations appear to be the result of local interactions

between inhibitory local and excitatory projection neurons (within the bulb of vertebrates, the procerebral lobe of *Limax*, or the antennal lobe of insects), and to reflect the coherent activity of large numbers these neurons.

Transient synchronization of overlapping neuronal groups. The existence both of oscillatory mass activity and of temporal activity patterns in individual neurons in the first olfactory relay of amphibians, fish, mammals, mollusks and insects suggests that the distributed activity patterns described here for the locust may exist also in many other animals. Our preparation, however, appears to be the only one so far where all three phenomena have been observed together and seen to 'interlock' in a coherent fashion, showing transient synchronization of neuronal sets and progressive transformation of a coherently active neuronal population. The separate pieces of evidence from vertebrates and mollusks seem to be compatible with our hypothesis of stimulus representation and coding in the olfactory system, but it remains to be seen if they can all be concurrently observed there also. Optical imaging in the salamander (Cinelli et al., 1995), for example, certainly give support to the idea that odor representation in the olfactory bulb is distributed and combinatorial.

Chapter 3: Odor encoding by temporal sequences of firing in oscillating neural assemblies

Abstract

Stimulus-evoked oscillatory synchronization of neuronal activity has been observed in many systems, yet the possible functions of such rhythmic synchronization in neural coding remain largely speculative. In the locust, odors appear to be represented by dynamic ensembles of transiently synchronized neurons. We now report that the components of these ensembles change in a stimulus-specific manner and with a high degree of reliability on a cycle-by-cycle basis during an odor response. Thus, information about an odor is contained in the precise temporal sequence in which these ensembles are updated during an odor response. Neural coding with oscillations thus allows combinatorial representations in time as well as in space.

Although stimulus-evoked oscillations of brain potentials (caused by synchronized neural activity) have now been known for about fifty years (Adrian, 1942; Freeman, 1960; Gray & Singer, 1989; Gelperin & Tank, 1990; Laurent & Naraghi, 1994), the roles, if any, that they might play in information coding remain largely speculative (Milner, 1974; von der Malsburg, 1986; Hopfield, 1995). We tested two possible functional hypotheses of temporal codes that might use oscillations. The first proposes that oscillations, by virtue of their periodic nature, allow the phase of neural signals (i.e., the timing of action potentials relative to a specific or common reference during each cycle) to be a coding parameter. Different (and possibly coexisting) stimuli could thus be represented by different neural assemblies respectively defined by a common phase of activity (Gray & Singer, 1989; von der Mals-

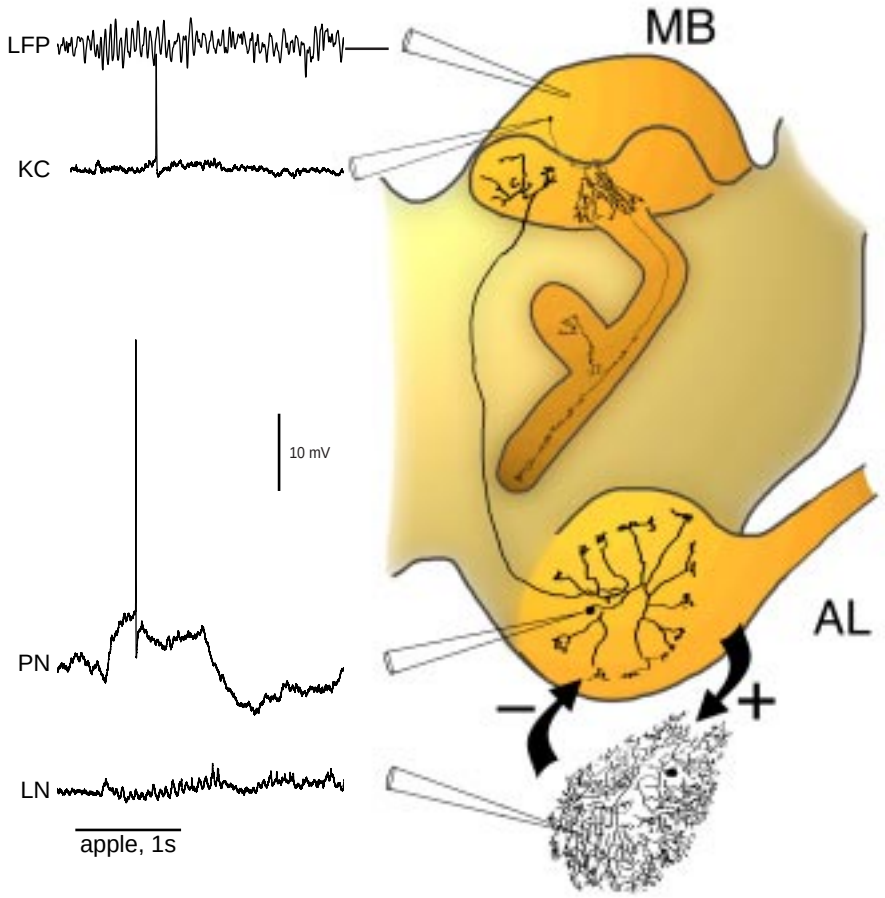

Figure 1. The locust olfactory system. Receptor afferents project from the antenna (not shown) to the antennal lobe (AL). The AL consists of projection neurons (PNs) which are spiking, excitatory cells with discrete glomerular arborization patterns, and local neurons (LNs) which are nonspiking, inhibitory cells with global arborization patterns. Projection neurons project to Kenyon cells (KC) in the mushroom body (MB). All three cell types experience odor-evoked membrane potential oscillations as shown in representative intracellular recordings at left (apple odor delivery indicated by solid bar, 1 s). Oscillatory synchronization of population activity can be seen in the local field potential (LFP) recorded in the mushroom body (here low-pass filtered at 50 Hz). Cobalt fills courtesy of G. Laurent.

---

burg, 1986; Hopfield, 1995). If true, this hypothesis predicts that the neural assemblies activated by different stimuli should synchronize at different phases. The second hypothesis rather proposes that oscillations allow the rank order (e.g., cycles

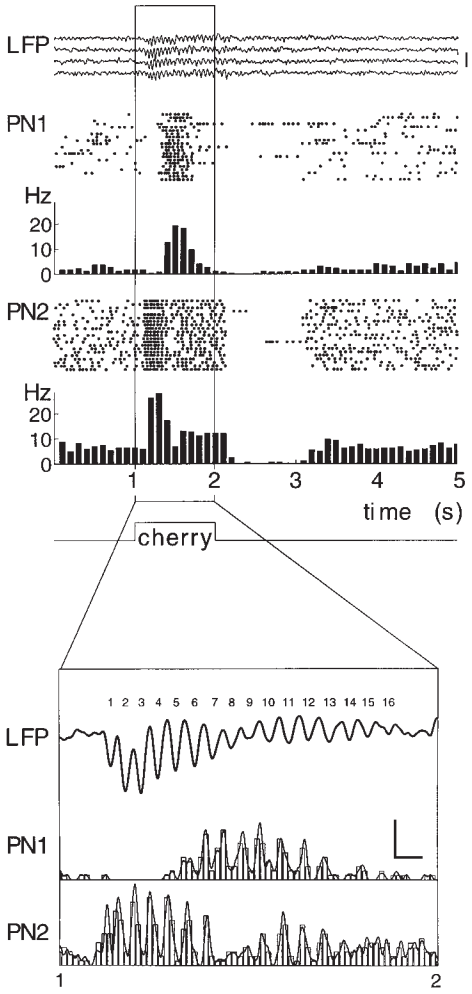

Figure 2. Top: Rasters and peri-stimulus histograms (PSTHs) of the responses of two simultaneously recorded antennal lobe PNs to the odor cherry (21 trials at 0.1 Hz, aligned on the odor delivery pulse). The local field potential (LFP) recorded in the ipsilateral mushroom body during trials 1-4 are shown. Each PN and the LFP were recorded with separate extracellular glass microelectrodes. Calibration (LFP): 500 mV. Bottom: Fine temporal structure of the PNs' responses during the 1-2 s epoch in figure 1. Spikes produced by each PN over the 21 trials were convolved one at a time with a 5 ms-wide Gaussian function (continuous lines), giving a smooth firing probability distribution free of binning artifacts. The LFP trace is the average of the 21 LFP traces, indicating a very tight stimulus-locking with this odor. Calibration: horizontal, 50 ms; vertical, 30 Hz or p=0.03 of firing within a 1 ms bin.

1, 2 and 4 of the oscillation) of action potentials produced by participating neurons to be coding parameters. In this scheme, the order of recruitment of neurons in an oscillating assembly should be stimulus-specific.

To test these hypotheses, we used the olfactory antennal lobe of the locust *Schistocerca americana* (anatomy shown in Fig. 1, reprinted here from Chapter 1 for reference), in which individual odors are represented combinatorially by oscillating and dynamic neural assemblies formed by about 10% of a total of about 830

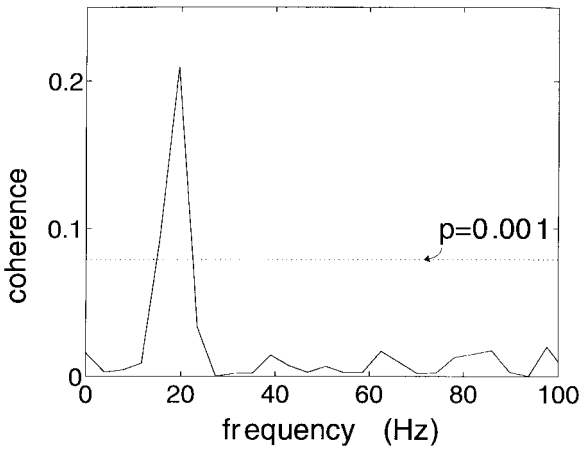

Figure 3. Coherence function (varies between 0 and 1) calculated for the spikes produced by the two PNs over the 1 s epoch in figure 2.

neurons (Laurent & Davidowitz, 1994; Laurent et al., 1996; Wehr & Laurent, 1996). We recorded simultaneously the responses of small ensembles (2-5) of these projection neurons (PNs)— the analogs of the mitral-tufted cells of the vertebrate olfactory bulb— *in vivo*, to airborne odorants. Fig. 2 (top) illustrates the temporally modulated responses of two PNs to a cherry odor. While both neurons responded partly with an increased firing rate to this odor, their peaks of activity did not coincide and the durations of increased firing differed between them. The fine temporal structure of these responses, shown at the bottom of Fig. 2, reveals that the firing probability of each PN varied rhythmically and that the timing of either neuron's activity was locked to the other's and to the field potential oscillation. The coherence (normalized cross power) of firing of these two PNs over the 1 second response period was significantly different from zero ($p<0.001$) at 20Hz, the frequency of the field potential oscillations (Fig 3), indicating tightly coherent firing.

We presented 13 odors and their mixtures and measured the phase of activity of each neuron relative to the field potential (not shown) or to the other neuron (Fig. 4), for all odors with which these neurons phase-locked to the field potential, using

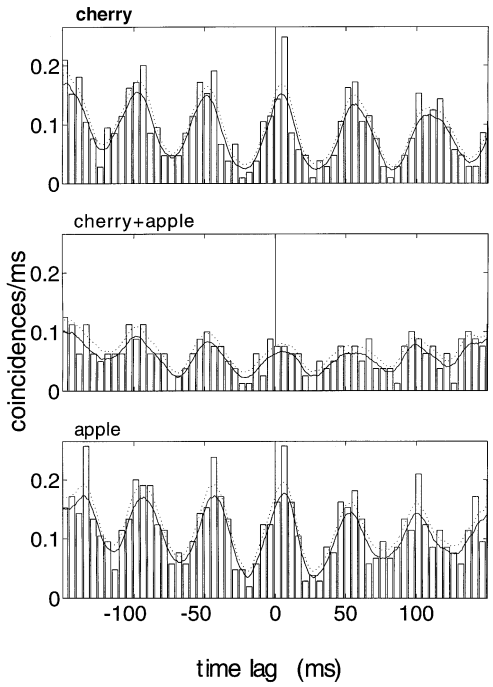

Figure 4. Cross-correlation functions calculated between the spike trains produced by both PNs in figure 1-2 in response to two odors and their 1:1 mixture. Spike coincidences were binned into 5 ms bins or convolved with 5 ms wide gaussian (solid lines). Dotted lines indicated one standard deviation from the mean.

cross-correlation techniques. Fig. 4, for example, indicates that, while these two neurons fired and phase-locked in response to cherry, apple, or a mixture of both, the slight phase difference between their action potentials was constant and thus, not odor specific. This experiment was repeated with 5 pairs of PNs and 17 'neuron pair-odor' combinations for which coherence values were significant at $p<0.01$ or better. In no case did the phase of action potentials relative to the field potential or to action potentials of other participating neurons appear to vary with, and thus participate in encoding, the stimulus.

We next considered the second hypothesis. Fig. 2, for example, indicates that, while both neurons were synchronized in response to cherry, coincident firing of both PNs occurred only during certain cycles of the oscillatory ensemble response (e.g., cycles 6-7, 10-13), and never during other cycles (e.g., 1-4). This information cannot be extracted by cross-correlation analysis (Fig. 4), which aver-

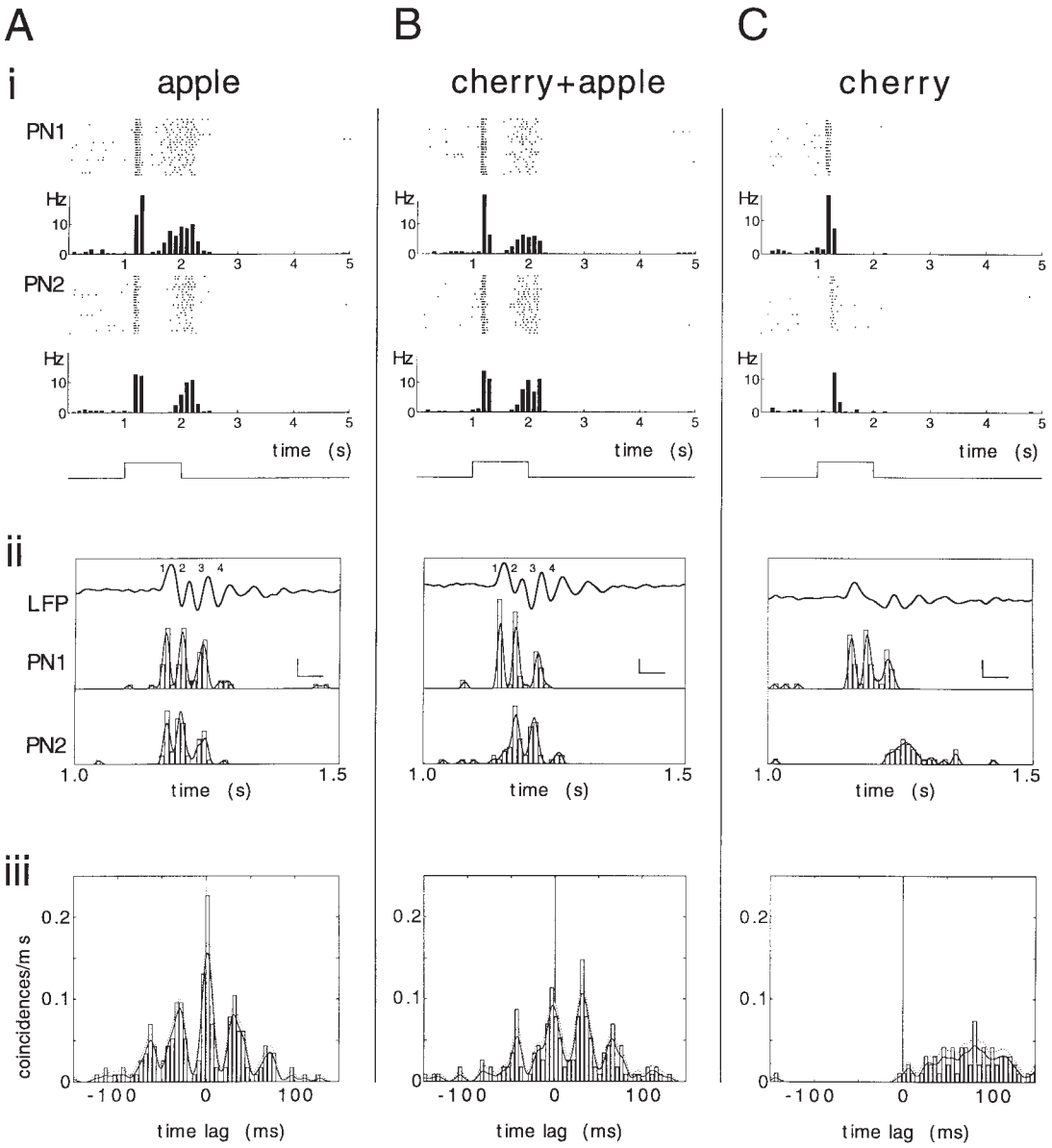

Figure 5. Stimulus identity is encoded in part by the fine temporal features of firing of groups of neurons. A-C: Responses of two PNs (different animal than in Fig. 2) to two odors (A, C) and their 1:1 mixture (B). i: Rasters and PSTHs constructed as in Fig. 2. ii: Fine temporal structure of the PNs' responses during the 1-1.5 s epoch (representation as in Fig. 3; bin size: 10 ms; vertical calibration: 20 Hz or p=0.02 of firing within a 1 ms bin). iii: Cross-correlation functions calculated with the PN spike trains (as in figure). Note the similarity of both neurons' overall responses to

(continued on next page)

ages together successive events, thereby obscuring temporal details of correlated activity. Are such temporal patterns stimulus specific? Figure 5Ai,Bi illustrates the responses of a different pair of neurons to the odor apple and the mixture cherry+apple. In both cases, the two neurons produced remarkably similar responses: a short 'burst' of action potentials, a period of silence, and a second, longer period of elevated activity. These responses (rasters and peristimulus histograms) appear, at first glance, to be identical for both odors. Consider now their fine temporal structure during the initial part of the response (Figure 5Aii, Bii). Whereas both PN1 and PN2 reliably fired simultaneous action potentials during each of the first three cycles of the LFP oscillation in response to apple (Figure 5Aii), PN2 failed to fire during cycle 1 when the mixture was presented, resulting in an apparent relative shift of the two PNs' firing by one cycle (Fig.5Bii). Such 1- or 2-cycle relative shifts were observed for several other odor combinations to which both neurons responded (Figure 7). The skewness of the cross-correlation functions calculated over the initial epoch of the two PNs' responses to odors could be indicative of the absence (e.g.,Figure 5Aiii) or presence (e.g., Figure 5Biii) of a sequential activation of the two neurons, but could not reveal the exact temporal structure of these sequences. Sliding window cross-correlation analysis (Figure 6A) of the response to cherry+apple demonstrated that these neurons were tightly

---

Figure 5 (cont.)

apple and cherry+apple (Ai, Bi), but the striking difference between the fine structures of their spike trains (Aii, Bii). Note that the cross-correlation function is symmetrical about the y-axis at x=0 zero time lag) for apple (indicating near perfect average synchrony), but that it is skewed to the right (meaning that PN1 fired one cycle earlier on average than PN2) for cherry+apple. The exact temporal sequence of activation, however, can only be seen in ii. Note finally that the response to cherry alone was shorter in both neurons (it lacked the second excitatory epoch, Ci), and that only PN1 showed an oscillatory response to this odor (Cii, iii).

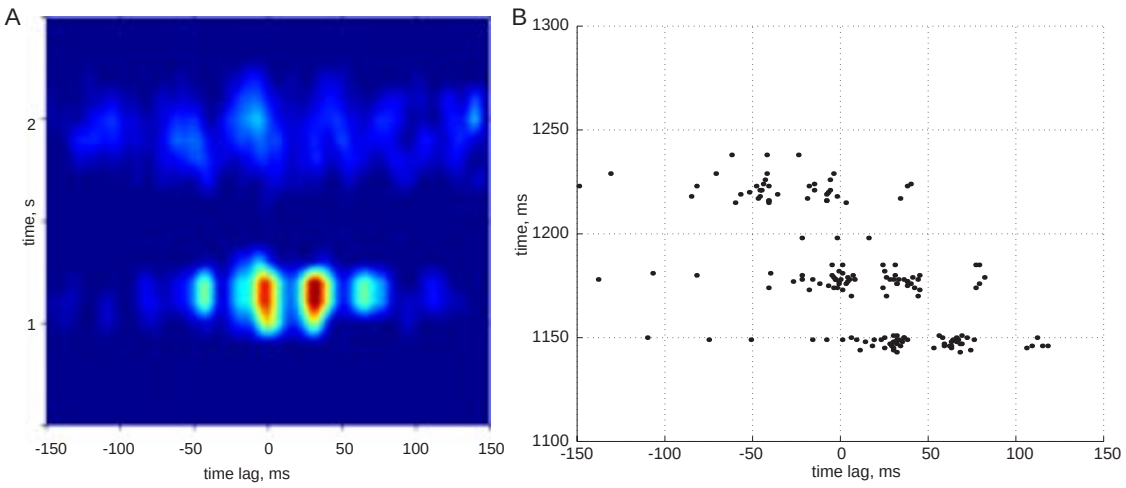

Figure 6. Joint time-correlation representations of the response to cherry+apple. **A**. Spike trains shown in Fig. 5Bi were used to calculate the sliding window cross-correlation (for details on methods, see Chapter 1, Methods). These two PNs showed a ~200 ms epoch of strong oscillatory synchronization between 1 and 1.5 s. The second epoch of firing around 2 s showed much weaker synchronized oscillations. **B**. Spike trains from the first firing epoch (1-1.5 s, shown in Fig. 5Bii) plotted as a function of time lag (x-axis) and time throughout the trial (y-axis). Note that the vertical scale is expanded relative to A. For each trial, the spike train from PN2 was plotted with each PN1 spike time fixed at 0 lag (on the x-axis) and its time of occurrence (on the y-axis), so that the number of dots is the product of the spike counts of the two neurons. This representation is related (but not equivalent) to the sliding window cross-correlation. Note the precise phase-locking on the first cycle (illustrated by the tight clusters of dots at the bottom), which becomes progressively weaker by the third cycle (top).

---

synchronized during the initial 'burst' of firing, but much less so during the second epoch of firing later in the trial. Note that the peaked structure of the cross-correlation histogram shown in Fig. 5Biii results from its calculation being restricted to the 1-1.5 s epoch of strongly synchronized firing. Figure 6B shows an alternative representation of firing correlations as a function of time, similar (but not equivalent) to the sliding window cross-correlation. Here individual spikes are plotted as dot ras-

ters, demonstrating the fine structure of firing correlations on a cycle-by-cycle basis. The precise phase-locking on the first cycle is illustrated by the tight clusters of dots at the bottom, when PN1 leads PN2 by one cycle. On the second and third cycles the two PNs are synchronized at zero lag, and the phase locking becomes progressively weaker by the third cycle at the top. Note that in the sliding window cross-correlation (Fig. 6A) all of these action potentials are averaged together in a single window (which must span multiple cycles).

These fine temporal patterns were highly reliable. The firing probability of a PN during a given cycle could exceed 0.9 (for example, cycle 1 for PN1 in response to cherry+apple, Fig. 7 and Table 1), indicating participation of this PN in the odor-encoding assembly during this cycle of almost every trial. In addition, the firing of one PN during a given cycle often had some predictive value about the behavior of another PN during the same, or a different cycle. For example, although the firing probability of PN2 at cycle 3 was 0.4 in response to geraniol+cherry, this probability rose to 0.67 if it was known that PN1 had fired at cycle 1 of the same trial (Table 1, Fig. 7). Similarly, whereas the firing probability of PN1 at cycle 1 was 0.6 in response to this odor, it rose to 1.0 if it was known that PN2 would also fire at cycle 3 (Table 1, Fig. 7). These results show that odors can reliably evoke specific sequences of activity across neural assemblies.

The fine temporal structure of PN responses to mixtures were not simple or predictable combinations of their responses to the components presented separately (compare Figs. 5A-C). Each odor, however complex, apparently evoked activity in its own specific neuronal set and its own specific sequence of activity. For example, unique patterns are discernible in the firing probabilities of the two PNs in Fig. 5 in response to many other odors probability greater than 0.3 for each

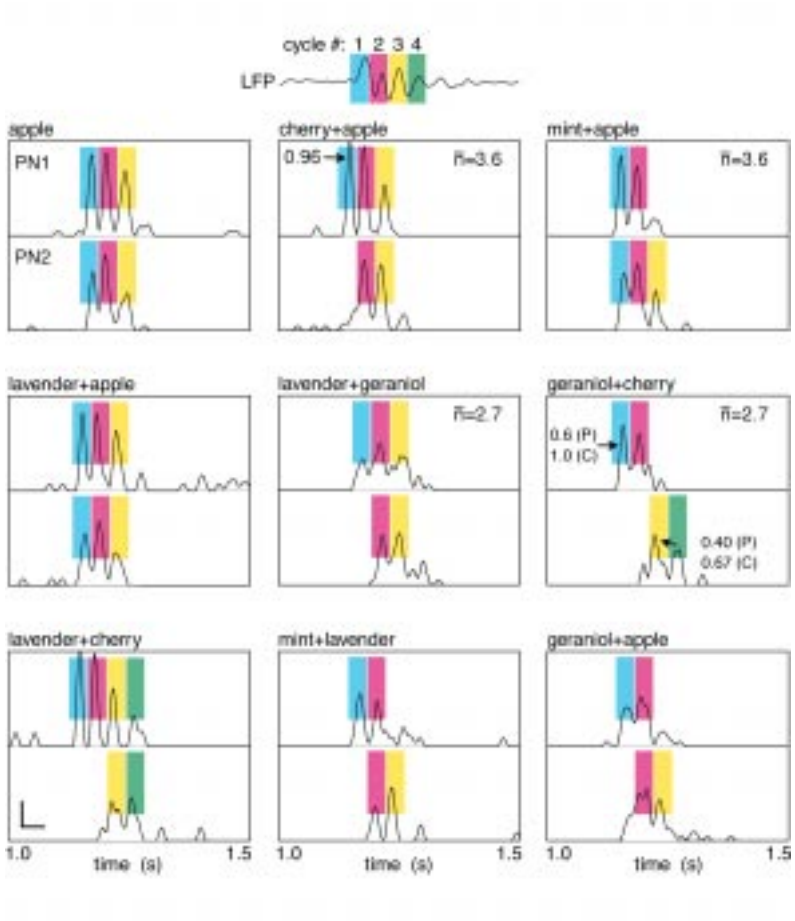

Figure 7. Information about an odor can be gained from the temporal structure of firing of the neurons activated in periodic synchrony. The temporal evolution of the firing probabilities of the two PNs in Figure 5 in response to nine complex odors is displayed here. If the firing probability of either PN exceeded a given threshold (P=0.3) during one oscillation cycle of the response, the neuron's action potential was assigned a color corresponding to the cycle in which it occurred. A colored box thus indicates that the corresponding PN fired an action potential during that cycle with a probability P>0.3 (integrated over the 20 ms period centered on the peak firing probability), The averaged LFP in response to apple is shown at the top, with each oscillation cycle denoted by its color. Each odor can thus be represented by a particular colored pattern that contains more information about odor identity than spike count alone. For example, whereas cherry+apple and mint+apple each produced an average of 3.6 action potentials per trial in the two PNs over the first 3 cycles, the two odors could be discriminated because these action potentials occurred in a different order with each odor. Similarly, lavender+geraniol and geraniol+cherry each produced an average of 2.7 action potentials per trial in the two PNs over the first four cycles, but the two odors could be discriminated by the sequence of these action potentials.

Table 1 firing probabilities of neurons in response to odors

cherry+apple

prior probabilities:

	cycle 1	cycle 2	cycle 3
P(PN1)	**0.96**	0.87	0.39
P(PN2)	0.04	0.70	0.52

joint probabilities: P(PN1,PN2)

		PN1		
		cycle 1	cycle 2	cycle 3
	cycle 1	0.04	0.04	0
PN2	cycle 2	0.65	0.61	0.26
	cycle 3	0.48	0.43	0.22

conditional probabilities: P(PN1|PN2)

		PN1		
		cycle 1	cycle 2	cycle 3
	cycle 1	1.0	1.0	0
PN2	cycle 2	0.94	0.88	0.38
	cycle 3	0.92	0.83	0.42

conditional probabilities: P(PN2|PN1)

		PN1		
		cycle 1	cycle 2	cycle 3
	cycle 1	0.05	0.05	0
PN2	cycle 2	0.68	0.70	0.67
	cycle 3	0.50	0.50	0.56

geraniol+cherry

prior probabilities:

	cycle 1	cycle 2	cycle 3	cycle 4
P(PN1)	**0.60**	0.50	0	0
P(PN2)	0	0	**0.40**	0.30

joint probabilities: P(PN1,PN2)

		PN1			
		cycle 1	cycle 2	cycle 3	cycle 4
	cycle 1	0	0	0	0
PN2	cycle 2	0	0	0	0
	cycle 3	0.40	0.30	0	0
	cycle 4	0.20	0.20	0	0

conditional probabilities: P(PN1|PN2)

		PN1			
		cycle 1	cycle 2	cycle 3	cycle 4
	cycle 1	—	—	—	—
PN2	cycle 2	—	—	—	—
	cycle 3	**1.0**	0.75	0	0
	cycle 4	0.67	0.67	0	0

conditional probabilities: P(PN2|PN1)

		PN1			
		cycle 1	cycle 2	cycle 3	cycle 4
	cycle 1	0	0	—	—
PN2	cycle 2	0	0	—	—
	cycle 3	**0.67**	0.60	—	—
	cycle 4	0.33	0.40	—	—

Table 1: Action potentials of one PN during a given oscillation cycle have predictive value about the likelihood of firing of another PN during the same or a different cycle. Firing probabilities of the two PNs in Figures 2 and 3 during the fist few cycles are shown for cherry+apple (left) and geraniol+cherry (right). The **prior** probability is the probability that a PN fired and action potential in a given cycle. The **joint** probability P(PNx, PNy) is the probability that PNs x and y fired together during the same trial, with a specific temporal relationship (for example, PN1 in cycle 1 and PN2 in cycle 3). The **conditional** probability P(PNy|PNx) is the probability that PNy fired an action potential during a given cycle, given that PNx fired an action potential in the same or a different cycle of the same trial (for example, the conditional probability that PN2 fired an action potential in cycle 3, given that PN1 had fired in cycle 1 of the same trial, was 0.67 in response to geraniol+cherry). When conditional probabilities so calculated were greater than the corresponding prior probabilities, they exceeded them by an amount varying between 0 and 0.45. The average increase was 0.21 + 0.085.

PN and cycle is indicated by a colored box. This representation reveals six different patterns for these nine odors (Figure 7), indicating that knowing the average temporal firing behavior of these two neurons over four oscillation cycles provides

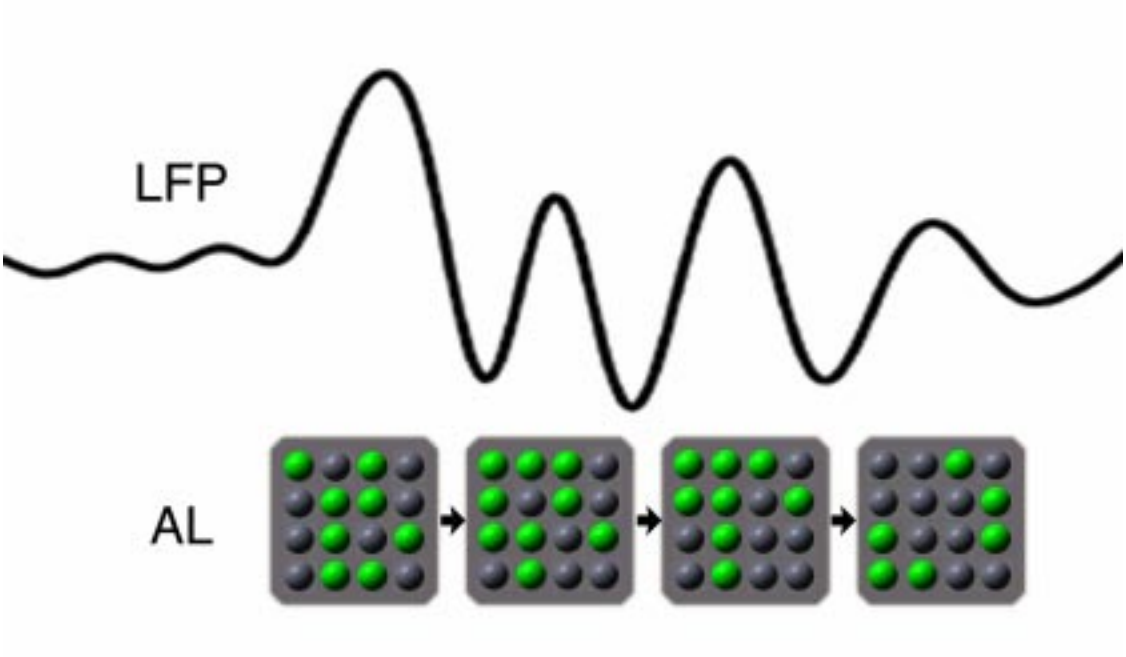

Figure 8. Depiction of odor-specific sequence of synchronized ensembles of projection neurons in the antennal lobe (AL). During each cycle of the LFP oscillation (solid curve at top), a "snapshot" depicts the state of the antennal lobe. Dark circles represent quiescent PNs, while light circles represent the ensemble of PNs firing a synchronous action potential during that cycle.

---

a 66 percent chance of correct odor identification. Ignoring this temporal information would, by contrast, provide only a 33 percent chance of correct identification (three different spike counts for nine odors), a probability similar to that provided by considering the termpoal firing behavior of only one of these two PNs (3 different temporal patterns for 9 odors in each PN, Figure 7). In reality, PN firing is probabilistic and average firing probabilities are not available to the animal on a single odor sampling. Information is, therefore, probably gathered from multiple neurons at once as well as over several oscillations cycles. Previous results indicate that odors are probably represented by about 100 neurons (Laurent & Davidowitz, 1994; Laurent, 1996); only a subgroup of these are likely to be coactive during any given oscillation cycle.

Summary

In summary, we have shown that odors can be represented by ensembles of synchronized neurons that are updated non-randomly at each cycle of an oscillatory activation. Information about the odor smelled is present not in the phase of the active neurons, which is invariant, but rather in their identity and in the temporal sequence in which they are recruited. The firing probability of individual neurons during one cycle of the response can be linked to that of other neurons during the same or other cycles, indicating deterministic and stimulus-specific sequential activation of groups of neurons. In principle, the timing of these odor-encoding sequences need not be precisely locked to the stimulus, although it is this feature which allowed us to detect them. We propose that oscillations are a means to encode stimuli in a temporal combinatorial fashion. Stimuli can thus be represented both by spatial (instantaneous) ensembles— *i.e.*, the neurons activated together during any one cycle— and by temporal sequences (which are expressed by individual or groups of neurons over several cycles). We conclude that this sequence of synchronized ensembles (depicted in Fig. 8) is stimulus-specific, and suggest that it may, in fact, be part of the neural code for odors in this system.

Chapter 4: Relationship between afferent and central temporal patterns in the locust olfactory system

Abstract

Odors evoke synchronized oscillations and slow temporal patterns in antennal lobe neurons, and fast oscillations in the mushroom body local field potential (LFP) of the locust. What is the contribution of primary afferents in the generation of these dynamics? We addressed this question in two ways. First, we recorded odor-evoked afferent activity in both isolated antennae and intact preparations. Odor-evoked population activity in the antenna and the antennal nerve consisted of a slow potential deflection, similar for many odors. This deflection contained neither oscillatory nor odor-specific slow temporal patterns, while simultaneously recorded mushroom body LFPs exhibited clear 20-30 Hz oscillations. This suggests that the temporal patterning of antennal lobe and mushroom body neurons is generated downstream of the olfactory receptor axons. Second, we electrically stimulated arrays of primary afferents *in vivo*. A brief shock to the antennal nerve produced compound PSPs in antennal lobe projection neurons, with two peaks at a ~50 msec interval. Prolonged afferent stimulation with step, ramp, or sine-shaped voltage waveforms evoked sustained 20-30 Hz oscillations in projection neuron membrane potential and in the mushroom body LFP. Projection neuron and mushroom body oscillations were phase-locked and reliable across trials. Synchronization of projection neurons was seen directly in paired intracellular recordings. Pressure injection of picrotoxin into the antennal lobe eliminated the oscillations evoked by electrical stimulation. Different PNs could express different temporal patterns in response to the same electrical stimulus, as seen for odor-evoked responses. Conversely, individual projection neu-

rons could express different temporal patterns of activity in response to step stimulation of different spatial arrays of olfactory afferents. These patterns were reliable, and remained distinct across different stimulus intensities. We conclude that oscillatory synchronization of olfactory neurons originates in the antennal lobe and that slow temporal patterns in projection neurons can arise in the absence of temporal patterning of the afferent input.

Fast stimulus-evoked oscillations in the brain have now been known for over 50 years (Adrian, 1942, 1950). The functional significance of these oscillations remains controversial, although oscillatory synchronization has been shown to be stimulus-specific in a few systems (Gray et al., 1989; Wehr and Laurent, 1996), and experimental desynchronization impairs fine discrimination of odors in the honeybee (Stopfer et al., 1997). Olfactory systems across phyla display, in addition to this fast oscillatory synchronization, complex slow temporal patterns of excitation and inhibition in projection neurons of the first synaptic area, namely, the olfactory bulb in vertebrates and the antennal lobe in insects (Christensen and Hildebrand, 1987; Kauer, 1974). The functional significance of these slow temporal response patterns is also unclear. The role of such temporal coding in vision, for example, remains controversial (McClurkin et al., 1991; Shadlen and Newsome, 1998). The slow temporal patterns in the locust olfactory system are odor- and neuron-specific, and thereby shape the population of activated, rhythmically synchronized projection neurons into an evolving sequence of synchronized oscillatory assemblies which contains information about the odor presented (Laurent and Davidowitz, 1994; Laurent et al., 1996; Wehr and Laurent, 1996). Odors thus appear to be encoded by dynamic neural ensembles, whose components and update are both stimulus-specific (Laurent, 1996).

While oscillatory synchronization in olfactory bulb and antennal lobe is thought (Rall and Shepherd, 1968; Freeman, 1975) or known to involve fast inhibitory feedback (MacLeod and Laurent, 1996), the (possibly distinct) mechanisms by which oscillations are generated in

other sensory systems remain unknown. In the visual system, for example, the onset of oscillatory firing is not stimulus-locked (Gray et al., 1989), whereas it can be so in the locust olfactory system (Wehr and Laurent, 1996). What, therefore, is the contribution of primary afferents in the generation of these dynamics? Could oscillatory synchronization of projection neurons be driven by temporal structure in the afferent input? The vertebrate olfactory epithelium, olfactory bulb, and piriform cortex are each capable of generating oscillations in isolation, suggesting that these structures share a matched resonant capability, rather than any one driving the other (Freeman, 1962, 1968; K Dorries and J Kauer, unpublished observations). Here we investigate the degree to which this is true of the locust olfactory system.

The mechanisms by which odor-evoked slow temporal patterns are generated in projection neurons and mitral/tufted cells are even less well understood. Although they are thought to involve lateral synaptic interactions (Christensen et al., 1993; White et al., 1992; Meredith, 1986, 1992), the details of these interactions are unknown and only rarely have been the subject of speculation. Here we examine the extent to which these dynamics might be driven by temporal structure in the afferent input, or alternatively, might be generated by the intrinsic circuitry of the antennal lobe.

Materials and methods

The preparation: Experiments were carried out *in vivo* on 125 adult female locusts (*Schistocerca americana*) taken from a crowded colony. Animals were restrained dorsal side up. The head was immobilized with beeswax, and a watertight beeswax cup was built around the head for saline superfusion. A window was opened in the cuticle of the head capsule, between the compound eyes, and air sacs on the anterior surface of the brain were carefully removed. For stability, the esophagus was sectioned anterior to the brain, and the gut was removed through a distal abdominal section which was then ligatured. The brain was treated with protease (Sigma type XIV), gently desheathed, and supported with a small metal plat-

form. The head capsule was continuously superfused with oxygenated physiological saline (in mM: 140 NaCl, 5 KCl, 5 $CaCl_2$, 4 $NaHCO_3$, 1 $MgCl_2$, 6.3 HEPES, pH 7.0) at room temperature. Picrotoxin (PCT, 500 picoliters of 1mM solution in locust physiological saline) was pressure injected into the center of the antennal lobe using a glass micropipette (2 mm tip diameter) connected to a pneumatic picopump (WPI, Sarasota, FL).

Electrical stimulation: The antennal nerve was cut distal to its bifurcation, and the antenna was removed. The cut ends of both antennal nerve branches were drawn into a polyethylene suction electrode, or (in some experiments) each branch was drawn into a separate suction electrode (see Fig. 1). The antennal nerve was desheathed from the antennal lobe up to the bifurcation, and penetrated with a planar array of 4 tungsten microelectrodes (etched to a 1 mm tip and insulated with Formvar, impedance 2-5 MW), which were placed across the width of the nerve, proximal to the bifurcation. Bipolar electrical stimuli were delivered between any two of the four tungsten electrodes, indicated in Figures 9-11 by the notation TiTjn for voltage applied from the i^{th} to the j^{th} electrode, with TiTjr indicating the reversed polarity. The suction electrodes used a common AgCl wire in the bath as reference. Together, the suction electrodes and array allowed up to 15 stimulus configurations. In some experiments the antenna was left intact to enable natural stimulation with airborne odors; in these experiments only the array was used for electrical stimulation. Voltage pulses were produced with a programmable pulse generator (AMPI, Jerusalem, Israel) and for voltage shock or step stimuli, were applied via a passive stimulus isolator (Grass Instr., West Warwick, RI). Ramp or sine-shaped voltage waveforms were produced with an analog function generator in single cycle mode (Hewlett-Packard, Palo Alto, CA), DC amplified (Brownlee Precision Instr., Santa Clara, CA), and applied via a stimulus isolator. In some experiments (Figs. 4-8) the stimulus isolator was not used, and the resulting stimulus artifact in the LFP was minimized by digitally high pass filtering at 5 or 10 Hz (as noted in figure captions), but in PNs remains evident as a downward trend in membrane potential. For KC recordings, voltage shocks were applied with a 50 mm stainless steel bipolar stimulating electrode placed in the center of the antennal

lobe.

Olfactory stimulation: The open ends of a set of 20 stainless steel tubes (0.5 mm inner diameter) were placed 2.5 cm from the antenna, angled so that they converged onto the antenna. The other end of each tube was connected via polyethylene tubing to a 2 ml chamber which contained a 1 cm^2 piece of filter paper, on which was deposited 10 ml of one of the following odors: iso-amyl acetate (iaa), citral, cineole, geraniol, hexanol, octanol (Sigma, St. Louis, MO), apple blossom potpourri oil (Gilbertie's Herb Gardens, Easton, CT), spearmint oil (Flavco, Mansfield, OH) or no odorant (air). The chambers were connected in parallel to a common air pressure injection system via a set of valves, so that electronically controlled gentle pressure pulses (0.3 liters/min, insufficient to visibly bend the antenna) could be delivered to the animal. Source air was cleaned and dried by passing through activated charcoal and drierite. Odorant pulses of 0.5 or 1 sec duration were delivered at 0.1 Hz. For isolated antennal recordings, 5 ml polystyrene serological pipettes were used in place of the stainless steel tubes.

Electrophysiology: Intracellular recordings were made using conventional sharp glass microelectrodes pulled with a horizontal puller (Sutter Instr., Novato, CA), which were filled with either 0.5 M KAcetate (for PNs) or a modified patch solution (for KCs, in mM: 155 KAsp, 1 $CaCl_2$, 1.5 $MgCl_2$, 10 EGTA, 2 ATP, 10 HEPES, ~3 Glucose adjusted to give 380 mOsm, pH 7.0; Laurent et al., 1993) and had DC resistances of 100-300 MW. Local field potential (LFP) and antennal nerve recording electrodes had ~1 mm tips with DC resistances of 1-10 MW and were filled with locust physiological saline. For antennal nerve recordings, a ported electrode holder was used and gentle negative pressure was applied with a 10 cc syringe. For electro-antennograms (EAGs) from isolated antennae, two segments were removed from the distal end of the antenna, and each end of the antenna was placed in a glass capillary (tip diameter 0.68 mm) filled with physiological saline. All recordings were done in bridge mode using an Axoclamp-2A (Axon Instr., Foster City, CA) or an SEC-10L (NPI Electr., Tamm, Ger-

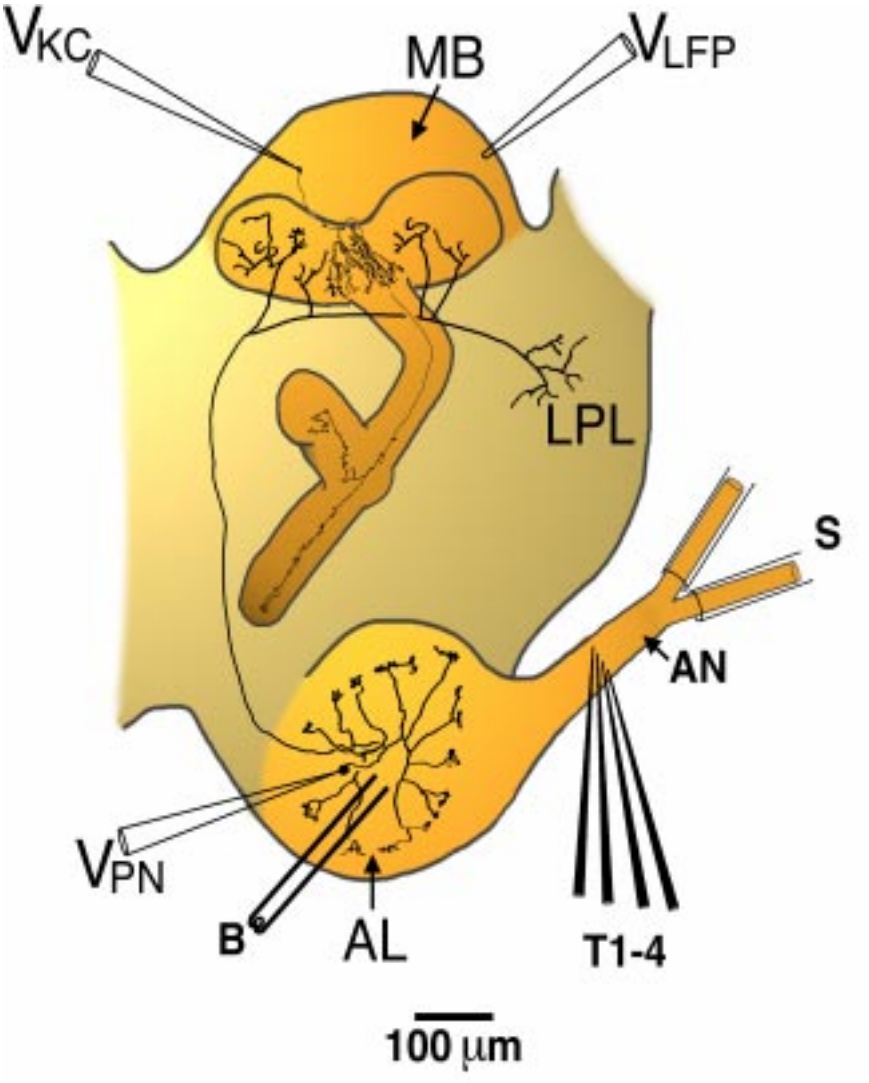

Figure 1. Anatomy cartoon showing configuration of stimulating and recording electrodes. S: suction electrode, AN: antennal nerve, T1-4: planar array of tungsten stimulating electrodes, AL: antennal lobe, B: bipolar stimulating electrode, V_{PN}: projection neuron intracellular recording electrode, V_{KC}: Kenyon cell intracellular recording electrode, MB: mushroom body, V_{LFP}: local field potential recording electrode, LPL: lateral protocerebral lobe.

many) amplifier, and stored to digital audio tape (DAT; Micro Data Instr., Woodhaven, NY; 5.5 kHz sampling rate). The DAT recorder included an analog 8-pole bessel anti-aliasing filter. Data were redigitized from DAT at 5 kHz (National Instruments: LabVIEW software and NBMIO16L hardware) after DC amplification and anti-alias filtering at 3 kHz (Brownlee Precision Instr., Santa Clara, CA).

Analysis: LFPs were digitally low-pass filtered at 50 Hz. Antennal and antennal nerve recordings were digitally low-pass filtered at 300 Hz. Digital filtering was non-causal (i.e., introduced no phase distortion). Decay time constants for EAGs from isolated antennae were

obtained by fitting, in a least squares sense, the falling region (mean of 5 trials) from 90% to 30% of peak amplitude with the equation $e^{-\frac{t}{\tau}+\kappa}$ where κ is a constant and τ is the reported decay time constant. Spectral and cross-correlation analyses were done on the 1.5 sec response periods of each trial, except for the experiment shown in Fig. 2, in which they were done on the entire 10 sec trial (for both antennal nerve recordings and LFP). Cross-correlations were done on mean-subtracted traces and are thus mathematically equivalent to cross-covariances. Power spectra were computed by concatenating response periods from a block of trials and then estimating the power spectral density by Welch's averaged periodogram method (Welch, 1967). Coherence was computed by separately obtaining cross-power and power spectra as above; coherence was then given by the ratio of the magnitude-squared cross-power to the product of the powers of each signal. Mean membrane potentials were computed by first subtracting the pre-stimulus resting potential from each trace, and simply computing the mean across trials. Peri-stimulus-time histograms (PSTHs) were constructed by averaging spike times (obtained by using a threshold discriminator algorithm on the intracellular signals) across blocks of trials aligned on the stimulus command, using bins of 25 msec. All off-line analysis was performed with MATLAB (The MathWorks, Inc.). Results are based on 101 single PN intracellular recordings and 18 paired PN intracellular recordings in 31 animals (including 6 PNs successfully held through PCT injection), 212 KC intracellular recordings in 74 animals, 9 *in vivo* antennal nerve recordings in 11 animals, and 17 isolated antennal recordings from 9 animals.

Results:

Temporal structure of the afferent input

Presentation of odors to an antenna produced a slow potential deflection in the ipsilateral electro-antennogram (EAG), which peaked some time after the end of the odor pulse, and

took several seconds to decay. Figure 2a shows a simultaneous recording of the antennal nerve EAG and the mushroom body LFP in response to presentation of iso-amyl acetate. Fast oscillations were clearly present in the LFP, but none were seen in the population activity of the primary afferents. Power spectra of the mushroom body LFP showed a peak at 20 Hz. No such peak was seen in the antennal nerve spectrum of the same trials (Fig. 2a, inset). Figure 2b shows EAGs from an isolated antenna in response to air and several odors. These responses were consistent across trials, as can be seen from the mean of 5 trials (black) superimposed on the trace of a typical trial (gray). No oscillatory activity or slow temporal patterns were seen in the responses to these odors. If normalized to the same peak amplitude, these odor responses were essentially indistinguishable, except for their decay time constants, which ranged from 0.4 to 1.0 sec.

Central oscillatory synchronization evoked by electrical stimulation of primary afferent axons

To test whether oscillatory activity in the antennal lobe could be evoked by direct activation of the primary afferent axons, we removed the antenna and stimulated the antennal nerve electrically with a suction electrode. A brief (500 msec) shock produced a compound PSP in PNs, that typically contained a second peak ~50 msec after the first (see Fig. 3a). The mushroom body LFP typically showed a single, biphasic deflection. Traces from two consecutive trials at the same intensity are superimposed, showing the consistency of the response. Single shock stimulation of PN axons in the antennal lobe also gave rise to compound EPSPs in their synaptic targets in the mushroom body (Kenyon cells, Fig. 3b). As seen for PNs in response to antennal nerve stimulation, these consecutive Kenyon cell EPSPs were separated by ~50 msec.

Because odor-evoked afferent input is sustained (e.g., see Fig. 2), we next asked whether sustained electrical stimulation of the primary afferents could generate sustained oscillatory

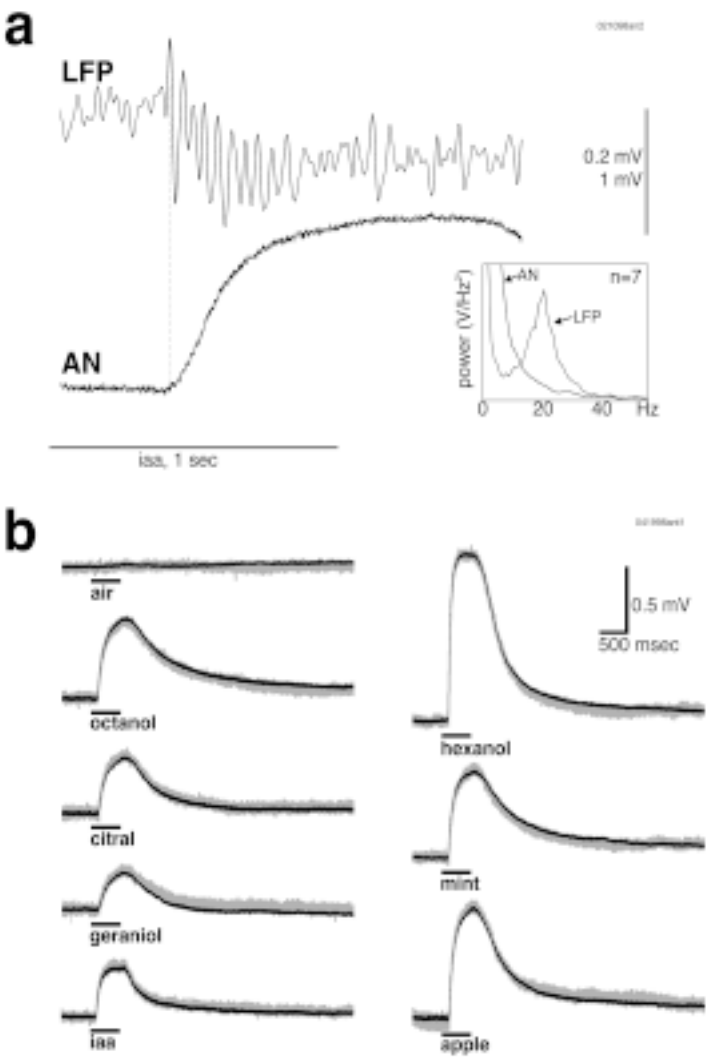

Figure 2. Odor presentation evoked fast oscillations in the mushroom body LFP, but no such oscillations were seen in simultaneously recorded antennal nerve activity. **a:** Presentation of iso-amyl acetate (iaa). The antennal nerve recording showed a slow potential which took several seconds to decay. Odor presentation indicated by horizontal bar. Onset of odor responses indicated by dotted line. Inset: Power spectrum of unfiltered mushroom body LFP (responses to seven consecutive iaa presentations) shows a peak at 20 Hz, while no such peak is seen in the antennal nerve spectrum of the same trials. **b**: EAG recordings from an isolated antenna in response to charcoal-filtered, dried air and seven odors. The mean of five trials (dark line) is superimposed on a typical single trial (gray line). No oscillatory activity or slow temporal patterns were seen in the EAGs in response to these odors. 500 msec odor presentation indicated by horizontal bar.

activity. Prolonged electrical stimulation of the antennal nerve (using a 500 msec voltage step) generated rhythmic, summating EPSPs in PNs. Three cycles were evoked in the example shown in Fig. 3c. Two consecutive trials at the same intensity are superimposed, showing the consistency of the response. The inter-stimulus interval was 30 sec; with intervals less than 20 sec, successive responses decreased in amplitude and duration (data not shown). Using this step stimulation protocol, oscillations were often (cf. Fig. 4-8), though not always (Fig. 3c), seen in the mushroom body LFP. The shape of the voltage waveform used for nerve stimulation affected the duration of the evoked oscillatory activity. Stimulation of the antennal nerve with sine (Fig. 3d) or ramp (Fig. 3e) shaped voltage stimuli, for example, generated sustained oscillations in PN membrane potential and in the mushroom body LFP. In Fig. 3f, a PN was held hyperpolarized by current injection to prevent spiking and enhance

the voltage ramp-evoked EPSPs. The precise synchronization of PN membrane potential and mushroom body LFP can be seen directly from the traces (Fig. 3f), from the cross-correlation of those two traces (Fig. 3g), and from the peak at ~30 Hz in the coherence function (Fig. 3h). The consistency of synchronized PN-LFP oscillations evoked by electrical stimulation of the afferent axons can be seen in Fig. 4, where traces from six consecutive trials are superimposed.

The LFP oscillations evoked by odors reflect rhythmic inputs carried by synchronized PN assemblies to the mushroom body. The synchronization of PN and LFP oscillations in response to electrical afferent stimulation suggests that electrical stimuli, like odors, activate synchronized PN assemblies. This was shown directly using paired intracellular recordings from PNs (Fig. 5a). The subthreshold membrane potential oscillations of these two PNs are consistently synchronized. Alternating EPSPs and IPSPs can be seen in PN1. The same electrical stimulus sometimes produced different temporal patterns of subthreshold activity in two PNs, as seen in the pair in Fig. 5b. Electrical stimulation consistently evoked an initial (suprathreshold) EPSP in PN1, while it evoked an initial IPSP followed by later EPSPs in PN2. Accordingly, the stimulus-evoked firing patterns of the two PNs differed: PN1 always fired on the first cycle of the oscillation, whereas PN2 was prevented from firing by the initial inhibition, and thus tended to fire later in the trial. These patterns are reminiscent of the different oscillatory sequences of firing seen in response to odor presentation (Wehr and Laurent, 1996).

PN desynchronization by picrotoxin injection

The synchronized PN and LFP oscillations evoked by odor presentation are abolished by focal injection of PCT into the antennal lobe (MacLeod and Laurent, 1996). Does PCT also block oscillations evoked by electrical stimulation of the primary afferents? To address this question, we injected PCT into the antennal lobe while recording from a PN and the mush-

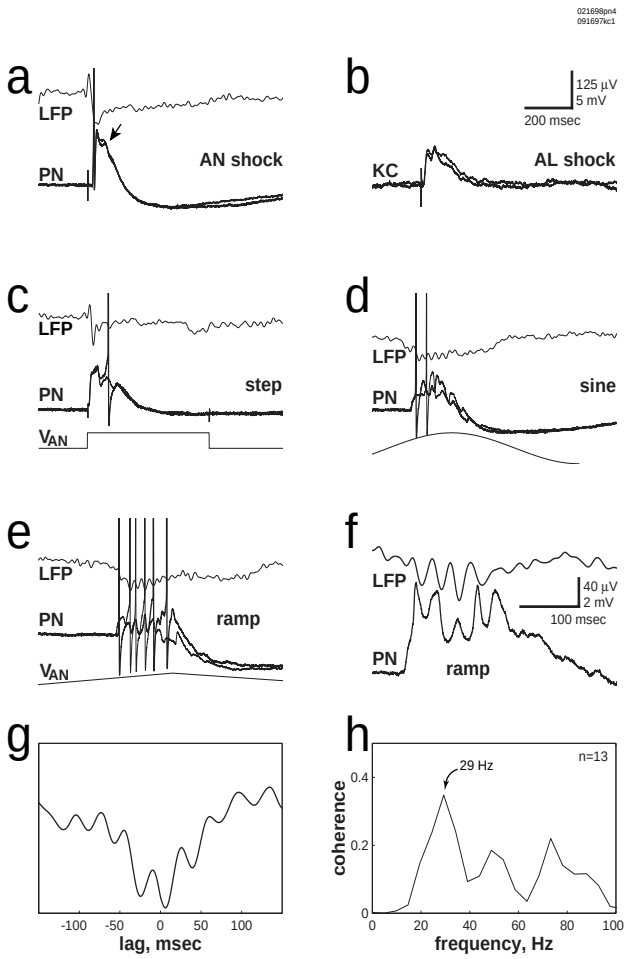

Figure 3. **a**: Shock of the antennal nerve with a suction electrode produced a suprathreshold compound PSP, which contained a second peak (indicated by an arrow) ~50 msec after the first. Two consecutive trials at the same intensity are superimposed (heavy and fine lines). **b:** Shock of the AL produced a compound PSP in an intracellularly recorded KC, with two peaks at a ~50 msec interval. Two consecutive trials at the same intensity are superimposed (heavy and fine lines). **c**: Prolonged (step) electrical stimulation of the antennal nerve with an electrode array generated membrane potential oscillations in PNs. Here three cycles are evoked. Two consecutive trials at the same intensity are superimposed (heavy and fine lines). **d-e**: Prolonged electrical stimulation of the antennal nerve with a suction electrode using sine or ramp-shaped stimuli generated sustained oscillations in PN membrane potential and in the mushroom body LFP. **f-g**: The PN was hyperpolarized by current injection of -0.2 nA. **f:** Note the synchronization of PN membrane potential and mushroom body LFP. **g**: Cross-correlation of traces in f. **h**: Coherence function of PN membrane potential and unfiltered mushroom body LFP, computed over 13 trials. **a**, **c**-**h** from the same PN.

---

room body. PCT disrupted the oscillations evoked by electrical stimulation in both PNs and mushroom body LFP. Figure 6a shows a typical trial both before (heavy line) and after (fine line) PCT injection, illustrating the loss of rhythmicity in both membrane potential and LFP. The amplitude of the synaptic response in PNs was increased after PCT injection, presumably due to the block of fast inhibitory feedback (MacLeod and Laurent, 1996). The desynchronization of PNs can also be seen in the decreased coherence between PN membrane potential and LFP after PCT injection (Fig. 6b). Finally, the consistency of oscillatory responses before, and of non-oscillatory responses after, PCT injection can be seen in averages calcu-

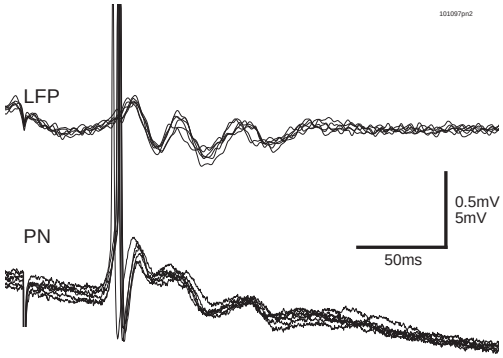

Figure 4. Consistency of synchronized PN-LFP oscillations is shown by superposition of traces from six consecutive trials (different animal from Fig. 3). LFP filtered at 5-50 Hz.

lated over many consecutive trials (Fig. 6c-d).

Oscillatory activity could be evoked only over a relatively narrow range of stimulus intensities (Fig. 7). In this preparation, rhythmicity was absent at intensities below 110 mV, and only one or two cycles were generated for 110 mV. For stimulus intensities between 120 and 150 mV, regularity and rhythmicity were increased and up to 6 cycles could be evoked. For intensities greater than about 150 mV, oscillatory responses were curtailed and rhythmicity was finally replaced by brief initial excitation followed by long-lasting inhibition in PNs, and by a population spike in the mushroom body LFP (Fig. 7a). After PCT injection, no stimulus intensity could evoke oscillations (Fig 7b).

Temporal patterns evoked by stimulation of spatial arrays of afferents

To stimulate different arrays of afferent fibers, we first took advantage of the fact that the antennal nerve has two branches (Fig. 1), and used a separate suction electrode to stimulate each branch. Stimulation of either branch evoked the same basic temporal pattern in a given PN. Figure 8, for example, shows a simultaneous recording from two PNs and the LFP in response to stimulation of each branch (a and b) of the antennal nerve. In PNs which showed an initial inhibitory response (as did PN2 in Fig. 5b), the response was similarly initially inhibitory for stimulation of either branch of the antennal nerve. In no case did a PN respond with different temporal patterns for stimulation of the two branches of the antennal nerve.

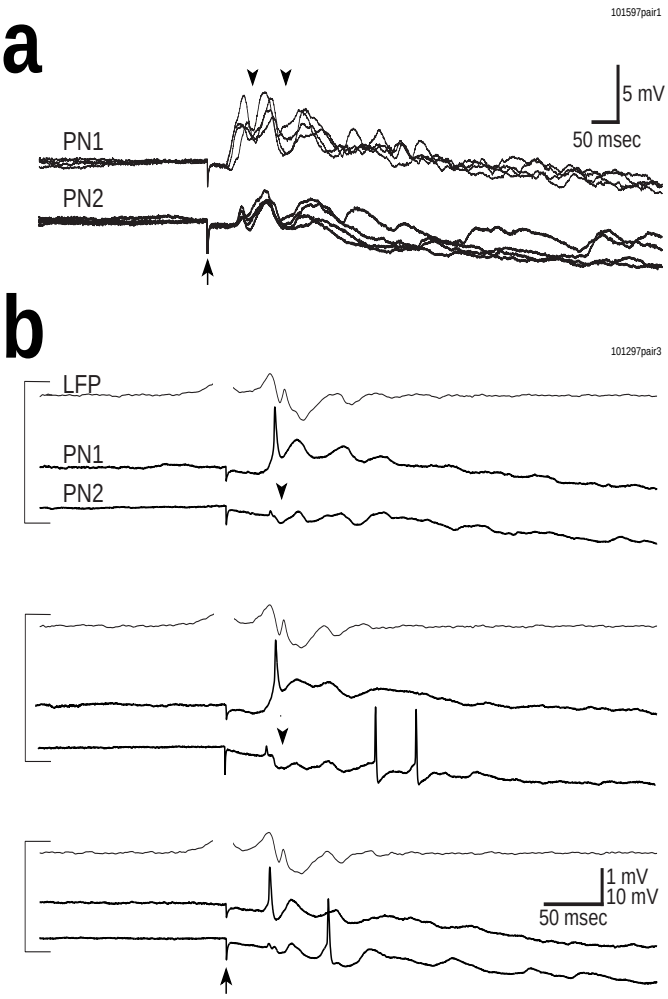

Figure 5. Synchronization between PNs could be seen directly in paired intracellular recordings. **a:** Four consecutive traces are superimposed, showing consistent synchronization of the subthreshold membrane potential oscillations in these 2 PNs. IPSPs are indicated by arrowheads. **b**: Membrane potential of 2 PNs and the mushroom body LFP all showed synchronized oscillations (LFP filtered at 5-50 Hz). PN1 consistently receives an initial EPSP in response to electrical stimulation, whereas PN2 received an initial IPSP (arrowheads), followed by EPSPs later in the trial. This suggests that different PNs can receive different temporal patterns of inputs from the same electrical stimulus. **a-b:** 500 msec step electrical stimulation by suction electrode, onset indicated by arrow.

We then inserted an array of four tungsten stimulating electrodes across the antennal nerve. By choosing any two of the electrodes and applying bipolar stimulation between them, we hoped to stimulate different subsets of the primary afferent fibers, thereby mimicking the ability of odorants to activate different subsets of olfactory receptor neurons. Activating different afferent fiber sets with the same step stimulus generated different temporal response patterns in PNs. In Fig. 9a, these different patterns are apparent in the sub-threshold activity. Single (heavy line) and mean (fine line) responses are superimposed to show the reliability of the different temporal patterns. This example is typical in that the different temporal patterns were often either a brief, short latency, monophasic response (as with T1T2r), or a sustained, long latency, structured response (as with T1T2n). These different temporal patterns re-

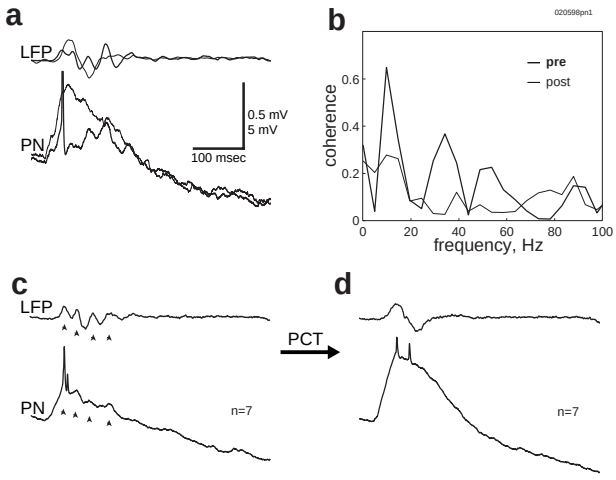

Figure 6. Pressure injection of PCT into the AL disrupts the oscillations evoked by electrical stimulation in both PNs and LFP. **a**: Single trial responses of PN and LFP evoked by step electrical stimulation (with a suction electrode) before (heavy line) and after (fine line) PCT injection. Rhythmicity in both membrane potential and LFP is abolished after injection (LFP filtered 10-50 Hz). Response amplitude also increased after PCT (PN hyperpolarized by -0.5 nA). **b**: Coherence between PN membrane potential and unfiltered mushroom body LFP computed over seven trials both before (pre) and after (post) PCT injection. The peak at ~30 Hz is absent after PCT injection. **c-d**: Mean membrane potential and LFP computed before (**c**) and after (**d**) PCT injection for the same 14 trials as in **b**. Rhythmic EPSPs and phase-locked LFP oscillations in **c** indicated by arrowheads.

---

mained different across stimulus intensities, as shown in Fig. 9b. Thus the different temporal patterns cannot be a simple effect of differential recruitment of the *same* population of afferents by the different stimulating electrodes. For stimulus T1T2r, the mean response latency was 6.9 $\pm$ 0.5 msec (antennal nerve conduction time not subtracted) and did not vary with stimulus intensity. For stimulus T1T2n, however, the latency clearly decreased with increased stimulus intensity.

In some PNs, different spatial patterns of afferent stimulation evoked many different firing patterns. These firing patterns can be seen in individual traces (Fig. 10a), and their reliability can be seen from rasters and peri-stimulus time histograms (Fig. 10b). Delayed firing could be caused by an early inhibition, as with stimulus T3T4n, or by a delayed excitation, as with stimulus T1T2r. Five consecutive trials in response to stimulus T3T4n demonstrate the consistency of the response (Fig. 10c).

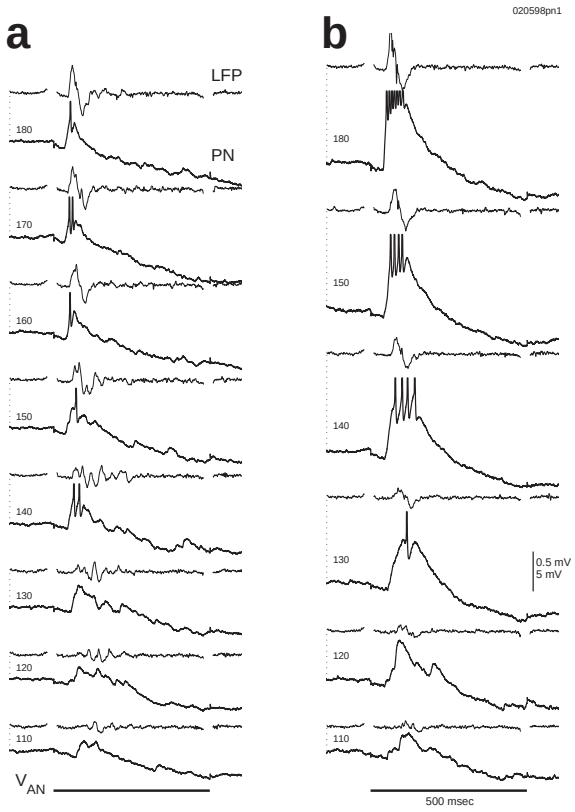

Figure 7. Intensity series showed that PCT effects cannot be attributed to change in stimulus threshold (same PNs as in Fig. 6). **a**: Oscillations are only evoked within a range of stimulus intensities (below which one or no cycles are evoked, above which only a population spike is evoked). **b**: After PCT, no stimulus intensity can evoke oscillations.

Do the temporal patterns evoked by different spatial stimulus arrays bear any relation to the temporal patterns evoked by different odors? To address this, the antennal nerve was electrically stimulated in a preparation in which the antenna had been left intact, so as to enable the presentation of odors. Response to odors and electrical stimulation are shown in Fig. 11 for a single PN. Three trials are superimposed for each stimulus. Apple and citral evoked an initial inhibition followed by a sustained excitation. Cineole caused an initial excitation followed by inhibition. IAA produced a mixed response with an initial subthreshold excitation, followed by epochs of inhibition and then excitation. This spectrum of temporal patterns for different odors is typical for PNs (Laurent and Davidowitz, 1994; Laurent et al., 1996). Electrical stimulation with either T3T4r or T1T2n evoked an initial inhibition followed by excitation, similar to the responses to apple and citral. Close examination of the response to T1T2n reveals a fast initial IPSP followed by a slow inhibitory component. In contrast, the

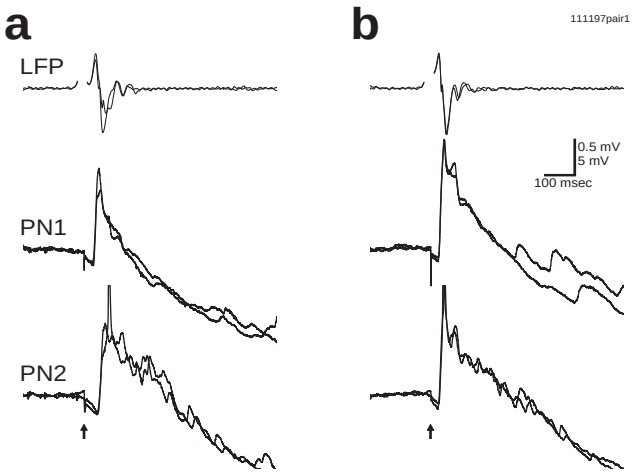

Figure 8. Stimulation of either branch (**a** and **b**) of the antennal nerve evokes the same temporal pattern in a given PN. Two consecutive trials at the same intensity are superimposed, showing the consistency of the response. LFP filtered 10-50 Hz. 500 msec step electrical stimulation, onset indicated by arrow.

the response to T1T3r consisted of a fast, subthreshold EPSP followed by a slow inhibitory component. No electrical stimulus produced an initial supra-threshold excitation for this PN.

Discussion:

Connectivity between olfactory afferents and antennal lobe neurons

In *Manduca sexta*, primary olfactory afferents are thought to synapse directly only onto inhibitory local interneurons; PN excitation must therefore be polysynaptic, via disinhibition. Electrical stimulation of the antennal nerve generally causes an early IPSP, followed by a later excitation of PNs (Waldrop et al., 1987; Christensen and Hildebrand, 1988; Christensen et al., 1993). In the cockroach (*Periplaneta americana*), however, ultrastructural studies indicate direct afferent connections onto PNs (Distler and Boeckh, 1996, 1997). In the locust, short latency and consistent EPSPs were commonly seen in PNs in response to electrical stimulation of the antennal nerve, a result not obtained with *Manduca* PNs (Waldrop et al., 1987; Christensen et al., 1993). The short latency and its low variance are consistent with monosynaptic connections between locust olfactory afferents and PNs—as shown morphologically

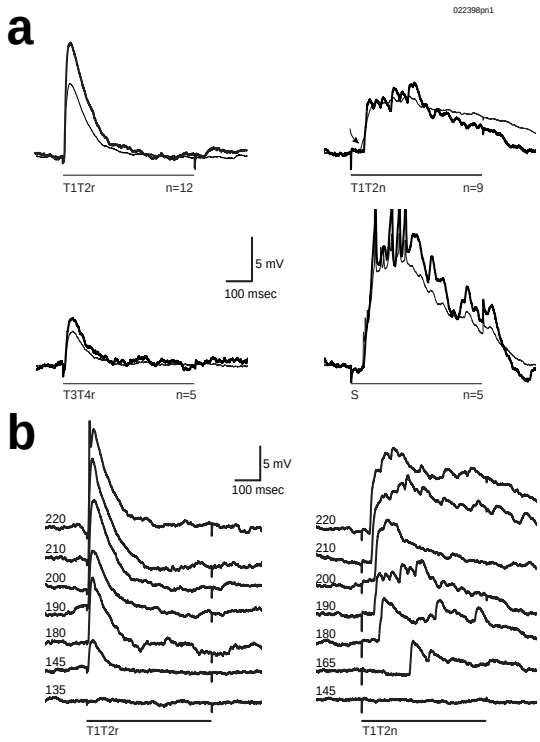

Figure 9. **a:** Stimulating different subsets of afferent fibers generated different temporal PN response patterns. In this PN different patterns are apparent in the sub-threshold activity. Single (heavy) and mean (fine) responses are superimposed. Increased latency (and increased latency variability, see mean) indicated by arrow. **b:** Intensity series shows that the different temporal patterns remained distinct across intensities. Intensities are in mV. For T1T2n but not for T1T2r, latency was a function of stimulus intensity.

for *Periplaneta*—although direct proof awaits ultrastructural or direct electrophysiological evidence.

Oscillatory synchronization

Odor-evoked oscillatory activity in the locust olfactory system is thought to be generated by the intrinsic circuitry of the antennal lobe. This hypothesis is supported by two previous findings. First, odor evoked oscillations in antennal lobe PNs persist after ablation of the mushroom body (Laurent and Davidowitz, 1994), suggesting that the antenna and antennal lobe are sufficient for oscillatory synchronization of PNs during odor responses. Second, focal injection of PCT into the antennal lobe abolishes fast IPSPs in PNs, phase locking of PNs to the mushroom body LFP, and finally, LFP oscillations (MacLeod and Laurent, 1996). These results demonstrate that inhibitory synapses of local neurons onto PNs are necessary for their oscillatory synchronization. The possible contribution of rhythmic and synchronized

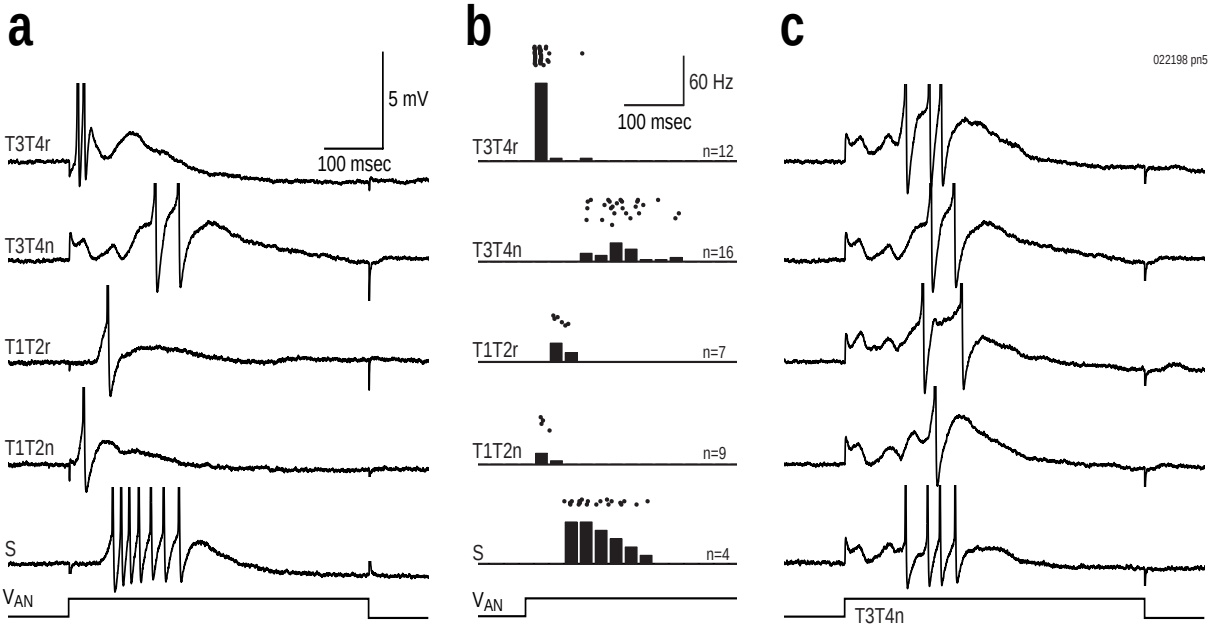

Figure 10. In some PNs, different spatial patterns of afferent stimulation (500 msec step, V_{AN}) evoked many different firing patterns. **a:** Firing patterns can be seen in individual traces. Delayed firing in S is due in part only to conduction time along the antennal nerve. **b:** Peri-stimulus time histograms (25 msec bins) and rasters show reliability of firing patterns. **c:** Five consecutive trials in response to stimulus T3T4n show the consistent early inhibition and late firing.

---

afferent input from the antenna, however, could not be ruled out. Although no evidence exists for reciprocal coupling between olfactory receptor neurons, such connections could in principle participate in the generation of synchronized activity in the antennal lobe. Indeed, recent results from the salamander suggest that afferent synchronization and rhythmic odor-evoked activity can be recorded in the olfactory epithelium even after connections to the olfactory bulb have been severed (Dorries and Kauer, 1996, unpublished observations). Are locust antennal olfactory receptor neurons rhythmically and coherently active during odor responses? Simultaneous extracellular population recordings from the antennal nerve and the mushroom body revealed odor-evoked 20-30 Hz oscillations in the mushroom body LFP, but not in the primary afferents. These results collectively show that the 20-30 Hz oscillations seen in the antennal lobe and mushroom body originate in the antennal lobe. This was confirmed in experiments in which olfactory receptor axons were stimulated electrically, thereby

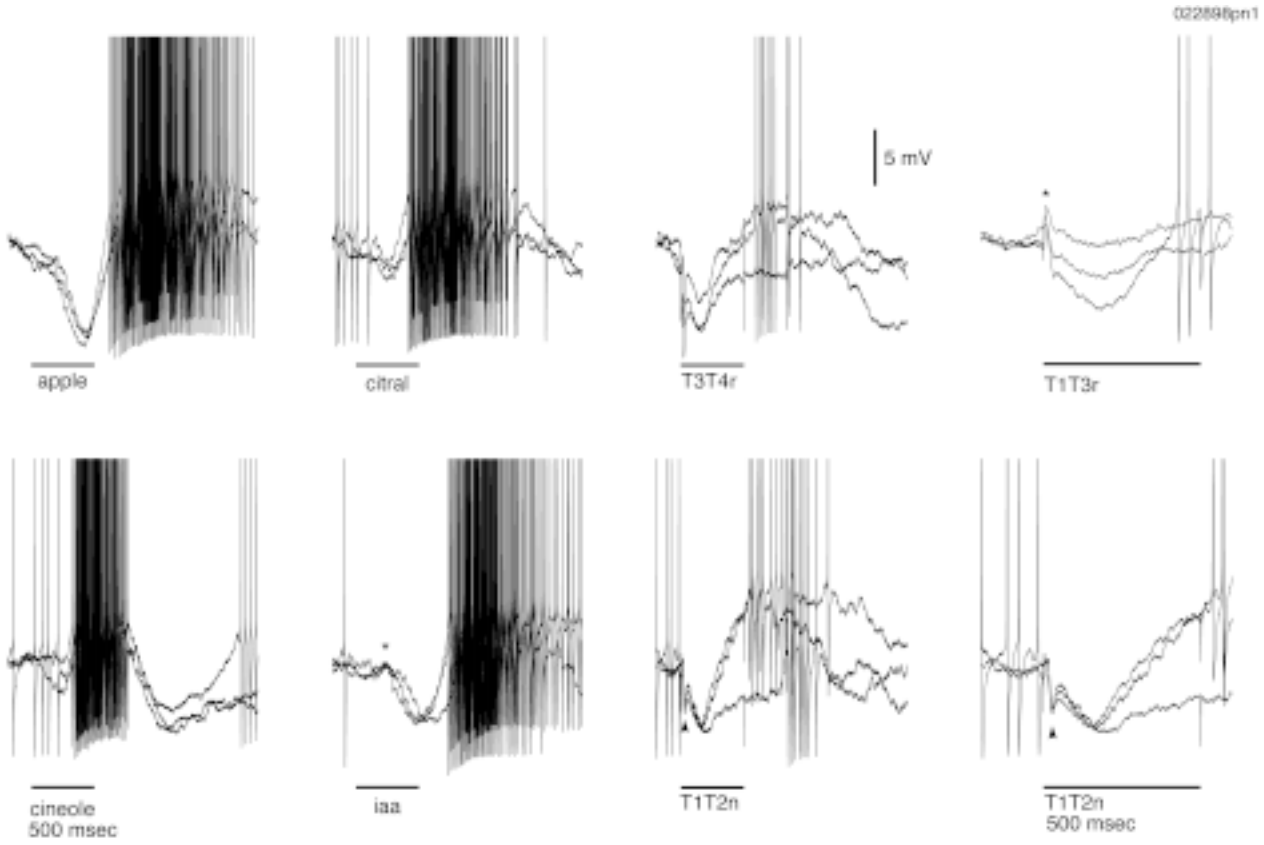

Figure 11. Responses to odors and electrical stimulation in the same PN. Three superimposed trials in each condition. Apple and citral evoke initial inhibition followed by an epoch of excitation. Cineole leads to initial excitation followed by inhibition. Presentation of iaa evokes a mixed response with a weak subthreshold initial excitation (*), followed by epochs of inhibition and then excitation. Electrical stimulation with either T3T4r or T1T2n evokes initial inhibition, followed by excitation. Close examination of the response to T1T2n reveals a fast initial IPSP (arrowhead) followed by a slow inhibitory component. Response to T1T3r consists of a fast, subthreshold EPSP (*) followed by a slow inhibitory component.

---

eliminating the possibility of afferent induced rhythmic synchronization of olfactory receptors. Single shocks to the antennal nerve evoked compound EPSPs with two peaks at a ~50 msec interval in antennal lobe PNs. LFPs two synapses downstream (in the mushroom body) usually failed to reveal more than a single wave of activity. Single shocks delivered directly to the antennal lobe PNs, however, evoked compound EPSPs in mushroom body Kenyon cells,

also with successive peaks at a ~50 msec interval. These results indicate that simple suprathreshold activation of antennal lobe PNs (either synaptically from the antennal nerve, or directly, using an extracellular stimulating electrode) caused at least two consecutive waves of activation in these and possibly other PNs, at a frequency identical to that of odor-evoked responses. Such activity, however, was not sustained, unless unpatterned electrical stimulation was maintained. In this case, oscillatory activity in PNs and in the LFP could be sustained for many cycles. This demonstrates that non-specific, temporally unstructured afferent input can cause sustained oscillatory activity in the antennal lobe and mushroom body networks, likely via activation of the antennal lobe reverberatory circuitry.

Our results for single shock stimulation are very similar to those obtained in vertebrates, where shock stimuli delivered to the olfactory nerve—analogous to the antennal nerve in insects—evoke damped gamma oscillations in field potentials and mitral cell firing in the olfactory bulb (Freeman, 1962, 1972, 1974). Shocks delivered to the lateral olfactory tract—analogous to the PN axon tract in insects—evoke damped field potential gamma oscillations in their target area, the piriform cortex (Freeman, 1959; Haberly and Shepherd, 1973; Rodriguez and Haberly, 1989; Ketchum and Haberly, 1991, 1993). As seen in those experiments, oscillatory activity in the locust antennal lobe could only be evoked within a narrow range of stimulus intensities. These dynamics have been replicated in realistic (Wilson and Bower, 1992) and abstract (Li and Hopfield, 1989; Freeman, 1987) models of mammalian olfactory bulb and piriform cortex.

Finally, focal injection of PCT, a vertebrate $GABA_A$ and insect ionotropic GABA receptor antagonist, abolished electrically evoked oscillatory synchronization in the antennal lobe. The fact that no stimulus intensity could evoke oscillations after PCT injection shows that the effect could not be attributed to a change in stimulus threshold. These results indicate that the inhibitory synapses from local GABAergic neurons onto PNs are necessary for oscillatory synchronization, whether the afferents are stimulated by odorants or electrically. Modeling

studies have shown that inhibition can synchronize neural firing (van Vreeswijk et al., 1994; Jefferys et al., 1996). We conclude that oscillatory synchronization of antennal lobe neurons is a result of the intrinsic connectivity of olfactory afferents, local, and projection neurons in the antennal lobe.

Slow temporal patterns

Odors evoke slow temporal patterns of activity in PNs. These usually consist of successive epochs of excitation, inhibition, and absence of activity. Different odors evoke different temporal patterns in a given PN, and a given odor evokes different temporal patterns in simultaneously recorded PNs (Laurent and Davidowitz, 1994; Laurent et al., 1996; Wehr and Laurent, 1996). Similar slow temporal patterns are also seen in PNs in other insects (Christensen and Hildebrand, 1987, 1988; Waldrop et al., 1987; Waldrow, 1977; Sun et al., 1993), as well as in mitral cells of the vertebrate olfactory bulb (Kauer, 1974; Meredith, 1986; Hamilton and Kauer, 1989). Interestingly, the slow temporal patterns evoked by odors in locust PNs persist in the presence of PCT (MacLeod and Laurent, 1996). This suggests that the mechanisms which generate them are distinct from those which generate synchronous oscillations. What, therefore, are these underlying mechanisms? One hypothesis is that the slow temporal patterns seen in PNs are driven by slow temporal patterns in the afferent input. For example, olfactory receptor neurons could respond with different time courses to different ligands due to perireceptor events (Pelosi, 1996), competitive binding interactions at receptors, combinations of multiple odor-activated membrane conductances (Restrepo et al., 1996), or differential activation of (possibly interacting) second messenger cascades (Restrepo et al., 1996). Alternatively, these temporal patterns could be generated by complex dynamics resulting from intrinsic antennal lobe circuitry. To try and distinguish between these two (non-exclusive) possibilities, we first recorded the population activity of the antennal nerve in response to odor presentation to the antenna, and showed that it contains no odor-specific slow temporal patterns. An absence of slow odor-evoked temporal patterns in the population ac-

tivity does not exclude, however, the possibility that temporal patterns exist in individual or classes of olfactory receptor neurons. Indeed, the many slow temporal patterns seen in PNs are typically not reflected in the mushroom body LFP, i.e., in their averaged activity. We addressed this issue in two ways. First, we attempted to record odor responses from single receptor axons. All attempts failed, probably due to the small size (~0.1 mm diameter) of the afferent axons. Direct recordings from the peripheral sensilla—e.g., as done with moth (Kaissling, 1986)—were unsuccessful (but see Kafka, 1970; Hansson et al., 1996). Failing this, we used a second method, in which afferents were stimulated electrically from their axons, using constant voltage waveforms. The results showed that identical and unpatterned afferent stimuli could activate different temporal response patterns in simultaneously recorded PNs. These response patterns closely resembled those evoked by odor presentation in intact animals, in which PN firing is often cycle-specific (Wehr and Laurent, 1996). In addition, activation of different *spatial* arrays of afferent axons, using identical electrical stimulus waveforms, could often cause different *temporal* response patterns in individual PNs. These responses were shaped by the same features (EPSPs, IPSPs, periods of silence) as seen during responses to odors. This indicates that temporal patterning of the olfactory afferent input is not required for shaping complex response patterns in PNs. Simple depolarization of single PNs by constant intracellular current injection never produced such temporal response patterns in them. We conclude that the complexity of PN odor response patterns (oscillatory synchronization *and* slow temporal patterns) results in great part from the synaptic interactions *within* the antennal lobe. Although the contribution of temporal activity patterns in the olfactory receptor neurons cannot be excluded, our results indicate that PNs are not simple relay neurons for the afferent input. Rather, their output to downstream areas is profoundly shaped by lateral interactions within the antennal lobe, and these interactions are input specific. This confirms earlier reports showing that simultaneously recorded PNs which respond to the same odor often respond in a correlated manner from trial to trial [i.e., the firing of one PN during one cycle on a given trial has predictive value about the firing of the other recorded PN, in that or a different cycle, on the same trial (Wehr and Laurent, 1996)]. How slow

temporal response patterns arise from these lateral interactions, however, remains largely speculative. Although realistic models of the olfactory bulb produce complex temporal response patterns in mitral cells, the mechanisms for their generation are not understood in detail (White et al., 1992). Meredith (1986, 1992) has proposed that slow temporal patterns in mitral cells are a result of non-monotonic intensity response functions, combined with the necessarily finite rate of intensity increase associated with the onset of an odor pulse. The fact that slow temporal patterns are evoked in PNs by step electrical stimuli, which are not subject to the rise time limitations of odor stimulation, suggests that the temporal structure of these responses is generated by reverberatory lateral interactions within the antennal lobe, without dependence on the rate of intensity increase or non-monotonicity of PN intensity response functions.

These results demonstrate that the computations performed by the antennal lobe include, in addition to a spatial mapping of odor information (Hildebrand and Shepherd, 1997), a coordinate transformation from *spatial* input patterns into *temporal* output patterns. To our knowledge, this is the first report of such a transformation in a sensory system, though stimulus-related information has been demonstrated in higher principal components of visual cortical neuron responses in primates (McClurkin et al., 1991; Richmond and Optican, 1987). The existence of such transformations is well known in motor systems, where (for example) stimulation of so-called command neurons can elicit specific and complex motor outputs (Larimer, 1988) which presumably involve temporal patterns of firing in neural assemblies. The functional significance of such a transformation in a sensory system is unclear. Piriform cortex has been proposed to function as a content-addressable memory (Haberly and Bower, 1989), as suggested by its recurrent architecture and the demonstration of LTP in the afferent and associative pathways (Kanter and Haberly, 1990). Recurrent network models incorporating time delays (Tank and Hopfield, 1987), or fast and slow feedback (Kleinfeld, 1986; Sompolinsky and Kanter, 1986), have time-dependent energy landscapes, and thereby attractors which are not fixed points but sequences. Thus piriform cortex, by virtue of its fast and slow associa-

tive feedback pathways, could store and recognize spatiotemporal patterns of inputs from the olfactory bulb (Ketchum and Haberly, 1991). The mushroom body in insects contains putative feedback pathways in the protocerebral lobe (Mobbs, 1982; Gronenberg, 1987; MacLeod and Laurent, 1997), and has been implicated in learning and memory (Menzel and Muller, 1996; Davis, 1993). These circuits may therefore be able to store and recognize spatiotemporal input patterns from the antennal lobe, which consist of rhythmic sequences of synchronized PN assemblies shaped by slow temporal patterns in participating PNs.

Conclusions

The hypothesis that odors are encoded by dynamical (evolving) ensembles of synchronized and oscillating neurons was first formulated by Laurent and Davidowitz (1994). Previous work had demonstrated that odors evoked oscillations in Kenyon cells and the local field potential of the mushroom body (Laurent and Naraghi, 1994), and recordings from local and projection neurons in the antennal lobe suggested that these were generated by rhythmic inputs from a succession of synchronously oscillating odor-specific assemblies of projection neurons (Laurent and Davidowitz, 1994). The work described in Chapter 2 (which appeared in Laurent et al., 1996) confirmed and extended these results, demonstrating that odors evoke specific temporal response patterns in projection neurons in the antennal lobe, such that different neurons responded with different temporal patterns to a given odor, and individual neurons responded with different temporal patterns to distinct odors. These patterns were consistent across repeated odor presentations, and different patterns could be quantitatively compared by computing the relative distances between responses. Oscillatory synchronization between antennal lobe neurons could be seen from their membrane potential responses to a single odor presentation (Laurent and Davidowitz, 1994), or from spike trains averaged across several presentations (Laurent et al., 1996). Because the participation of individual neurons in a synchronized oscillatory ensemble was usually transient, occurring during precise epochs of an odor response, the oscillating ensemble evolves over time—forming a succession of synchronized ensembles, with a new and different (but partially overlapping) ensemble for each successive epoch. These epochs were presumed to last hundreds of milliseconds based on the time course of slow temporal patterns seen in PNs.

This odor-coding hypothesis was very much refined by the work described in Chapter 3 (which appeared in Wehr and Laurent, 1996). Essentially, the fine temporal structure of the succession of ensembles could be more precise and informative than was previously thought. This refinement resulted from the demonstration that these ensembles could change in a stimulus-specific manner and with a high degree of reliability on a cycle-by-cycle basis during an odor response. Thus, information about an odor is contained in the precise temporal sequence in which these ensembles are updated during an odor response. The reliability of these oscillatory *sequences* of firing was demonstrated by the predictive value that the firing of one PN during a given cycle often had about the behavior of another PN during the same, or a different cycle. Transient oscillatory synchronization can be detected with sliding window cross-correlation techniques, but is best quantified using spectral techniques, with which odor-evoked synchronization was shown to be highly significant. As was demonstrated in Chapter 2 for slow temporal patterns, the fine temporal structure of PN responses to mixtures were not simple linear or predictable combinations of their responses to the components presented separately. Each odor, however complex, apparently evoked activity in its own specific neuronal set and its own specific sequence of activity. Information about the odor smelled was present not in the phase of the active neurons, which was invariant, but rather in their identity and in the temporal sequence in which they were recruited.

Finally, Chapter 4 (to appear in Wehr and Laurent, 1998) addressed the mechanisms with which the locust olfactory system generates the evolving oscillatory synchronization described in Chapters 2-3. Previous results (Laurent and Davidowitz, 1994; MacLeod and Laurent, 1996) had suggested that oscillatory synchronization results from network properties in the antennal lobe, but the contribution of afferent activity to this synchronization and to the slow temporal patterns was un-

known. Simultaneous extracellular population recordings from the antennal nerve and the mushroom body revealed odor-evoked 20-30 Hz oscillations in the mushroom body LFP, but not in the primary afferents. Furthermore, oscillatory synchronization was evoked by electrical stimulation of the afferent axons, demonstrating that non-specific, temporally unstructured afferent input can cause sustained oscillatory activity in the antennal lobe and mushroom body networks. Identical and unpatterned electrical stimulation of the afferents could activate different temporal response patterns in simultaneously recorded PNs. These response patterns closely resembled those evoked by odor presentation in intact animals. Activation of different *spatial* arrays of afferent axons, could often produce different *temporal* response patterns in individual PNs. We conclude that the complexity of PN odor response patterns (oscillatory synchronization *and* slow temporal patterns) results in great part from the synaptic interactions *within* the antennal lobe. The computations performed by the antennal lobe therefore include, in addition to a spatial mapping of odor information, a coordinate transformation from *spatial* input patterns into *temporal* output patterns. To our knowledge, this is the first report of such a transformation in a sensory system.

How is oscillatory synchronization decoded by downstream areas? To address this question, MacLeod et al. (1998) recorded from a population of neurons in the β-lobe, two synapses downstream from the antennal lobe. These neurons showed odor responses whose specificity was degraded when their inputs were desynchronized by PCT. This degradation of selectivity consisted of the appearance of responses to new odors, and a loss of discriminability of spike trains evoked by different odors. In contrast, such loss of information was never seen in the PNs whose activity had been desynchronized, suggesting that the loss is due to PN desynchronization and that the β-lobe neurons are sensitive to the temporal struc-

ture of their inputs. These results demonstrate that information encoded in time across ensembles of neurons converges onto single neurons downstream in the pathway.

Is oscillatory synchronization meaningful to the animal? The fact that the oscillatory sequence of synchronized PN ensembles evoked by an odor contains information about the stimulus does not demonstrate that this information is actually used by the animal. For example, because cricket call frequency varies with the ambient temperature, information about the temperature is encoded in cricket calls—and although this information can be decoded by the experimenter, it is not known to be used by the animal in any way. Similarly, the odor-specific oscillatory synchronization described in this thesis could be epiphenomenal, although this seems unlikely given the widespread occurrence of such oscillations in olfactory and other sensory systems across phyla. This question was addressed directly by Stopfer et al. (1997) using proboscis extension response (PER) conditioning in the honeybee. These experiments (described in Chapter 1) took advantage of the fact that picrotoxin, an insect ionotropic GABA receptor antagonist, selectively disrupts oscillatory synchronization of locust and honeybee PNs without affecting their slow temporal response patterns (MacLeod and Laurent, 1996; Stopfer et al., 1997). Honeybees can be trained to selectively extend their proboscis for one odor but not others. Desynchronization using PCT impaired the ability of bees to discriminate between molecularly similar odors (e.g., hexanol and octanol), but did not affect their ability to discriminate molecularly different odors (e.g., octanol and geraniol). These results demonstrate that oscillatory synchronization in the insect olfactory system not only contributes to the selectivity of downstream neurons (MacLeod and Laurent, 1998), but actually participates in odor encoding, and is in fact necessary for fine odor discrimination.

Converging evidence from single unit electrophysiology, spatial activity mapping, and molecular biology (e.g., Mori et al., 1992; Cinelli et al., 1995; Friedrich and Korsching, 1997; Mombaerts et al., 1996) has demonstrated that different odorants activate overlapping yet unique sets of glomeruli. Similarly, stable odor-specific spatial patterns of oscillatory EEG amplitude have been seen in the olfactory bulbs of trained rabbits (Viana Di Prisco and Freeman, 1985). Taken together, these results suggest to Freeman that during training, reinforcement of spatial patterns of co-activated mitral cells leads to the formation of neural assemblies (Hebb, 1949), which produce odor-specific and stable spatial patterns of oscillatory EEG amplitude over the entire bulb. To other investigators, the spatial mapping of odor information has suggested that the glomerulus serves as a functional unit for the processing and coding of odor information, and that odor quality is represented by a spatial code in the olfactory bulbs of vertebrates and the antennal lobes of arthropods. However, the fact that normal glomerular organization of the antennal lobes may not be necessary for odor-modulated flight in female moths (Willis et al., 1995) poses a challenge to this view. Furthermore, as discussed in Chapter 1, the demonstration of spatial maps in the olfactory system does not establish that neural space encodes odor quality information (except to the experimenter). Whether the information contained in spatial activity patterns is actually decoded by downstream neurons using position (rather than identity) and used for odor perception by the animal, remains untested. Certainly the identity of active neurons encodes information (for the animal), but it is not yet clear whether there is a meaningful distinction between the identity of those neurons and their spatial location per se. One interpretation of the results of Stopfer et al. (1997) is that the spatial pattern (or set) of activated glomeruli is different for molecularly different odors, and is thereby sufficient to support discrimination between them. For similar odors the patterns of

activated glomeruli may be highly overlapping, and the additional information carried by oscillatory synchronization of PNs appears to be necessary for discrimination. Odors therefore appear to be represented by a combinatorial code both in time and in space.

Stimulus-dependent neuronal synchronization has been observed in many systems; one of the most widely studied currently is the mammalian visual system. In the visual cortex, as discussed in Chapter 1, stimulus-evoked synchronous oscillatory activity in the gamma (20-70 Hz) frequency range has been recorded at many different spatial scales in the cat and monkey (Gray and Singer, 1989; Gray et al., 1989; Eckhorn et al., 1988; Gray and DiPrisco, 1997; Livingstone, 1991). The degree of synchronization depends on global stimulus properties, and therefore may play a role in image segmentation and visual feature integration.

While enormous progress has been made in understanding how an image is analyzed by single neurons with diverse feature selectivities, the mechanisms with which these visual features are integrated for global computations such as figure-ground segmentation are essentially a mystery. A central difficulty, termed the 'binding problem,' arises from the distributed representation of any visual object across different cortical areas. This distributed neuronal activity must somehow be identified as corresponding to the same object, and integrated without interfering with coexisting activity patterns corresponding to other visual objects. These problems of figure segmentation and feature binding cannot be flexibly solved using only a rate code, because relationships between features cannot be encoded along with the features themselves. The temporal correlation hypothesis suggests that neuronal synchronization provides a dynamic, flexible mechanism for this integration (Milner, 1974, von der Malsburg, 1981; von der Malsburg and Schneider, 1986;

Gray, 1994; Singer and Gray, 1995). The demonstration of stimulus-evoked oscillatory synchronization in visual cortex has been used to support this hypothesis.

While the temporal correlation hypothesis has received a great deal of experimental and theoretical attention, both the mechanisms and functional significance of oscillatory synchronization in the mammalian visual system remain unknown. The mechanisms are likely to include cortical network properties, but reports of a novel class of fast rhythmic intrinsically bursting neurons (termed 'chattering cells') in cat visual cortex suggest that a specialized subset of cortical neurons could recruit large populations of cells into synchronously firing assemblies. Direct demonstration of this proposed synchronization mechanism will be extremely difficult, requiring intracellular recording from a chattering cell, simultaneously with extracellular recordings from multiple other cells coupled to that chattering cell— *in vivo,* during presentation of optimal visual stimuli. Even after such a heroic effort, without demonstrating selective disruption of synchronization by interfering with the putative mechanisms, causality will be difficult to establish. In contrast, the mechanism by which oscillatory synchronization is generated in the insect olfactory system has now been fully and directly demonstrated to emerge from network properties in the antennal lobe, namely, reciprocal excitation and inhibition among local and projection neurons. Selective desynchronization by blocking fast GABAergic inhibition has demonstrated a causal relationship, and together with the demonstration of oscillatory synchronization in response to electrical stimuli, these results show that the excitatory and inhibitory circuitry in the antennal lobe are both necessary and sufficient for generation of oscillatory synchronization.

The functional significance of oscillatory synchronization in the mammalian visual system also remains unknown, although several findings suggest that it plays

a role in visual integration and segmentation. The stimulus-dependence of synchronization shows that it contains information about the stimulus, but whether this information is used by the animal has not been demonstrated. Unlike insects, in which the effect of PCT-induced desynchronization on odor discrimination was directly tested, in mammals there are no means yet known to experimentally interfere with synchronization. The strength of synchronization can be correlated with different behavioral conditions, and such correlations have been reported and support a role for synchronization in visual perception. For example, strabismic cats exhibit interocular rivalry (humans with early onset strabismus do also, so that signals conveyed by the two eyes are not perceived simultaneously but in alternation), and interocular suppression can be measured in cats by tracking eye movements. Strength and regularity of synchronization between cortical neurons evoked by dichoptic stimulation was increased for the dominant eye, and decreased for the suppressed eye (Fries et al., 1997). These differential changes were not associated with changes in firing rate, suggesting that degree of synchronization (rather than firing rate) determines which signals are perceived by the animal. A direct, causal demonstration of a functional role for synchronization in visual perception would require experimental desynchronization of neuronal ensembles, ideally without affecting firing rates—an experiment which has as yet only been possible in the insect olfactory system.

Stimulus-evoked oscillatory synchronization has also been long known in the vertebrate olfactory system, and similar to the insect olfactory system is thought to be generated (at least in the olfactory bulb) by network interactions between mitral and granule cells. While bulb circuitry is very well studied *in vitro*, the mechanisms for odor-evoked oscillatory synchronization await direct demonstration. In addition, the functional significance of these oscillations has not been addressed. Stimu-

lus- or task-dependent synchronization has also been reported in auditory cortex (non-oscillatory, DeCharms and Merzenich, 1996), the somatosensory system (Nicolelis et al., 1995), motor cortex (Donoghue et al., 1998), and frontal cortex (non-oscillatory, Vaadia et al., 1995). While these reports suggest that synchronization may be a widespread phenomenon in the brain, questions about mechanisms and functional significance cannot be addressed until the basic phenomena are more completely explored and characterized.

Both oscillatory population activity and complex temporal response patterns in individual neurons are well established in the first olfactory relay of amphibians, mammals, mollusks and insects, suggesting that the odor-evoked succession of oscillatory ensembles in the insect antennal lobe may also occur in many other animals, across phyla. The insect olfactory system appears to be the only preparation thus far in which oscillations, synchronization, and slow temporal patterns have been observed together and shown to ‘interlock’ into an odor-specific cycle-by-cycle oscillatory sequence of transiently synchronized neuronal ensembles. It is also the only system in which oscillatory synchronization has been directly demonstrated to play a role in stimulus encoding and perception, and the only system in which the decoding of information conveyed by oscillatory synchronization has been demonstrated in downstream neurons. The separate pieces of evidence from vertebrates and mollusks are compatible with our odor coding hypothesis, but it remains to be seen if they can all be concurrently observed there also.

Appendix A: Distinct rhythmic locomotor patterns can be generated by a simple adaptive neural circuit: biology, simulation, and VLSI implementation

Preface

This paper is unrelated to the work described in the main body of the thesis. It arose out of a collaboration with Sylvie Ryckebush, who performed the physiology and computational modelling described here (Ryckebusch et al., 1994). My contribution to this work was the VLSI circuit design, fabrication, and testing (Figs. 6-7).

Abstract

Rhythmic motor patterns can be induced in leg motor neurons of isolated locust thoracic ganglia by bath application of pilocarpine. We observed that the relative phases of levators and depressors differed in the three thoracic ganglia. Arguing that the central pattern generating circuits underlying these three segmental rhythms are probably very similar, we developed a simple model circuit which can produce either of the three activity patterns and characteristic phase relationships by modifying a single synaptic weight. We show results of a computer simulation of this circuit using the neuronal simulator NeuraLOG/Spike. We built and tested an analog VLSI circuit implementation of this model circuit which exhibits the same range of “behaviors” as the computer simulation. This multidisciplinary strategy will be useful to explore the dynamics of central pattern generating networks coupled to physical actuators, and ultimately should allow the design of biologically realistic walking robots.

It is now generally recognized that neural circuits are not hardwired ensembles of neurons with fixed properties, but rather form plastic and adaptable sets. Some of the clearest demonstrations of such neural plasticity have come from studies of central pattern generator circuits. Studies of the crustacean stomatogastric nervous system, for example, have established that the intrinsic properties of component stomatogastric neurons and the efficacies of their synaptic connections are subject to modulation by a large number of "neuroactive" substances, which can act on a wide range of temporal and spatial scales (Harris-Warrick et al., 1992). Altering neuronal and synaptic properties is one way of creating different 'functional' circuits from a fixed set of interconnected neurons. The traditional concept of a central pattern generator as a hardwired neural circuit which produces a fixed output pattern is thus being replaced by that of a "family" of circuits, a set of modifiable neurons and connections, which can be reorganized to produce different outputs as external and internal conditions change (Harris-Warrick and Marder, 1991; Marder and Weimann, 1992). Some examples of neural circuits that are used to generate the motor patterns underlying multiple behaviors come from the studies of *Tritonia* withdrawal and swimming (Getting and Dekin, 1985), crab forward and reverse scaphognathite beating (Simmers and Bush, 1983), *Pleurobranchaea* feeding, regurgitation, and rejection (McClellan, 1982), and the crustacean gastric and pyloric nervous system (Weimann et al., 1991).

Work on more complex central pattern generators (such as the flight system of the locust (Robertson, 1986) or the spinal cord of vertebrates (Grillner et al., 1991; Grillner and Wallén, 1985)) has shown that the identification of component neurons and their interconnections does not necessarily yield a clear functional understanding of the circuits. Such circuits are often more "complicated" than appears necessary to generate a limited set of observable behaviors. In addition, because a

central pattern generator circuit probably contains elements which serve several functions, it is hard to identify by inspection the components which are essential for the generation of a single behavior. In other words, the dissection of a complex circuit into its component parts does not necessarily lead directly to an understanding of the computational rules or algorithms that it employs. One of the clearest demonstrations of the limits of our intuition comes from a theoretical study of pairs of neurons connected through reciprocal inhibitory synapses (Wang and Rinzel, 1993). In this study, Wang and Rinzel showed that the behavior of such a circuit depends critically on the time constant of decay of the inhibitory synaptic conductance. If this time constant is short, the neurons oscillate in antiphase; if it is long, however, the neurons fire in synchrony, despite their inhibitory reciprocal coupling. Even seemingly simple ideas, therefore, need to be carefully tested and explored.

An alternative strategy to exhaustive electrophysiological analysis of complex circuits and characterization of their component neurons is to use a limited experimental data set to generate artificial models, whose behavior can then be exhaustively challenged. This strategy, in time, leads to new specific questions about the biological system that can be addressed experimentally, and to the gradual addition of constraints on the modelled circuit. We adopted such a multidisciplinary strategy in the study of central pattern generating circuits underlying terrestrial locomotion in insects. We focused on the thoracic circuits controlling the three pairs of legs of locusts. Because the front, middle, and hind legs have unique morphologies and functional roles during walking, we focused here on the differences between the patterns of rhythmic activity generated by the three segments. Arguing that, although different, these rhythms should be produced by similar central pattern generating networks (the three thoracic ganglia being essentially homologous repeats of a single ontogenetic design), we then attempted to design a simplified

generic circuit capable of producing all three output patterns. This paper describes one such successful circuit.

Although computer simulations are now widely used to model various aspects of neural systems, silicon (hardware) models are less commonly used. Yet silicon models are extremely useful in testing the ability of a model to function with real physical constraints such as noise and device imperfections (Mead, 1989). In addition, because silicon models operate in real time, feedback to the experimenter is immediate. Moreover, Very Large Scale Integrated (VLSI) circuits can be easily interfaced to mechanical actuators to build systems which interact with the environment, such as mobile robots (DeWeerth et al., 1991). Several types of spiking "neural" circuits have been successfully modelled in silicon hardware. Pulse stream encoding of information has been used in data communications applications and neural networks for a number of years (Murray et al., 1991; Mahowald et al., 1992). Ryckebusch et al. (1989) described silicon models of invertebrate central pattern generators using simple spiking neurons and synapses. Similar neuronal circuits have been used successfully in silicon models of auditory localization (Lazzaro and Mead, 1989) and the jamming-avoidance response of weakly-electric fish (LeMoncheck, 1992). A detailed model of a single neuron which explicitly included different membrane conductances and adaptation mechanisms was introduced by Mahowald and Douglas (1991). Our approach thus combined biological experiments, computer simulations, and silicon hardware designs, to study central pattern generators underlying terrestrial insect locomotion.

Methods

Electrophysiology

Experiments were performed on adult locusts *Schistocerca americana* of either sex, from our crowded laboratory colony. The results presented here were gathered from 44 different experiments.

The preparation. Experiments were performed on an *in vitro* thoracic preparation described previously (Ryckebusch and Laurent, 1993). Briefly, thoracic ganglia were removed from the thorax of the animal with the surrounding tracheal supply and air sacs undisturbed, and were pinned down in a chamber lined with Sylgard 184 (Dow Corning Co., Midland, MI). Leg motor nerves were carefully stripped of their surrounding connective tissue with a small hooked pin. The preparation was superfused with locust saline (mM: NaCl: 140; KCI: 5; $CaCl_2$: 5, $NaHCO_3$: 4, $MgCl_2$: 1, N-2-hydroxyethylpiperazine-N'-2-ethanesulfonic acid (Hepes): 6.3; pH 7.0) supplemented with 2.5% (wt/vol) sucrose. Air was supplied to the ganglia by teasing open the tracheae at the surface of the saline. A stock solution of 10^{-2} M pilocarpine hydrochloride (Sigma) was prepared in advance, and was added to the saline to final bath concentrations of 10^{-5} to 10^{-4} M. The preparation remained healthy for at least 4 or 5 hours at 20 to 26°C.

Recordings. The electrical activity of different leg motor nerves was monitored extracellularly using polyethylene suction electrodes. Data were recorded on an eight-channel Digital Audio Tape recorder sampling at 5 kHz (Sony/Biologic), and were displayed on a Gould TA4000 chart recorder.

Anatomy and nomenclature. The muscles are numbered according to Snodgrass (1929), except where a variant is now more commonly used in the literature. The nerves are numbered according to Bräunig (1982). Motor neurons are designated by commonly used abbreviations or by the name of the muscle group that they innervate. Detailed descriptions of the innervation of the leg musculature can be found in Campbell (1961), Bräunig (1982), and Siegler and Pousman (1990a).

Analysis. Electrophysiological recordings were analyzed off-line with a Macintosh II microcomputer, after digitization at 2 to 8 kHz with a National Instruments NBMI016L AD/DA interface. The software packages used for data analysis were Spike Studio (Eli Meir, Cornell University), Matlab (The MathWorks), and Kaleidagraph (Abelbeck Software).

The centrally generated rhythm observed in the present experiments was characterized by two main phases, hereafter referred to as the **levator** and **depressor** phases, corresponding to the activities of levators and depressors of the trochanter. The onset of a burst of activity in trochanteral levators was chosen as the reference for the rhythmic activity. A period is defined as the interval from the onset of a levator burst to the onset of the next levator burst.

Computer simulations

Spike: Event-Driven Simulation. "Spike" is a fast event-driven simulator written by Lloyd Watts (Caltech, Synaptics), optimized for simulating networks of spiking neurons and synapses. The key simplifying assumption in Spike is that all currents injected into a cell may be composed of piecewise-constant pulses (i.e.,

boxcax pulses). All integrated membrane voltage trajectories are therefore piecewise linear in time. This simple representation is well-suited for investigating system-level questions that rely on detailed spiking behavior. The simulator operates by maintaining a queue of scheduled events. The occurrence of one event (i.e., an action potential) usually causes later events to be scheduled in the queue (i.e., end of refractory period, end of post-synaptic current pulse). The total current injected into a neuron is integrated into the future to predict the time of firing, at which time a neuron spike event is scheduled. If any of the current components being injected into the cell subsequently change, the spike event is rescheduled. The simulator runs until the queue is empty or until the desired run-time has elapsed.

NeuraLOG. Neural Schematic Capture. "NeuraLOG" is a schematic entry tool, which allows the convenient entry of "neural" circuit diagrams, consisting of neurons, synapses, test inputs, and custom symbols. NeuraLOG is a customization by Lloyd Watts of the program AnaLOG, by John Lazzaro and Dave Gillespie (Caltech). The parameters of the neural elements are entered directly on the schematic diagram; these parameters include the neuron refractory period, duration and intensity of the post-synaptic current pulse following an action potential, saturation value of summating post-synaptic currents, tonic input currents, axonal delays, etc. Custom symbols can be defined, so that arbitrarily complex hierarchical designs may be made. For example, one can create a complex "neuron" (e.g., bursting neuron) containing many neuron and synapse primitive elements. Spiking inputs may be supplied as external stimuli in a number of formats, including single spikes, periodic spike trains, periodic bursts, (Poisson) random spike trains, and gaussian-jittered periodic spike trains. Textual input to Spike is also possible, to allow simulation of algorithmically-generated circuit topologies too complex to specify graphically.

NeuraLOG and Spike were both created by Lloyd Watts, and are distributed under the GNU General Public Licence. Send email to lloyd@pcmp.caltech.edu for information.

Neuron and Synapse Models. The model neuron and synapse circuit primitives we used both in our simulations and in the VLSI implementation were developed by Lloyd Watts as abstract models which capture some of the basic characteristics of biological neurons and synapses. These circuit elements are the primitive elements in the NeuraLOG/Spike simulator described above. Since both the neuron and synapse circuits were designed as electronic VLSI circuits, it is relatively straightforward to implement in VLSI a given model circuit which was designed and sirnulated using NeuraLOG/Spike. Detailed mathematical analysis of the neuron circuit at the transistor level can be found in Sarpeshkar et al. (1992). General descriptions of the circuit models and the simulation tools can be found in Watts (1992, 1993). We will briefly describe these circuits here in biological terms. The model neuron circuit is similar to a Hodgkin-Huxley sodium-potassium conductance pair. This neuron circuit takes as its input a current, and generates as its output a train of pulses whose height is determined by the voltage of the power supply (typically 5 volts). The pulses are fired only if the input node, which is integrating the input current, reaches the threshold voltage. The firing frequency increases with the input current until the upper frequency limit (saturation) set by the refractory period is reached. The neuron circuit has three parameters: a threshold, a pulse width, and the refractory period of the action potential. The circuit operations underlying the generation of a pulse can be described in biological terms as follows. A persistent “sodium conductance” causes the rising phase of the action potential. The “sodium conductance” activates, after a delay, a “potassium conduc-

tance" that is coupled to it. This "potassium conductance" restores the membrane potential to its "resting" value and causes the falling phase of the action potential. The "potassium conductance" inactivates slowly in a time-dependent (but not voltage-dependent) manner, causing a "refractory" period after the firing of the action potential.

A simplified synaptic cleft model is the basis for the synapse circuit. An action potential from the presynaptic "neuron" causes the release of "neurotransmitter" into the synaptic cleft, where it remains for a controlled duration. While "neurotransmitter" is in the cleft, a constant current is injected into the postsynaptic cell. The "synapse" circuit therefore has two parameters: the duration of a synaptic event and the synaptic current which flows into the postsynaptic cell. Any number of "synapses" can be connected to a "neuron" circuit.

VLSI implementation

The VLSI implementation of the neuron circuit contains eight transistors and can operate over wide ranges of firing frequency, pulse width, refractory period, and threshold. The firing frequency can be varied from 0.1-0.5 Hz to 100 kHz. The pulse widths and refractory periods of the action potentials can be varied from a few tens of microseconds to hundreds of milliseconds. The threshold for firing can be varied from approximately 0.7 volts to the power supply voltage (5 volts). A typical neuron with its synaptic inputs measures approximately 100 x 250 μm (Fig. 6B). The entire 3-neuron circuit contains 97 transistors and measures 400 x 600 μm. VLSI circuits were designed using the layout editor LEdit (Tanner Research) on a Hewlett Packard workstation. The chip was fabricated in a standard 2-micron double-poly CMOS (Complementary Metal-Oxide Semiconductor) process on a 2

x 2 mm 40-pin die (TinyChip) (Fig. 6A). Chip fabrication was provided by the Defense Advanced Research Projects Agency and through the MOSIS service. Data acquisition was performed using a Macintosh microcomputer with a National Instruments NBMI016L AD/DA interface running Matlab (The MathWorks).

Abbreviations

CI	common inhibitor
CMOS	Complementary Metal-Oxide Semiconductor
dep	depressor
Df	fast depressor trochanteris
Ds	slow depressor trochanteris
lev	levator
troch	trochanter
VLSI	Very Large Scale Integrated

Results

Pro- , meso-, and metathoracic ganglia produce different rhythmic patterns

Metathoracic rhythm

The rhythmic patterns evoked in leg motor neurons in isolated metathoracic ganglia by pilocarpine have been described in detail in Ryckebusch and Laurent (1993). Those results are summarized here for the purposes of comparison.

The frequency of the pilocarpine-induced rhythm increased approximately lin-

early from 0 to 0.2 Hz with concentrations of pilocarpine from 10^{-5} to 10^{-4} M. For each hemiganglion, the rhythm was characterized by two main phases: a **levator** phase, during which the anterior coxal rotator, levators of the trochanter, flexors of the tibia, and common inhibitory motor neurons were active; and a **depressor** phase, during which depressors of the trochanter, extensors of the tibia, and depressors of the tarsus were active. During normal walking these two phases would correspond to the swing and stance phases of a step of the hind leg, respectively. Trochanteral depressor activity followed the trochanteral levator bursts with a short, constant interburst latency such that activity in the two antagonistic groups did not overlap. The levator phase was short in comparison to the cycle period (0.5 to 2 sec, or 10% to 20% of the period), and was independent of the cycle period. The interval between the end of a levator burst and the beginning of the following one thus increased with cycle period. The depressor phase was more variable, and was usually shorter than the interval between successive levator bursts. A second depressor burst was sometimes observed during the latter half of a cycle. This second burst generally coincided with a levator burst on the contralateral side and always ended before the onset of the ipsilateral levator burst.

All depressor trochanteris motor neurons were active during the same phase, although their spiking thresholds differed substantially. In inactive preparations (no pilocarpine), *Df* was silent and *Ds* was tonically active. At low levels of activity, the tonic firing of *Ds* was interrupted during the bursts of trochanteral levator activity; this interruption was followed by a transient increase in firing frequency. Variations of the instantaneous firing frequency of *Ds* were mirrored by those of the membrane potential of *Df*, which was hyperpolarized during a levator burst, and depolarized immediately after it. As the level of activity increased, the tonic firing of *Ds* ceased, and short, clearly defined, bursts of action potentials emerged. *Df* action

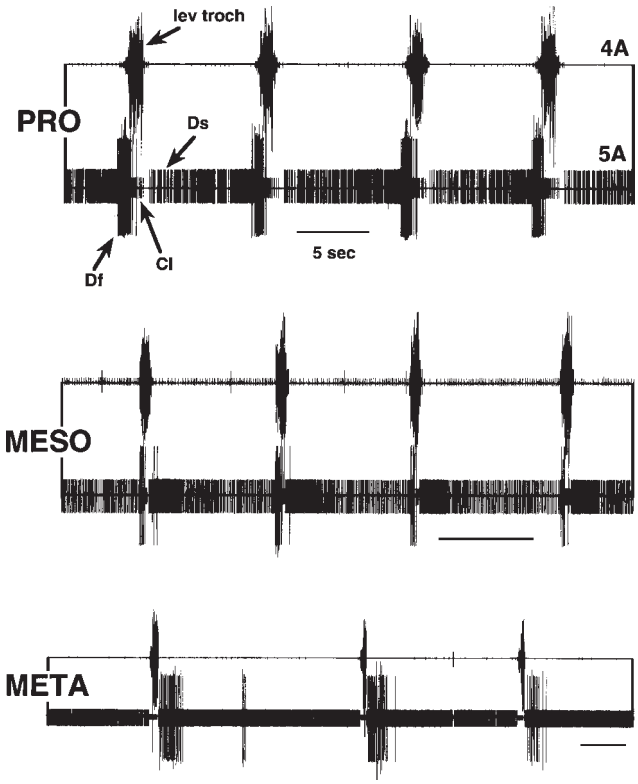

Figure 1. Rhythmic patterns of activity of levator and depressor trochanteris motor neurons in isolated pro-, meso-, and metathoracic ganglia. In each pair of traces, the top trace is an extracellular recording of nerve 4A (trochanteral levators) and the bottom trace is an extracellular recording of nerve 5A (trochanteral depressors, CI). Pilocarpine: 10^{-5} M (pro), 10^{-5} M (meso), 3×10^{-5} M (meta) (Scale bar: 5 sec).

potentials were often observed when *Ds* reached its peak instantaneous firing frequency.

Prothoracic rhythm

We recorded extracellularly from leg motor nerves 4A (trochanteral levators) and 5A (trochanteral depressors) of isolated prothoracic ganglia. From nerve 4A, we recorded the activity of up to 10 motor neurons. From nerve 5A, we recorded the activity of the fast and slow trochanteral depressors *Df* and *Ds* and a common inhibitory motor neuron CI (Fig. 1). In inactive preparations (no pilocarpine), *Df* was silent and *Ds* was tonically active. The prothoracic rhythmic motor patterns recorded in the presence of pilocarpine differed in several respects from the metathoracic ones. During rhythmic activity, *Ds* maintained a high tonic firing rate, and was periodically inhibited during the bursts of trochanteral levator activity (Fig. 1,

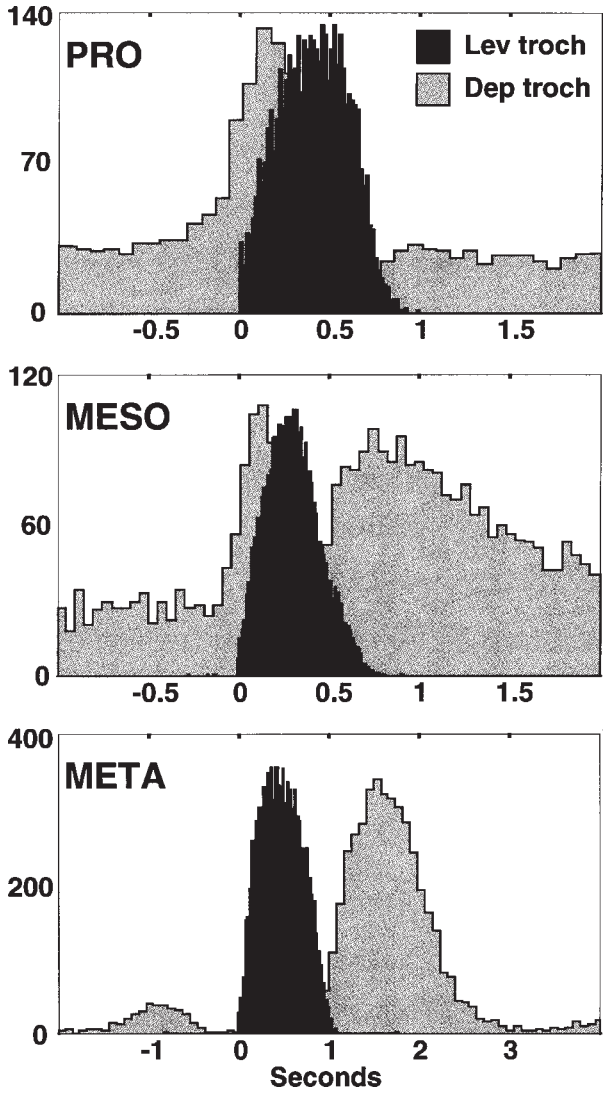

Figure 2. Spike frequency histograms of trochanteral levator and depressor motor neuronactivity as shown in Fig. 1. Data is compiled from 30 (pro), 132 (meso) and 53 (meta) periods of activity from single continuous recordings. The reference is the onset of a burst of trochanteral levator action potentials. The scale on the ordinate is the total number of action potentials in each bin, and represents a cumulative total for all of the periods of activity that were analyzed.

top). The rhythmic activity could be elicited at lower concentrations of pilocarpine (ca. 10^{-5} M) than that which was typically used for the metathoracic ganglion (5 x 10^{-5}-10^{-4} M). The frequencies (inverse of cycle period) typically recorded were higher than those in the metathoracic ganglion at similar concentrations of pilocarpine. Although both prothoracic trochanteral levator burst durations and interburst intervals were shorter than the metathoracic ones, the higher frequency was mainly due to shorter intervals between trochanteral levator bursts (Figs. 1 and 2). Whereas metathoracic *Ds* and *Df* fired at the highest rate immediately after a trochanteral levator burst, the highest firing frequency of prothoracic *Ds* and *Df* occurred before

trochanteral levator bursts (Figs. 1 and 2). Overlap between levator and depressor activities was often observed at the beginning of a trochanteral levator burst (Fig. 2). In the isolated prothoracic ganglion, we typically did NOT observe a postinhibitory increase in depressor firing frequency after a trochanteral levator burst, although the latency between the end of a levator burst and resumption of tonic firing of *Ds* was shorter than that observed in the metathoracic ganglion (Fig. 2). Whereas in the metathoracic ganglion we often saw coupling between depressors and the contralateral levators (i.e., the firing frequency of depressors increased during a contralateral levator burst), we rarely saw such bilateral coupling in the prothoracic ganglion. (A detailed analysis of intersegmental coupling is the object of a following publication.)

Mesothoracic rhythm

The rhythmic activity recorded in the mesothoracic ganglion was similar in most respects to that in the prothoracic ganglion, as described above. The main difference observed was that the depressor motor neurons (*Ds* and *Df*) had marked peaks of activity both immediately before and after a levator burst (Figs. 1 and 2). This pattern of activity was somewhat variable: In some preparations, the mesothoracic depressors fired maximally before the levator burst (as was described for the prothoracic ganglion); in other preparations, the depressors fired maximally after a levator burst (as was observed in the metathoracic ganglion); in still other preparations, depressor activity was equally high both before and after a levator burst. In most preparations, each of these patterns occurred at some time. The frequencies of the rhythmic activity were similar to those of the prothoracic ganglion, as described above.

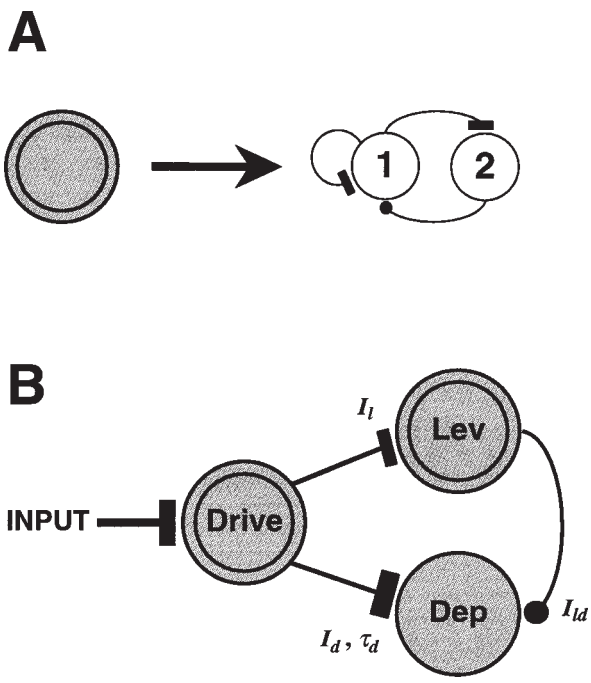

Figure 3. An abstract model circuit for generating pro-, meso-, and metathoracic motor patterns. **A**. A "bursting" neuron can be modeled by two "cells" connected by reciprocal synapses. Cell 1 makes a weak excitatory synapse onto cell 2. Cell 2 makes a strong inhibitory synapse onto cell 1. In addition, cell 1 makes an excitatory connection onto itself (positive feedback). With the addition of a small excitatory input drive into cell 1, the output of cell 1 consists of bursts of action potentials separated by a silent period. Note that in such a model circuit, cells 1 and 2 represent state variables rather than actual cells. **B**. Three-neuron model circuit, consisting of a "Drive" neuron and levator (Lev) and depressor (Dep) motor pool drivers. Drive and the levator motor pool driver are bursting neurons. Filled bars represent excitatory synapses, and filled circles represent inhibitory synapses. The three motor patterns (pro-, meso- and metathoracic) can be obtained by modifying the strength of the excitatory synapse between Drive and the levator neurons (I_l). For details see Results and Appendix.

A simple configurable model circuit

The aim of the simulation studies described here was to test model circuit designs which could produce the different motor patterns recorded in the isolated pro-, meso-, and metathoracic ganglia. The goal of this modelling study was therefore to explore possible circuit designs of a central pattern generator which would be flexible enough to produce all of these motor patterns. Such modulation of the motor pattern should be achievable by simple and biologically realistic mechanisms in the model circuit. The actual structures of the biological circuits, however, are

unknown at this point. Such a circuit was designed using abstract models of neurons and synapses using the NeuraLOG/Spike circuit simulator (see Methods). It should be emphasized that this circuit was designed so that it would be both simple and easy to implement using available VLSI technology (see below).

The bursting neuron

A bursting neuron, which produces rhythmic bursts of action potentials, was constructed using two primitive neuron circuits (Fig. 3A). Two neuron circuits were needed to obtain an equivalent neuron with enough state variables to generate bursting behavior. In Appendix B, we describe another bursting neuron model which uses only a single cell, but requires a more sophisticated model of the synapse. In the burster circuit (Fig. 3A), cell 1 makes a weak excitatory synapse onto cell 2. Cell 2, in turn, makes a strong inhibitory synapse onto cell 1. In addition, cell 1 makes an excitatory feedback synapse onto itself. In response to an excitatory input drive (such as a constant current or a train of action potentials fed through an excitatory synapse), cell 1 fires bursts of action potentials. The activity of cell 1 is taken to be the output of the bursting neuron. The firing frequency of cell 1 during a burst is determined by the magnitude of its positive feedback current. The duration of the burst is determined by the strength of the excitatory synapse from cell 1 to cell 2, and the interval between bursts is determined by the strength of the excitatory input drive into cell 1. The burst duration and interburst interval are therefore independently determined.

The central pattern generator circuit

The entire model circuit, shown in Fig. 3B, is composed of two bursting neu-

rons as described above (Drive and Lev) and one non-bursting neuron (Dep). Lev represents the drive to the pool of trochanteral levator motor neurons, and Dep represents the drive to the pool of trochanteral depressor motor neurons. For simplicity, we will often refer to Dep and Lev as levator and depressor neurons. Since connections between motor neurons do not occur in the locust circuits, we consider levator and depressor motor neurons to be followers, rather than fundamental components of the central pattern generating circuits. The connections shown between Lev and Dep in the model circuit are therefore not connections between pools of motor neurons, but between the central drives to these motor neurons.

In this model circuit, Drive makes excitatory synapses onto Lev and Dep, and Lev makes an inhibitory synapse onto Dep. The ability of this circuit to produce the different patterns of levator and depressor activity depends on the relative strengths of the excitatory synapses, I_l and I_d. In particular, by simply modifying the strength of I_l, the output of the circuit can be changed from a prothoracic-like pattern, where the activity of Dep precedes Lev, to a metathoracic-like pattern, where the activity of Dep follows the activity of Lev. Intermediate mesothoracic-like patterns are obtained in the transition region between prothoracic and metathoracic patterns. The operation of the model circuit can be understood as follows: Drive receives a constant depolarizing input, which causes it to burst rhythmically (see previous description of burster neuron). When Drive is active, it excites both Lev and Dep. If I_l is weaker than I_d, Dep reaches threshold sooner than Lev, and fires as long as it is being driven. Once Lev reaches threshold, it fires a burst of action potentials, inhibiting Dep. Since Lev is a bursting neuron, its burst of activity eventually ends. This first pattern, shown in Fig. 4 (PRO), is similar to the prothoracic rhythmic pattern described above (Figs. 1 and 2). Note that Fig. 4 shows the outputs of two different depressor neurons (a “fast” depressor Dep*f* and a “slow” depressor Dep*s*)

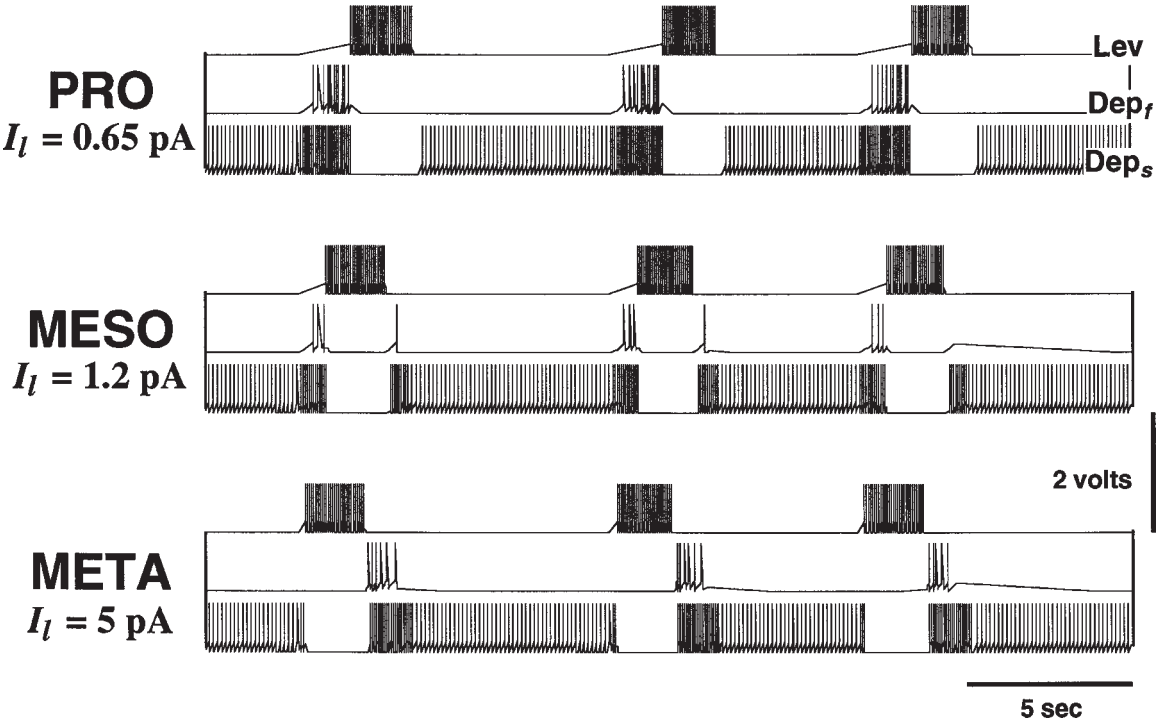

Figure 4. Results of the simulation of the model circuit shown in Fig. 3B using NeuraLOG/Spike. Shown are levator (Lev) and depressor (Dep) activities for three different values of I_l, the synaptic strength of the excitatory synapse from Drive to Lev (Fig. 3B). In this simulation, two different Dep neurons were simulated, one fast (Dep*f*) and one slow (Dep*s*). In the three sets of traces, the top trace is the output from Lev, the middle trace is the output from Dep*f*, and the bottom trace is the output from Dep*s*. Compare with Fig. 1 (Scale bars: 5 secs, 2 volts).

---

with different thresholds. The activities of these neurons differ only in that Dep*s* fires tonically in its resting state. Compare with the activities of the biological neurons *Df* and *Ds* (Fig. 1, lower traces).

If, on the other hand, I_l is stronger than I_d, Lev reaches threshold sooner than Dep. Once Lev begins to spike, Dep is inhibited. Only when Lev stops firing is Dep released from inhibition sufficiently to fire a burst of action potentials. This pattern, shown in Fig. 4 (META), is similar to the metathoracic rhythmic pattern described above and shown in Figs. 1 and 2. In order for Dep to fire a burst of action potentials

upon release from inhibition, it must receive sufficient excitatory input to drive it to threshold. This can be accomplished in this model circuit in either of two ways. (i) If Drive has a longer burst duration than Lev ($t > t_l$), Dep will continue to receive excitatory input from Drive once it is no longer being inhibited by Lev. This is a simple condition to achieve, since the burst durations of Drive and Lev can be controlled independently. If, however, the burst duration of Drive is set too long, Lev may be depolarized enough to generate another burst, leading to anomalous "double bursts" in the activity of Lev. (ii) In the simulation, the excitation to Dep was prolonged by making the time constant of decay of the excitatory current I_d very long. As a consequence, Dep is being depolarized by a persistent excitatory current for a certain time τ_d after the Drive burst terminates. The mathematical analysis shown in Appendix A is general enough to allow one or both of the conditions to hold.

For intermediate values of the synaptic strength I_l, Dep fires a burst of action potentials both before and after a burst of activity in Lev. This output is therefore similar to the mesothoracic rhythmic pattern (Figs. 1, 2, and 4).

Spike frequency histograms of the simulation output are shown in Fig. 5. This figure should be compared with Fig. 2, which shows the spike frequency histograms of electrophysiological data from locust thoracic ganglia. One difference between the figures is the shape of the levator spike frequency histogram. This histogram is bell-shaped in Fig. 2, whereas it is square in Fig. 5. This difference is mainly due to the different numbers of neurons whose activity is represented in the histograms. In Fig. 2, data was obtaining by pooling all of the trochanteral levator action potentials on nerve 4A, which included up to 10 motor neurons with different thresholds. As can be seen from Fig. 1, a trochanteral levator burst consists of

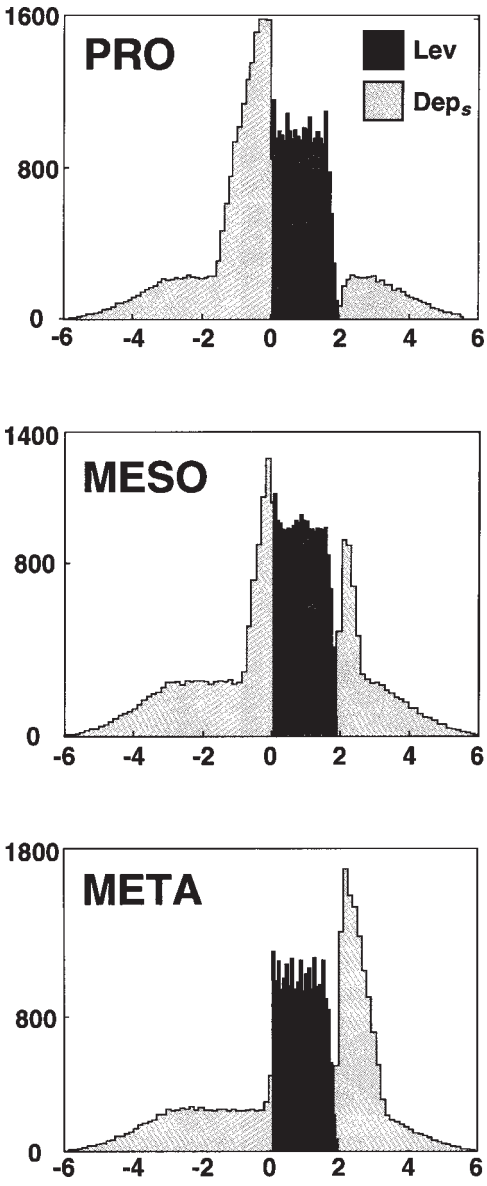

Figure 5. Spike frequency histograms of the simulated trochanteral levator and depressor neuron activities shown in Fig. 4. Data compiled from 238 periods of activity from single continuous output traces. The reference is the onset of a burst of trochanteral levator action potentials. The scale on the ordinate is the total number of action potentials in each bin, and represents a cumulative total for all 238 periods of activity that were analyzed. Compare with Fig. 2.

action potentials from many different motor neurons, with the largest number of neurons participating near the middle of a burst. In contrast, the simulation in Fig. 5 only included a single levator neuron (Lev). A similar bell-shaped distribution would be obtained by pooling the activities of many levator motor neurons driven by Lev, but with different thresholds.

In Fig. 2, substantial overlap between activities of the levators and depressors of the trochanter can be seen, particularly for the pro- and mesothoracic patterns.

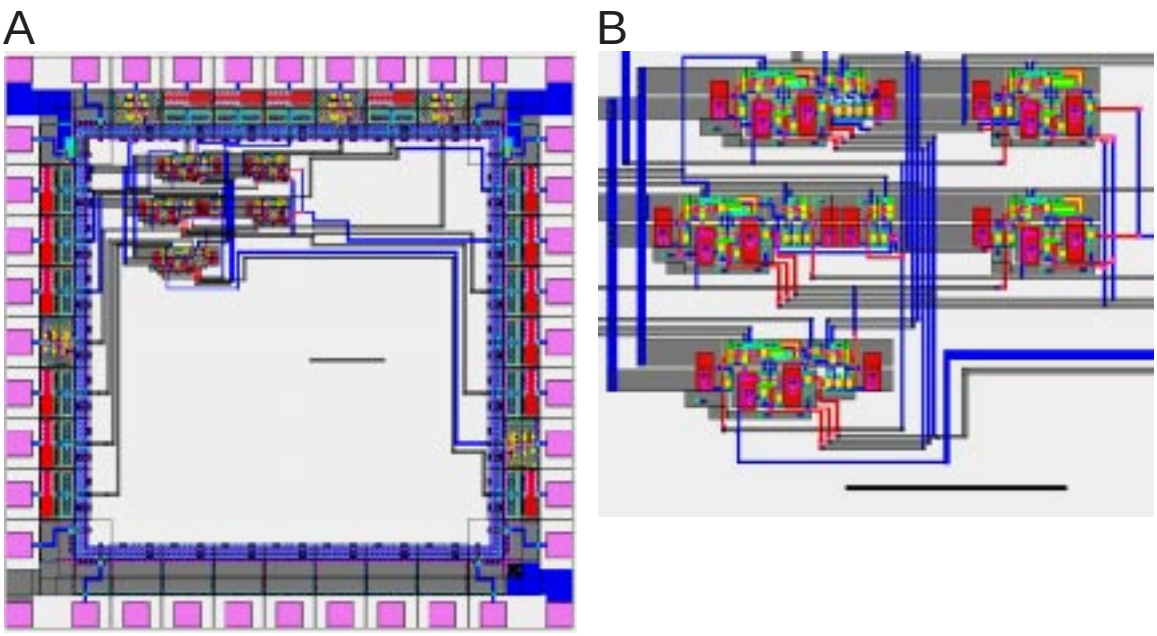

Figure 6. A VLSI implementation of the model circuit shown in Fig. 3. **A**. Graphical design of the entire chip, measuring 2 x 2 mm. The model circuit is in the upper left corner of the chip (Scale bar: 250 μm). **B**. Expanded view of a single non-bursting neuron circuit (Scale bar: 50 μm).

This overlap is much smaller in the simulation histograms in Fig. 5. Such overlap can be obtained in the simulation by weakening the inhibition between the levators and depressors, which would allow some co-activity between the antagonists (Fig. 3B).

VLSI Implementation

We designed, fabricated, and tested a VLSI implementation of the simulated model circuit described above (see Methods). Fig. 6A shows a picture of the entire VLSI chip layout, and Fig. 6B shows the depressor neuron layout. The electronic circuit implemented on the chip was essentially the same as the simulated circuit, since, as described in Methods, the circuit primitives used in the simulator were developed on the basis of existing electronic circuits. The different parameters in

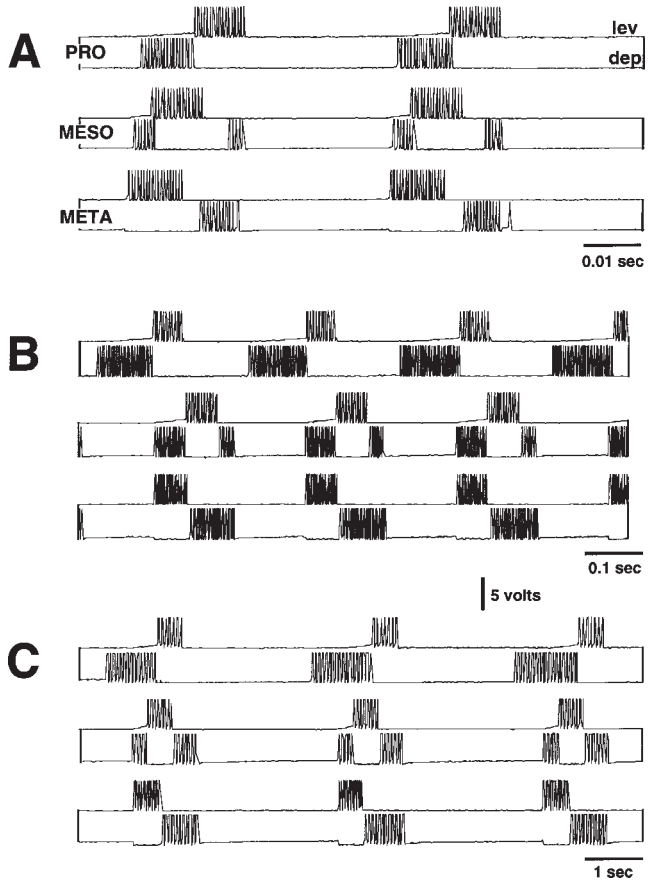

Figure 7. Output of the VLSI circuit. **A**. Output of electronic levator and depressor neurons for three different settings of the synaptic strength I_l (see Fig. 3). This synaptic strength is modified by changing the gate voltage on a single transistor. In the three sets of traces, top trace is output from a "levator" neuron and bottom trace is output from a "fast depressor" neuron. Compare with Figs. 1 and 4. **B-C**. Same figure as in A, except that the chip is operating at different time scales (note scale bars in A, B, and C). The circuit can operate over four orders of magnitude of frequency.

the model were represented as voltages which could be externally controlled. The synaptic strength I_l (Fig. 3B) was represented as a single voltage parameter. Fig. 7 shows voltage outputs of the chip operating at different frequencies. Fig. 7A, for example, shows the output from the levator and depressor drives for three different values of I_l. As was shown in the simulation (Figs. 4 and 5), as I_l is increased, the output of the circuit moves smoothly from a prothoracic (top) to a mesothoracic (middle), and finally to a metathoracic (bottom) rhythmic pattern. All other circuit parameters were unchanged. Figs. 7B and 7C show the same behavior as Fig. 7A, but at different time scales. In each case, the circuit parameters were adjusted for operation of the circuit at a given time scale, but only I_l was then modified to generate the pro-, meso-, and metathoracic rhythmic patterns. We verified that the chip can operate in a stable manner in the frequency range of 0.1 to 10OHz.

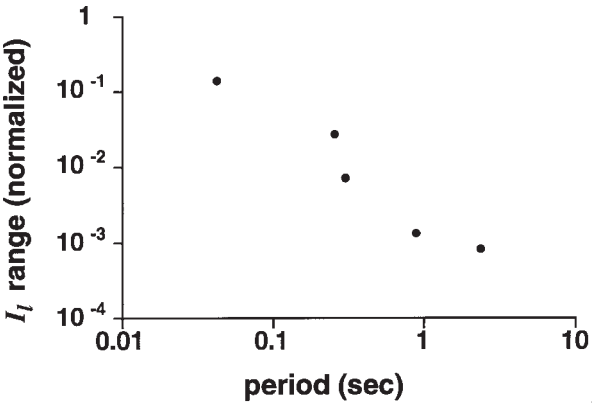

Figure 8. Range of the synaptic current I_l as a function of the period. The range of I_l is defined as the difference in synaptic current required to switch the circuit from a "prothoracic" rhythm to a "metathoracic" rhythm (I_l(meta) - I_l(pro)). Since the synaptic currents in the chip could not be measured, values of the currents were estimated from voltage measurements and normalized. The range was determined for five different time scales, represented on the abscissa as the period. Note that both the current range and the period are plotted on log scales. That the circuit is more stable at higher frequencies of operation (smaller periods) can be attributed to the larger ranges over which parameters can be modified at these frequencies.

The circuit was most stable (i.e., the operating range of circuit parameters was widest) at higher frequencies of operations. In an attempt to quantify the decreased circuit stability at lower frequencies of operation, we studied the operating range of a single parameter (I_l) for different time scales of circuit operation (Fig. 8). We chose the synaptic current I_l since it is this parameter that determines the output of the circuit model. For each frequency of circuit operation, we measured the amount by which I_l needed to be changed to switch from a prothoracic to a metathoracic pattern (defined to be the "range" of I_l). On the chip, I_l is determined by externally setting the voltage on the gate of a single transistor. Since the synaptic currents in the chip could not be measured, I_l was estimated from the gate voltage and was normalized. The range of I_l was determined for five different frequencies of circuit operation (Fig. 8). As can be seen in Fig. 8, the range of I_l decreased monotonically as the cycle period increased. This is because slow operation of the circuit is achieved by reducing all currents in the electronic circuitry. Therefore, excursions

in circuit parameters needed to switch between two states are correspondingly smaller. Since all of the currents in the circuit are smaller at lower frequencies, we would expect the operating ranges of all of the different circuit parameters to decrease in a similar way. This decrease in operating range of the parameters is closely related to the increased instability of the circuit at lower frequencies. When currents are very small, instabilities due to noise and device imperfections have a greater effect on circuit operation.

Mathematical analysis

We developed a simple theoretical analysis of the circuit model shown in Fig. 3B and described above. The mathematical details can be found in Appendix A. We computed expressions which describe the behavior of the circuit as I_l is varied. These expressions express the widths of the bursts of activity of depressor drives before and after a levator burst as functions of I_l (Fig. 9A). In Fig. 9A, we can see that the width of the depressor burst which precedes a levator burst (*w1*) decreases as I_l increases, and the width of the depressor burst which follows a levator burst (*w2*) increases as I_l increases. Different regions of the graph (shaded area, delimited by asymptotes) correspond to the production of pro-, meso-, and metathoracic rhythmic patterns. For small values of I_l, *w2* = 0 and the depressor activity precedes the levator activity. This corresponds to the prothoracic rhythm. For intermediate values of I_l, both *w1* and *w2* are greater than zero, and the depressor activity both precedes and follows a levator burst. This corresponds to the mesothoracic rhythm. For large values of I_l, *w1 = 0* and the depressor activity follows the levator activity. This corresponds to the metathoracic rhythm. In Fig. 9B, we show measured values of *w1* and *w2* from the output of the integrated circuit as I_l is varied. The solid lines are fits of the forms given by the theoretical expressions

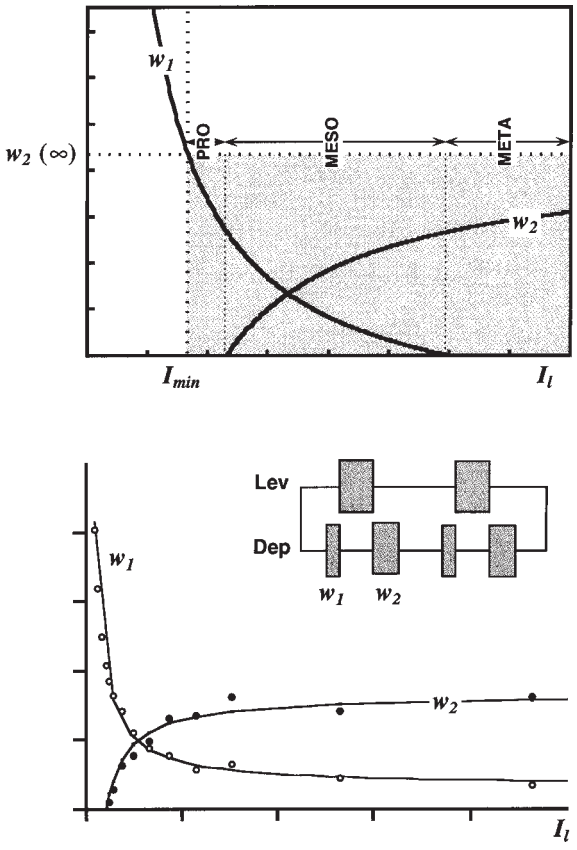

Figure 9. Comparison of chip performance and theoretical analysis. **A**. Graph of theoretical expressions for *w1* and *w2* (see Appendix and inset in Fig. 9B) as a function of the magnitude of I_l, the excitatory current from Drive to the levator motor pool driver (Fig. 3). Solutions lie within the shaded rectangle delimited by the asymptote *W2*(∞) and the constraint I_{min}. See Results and Appendix for details. **B**. Measured values of *w1* and *w2* from integrated circuit output, as a function of the current I_l. Solid lines are fits of the form given by the theoretical expressions derived in the Appendix and plotted in A. Because I_l was modified by changing a voltage on the integrated circuit, exact current values could not be determined. The current on the abscissa is therefore a normalized current.

for *w1* and *w2* (see Appendix A). Note that since I_l is controlled by a voltage, exact values of the current, I_l could not be determined. The abscissa therefore represents a normalized current.

Discussion

We have shown that pilocarpine induces rhythmic activity in leg motor neurons of isolated locust pro-, meso-, and metathoracic ganglia. The patterns recorded in the three ganglia differed in their sensitivities to pilocarpine, their frequencies, and the phase relationships of motor neuron antagonists. The different patterns we

observed could be generated by a simple adaptable model circuit, which was both simulated and implemented in VLSI hardware.

Locomotor rhythm generation in thoracic segments

Given that locomotor rhythms could be induced by pilocarpine in the isolated locust metathoracic ganglion (Ryckebusch and Laurent, 1993), it is perhaps not surprising that such rhythms could also be recorded in isolated pro- and mesothoracic ganglia. This result supports the idea that there exist distinct pattern generating circuits for leg movements in each thoracic ganglion or hemiganglion. This is in contrast to other insect central pattern generators (CPGs), such as those underlying flight and ventilation. The flight central pattern generator, which controls two sets of wings in the locust, is known to be distributed in both the meso- and the metathoracic ganglia (Robertson and Pearson, 1983; 1985; Robertson, 1986). It has been established that ventilatory rhythms are produced by a dominant central pattern generator in the metathoracic ganglion; indeed, respiratory rhythms recorded in the pro- and mesothoracic ganglia cease when the connectives to the metathoracic ganglion are sectioned (Farley et al., 1967; Miller, 1960, 1966, 1967).

Perhaps more surprising is our finding that the phases and frequencies of the evoked rhythms differ in the three thoracic ganglia. These differences in rhythmic patterns may reflect the intrinsic physical differences between the three pairs of insect legs. The front legs are oriented toward the front of the body, whereas the hind legs are oriented toward the rear. This implies that the intrinsic locomotor rhythms for these legs must differ, as the sequence of levator and depressor activity (protraction and retraction) would be different during a step. Cruse (1976) has found that the three pairs of legs in stick insects have different functions during

walking and the maintenance of posture. During horizontal walking, the foreleg has primarily a feeler function, while the middle leg has a supportive function and the hind leg has both supportive and propulsive functions. These roles can change, however, if the insect walks on a non-horizontal surface, which implies that individual segmental oscillators, already tuned in a segment-specific manner, in addition must have the capability of adapting their output in response to the changing functional role of the limb which they move.

Differences in intrinsic frequencies of the segmental rhythms might also be related to the morphological differences of the limbs. It has been observed in behavioral experiments that, during tethered walking, the insect hind leg can exhibit either 1:1 or 1:2 coupling with the front and middle legs (N. Hatsopoulos, personal communication; Graham 1978a,b); i.e., the front and middle legs occasionally make two steps for one step of the hind leg. Since the hind leg is longer than the front or middle legs, it compensates for a missed step by making a larger amplitude step at the next cycle. That the step frequencies of the hind leg are lower than those of the front and middle legs in walking animals is consistent with the finding that locomotor patterns recorded from isolated metathoracic ganglia are slower than those produced by the pro- and mesothoracic ganglia. Several models of insect walking have in fact proposed an anterior-posterior gradient of frequencies for the thoracic segments, with the hind segment having the lowest intrinsic frequency (Wilson, 1966; Graham, 1977; reviewed in Graham, 1985). Such a frequency gradient appears to be necessary to produce appropriate phase lags and coupling between the legs, and can also explain the occasional absences of rear leg protractions. It will be interesting to study the patterns of activity of the other motor neuron pools such as the tibial and tarsal motor neurons and compare them to the corresponding metathoracic patterns (Ryckebusch and Laurent, 1993). We already established,

however, that the phase relationships between trochanteral antagonists are tuned in a segment-specific manner.

Adaptable neural circuits

Our basic assumption in designing a model pattern generating circuit was that the locomotor circuits in segmentally homologous thoracic ganglia were likely to be very similar, despite the different rhythmic output patterns they generated. In the model we devised, the output pattern could be switched between those characteristic of the pro-, meso-, and metathoracic ganglia by modifying a single synaptic coupling parameter in the circuit. There are now numerous examples of biological pattern generating circuits which can produce several rhythmic patterns: the pyloric and gastric mill rhythms in the stomatogastric system of crabs (Weimann et al., 1991); withdrawal and swimming in *Tritonia* (Getting and Dekin, 1985), forward and backward scaphognathite beating in crabs (Simmers and Bush, 1983); jumping and kicking in the locust (Gynther and Pearson, 1989), to name only a few. In some of these systems, the switch from one pattern to another is accomplished under the action of a neuromodulator which alters cellular and synaptic properties of the circuit elements. For example, the crustacean gastric mill motor pattern can be switched from “squeezing” to “cut-and-grind” mode under the action of the peptide proctolin (Heinzel and Selverston, 1988; Heinzel, 1988). Although in most systems the detailed mechanisms by which neuromodulators alter circuit properties are not known, the modification of a synaptic strength to alter circuit dynamics has been demonstrated in the crustacean stomatogastric nervous system, where application of the peptide proctolin potentiates the inhibitory synapse from the inferior cardiac (IC) neuron to the gastric mill (GM) neurons, causing the GM neurons to switch from a gastric to a pyloric pattern of activity (Weimann, 1992).

Although any biological pattern generator is likely to be far more complex than the simple model which we have designed, some of the mechanisms we propose could be imbedded in a larger neural circuit. Some simple central pattern generator circuits, such as that underlying feeding in the snail *Lymnaca stagnalis* (Benjamin and Elliott, 1989) have been shown to use mechanisms similar to those employed by our model circuit. The Slow Oscillator (SO) in *Lymnaea* plays a role much like that of Drive in our model circuit. SO initiates, maintains, and controls the frequency of the snail feeding pattern, provided it receives a constant depolarizing input. SO is the primary source of excitatory drive to a small network of interneurons forming the central pattern generator, which in turn provides the drive to a set of buccal motor neurons. The interneurons (Nl, N2, and N3) which form the core of the central pattern generator produce rhythmic output as a result of their intrinsic properties (e.g., endogenous bursting, postinhibitory rebound, plateau potentials) as well as their synaptic connections. Nl and N2 form a network reminiscent of the design of our two-neuron “bursting” neuron, with slow excitation from Nl to N2 and delayed inhibition from N2 to Nl. N3 is first inhibited by Nl, and then produces a postinhibitory burst of action potentials, which is similar to the Lev-Dep interaction in our model network.

Design of realistic walking robots

The VLSI implementation of the model circuit we designed operated robustly over 4 orders of magnitude of frequency, despite physical constraints such as noise and device imperfections. The chip exhibited the behavior predicted by theoretical calculations and computer simulations. Because a complete understanding of biological sensory-motor systems requires an understanding of the real-world context

within which they operate, physical models of biological circuitry can be valuable tools for the neurobiologist. Designing physical devices such as sensory systems and mechanical actuators that interact with the real world need not be the exclusive domain of the engineer. Physical devices such as walking robots could provide biologists with a platform on which to test ideas about the design of biological circuitry. We will use such techniques, for example, to explore the intersegmental coupling between thoracic locomotor circuits, as well as the role of sensory information in shaping motor outputs. We believe that such an interdisciplinary approach will help to uncover the design principles of the biological circuit, while at the same time allowing the design of more adaptable walking robots.

Acknowledgments

Supported by grants from NIH and ONR to GL. GL is a Searle, Alfred P. Sloan, and McKnight scholar. SR was supported by fellowships from AT&T, ONR, and an NIH Training Grant. MW was supported by an ONR fellowship. We would like to thank Dr. Ari Berkowitz, Dr. Nicho Hatsopoulos and Christine Chee-Ruiter for their thoughtful comments on previous drafts of this manuscript; and Drs. Lloyd Watts and Nicho Hatsopoulos for useful discussions. We are particularly indebted to Dr. Lloyd Watts for incorporating many useful features in Spike and NeuroLOG during the course of this work, and to Dr. Carver Mead for providing support and laboratory space.

Appendix *i*: A mathematical description of the levator-depressor model

Variables

C: Capacitance of neurons

V_T: Neuron spike threshold

I_l: Magnitude of excitatory synaptic current from Drive to Lev

I_d: Magnitude of excitatory synaptic current from Drive to Dep

I_{ld}: Magnitude of inhibitory synaptic current from Lev to Dep

τ_d: Duration of synaptic current from Drive to Dep

$w1$: Duration of Dep burst preceding Lev burst

$W2$: Duration of Dep burst following Lev burst

t: Duration of Drive burst

t_l: Duration of Lev burst

Assumptions

1. The excitatory synapse from Drive to Dep is strong (I_d is large). We assume that $I_d >> I_l$ for the pro- and mesothoracic solutions.

2. Inhibition of Dep by Lev is stronger than the excitatory drive to Dep ($|I_{ld}| > I_d$).

3. The synaptic current I_d persists for a time t_d. All other synaptic currents decay quickly.

Derivations

Given the above assumptions, one can derive the following expressions for *w1* and *W2* :

$$W1 = \frac{CV_T}{I_l} - \frac{CV_T}{I_d} \qquad (1)$$

$$W2 = t + \tau_d - t_l - \left(\frac{CV_T}{I_l} - \frac{CV_T}{I_d}\right) \qquad (2)$$

We can see from (2) that $w2 > 0$ if t or τ_d are sufficiently large, as was described above (see Results). $t > t_l$ if the Drive burst is longer than the Lev burst. That τ_d is large is the same as saying that the excitatory drive to Dep has a slow time constant of decay. One or both of these conditions need to be true to obtain a positive value for *w2 .*

Constraints

For this circuit to operate in the desired range, the current I_l must satisfy the following constraint, represented graphically in Fig. 9A by a vertical dashed line:

$$I_l > I_{min} = \frac{CV_T}{t} \qquad (3)$$

This constraint expresses the requirement that the time needed for Lev to charge its membrane to threshold must be less than *t*, the duration of the Drive burst.

If $I_I < I_{min}$ **,** Lev will remain silent, and Dep will receive excitatory input from Drive but no inhibition.

Asymptotes

$$W2(\infty) = \lim_{I_I \to \infty} W2 = t + \tau_d - t_l + \frac{CV_T}{I_d} \qquad (4)$$

$$\lim_{I_I \to \infty} W1 = -\frac{CV_T}{I_d} \qquad (5)$$

Solutions of interest

1. Prothoracic solution (*w2* = 0)

This solution will occur when

$$I_{min} < I_I < \frac{C V_T}{t - t_l + \tau_d} \qquad (6)$$

The solution only exists when $t_l > \tau_d$ (i.e., if the duration of a Lev burst is longer than the duration of the excitatory drive to Dep).

2. Mesothoracic solution ($w1 > w2$)

$$\frac{C\,V_T}{t - t_l + \tau_d} < I_l < \frac{2\,C\,V_T}{t - t_l + \tau_d} \qquad (7)$$

3. Mesothoracic solution ($w1 \leq w2$)

$$\frac{2\,C\,V_T}{t - t_l + \tau_d} \leq I_l < I_d \qquad (8)$$

4. Metathoracic solution ($w1 = 0$)

This solution will occur when $I_l \geq I_d$.

Appendix *ii*: An alternative design for the bursting neuron using summating synapses

We describe here an alternative design for a bursting neuron using new features recently incorporated in the NeuraLOG/Spike simulator. In the earlier version of the simulator, synaptic events consisted of square pulses of "neurotransmitter" with a fixed amplitude and duration (see Methods). These events did not summate; i.e., if two presynaptic action potentials occurred in close succession, the amplitude of the "neurotransmitter" released at the synapse as a result was no greater than that caused by a single action potential. The only effect of a presynaptic train of action potentials was to prolong the duration of the presence of "neurotransmitter" in the "synaptic cleft." The design of a bursting neuron as a two-neuron circuit was a direct consequence of this limitation of the simulator. Indeed, to build a neuron capable of slow membrane potential oscillations, a mechanism is needed for storing the "history" of the activity of the neuron. In biological neurons, this can be accomplished by the accumulation of intracellular calcium caused by the generation of action potentials. The intracellular calcium concentration is a representation of the time integral of the spiking history of the neuron. In the bursting neuron circuit described above (see Fig. 3A and Results), cell 2 was used to store information about the activity of cell 1. Repeated action potentials from cell 1 led to the gradual depolarization of cell 2. A new feature of NeuraLOG/Spike allows the "neurotransmitter" at a "synaptic cleft" to summate. If a second action potential occurs before the end of the pulse of "neurotransmitter" due to the first action potential, the net amount of "neurotransmitter" during that time will be twice as large. In addition to the magnitude and duration of a synaptic event, the number of pulses which can be summated (i.e., the maximum amount of neurotransrnitter in the synaptic cleft) can now also be specified as parameters in the simulator. This new feature allows

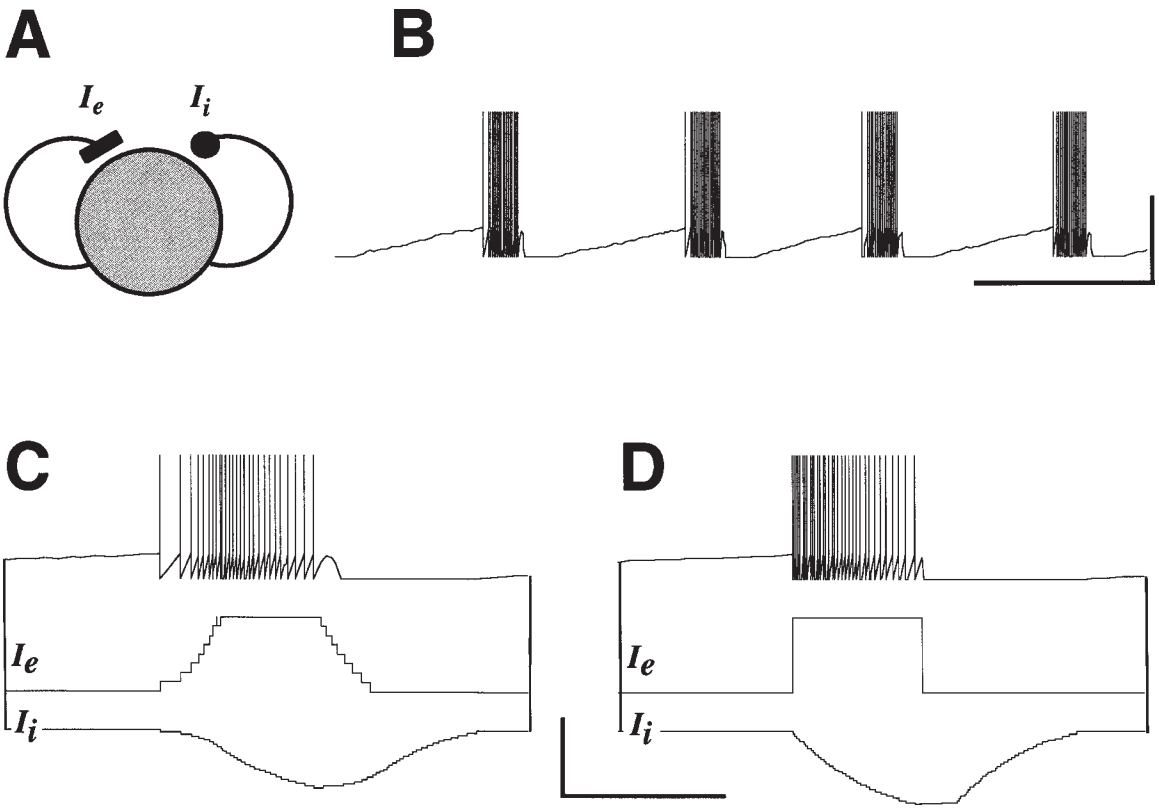

Figure 10. An alternative model for the bursting neuron. **A**. Using an improved synapse model (see Appendix B), a bursting neuron can be represented by a single neuron with excitatory and inhibitory feedback conductances. **B**. Output of the bursting neuron in response to a constant excitatory input, simulated using NeuraLOG/Spike (Scale bars: 1 volt, 10 sec). **C-D**. Expanded view of a single burst (top trace), excitatory (middle), and inhibitory (bottom) feedback currents for different characteristics of the excitatory feedback current I_e, as described in Appendix B (Scale bars: 1 volt, 2 sec). Note that, here, different firing patterns *within* a burst can be achieved by changing the properties of the excitatory feedback I_e.

---

a bursting neuron to be implemented by a single “neuron” circuit (Fig. 10A) with excitatory and inhibitory feedback conductances. When the neuron has reached threshold in response to an excitatory current input, it will begin to fire action potentials at a rate determined by the characteristics of the excitatory feedback in much the same way as the previous bursting neuron circuit (Fig. 3A). While the neuron is

firing, a slow feedback inhibition builds up. The summating property of the synapse allows the inhibition to slowly increase during the course of the burst. As the cumulative inhibition increases, the frequency of action potentials decreases until the neuron eventually stops firing (Fig. 10B). The firing frequency of the neuron during a burst thus depends on the interaction between the excitatory and inhibitory feedback. Figs. 10C and D show how the characteristics of a burst can be modified by changing the excitatory feedback conductance. If this excitatory feedback is small and slowly increasing, the firing frequency of the neuron will increase during the burst, reach a peak, and then decrease again (Fig. 10C). If, on the other hand, this excitatory feedback very quickly reaches its maximum amplitude, the firing frequency of the neuron will be highest at the beginning of a burst, and will slowly decrease during the course of a burst (Fig. 10D). Although the ability of NeuraLOG/Spike to simulate summating synapse makes it possible to simulate much more sophisticated circuits, this new feature will currently not be useful to the VLSI chip designer who uses NeuraLOG/Spike to develop hardware models, since there does not yet exist a VLSI circuit implementation of the summating synapse.

Appendix B: Simultaneous Paired Intracellular and Tetrode Recordings for Evaluating the Performance of Spike Sorting Algorithms

Preface

This paper is also unrelated to the work described in the main body of the thesis. It arose out of a collaboration with John Pezaris and Maneesh Sahani, and will appear in Wehr et al. (1998).

Abstract

Understanding the function of neural ensembles is increasingly recognized to require simultaneous recordings from multiple neurons. One technique for recording from several neurons at once is multiunit recording, in which the signal from an electrode contains spike waveforms from multiple neurons. This approach requires the use of a spike sorting algorithm to assign each spike waveform to a candidate source. Evaluating the performance of spike sorting algorithms requires *a priori* knowledge of the "right answer": the correct classification for a given multiunit recording. Intracellular recording can unambiguously assign spikes to a single neuron, thus providing the correct classification if signals from that neuron simultaneously appear in a multiunit recording. Further, paired intracellular recording from two neurons appearing in a multiunit recording allows the unambiguous resolution of spike waveform overlaps. We present here a data set consisting of single and paired intracellular recordings from neurons which were concurrently recorded on a tetrode. We use this data to evaluate currently used spike sorting algorithms for isolated as well as overlapped events. In addition, these data are used to address

the following fundamental questions about the properties of extracellularly recorded waveforms: Do extracellular spikes combine additively, so that an overlapped event is the simple superposition of the two component events? Can the spike-to-spike variability of the action potential shape from a given cell be quantitatively described? Independent intra- and extracellular observations of the same spiking neuron allow us to address these questions directly.

Until recently, the function of neural assemblies was typically inferred from repeated recordings of single neurons. This inference depends critically on the assumption that time-dependent interactions between neurons can be neglected. With the advent of electrophysiological techniques for simultaneously recording from multiple neurons, many groups have found evidence for temporal interactions between neurons (Gray, 1994; Nicolelis et al., 1997; Singer and Gray, 1995). This suggests that in order to understand the function of neural ensembles, simultaneous recording from multiple neurons is crucial.

Many types of electrodes can record action potentials simultaneously from multiple neurons. It is, however, difficult to unambiguously assign each waveform to a distinct neuron. For example, a conventional metal electrode placed in neural tissue can often record spikes from several neurons, but the spike waveforms from these cells may appear quite similar, hampering the task of identifying the source for each spike. Several algorithms have been devised to solve this spike sorting problem. Some methods extract characteristic parameters from each spike, such as height and width, and then search for distinct clusters in the parameter space, while others use the entire spike waveform (Fee et al., 1996) and include explicit noise models (Lewicki, 1994).

Particularly troublesome are overlapping waveforms generated when two neighboring neurons fire near enough in time that the individual action potential waveforms interfere at the single recording site. Some algorithms attempt to resolve these overlaps, for example by subtracting candidate spike waveforms and searching for remaining candidates. Other spike sorting algorithms merely discard overlap events.

Multiwire electrodes, such as tetrodes (Recce and O'Keefe,1989), offer significant advantages in addressing the spike sorting problem (Fee et al., 1996; Sahani et al., 1998a,b; Gray et al., 1995). These electrodes, essentially bundles of fine wires, use close-packed recording sites to generate multiple views of the electrical landscape at the electrode tip. A cell which is closer to one site will produce a larger waveform on that site than at other, slightly more distant recording sites. Since each cell has a unique spatial position, and thus a unique pattern of distances to each recording site, each neuron should in principle have a characteristic pattern of waveforms across the multiple channels. All that is required is an algorithm for decoding the four tetrode signals into the spike trains of the different neurons that were recorded. Several such algorithms have been devised; these face many of the same challenges as single electrode spike sorting algorithms.

Evaluating the performance of a spike sorting algorithm, whether for single electrodes or for tetrodes, requires that we know the "right answer." Running a spike sorting algorithm on a multiunit recording will produce inferred spike trains from some inferred number of neurons. In order to know how well an algorithm is doing, one must have access to the true spike trains to see if and how they differ from the output of the algorithm. Knowledge of the true spike trains is essential for

developing an algorithm or for comparing its performance to that of other algorithms.

Currently this type of performance evaluation is done using synthetic data sets, so that the right answer is known *a priori*. Synthesizing such a data set requires assumptions, such as how the signals add *in situ*, how the noise adds, and what the distributions of noise and spike waveform shapes are, among others. These assumptions may in fact overlap with those on which the spike sorting algorithms themselves depend. Thus synthetic data sets are not suitable for testing the validity of these assumptions, and are perhaps not optimal for evaluating the performance of spike sorting algorithms.

To test these assumptions directly, and thereby objectively evaluate the performance of a spike sorting algorithm, we need real data (multiunit recordings) for which we know the right answer. Intracellular recording can provide the membrane potential of a single neuron, and thus the right answer: unambiguous assignment of spikes to a known neuron. Thus one could determine one of the true spike trains in a tetrode recording by simultaneously recording intracellularly from one of the neurons which is being recorded by the tetrode. This holds equally well for single electrode multiunit recordings, which can be considered as a special case of tetrode recordings (in which three of the four signals are discarded). Resolution of spike waveform overlaps requires the identity and spike times of both neurons involved (at least for two-spike overlaps). This requires simultaneous intracellular recording from two of the neurons appearing on the tetrode signal.

Two other yet unanswered questions are also addressed here. Existing algorithms for the decomposition of spike overlaps depend critically on the assumption

of linearity, but the linearity of overlaps remains untested. Do extracellular spikes combine additively, so that an overlapped event is the simple superposition of the two component events? A second question regards intrinsic spike waveform variability. Can the spike-to-spike variability of the extracellular action potential shape from a given cell be quantitatively described? Only with spikes independently known to arise from a single neuron can this variability be characterized.

Methods

The preparation: Experiments were carried out *in vivo* on adult female locusts (*Schistocerca americana*). Animals were restrained dorsal side up, the head was immobilized with beeswax, and a watertight beeswax cup was built around the head for saline superfusion. A window was opened in the cuticle of the head capsule, between the compound eyes, and air sacs on the anterior surface of the brain were carefully removed. For stability, the esophagus was sectioned anterior to the brain, and the gut was removed through a distal abdominal section which was subsequently ligatured. The brain was treated with protease (Sigma type, XIV), gently desheathed, and supported with a small metal platform. The head capsule was continuously superfused with oxygenated physiological saline (in mM: 140 NaCl, 5 KCl, 5 $CaCl_2$, 4 $NaHCO_3$, 1 $MgCl_2$, 6.3 HEPES, pH 7.0) at room temperature.

Electrophysiology: Intracellular recordings were made using conventional sharp glass microelectrodes pulled with a horizontal puller (Sutter P-87), which were filled with 0.5 M KAc and with DC resistances of 100-300 MΩ. Intracellular recordings were done in bridge mode using an Axoclamp 2A amplifier (Axon Instruments) from the third optic lobe (lobula). Data are based on 28 single neuron intracellular re-

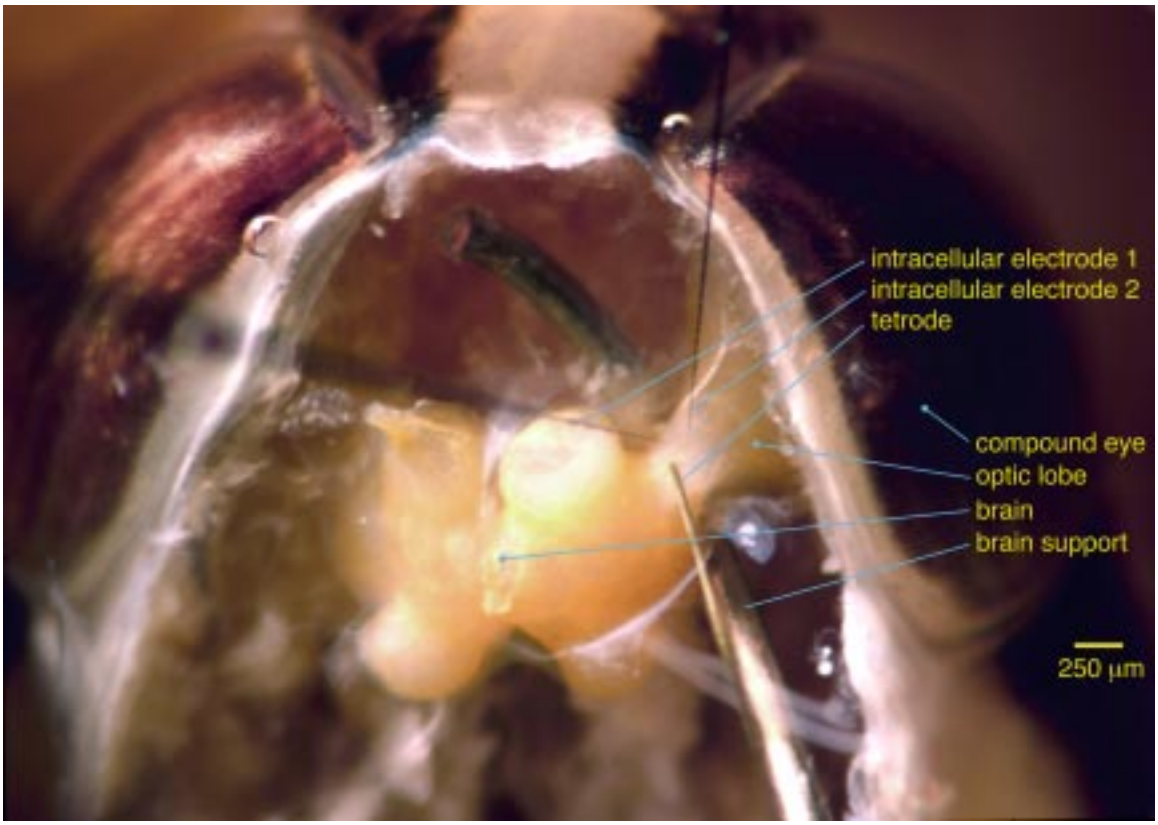

Figure 1. Photomicrograph of locust head capsule taken directly following a recording session.

cordings, and 6 paired intracellular recordings, from 7 animals. Tetrode recordings were made using 4 strands of 15 μm tungsten wire with FormVar insulation (California Fine Wire) twisted at ~10 turns/cm, which had impedances of 0.4-0.7 MΩ at 1 kHz. The tip was freshly cut at an acute angle using fine surgical scissors before each penetration. Tetrode recordings were done in the lobula, 50-100 μm medial to the site of intracellular recordings (see Figure 1). Recordings were made of spontaneous activity under these conditions for up to 15 minutes at a time. The retinotopic organization of the insect optic lobes, combined with the existence of large integrative neurons in the lobula, allowed simultaneous intracellular impalement of tetrode-recorded neurons at distances of up to a hundred microns from the tetrode tip.

Data acquisition: All signals were amplified and low-pass filtered at 10 kHz (tetrode signals were additionally high-pass filtered at 0.1 Hz) using an 8-pole analog Bessel filter (BrownLee Precision), digitized at 50 kHz with 16-bit resolution (Tucker Davis Technologies), and stored on the hard disk of an IBM-compatible PC. The continuous voltage recordings were processed off-line using in-house packages written for Matlab. The recordings were digitally high-pass filtered at 250 Hz and events were obtained by threshold detection on either the tetrode or intracellular signals only. The peak values for each event were extracted and clustered using established Expectation-Maximization (E-M) techniques (for details on the sorting algorithm used, see Sahani et al., 1998a,b). For details on covariance analysis, principal components analysis, and non-stationary components analysis, see Wehr et al. (1998).

Results and discussion

Figure 2 shows an example of simultaneously recorded traces from this experiment. Tetrode channels T1-4 are displayed at the top, and intracellular channels I1 and I2 are displayed underneath. This shows a typical tetrode recording where each of the large spikes appears across the four channels with a characteristic amplitude signature, with the simultaneous intracellular recordings shown in the two lower traces. The tetrode recording contains signals from (at least) four identifiable cells, two of which were impaled with the intracellular electrodes. This recording will be used as a running example for the remainder of this paper. Figure 3 shows the spike-triggered average waveforms of the six channels, triggered on each of the two intracellular channels. This reveals the tetrode waveform associated with action potentials from the two impaled cells shown in Fig. 2.

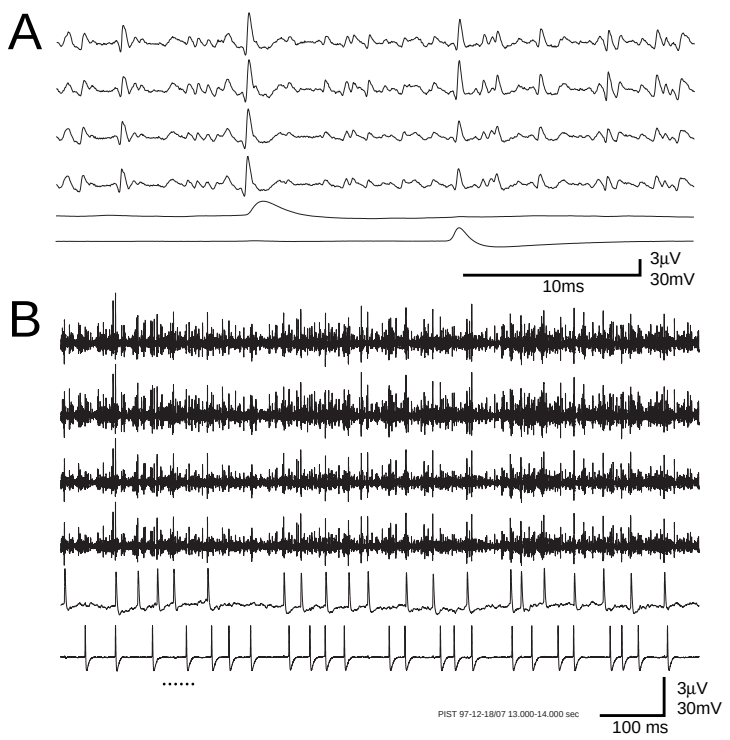

Figure 2. Example of simultaneously recorded raw traces. **A** is an expanded view of the region in **B** indicated by the horizontal dotted line below. In both **A** and **B**, the top four traces (T1-T4) are the four tetrode extracellular voltages, the bottom two traces (I1, I2) are the two intracellular voltages. The intracellular traces are unfiltered (except for anti-alias filtering at 10 kHz) to demonstrate their raw waveforms. Note that intracellular records in following figures are high-pass filtered at 250 Hz to facilitate accurate event detection, resulting in waveforms uncharacteristic of intracellular records. Based on the spike amplitudes, rising phase shapes, after-hyperpolarization amplitude, and synaptic background, I1 was likely impaled in a distal dendrite far from the spike initiation zone, whereas I2 was likely impaled in a primary neurite relatively near the spike initiation zone.

Spike sorting performance

We used these data to measure the performance of a spike-sorting algorithm based on maximum likelihood techniques (Sahani et al., 1998a,b). The algorithm consists of two stages. In the first stage, heuristics and robust fitting techniques were used to define clusters of events that belong to a single cell (for details see Sahani et al., 1998a,b). We did not attempt to exhaustively classify all spikes at this stage, and specifically rejected overlapped events.

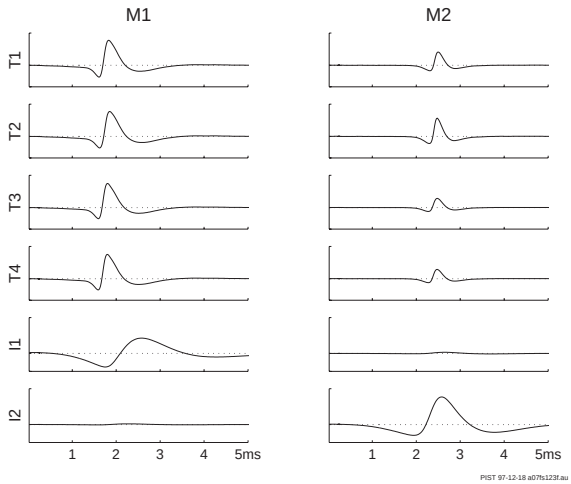

Figure 3. Spike-triggered average waveforms of the six channels, triggered on each of the two intracellular channels. M1 and M2 are the means of I1 and I2 events, respectively. The apparent phase delay between the extra- and intracellular signals is likely due to the high impedance of sharp glass microelectrodes.

Figure 4 shows the results of a clustering run. The models were fit in the eight-dimensional principal subspace. The data are plotted in the space of event peaks (Fig. 4a), and the optimal four-dimensional linear discriminant space (Fig. 4b). The dark green cluster (which corresponds to an impaled cell in this recording) would be difficult to isolate by hand, i.e., the cluster is not well isolated in Fig. 4a. The coordinate transformation which results in Fig. 4b, however, optimally isolated the clusters and shows good separation for the dark green cluster.

At the clustering stage we were most interested in the purity of each cluster. Two clusters corresponded to impaled cells (blue and dark green ellipses in Fig. 4). The blue cluster contained 862 spikes of which 831 (96.3%) came from a single cell (verified intracellularly). Only three additional spikes from that cell (0.4%) were misassigned to other clusters. The dark green cluster contained 190 events with 183 (96.3%) of these from the other impaled cell. Ten spikes from this cell (5.5%) were misassigned.

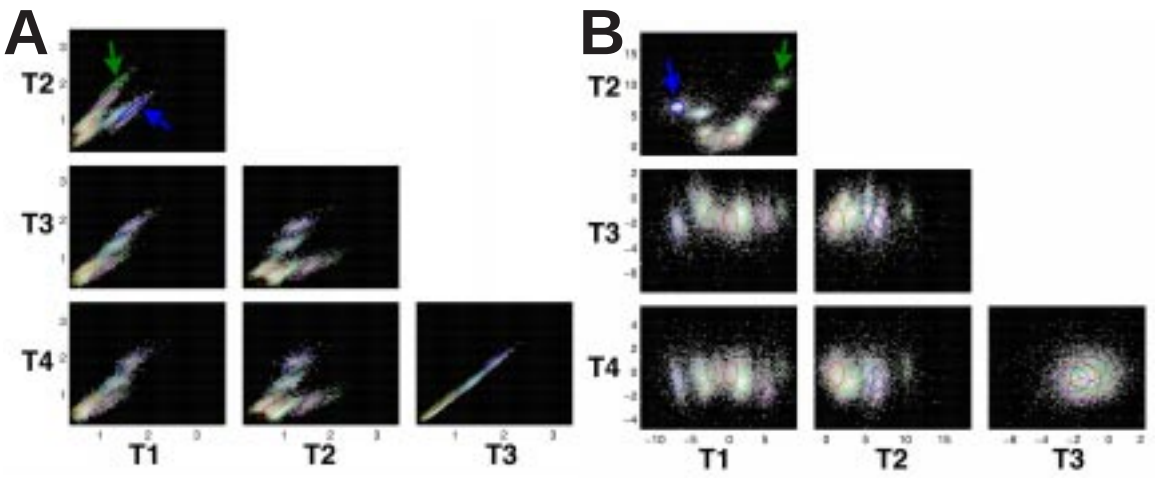

Figure 4. Clustergram plots of sorting output. The ellipses indicate fits generated from cluster analysis of the first eight principal components. The blue and dark green clusters (indicated by arrows) correspond to the impaled neurons. **A:** Action potential peak heights for each tetrode channel T1-T4 plotted against each other. Axes are in scaled volts. **B:** The same data transformed to the optimal four-dimensional linear discriminant subspace. This representation improves the discriminability of clusters. Axes are in arbitrary units.

At present we have not performed a strong test of the second stage of our sorting procedure due to difficulties with suitable decorrelation (whitening) of the signal. (Some features of the noise distribution in these data are different from those used to develop the sorting algorithm, which were recorded in primate parietal cortex). Note that this stage includes decomposition of overlap events. A preliminary run on unwhitened data was performed to detect spikes belonging to the blue cluster. There were a total of 1052 such spikes (taken from the intracellular data). Of these 999 were correctly detected (95.0%), however 124 additional spikes were incorrectly grouped in with these (11.8%). Such false-positives are likely to be reduced once the filtering procedure is correctly applied.

Linearity of overlaps

Do events overlap additively? That is, given two neural sources, do the signals combine linearly when recorded through an extracellular probe? To our knowledge the linearity of extracellular signals remains untested. The answer to this question is important because it determines if and how overlaps are decomposable.

For simplicity, consider the case where each of two cells fires exactly once. Figure 5a shows an overlap event between spikes from each impaled cell. If spike waveforms combine additively, we should be able to reconstruct the recorded overlap by taking the sum of the two waveforms recorded independently. Mathematically, this is expressed as follows:

$$v(t) = v_1(t-\tau_1) + v_2(t-\tau_2)$$

Where v is the observed voltage, v_1 is the voltage due to the spike from one cell, v_2 the voltage due to the spike from a second cell, and τ_1 and τ_2 are the firing times of the two cells.

Since spikes are short, we know that the equation above is true when τ_1 and τ_2 are very different. But what about when $\tau_1 \approx \tau_2$?

To experimentally verify the equation, we estimated v_1 and v_2 by averaging all events identified from intracellular traces I1 and I2, respectively (taking advantage of the assumption that $v_i(t) = 0$ for $t \neq 0$. We passed the intracellular voltages I1 and I2 independently through threshold detectors, sampled all 6 channels for 5 ms at

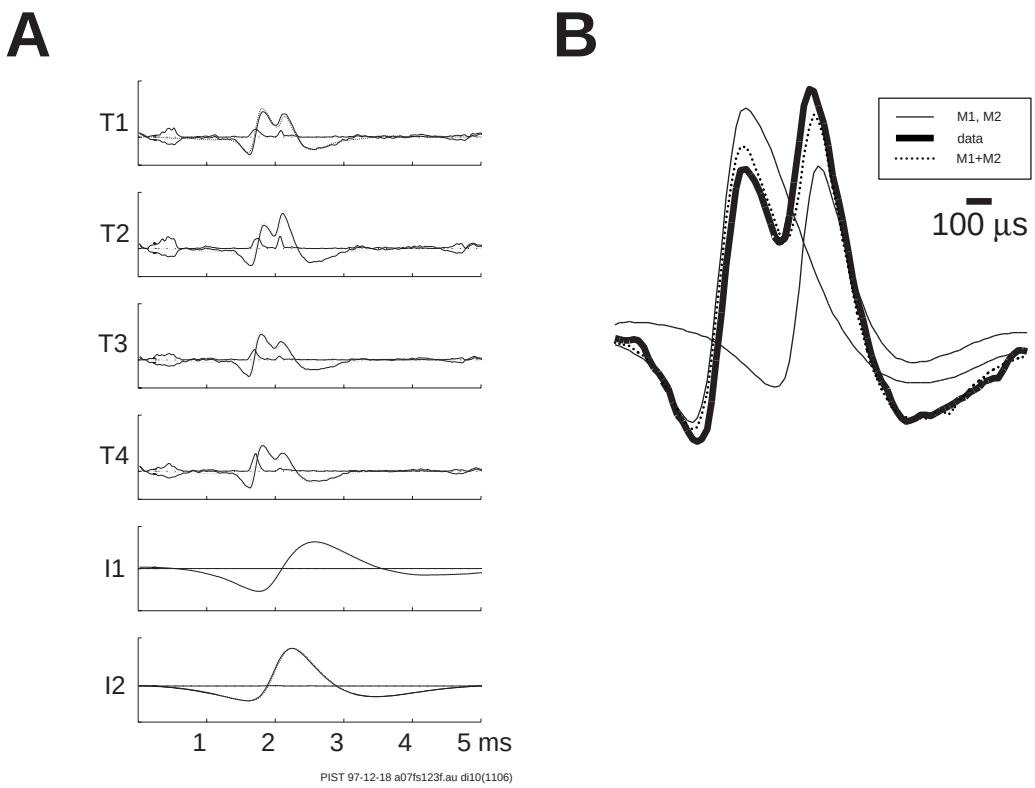

Figure 5. Spike waveform overlap. **A:** Overlap event seen across all six channels (heavy lines). T1-T4 are the tetrode channels and I1-I2 are the two intracellular recordings. The voltage predicted by additive combination is shown by dotted lines. Scaled square error between the actual and predicted voltage is shown by fine lines. **B**: Expanded view of T2, with the spike-triggered average from each neuron (M1 and M2, appropriately time-shifted) shown in fine lines, the recorded overlap shown by the heavy line, and the voltage predicted by additive combination (i.e., M1+M2) shown by the dotted line.

---

each crossing, and averaged over events. From these, we computed M1, the mean of all I1 events, and M2, the mean of all I2 events. These spike triggered averages are shown in Figure 3. By using the means, we assumed that the influence of any external interference was time-independent and evenly positive and negative, and therefore the mean reflected the underlying signal. Then, we selected the instances when the two cells fired at nearly the same time, and compared the actual record-

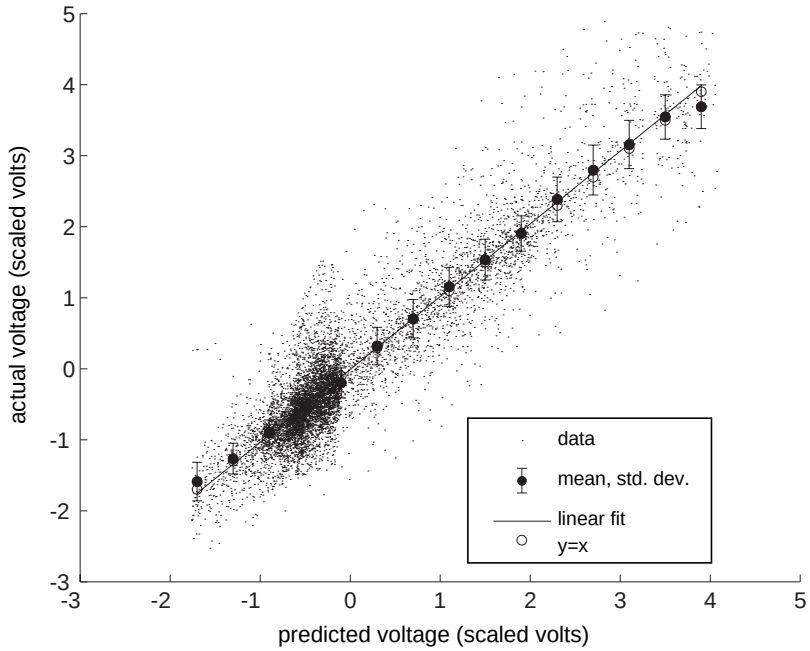

Figure 6. This plot shows, on a sample-by-sample basis for one channel, the values predicted by adding the two models M1 and M2 together with the appropriate time shift (as shown in Fig 5b), against the actual values seen for the 88 overlapped events in this recording. The solid line is the best linear fit to the points; the open circles show unity-slope; and filled symbols are the means and standard deviations for the data as partitioned along the horizontal dimension. The linear fit for this channel (T2) of our running example has a slope of 1.025 and an intercept of -0.01.

---

ing around these events to the sum of M1 and M2 shifted appropriately as determined by the intracellular signals. The results are depicted in Figs. 5-6. The predicted waveform (dotted lines in Fig. 5a) closely matches the actual waveform (heavy line). Fig. 5b is a closeup of one channel showing the components from each model (fine lines), their sum (dotted line), and the actual data (heavy line). For additively combined spikes, we would expect the simple sum of the models to accurately predict the shape of overlap events. Actual voltage is shown as a function of predicted voltage in Fig. 6, demonstrating that the additive prediction is valid

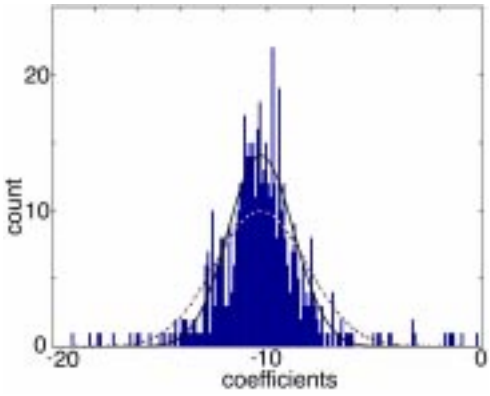

Figure 7. Histogram of first principal component coefficients. The dotted line is a Gaussian fit to the data, and the solid line is a fit with a combination of a Gaussian and a uniform distribution to describe the outliers. Non-spike noise appear to be Gaussian distributed.

across the entire voltage range. The region of increased density near 0 (baseline voltage) does not correspond to increased variance, as shown by the standard deviations (filled symbols) which were nearly constant across the entire voltage range. The increased density near 0 is a simple consequence of the voltage spending proportionally more time near that value (see Fig. 5a). The error distribution was the same across all voltages. This demonstrates that the actual value seen during overlaps closely matched the sum of shifted non-overlapped signals within experimental noise. We conclude that overlapping extracellular waveforms behave linearly.

Spike waveform variability

We selected all tetrode events associated with a single impaled cell and examined the resulting noise distribution. We aligned the events to the center of mass of the thresholded peak region of the extracellular trace. Fig. 7 shows a histogram of the coefficients of the first principal component of the resulting distribution. The dotted line indicates a Gaussian fit. The distribution exhibits strong tails that lead to severe non-normality. However, when we fit the distribution in a robust manner with a maximum likelihood (EM) technique, using a default uniform distribution to describe the outliers, we observed that the remainder was well modeled as Gaussian

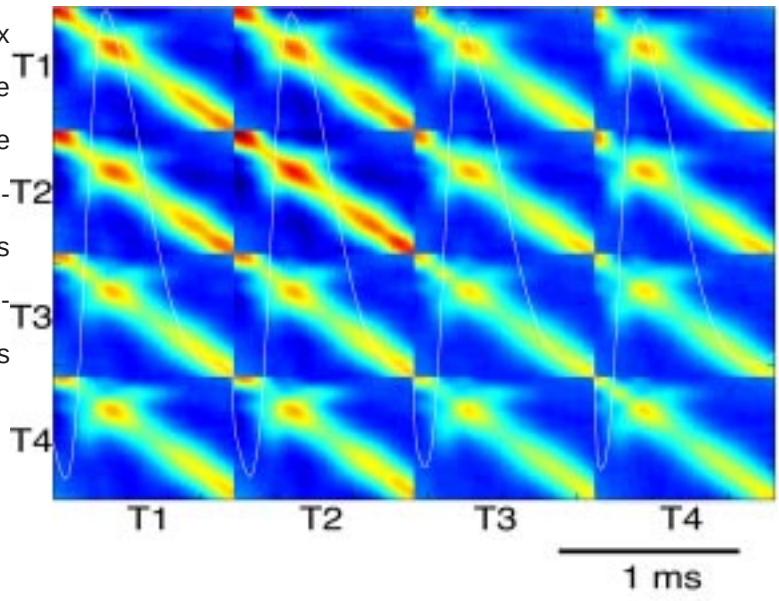

Figure 8. Full covariance matrix for tetrode channels T1-T4. The spike-triggered averages are overlaid for reference. High covariance is red, low covariance is blue. The non-uniform distribution along the diagonals indicates non-stationary covariance.

(solid line). Spike waveform variability therefore appeared to be Gaussian distributed after outliers were removed.

We then fit the distribution in the robust manner described above and examined the covariance of the Gaussian component (Fig. 8). The covariance was non-stationary, as can be seen by the non-uniform distribution along the diagonal. We then decomposed the covariance matrix into stationary and non-stationary parts by an EM algorithm equivalent to carrying out factor analysis in the Fourier-transformed space. By analogy with Principal Components Analysis, we call this Non-Stationary Components Analysis. Figures 9b and 9c show the stationary and non-stationary components of the covariance matrix, respectively. The matrix reconstructed from these two components (Fig. 9d) closely matched the original covariance matrix (Fig. 9a). The stationary component corresponds to additive background noise, whereas the non-stationary component corresponds to intrinsic spike waveform variability. From the non-stationary component of the covariance matrix, we computed the major modes of non-stationary variability, shown in Figure 10. These modes illustrate the ways in which spike waveforms varied from event to event.

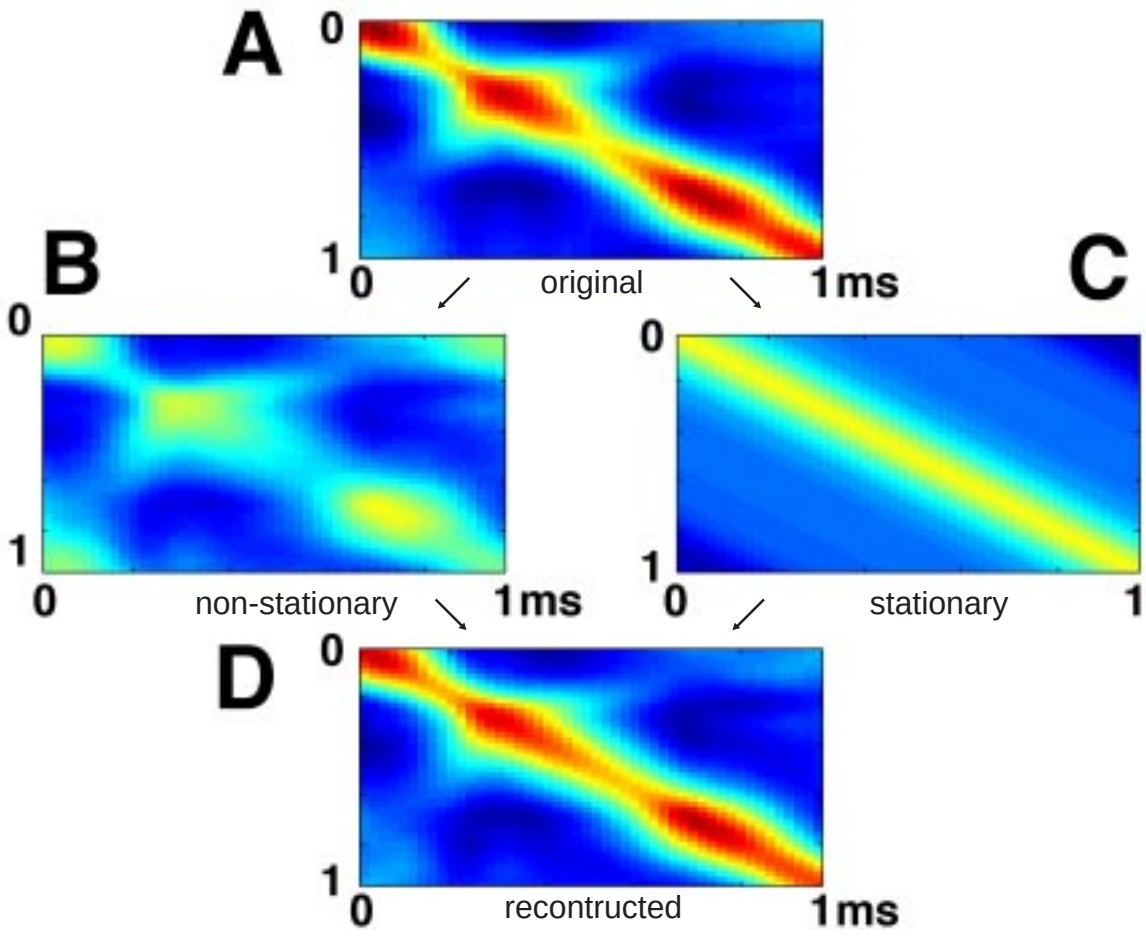

Figure 9. Decomposition of covariance for tetrode channel T2 (A) into stationary (C) and non-stationary (B) components. Reconstruction (D) from the two components closely matched the original (compare D to A). The stationary component of the covariance corresponds to non-spike noise which is independent of the spike waveform. The non-stationary component corresponds to intrinsic variability in the spike waveform from event to event.

For example, the first mode (dotted line) indicates that the predominant mode of variability was an increase in amplitude (both a higher peak and deeper trough) relative to the mean (heavy line). The second mode (dashed line) indicates a broadening of the action potential waveform compared to the mean. The third mode (fine line) corresponds to increased peak height and decreased trough depth, compared

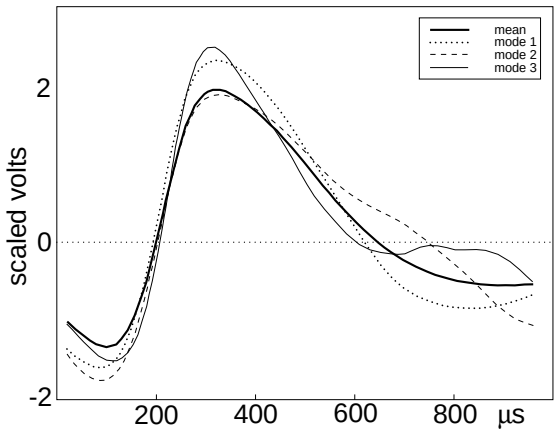

Figure 10. Modes of variability. The mean (heavy line) and first three modes of non-stationary variability about the mean are plotted here. Intrinsic variability in the spike waveform consisted of increased peak and trough amplitude (mode 1, dotted line), increased breadth (mode 2, dashed line), or increased peak height (mode 3, fine line), all relative to the mean.

to the mean.

Conclusions

In conclusion, preliminary analysis of simultaneous paired intracellular and tetrode recordings demonstrates that one spike sorting algorithm (Sahani et al., 1998a,b) performed 96% correct isolation and classification of signals from a tetrode. Current research efforts are also directed towards an algorithm for the resolution of spike waveform overlaps, and determining the performance of this algorithm on overlaps (on the tetrode recording) between the two intracellularly identified cells. Overlapping extracellular waveforms combine additively for the neurons we recorded from. Spike waveform variability could be decomposed into spiketime jitter, stationary Gaussian non-spike noise, and several modes of non-stationary variability. Data sets will be made available; for more information contact John Pezaris at pz@mit.edu.

Supported by NIH, NIMH, the Keck Foundation, the Alfred P. Sloan Foundation, NSF, and ONR.

References

Abeles M (1991) Cortoconics: neural circuits of the cerebral cortex. Cambridge: Cambridge University Press.

Abeles M, Bergman H, Margalit E, Vaadia E, Aertsen A (1993a) Spatio-temporal firing patterns in the frontal cortex of behaving monkeys. J Neurophysiol 70:1629-1638.

Abeles M, Prut Y, Bergman H, Vaadia E (1994) Synchronization in neuronal transmission and its importance for information processing. Progr Brain Res 102:395-404.

Abeles M, Prut Y, Bergman H, Vaadia E, Aertsen A (1993b) Integration, synchronicity, and periodicity. In: Brain theory: spatio-temporal aspects of brain function. Aertsen A (ed) Amsterdam: Elsevier pp 149-181.

Adrian E (1926) The impulses produced by sensory nerve endings. J Physiol (Lond) 61:49-72.

Adrian E (1942) Olfactory reactions in the brain of the hedgehog. J Physiol (Lond) 100:459-473.

Adrian E (1950) The electrical activity of the mammalian olfactory bulb. Electroenceph Clin Neurophysiol 2:377-388.

Adrian E (1951) Olfactory discrimination. L'Annee Psychol 50:107-113.

Adrian E (1956) The action of the mammalian olfactory organ. J Laryngol Otol 70:1-14.

Allison A, Warwick R (1949) Quantitative observations on the olfactory system of rabbit. Brain 72:186-197.

Amoore J, Buttery R (1978) Partition coefficients and comparative olfactometry. Chem Senses 3:57-71.

Astic L, Saucier D (1983) Ontogenesis of the functional activity of guinea-pig olfactory bulb: autoradiographic study with the 2-deoxyglucose method. Dev Brain Res 10:257-263.

Axel R (1995) The molecular logic of smell. Sci. American 273:154-159.

Baier H, Korsching S (1994) Olfactory glomeruli in the zebrafish olfactory system form an invariant pattern and are identifiable across animals. J Neurosci 14:219-230.

Belluscio L, Gold G, Nemes A, Axel R (1998) Mice deficient in G_{olf} are anosmic. Neuron 20:69-81.

Benjamin P, Elliott C (1989) Snail feeding oscillator: The central pattern generator and its control by modulatory interneurons. In: Neuronal and Cellular Oscillators, J Jacklet, ed. New York: Marcel Dekker pp 173-214.

Berger H (1929) Über das Elektrenkephalogramm des Menschen. Arch Psychiatr Nervenkrankheiten 87:527-570.

Bialek W, Owen W (1990) Temporal filtering in retinal bipolar cells: Elements of an optimal computation? Biophys J 58: 1227-1233.

Bialek W, Rieke F, van Steveninck R, Warland D (1991) Reading a neural code. Science 252:1854-1857.

Bignetti E, Cavaggioni A, Pelosi P, Persaud K, Sorbi R, Tirindelli R (1985) Purification and characterization of an odorant-binding protein from cow nasal tissue. Eur J Biochem 149:227-231.

Boeckh J, Ernst D, Sass H, Waldrow U (1984) Anatomical and physiological characteristics of individual neurones in the central antennal pathway of insects. J Insect Physiol 30:15-26.

Boekhoff I, Michel W, Breer H, Ache B (1994) Single odors differentially stimulate dual second messenger pathways in lobster olfactory cells. J Neurosci 14:3304-3309.

Boekhoff I, Tareilus E, Strotmann J, Breer H (1990) Rapid activation of alternative second messenger pathways in olfactory cilia from rats by different odorants. EMBO J 9:2453-2458.

Boudreau J (1964) Computer analysis of electrical activity in the olfactory system of the cat. Nature 201:155-158.

Boudreau J, Freeman W (1963) Spectral analysis of electrical activity in the prepyriform cortex of the cat. Exp Neurol 8:423-439.

Bouyer J, Montaron M, Rougeul A (1981) Fast fronto-parietal rhythms during combined focused attentive behavior and immobility in cat: cortical and thalamic localizations. Electroenceph Clin Neurophysiol 51:244-252.

Bouyer J, Montaron M, Vahnee J, Albert M, Rougeul A (1987) Anatomical localization of cortical beta rhythms in cat. Neuroscience 22:863-869.

Bredt D, Glatt C, Hwang P, Fotuhi M, Dawson T, Snyder S (1991) Nitric oxide synthase protein and messenger-RNA are discretely localized in neuronal populations of the mammalian CNS together with NADPH diaphorase. Neuron 7:615-624.

Bredt D, Snyder S (1994) Transient nitric-oxide synthase neurons in embryonic cerebral cortical plate, sensory ganglia, and olfactory epithelium. Neuron 13:301-313.

Breer H, Boekhoff I (1991) Odorants of the same odor class activate different second messenger pathways. Chem Senses 16:19-29.

Breer H, Boekhoff I, Tareilus E (1990) Rapid kinetics of second messenger formation in olfactory transduction. Nature 345:65-68.

Breer H, Klemm T, Boekhoff I (1992) Nitric oxide mediated formation of cyclic

GMP in the olfactory system. NeuroReport 3:1030-1032.

Bressler S (1984) Spatial-organization of EEGs from olfactory-bulb and cortex. Electroenceph Clin Neurophysiol 57:270-276.

Bressler S, Freeman W (1980)Frequency analysis of olfactory system EEG in cat, rabbit, and rat. Electroenceph Clin Neurophysiol 50:19-24.

Broillet M, Firestein S (1996a) Direct activation of the olfactory cyclic nucleotide-gated channel through modification of sulfhydryl groups by NO compounds. Neuron 16:377-385.

Broillet M, Firestein S (1996b) Gaseous second messengers in vertebrate olfaction. J Neurobiol 30:49-57.

Buck L, Axel R (1991) A novel multigene family may encode odorant receptors: a molecular basis for odor recognition. Cell 65:175-187.

Buonviso N, Chaput M (1990) Response similarity to odors in olfactory bulb output cells presumed to be connected to the same glomerulus: electrophysiological study using simultaneous single-unit recordings. J Neurophysiol 63:447-454.

Burrows M, Boeckh J, Esslen J (1982) Physiological and morphological properties of interneurons in the deutocerebrum of male cockroaches which respond to female pheromones. J Comp Physiol. [A] 145:447-457.

Cajal R (1890) Origen y terminacion de las fibras nerviosas olfatorias. Gazz Sanit

(Barcelona) 1-21.

Calvin W, Sypert, G. Fast and slow pyramidal tract neurons: Intracellular analysis of their contrasting repetitive firing properties in the cat. J Neurophys 39:420-434 (1976)

Chaput M, Holley A (1980) Single unit responses of olfactory bulb neurons to odor presentation in awake rabbits. J Physiol (Paris) 76:551-558.

Chase R (1985) Responses to odors mapped in snail tentacle and brain by [C-14]-2-deoxyglucose autoradiography. J Neurosci 5:2930-2939.

Chase R, Tolloczko B (1993) Tracing neural pathways in snail olfaction: from the tip of the tentacles to the brain and beyond. Microsc Res 24:214-230.

Chee-Ruiter C, Laurent G (1995) Odor-evoked antennal behavior in the cock-roach, *Periplaneta americana*. Soc Neurosci Abstr 21:134.

Cherubini E, Gaiarsa J, Ben-Ari Y (1991) GABA: an excitatory transmitter in early postnatal life. TINS 14:515-519.

Chess A, Simon I, Cedar H, Axel R (1994) Allelic inactivation regulates olfactory receptor gene expression. Cell 78: 823-834.

Christensen T, Harrow I, Cuzzocrea C, Randolph P, Hildebrand J (1995) Distinct projections of two populations of olfactory receptor axons in the antennal lobe of the sphinx moth *Manduca sexta*. Chem Senses 20:313-323.

Christensen T, Hildebrand J (1987) Male-specific, sex pheromone-selective projection neurons in the antennal lobes of the moth *Manduca sexta*. J Comp Physiol A 160:553-569.

Christensen T, Hildebrand J (1988) Frequency coding by central olfactory neurons in the sphinx moth *Manduca sexta*. Chem Senses 13:123-130.

Christensen T, Waldrop B, Harrow I, Hildebrand J (1993) Local interneurons and information processing in the olfactory glomeruli of the moth *Manduca sexta*. J Comp Physiol A 173:385-399.

Cinelli A, Hamilton K, Kauer J (1995) Salamander olfactory bulb neuronal activity observed by video rate, voltage-sensitive dye imaging. III. Spatial and temporal properties of responses evoked by odorant stimulation. J Neurophysiol 73:2053-2071.

Clark R (1979) Radiation of the metazoa. In: The origin of major invertebrate groups. House M (ed) London: Academic Press pp 55-101.

Costanzo R, O'Connell R (1978) Spatially organized projections of hamster olfactory nerves. Brain Res 139:327-332.

Cruse H (1976) The function of the legs in the free walking stick insect, Carausius morosus. J Comp Physiol 112:235-262.

Dahl A (1988) The effect of cytochrome P-450-dependent metabolism and other

enzyme activities on olfaction. In: Molecular neurobiology of the olfactory system. Margolis F, Getchell T (eds). Plenum Press, New York, pp 51-70.

Dal Monte M, Andreini I, Revoltella R, Pelosi P (1991) Purification and characterization of 2 odorant-binding proteins from nasal tissue of rabbit and pig. Comp Biochem B 99:445-451.

Davis R (1993) Mushroom Bodies And Drosophila Learning. Neuron 11:1-14.

Dawson T, Snyder S (1994) Gases as biological messengers: nitric oxide and carbon monoxide in the brain. J Neurosci 14:5147-5159.

de Belle J, Heisenberg M (1994) Associative odor learning in Drosophila abolished by chemical ablation of the mushroom bodies. Science 263:692-695.

DeCharms R, Merzenich M (1996) Primary cortical representation of sounds by the coordination of action potential timing. Nature 381: 610-613.

Delaney K, Gelperin A, Fee M, Flores J, Gervais R, Tank D, Kleinfeld D (1994) Waves and stimulus-modulated dynamics in an oscillating olfactory network. PNAS 91:669-673.

Delaney K, Hall B (1996) An *in vitro* preparation of frog nose and brain for the study of odor-evoked oscillatory activity. J Neurosci Methods 68:193-202.

DeWeerth S, Nielsen L, Mead C, Aström K (1991) A simple neuron servo. IEEE

Trans on Neural Networks 2-248-251.

Dϕving K, Belgaugh R (1977) Frequency of induced waves in the olfactory bulb in char (*Salmo alpinus* L.); a temperature dependence. Comp Biochem Physiol 56A:577-579.

Ding X, Coon M (1988) Purification and characterization of two unique forms of cytochrome P-450 from rabbit nasal microsomes. Biochemistry 27:8330-8337.

Ding X, Porter T, Peng H, Coon M (1991) cDNA and derived amino acid sequence of rabbit nasal cytochrome P-450NM6 (P450IIG1), a unique isozyme possibly involved in olfaction. Arch Biochem Biophys 285:120.

Dionne V (1992) Chemosensory responses in isolated olfactory receptor neurons from *Necturus maculosus*. J Gen Physiol 99:415-433.

Distler P, Boeckh J (1996) Synaptic connection between olfactory receptor cells and uniglomerular projection neurons in the antennal lobe of the American cockroach, *Periplaneta americana*. J Comp Neurol 370:35-46.

Distler P, Boeckh J (1997) Synaptic connections between identified neuron types in the antennal lobe glomeruli of the cockroach, *Periplaneta americana*. 1. Uniglomerular projection neurons J Comp Neurol 378:307-319.

Dohlman H, Thorner J, Caron M, Lefkowitz R (1991) Model systems for the study of seven-transmembrane-segment receptors. Annu Rev Biochem 60:653-

688.

Domino E, Ueki S (1960) An analysis of the electrical burst phenomenon in some rhinencephalic structures of the dog and monkey. Electroenceph Clin Neurophysiol 12:635-648.

Donoghue J, Sanes J, Hatsopoulos N, Gaal G (1998) Neural discharge and local-field potential oscillations in primate motor cortex during voluntary movements. J Neurophys 79:159-173.

Dorries K, Kauer J (1996) Field potential oscillations in frog and salamander olfactory bulb and epithelium. Soc Neurosci Abstr 22(3):2019.

Draguhn A, Traub R, Schmitz D, Jefferys J (1998) Electrical coupling underlies high-frequency oscillations in the hippocampus *in vitro.* Nature 394:189-192.

Dulac C, Axel R (1995) A novel family of genes encoding putative pheromone receptors in mammals. Cell 83:195-206.

Ezeh P, Davis L, Scott J (1995) Regional distribution of rat electro-olfactogram. J Neurophysiol 73:2207-2220.

Farley R, Case J, Roeder K (1967) Pacemaker for tracheal ventilation in the cockroach, Periplaneta americana. (L). J Insect Physiol 13:1713-1728.

Fee M, Mitra P, Kleinfeld D (1996) Automatic sorting of multiple-unit neuronal

signals in the presence of anisotropic and non-gaussian variability. J Neurosci Meth 69:175-188.

Felicioli A, Ganni M, Garibotti M, Pelosi P (1993) Multiple types and forms of odorant-binding proteins in the old-world porcupine *Hystrix cristata*. Comp Biochem B 105:775-784.

Firestein S (1991) A noseful of odorant receptors. TINS 14:270-272.

Firestein S, Picco C, Menini A (1993) The relation between stimulus and response in olfactory receptor cells of the tiger salamander. J Physiol (Lond) 468:1-10.

Firestein S, Werblin F (1987) Electrophysiological basis of the response of olfactory receptors to odorants and current stimuli. Ann NY Acad Sci 9:287-289.

Firestein S, Werblin F (1989) Odor-induced membrane currents in vertebrate olfactory receptor neurons. Science 244:79-82.

Flanagan D, Mercer A (1989) An atlas and 3-D reconstruction of the antennal lobes in the worker bee, Apis mellifera. Int J Insect Morphol Embryol 18:145-159.

Freeman W (1959) Distribution in time and space of prepyriform electrical activity. J Neurophysiol 22:644-665.

Freeman W (1960) Neurophysiol. 23, 111-131.

Freeman W (1962) Olfactory bulb response in the turtle. Nature 193:782-783.

Freeman W (1968) Effects of surgical isolation and tetanization on prepyriform cortex in cats. J Neurophysiol 31:349-357.

Freeman W (1972) Spatial divergence and temporal dispersion in primary olfactory nerve of cat. J Neurophysiol 35:733-744.

Freeman W (1974) Average transmission distance from mitral-tufted to granule cells in olfactory bulb. Electroenceph Clin Neurophysiol 36:609-618.

Freeman W (1975) Mass action in the nervous system. New York: Academic Press.

Freeman W (1978) Spatial properties of an EEG event in the olfactory bulb and cortex. Electroencephalogr. Clin. Neurophysiol. 44:586-605.

Freeman W (1987) Simulation of chaotic EEG patterns with a dynamic-model of the olfactory system. Biol Cybern 56:139-150.

Freeman W and Baird B (1987) Relation of olfactory EEG to behavior: Spatial analysis. Behav Neurosci 101:393-408.

Freeman W and Grajski K (1987) Relation of olfactory EEG to behavior: Factor analysis. Behav Neurosci 101:766-777.

Freeman W (1992) Nonlinear dynamics in olfactory information processing. In:

Olfaction, a model system for computational neuroscience. Davis J and Eichenbaum H editors, MIT Press, Cambridge Mass., London. pp 225-249.

Friedrich R, Korsching S (1997) Combinatorial and chemotopic odorant coding in the zebrafish olfactory bulb visualized by optical imaging. Neuron 18:737-752.

Fries P, Roelfsema P, Engel A, König P, Singer W (1997) Synchronization of oscillatory responses in visual cortex correlates with perception in interocular rivalry. PNAS 94:12699-12704.

Gabbiani F, Metzner W, Wessel R, Koch C (1996) From stimulus encoding to feature extraction in weakly electric fish. Nature 384:564-567.

Gault F, Leaton R (1963) Electrical activity of the olfactory system. Electroenceph Clin Neurophysiol 15: 299-304.

Gelperin A (1994) Nitric oxide mediates network oscillations of olfactory interneurons in a terrestrial mollusc. Nature 369:61-63.

Gelperin A, Kleinfeld D, Denk W, Cooke I (1996) Oscillations and gaseous oxides in invertebrate olfaction. J Neurobiol 30: 110-122.

Gelperin A, Tank D (1990) Odor-modulated collective network oscillations of olfactory interneurons in a terrestrial mollusc. Nature 345:437-440.

Gemne G, Dϕving K (1969) Ultrastructural properties of primary olfactory neurons in fish (*Lota lot* L). Am J Anat 126:457-475.

Georgopoulos A, Kalaska J, Caminiti J, Massey T (1982) J Neurosci 2:1527-1537.

Gesteland R, Lettvin J, Pitts W (1965) Chemical transmission in the nose of the frog. J Physiol (Lond) 181:525-559.

Getchell T (1974) Unitary responses in frog olfactory epithelium to sterically related molecules at low concentrations. J Gen Physiol 64:241-261.

Getchell T, Margolis F, Getchell M (1984) Perireceptor and receptor vents in vertebrate olfaction. Prog Neurobiol 23:317-345.

Getting P, Dekin M (1985) Mechanisms of pattern generation underlying swimming in Tritonia. IV. Gating of central pattern generator. J Neurophysiol 53:466-480.

Glaessner M (1984) The dawn of animal life. Cambridge: Cambridge University Press.

Golgi C (1875) Sulla Fina Anatomia dei bulbi olfactorii. Reggio-Emilia, Italy.

Gonzalez-Estrada M, Freeman W (1980) Effects of carnosine on olfactory bulb EEG, evoked potentials and DC potentials. Brain Research 202:373-386.

Gordon S, Zagotta W (1995) Localization of regions affecting an allosteric transition in cyclic nucleotide-activated channels. Neuron 14:857-864.

Graham D (1977) Simulation of a model for the coordination of leg movement in free walking insects. Biol Cybern 26:187-198.

Graham D (1978a) Unusual step patterns in the free walking grasshopper *Neoconocephalus robustus*. I. General features of the step patterns. J Exp Biol 73:147-157.

Graham D (1978b) Unusual step patterns in the free walking grasshopper *Neoconocephalus robustus*. II. A critical test of the leg interactions underlying different models of hexapod co-ordination. J Exp Biol 73:159-172.

Graham D (1985) Pattern and control of walking in insects. Advances in Insect Physiology 18:31-140.

Gray C, Di Prisco G (1997) Stimulus-dependent neuronal oscillations and local synchronization in striate cortex of the alert cat. J Neurosci 17:3239-3253.

Gray C, König P, Engel A, Singer W (1989) Oscillatory responses in cat visual cortex exhibit inter-columnar synchronization which reflects global stimulus properties. Nature 338:334-337.

Gray C, Maldonado P, Wilson M, McNaughton B (1995) Tetrodes markedly improve the reliability and yield of multiple single-unit isolation from multiunit recordings in cat striate cortex. J Neurosci Meth 63:43-54.

Gray C, McCormick D (1996) Chattering cells: superficial pyramidal neurons contributing to the generation of synchronous oscillations in the visual cortex. Science 274:109-113.

Gray C, Singer W (1989) Stimulus-specific neuronal oscillations in orientation columns of cat visual cortex. PNAS 86:1698-1702.

Gray C, Singer W (1989) Stimulus-specific neuronal oscillations in orientation columns of cat visual-cortex. PNAS 86(5):1698-1702.

Gray C, Skinner J (1988) Centrifugal regulation of neuronal activity in the olfactory bulb of the waking rabbit as revealed by reversible cryogenic blockade. Exp Brain Res 69:378-386.

Gray C (1994) Synchronous oscillations in neuronal systems: mechanisms and functions. J Comput Neurosci. 1:11-38.

Graystone P, Low B, Rogers J, McLennan H (1970) The induced wave activity of the olfactory bulb of toads, iguanas, and snakes. Comp Biochem Physiol 37:493-502.

Graziadei P, Monti-Graziadei G (1979) Neurogenesis and neuron regeneration in the olfactory system of mammals. 1. Morphological aspects of differentiation and structural organization of the olfactory sensory neurons. J Neurocytol 8:1-18.

Greer C, Stewart W, Kauer J, Shepherd G (1981) Topographical and laminar localization of 2-deoxyglucose uptake in rat olfactory bulb induced by electrical stimulation of olfactory nerves. Brain Res 217:279-293.

Grillner S, Wallén P (1985) Central pattern generators for locomotion, with special reference to vertebrates. Ann Rev Neurosci 8:233-261.

Grillner S, Wallén P, Brodin L, Lansner A (1991) Neuronal network generating locomotor behavior in lamprey: circuitry, transmitters, membrane properties, and simulation. Ann Rev Neurosci 14:169-199.

Gronenberg W (1987) Anatomical and physiological properties of feedback neurons of the mushroom bodies in the bee brain. Exp Biol 46:115-125.

Gustafsson M, Reuter M (1990) Flatworms as model organisms. In: The early brain. Gustafsson M, Reuter M (eds) pp 5-44. Abo: Abo Academy Press.

Guthrie K, Anderson A, Leon M, Gall C (1993) Odor-induced increases in c-fos mRNA expression reveal an anatomical “unit” for odor processing in olfactory bulb. PNAS 90:3329-3333.

Gynther I, Pearson K (1999) An evaluation of the role of identified interneurons in triggering kicks and jumps in the locust. J. Neurophysiol 61:45-57.

Gyorgyi T, Roby-Shemkovitz A, Lerner M (1988) Characterization and cDNA cloning of the pheromone-binding protein from the tobacco hornworn, *Manduca sexta*: a tissue-specific developmentally regulated protein.

PNAS 85:9851-9855.

Haberly L (1985) Neuronal circuitry in olfactory cortex: anatomy and functional implications. Chem Senses 10:219-238.

Haberly L, Bower J (1989) Olfactory cortex: Model circuit for study of associative memory? TINS 12:258-264.

Haberly L, Shepherd G (1973) Current density analysis of opossum prepyriform cortex. J Neurophysiol 36:789-802.

Hamilton K, Kauer J (1989) Patterns of intracellular-potentials in salamander mitral tufted cells in response to odor stimulation. J Neurophysiol 62:609-625.

Hammer M, Menzel R (1995) Learning and memory in the honeybee. J Neurosci 15: 1617-1630.

Hansson B, Ljungberg H, Hallberg E, Lofstedt C (1992) Functional specialization of olfactory glomeruli in a moth. Science 256:1313-1315.

Hansson B, Ochieng S, Grosmaitre X, Anton S, Njagi P (1996) Physiological responses and central nervous projections of antennal olfactory receptor neurons in the adult desert locust, *Schistocerca gregaria* (Orthoptera: Acrididae). J Comp Physiol A 179:157-167.

Hara T, Freeze M, Scott K (1973) Spectral analysis of olfactory bulbar responses

in rainbow trout. Jap J Physiol 23:325-333.

Harris-Warrick R, Marder E (1991) Modulation of neural networks for behavior. Ann Rev Neurosci 14:39-57.

Harris-Warrick R, Nagy F, Nusbaum M (1992) Neuromodulation of stomatogastric networks by identified neurons and transmitters. In: Dynamic Biological Networks: The Stomatogastric Nervous System. R Harris-Warrick, E Marder, A Selverston, M Moulins (eds) Cambridge: MIT Press pp 87-137.

Harrison T, Scott J (1986) Olfactory bulb responses to odor stimulation: analysis of response pattern and intensity relationships. J Neurophysiol 56:1571-1590.

Heinbockel T, Kloppenburg P, Hildebrand J (1998) Pheromone-evoked potentials and oscillations in the antennal lobes of the sphinx moth *Manduca sexta*. J Comp Physiol A 182:703-714.

Heinzel H-G (1988) Gastric mill activity in the lobster. II. Proctolin and octopamine initiate and modulate chewing. J Neurophysiol 59:551-565.

Heinzel H-G, Selverston A (1988) Gastric mill activity in the lobster. III. Effects of proctolin on the isolated central pattern generator. J Neurophysiol 59:566-585.

Herrada G, Dulac C (1997) A novel family of putative pheromone receptors in mammals with a topographically organized and sexually dimorphic distri-

bution. Cell 90:763-773.

Herrick C (1931) The amphibian forebrain. J Comp Neurol 53:55-69.

Herz R, Cupchik G (1992) An experimental characterization of odor-evoked memories in humans. Chem Senses 17:519-528.

Herz R, Cupchik G (1995) The emotional distinctiveness of odor-evoked memories. Chem Senses 20:517-528.

Hildebrand J (1995) Analysis of chemical signals by nervous systems. PNAS 92:67-74.

Hildebrand J (1996) Olfactory control of behavior in moths: central processing of odor information and the functional significance of olfactory glomeruli. J Comp Physiol A 178:5-19.

Hildebrand J, Shepherd G (1997) Mechanisms of olfactory discrimination: Converging evidence for common principles across Phyla. Ann Rev Neurosci 20:595-631.

Hobson J (1967) Respiration and EEG synchronization in the frog. Nature 213:988-999.

Holley A, Dϕving K (1977) Receptor sensitivity, acceptor distribution, convergence and neural coding in the olfactory system. In: Olfaction and Taste VI. Magnen J, MacLeod P (eds) IRL Press, London, pp 113-123.

Hopfield J (1995) Pattern recognition computation using action potential timing for stimulus representation. Nature 376, 33-36.

Hughes J, Hendrix D (1967) The frequency component hypothesis in relation to the coding mechanism in olfactory bulb. In: Olfaction and Taste II. Hayshi T (ed) Pergamon Press, Oxford pp 51-87.

Hughes J, Hendrix D, Wetzel N, Johnston J (1969) Correlations between electrophysiological activity from the human olfactory bulb and the subjective response to odiferous stimuli. In: Olfaction and taste III. Pfaffmann C (ed) Pergamon Press, Oxford pp 172-191.

Hughes J, Mazurowski J (1962) Studies of the suprocallosal mesial cortex of unanesthetized, conscious animals. II. Monkeys. C. Frequency analysis of responses from the olfactory bulb. Electroenceph Clin Neurophysiol 14:646-653.

Imamura K, Mataga N, Mori K (1992) Coding of odor molecules by mitral-tufted cells in rabbit olfactory bulb. I. Aliphatic compounds. J Neurophysiol 68:1968-2002.

Inamura K, Kashiwayanagi M, Kurihara K (1997) Blockage of urinary responses by inhibitors for IP_3-mediated pathway in rat vomeronasal sensory neurons. Neurosci Lett 233:129-132.

Ishii S, Kubokawa K, Kikuchi M, Nishio H (1995) Orientation of the toad, *Bufo*

japonicus, toward the breeding pond. Zoolog Sci 12:475-484.

Ivanova T, Caprio J (1992) Two transduction mechanisms in olfactory neurons. Soc Neurosci Abstr.

Jagadeesh B, Gray C, Ferster D (1992) Visually evoked oscillations of membrane potential in cells of cat visual cortex. Science 257:552-554.

Jahr C, Nicoll R (1982) An intracellular analysis of dendrodendritic inhibition in the turtle *in vitro* olfactory bulb. J Physiol (Lond) 326:213-234.

Jefferys J, Traub R, Whittington M (1996) Neuronal networks for induced ‘40 Hz’ rhythms. TINS 19:202-208.

Joerges J, Küttner A, Galizia G, Menzel R (1997) Representations of odours and odour mixtures visualized in the honeybee brain. Nature 387:285-288.

Johnston M, Simon S, Ramon F (1980) Interaction of anaesthetics with electrical synapses. Nature 286:498-500.

Jones D, Reed R (1989) Golf: an olfactory neuron specific G-protein involved in odorant signal transduction. Science 244:790-795.

Jourdan F, Duveau A, Astic L, Holley A (1980) Spatial distribution of 2-deoxyglucose uptake in the olfactory bulb of rats stimulated with two different odors. Brain Res 188:139-154.

Kafka W (1970) MolekulareWechselwirkungen bei der Erregung einzelner Riechzellen. Z vergl Physiologie 70:105-143.

Kaissling K (1986) Chemo-electrical transduction in insect olfactory receptors. Ann Rev Neurosci 9:121-145.

Kaissling K, Hildebrand J, Tumlinson J (1989) Pheromone receptor cells in the male moth Manduca sexta. Arch Insect Biochem Physiol 10:273-279.

Kaji S, Satou M, Kudo Y, Ueda K, Gorbman A (1975) Spectral analysis of olfactory responses of adult spawning spum salmon (Oncorhynchus keta) to stream waters. Comp Biochem Physiol 51A:711-716.

Kang J, Caprio J (1995) In vivo responses of single olfactory receptor neurons in the channel catfish, *Ictalurus punctatus*. J Neurophysiol 73:172-177.

Kanter E, Haberly L (1990) NMDA-dependent induction of long-term potentiation in afferent and association fiber systems of piriform cortex *in vitro*. Brain Res 525:175-179.

Kantor D, Lanzrein M, Stary S, Sandoval G, Smith W, Sullivan B, Davidson N, Schuman E (1996) A role for endothelial NO synthase in LTP revealed by adenovirus mediated inhibition and rescue. Science 274:1744-1748.

Kanzaki R, Arbas E, Strausfeld N, Hildebrand J (1989) Physiology and morphology of projection neurons in the antennal lobe of the male moth Manduca sexta. J Comp Physiol A 165:427-453.

Katoh K, Koshimoto H, Tani A, Mori K (1993) Coding of odor molecules by mitral-tufted cells in rabbit olfactory bulb. II. Aromatic compounds. J Neurophysiol 70:2161-2175.

Kauer J (1974) Response patterns of amphibian olfactory bulb neurones to odor stimulation. J Physiol (Lond) 243:695-715.

Kauer J, Cinelli A (1993) Are there structural and functional modules in the vertebrate olfactory bulb? Microsc Res Tech 24:157-167.

Kauer J, Moulton D (1974) Responses of olfactory bulb neurones to odour stimulation of small nasal areas in the salamander. J Physiol (Lond) 243:717-737.

Kauer JS (1991) Contributions of topography and parallel processing to odor coding in the vertebrate olfactory pathway. TINS 14:79-85.

Kauer JS, Shepherd GM (1977) Analysis of the onset phase of olfactory bulb unit responses to odour pulses in the salamander. J Physiol (Lond.) 272:495-516.

Kelly J, Wrynn A, Leonard B (1997) The olfactory bulbectomized rat as a model of depression: an update. Pharmacology & Therapeutics 74:299-316.

Ketchum K, Haberly L (1991) Fast oscillations and dispersive propagation in olfactory cortex and other cortical areas: A functional hypothesis. In: Olfac-

tion: A model system for computational neuroscience (Davis J, Eichenbaum H, eds), pp 69-100. Cambridge, MA: MIT Press.

Ketchum K, Haberly L (1993) Synaptic events that generate fast oscillations in piriform cortex. J Neurosci 13:3980-3985.

Kim M, Smith D (1997) Odorant binding proteins determine the chemical specificity of olfactory neurons. Meeting abstract, Neurobiology of *Drosophila*, Cold Spring Harbor Laboratory, p 105.

Kimura T, Suzuki B, Yamada A, Sekiguchi T, Mizukami A (1993) Response of oscillatory field potential to some conditioned odors in slug's brain. Zool Sci 9:1241.

Kleinfeld D (1986) Sequential state generation by model neural networks. PNAS 83:9469-9473.

Kleinfeld D, Delaney K, Fee M, Flores J, Tank D, Gelperin A (1994) Dynamics of propagating waves in the olfactory network of a terrestrial mollusc: an electrical and optical study. J Neurophysiol 72:1402-1419.

Krieger J, Ganssle H, Raming K, Breer H (1993) Odorant binding-proteins of *Heliothis-virescens*. Insect Biochem Mol Biol 23:449-456.

Krieger J, Raming K, Breer H (1991) Cloning of genomic and cDNA encoding insect pheromone binding-proteins: evidence for microdiversity. Biochim Biophys Acta 1088:277-284.

Kurahashi T, Lowe G, Gold G (1994) Suppression of odorant responses by odorants in olfactory receptor cells. Science 265:118-120.

Lam Y, Cohen L, Falk C (1998) Voltage-sensitive dye recording of odor elicited oscillations in the turtle olfactory bulb. J Physiol (Lond) 506:83-84.

Lancet D (1986) Vertebrate olfaction reception. Ann Rev Neurosci 9:329-355.

Land L (1973) Localized projection of olfactory nerves to rabbit olfactory bulb. Brain Res 63:153-166.

Land M, Collet T(1974) J Comp Physiol 89:331.

Larimer J (1988) The command hypothesis - a new view using an old example. TINS 11:506-510.

Laue M, Steinbrecht R, Ziegelberger G (1994) Immunocytochemical localization of general odorant binding protein in olfactory sensilla of the silkmoth *Antheraea polyphemus*. Naturewissenschaften 81:178-180.

Laurent G (1996) Dynamical representation of odors by oscillating and evolving neural assemblies. TINS 19:489-496.

Laurent G, Davidowitz H (1994) Encoding of olfactory information with oscillating neural assemblies. Science 265:1872-1875.

Laurent G, Naraghi M (1994) Odorant-induced oscillations in the mushroom bodies of the locust. J Neurosci 14:2993-3004.

Laurent G, Seymour-Laurent K, Johnson K (1993) Dendritic excitability and a voltage-gated calcium current in locust nonspiking local interneurons. J Neurophysiol 69:1484-1498.

Laurent G, Wehr M, Davidowitz H (1996) Temporal representations of odors in an olfactory network. J Neurosci 16:3837-3847.

Lazard D, Tal N, Rubinstein M, Khen M, Lancet D, Zupko K (1990) Identification and biochemical analysis of novel olfactory-specific cytochrome P450IIA and UDP-glucoronosyl transferase. Biochemistry 29:7433-7440.

Lazzaro J, Mead C (1989) A silicon model of auditory localization. Neural Computation 1:47-57.

Le Gros Clark W (1951) The projection of the olfactory epithelium on the olfactory bulb in the rabbit. J Neurol Neurosurg Psychiatr 14:1-10.

Leinder-Zufall T, Shepherd G, Zufall F (1995) Regulation of cyclic nucleotide-gated channels and membrane excitability in olfactory receptor cells by carbon monoxide. J Neurophysiol 74:1498-1508.

Leitch B, Laurent G (1996) GABAergic synapses in the antennal lobe and mushroom body of the locust olfactory system. J Comp Neurol 372:487-514.

LeMoncheck J (1992) An analog VLSI model of the jamming avoidance response in electric fish. IEEE Journal of Solid State Circuits 27(6).

Lewicki M (1994) Bayesian modeling and classification of neural signals. Neural Computation 6:1005-1030.

Li Z, Hopfield J (1989) Modeling the olfactory-bulb and its neural oscillatory processings. Bio Cybern 61:379-392.

Libet B, Gerard R (1939) Control of the potential rhythm of the isolated frog brain. J Neurophysiol 2:153-169.

Livingstone M (1996) Oscillatory firing and interneuronal correlations in squirrel monkey striate cortex. J Neurophysiol 75:2467-2485.

Longo V, Citti L, Gervasi P (1988) Biotransformation enzymes in nasal mucosa and liver of Sprague-Dawley rats. Toxicol Lett 44:289-297.

Lucero M, Horrigan F, Gilly W (1992) Electrical responses to chemical stimulation of squid olfactory receptor cells. J Exptl Biol 162:231-249.

MacKay-Sim A, Kesteven S (1994) Topographic patterns of responsiveness to odorants in the rat olfactory epithelium. J Neurophysiol 71:150-160.

MacKay-Sim A, Shaman P, Moulton D (1982) Topographic coding of olfactory quality: odorant specific patterns of epithelial responsivity in the salamander. J Neurophysiol 48:584-596.

MacLeod K, Bäcker A, Laurent G (1998) Who reads temporal information contained in synchronized spike trains? submitted.

MacLeod K, Laurent G (1996) Distinct mechanisms for synchronization and temporal patterning of odor-encoding neural assemblies. Science 274:976-979.

MacLeod K, Laurent G (1997) Effects of antennal lobe neuron desynchronization on odor responses of mushroom body extrinsic neurons in the locust. Soc Neurosci Abstr 23(2):1825.

Macrides F, Chorover S (1972) Olfactory bulb activity correlated with inhalation cycles and odor quality. Science 175:84-87.

Mafro-Neto A, Cardé R (1994) Fine-scale structure of pheromone plumes modulates upwind orientation of flying in moths. Nature 369:142-144.

Mahowald M, Douglas R (1991) A silicon neuron. Nature 354:515-518.

Mahowald M, Douglas R, LeMoncheck J, Mead C (1992) An introduction to silicon neural analogs. Semin Neurosci 4:83-92.

Maida R, Steinbrecht R, Ziegelberger G, Pelosi P (1993) The pheromone binding protein of Bombyx mori: purification, characterization, and immunocytochemical location. Insect Biochem Mol Biol 23:243-253.

Mair R (1982) Response properties of rat olfactory bulb neurons. J Physiol (Lond) 326:341-359.

Marchese S, Pes D, Scaloni A, Carbone V, Pelosi P (1998) Lipocalins of boar salivary glands binding odors and pheromones. Eur J Biochem 252:563-568.

Marder E, Weimann J (1992) Modulatory control of multiple task processing in the stomatogastric nervous system. In: Neurobiology of Motor Programme Selection, J Kien, C McCrohan, and B Winlow (eds) New York: Pergamon Press pp 3-19.

Martinez D, Freeman W (1984) Periglomerular cell action on mitral cells in olfactory bulb shown by current source density analysis. Brain Research 308:223-233.

Mathews D (1972) Response patterns of single units in olfactory bulb of the rat to odor. Brain Res 47:384-400.

Matsunami H, Buck L (1997) A Multigene family encoding a diverse array of putative pheromone receptors in mammals. Cell 90:775-784.

McClellan AD (1982) Movements and motor patterns of the buccal mass of *Pleurobranchaea* during feeding, regurgitation and rejection. J Exp Biol 98:195-211.

McClurkin J, Optican L, Richmond B, Gawne T (1991) Concurrent processing

and complexity of temporally encoded neuronal messages in visual perception. Science 253:675-677.

Mead C (1989) Analog VLSI and Neural Systems. Addison-Wesley: Reading, MA.

Mellon D, Sandeman D, Sandeman R (1992) Characterization of oscillatory interneurons in the protocerebrum of the crayfish. J Exp Biol 167:15-38.

Menco, B (1980) Qualitative and quantitative freeze-fractured studies on olfactory and nasal respiratory structures of frog, ox, rat, and dog. 1. A general survey. Cell Tissue Research 207:183-209.

Menzel R, Muller U (1996) Learning and memory in honeybees: From behavior to neural substrates. Ann Rev Neurosci 19: 379-404.

Meredith M (1981) The analysis of response similarity in single neurons of the goldfish olfactory bulb using amino acids as odor stimuli. Chem. Senses 6:277-293.

Meredith M (1986) Patterned response to odor in mammalian olfactory bulb: the influence of intensity. J Neurophysiol 56:572-597.

Meredith M (1992) Neural circuit computation: complex patterns in the olfactory-bulb. Brain Res Bull 29:111-117.

Meredith M, Moulton DG (1978) Patterned response to odor in single neurons of

goldfish olfactory bulb: influence of odor quality and other stimulus parameters. J Gen Physiol 71:615-643.

Michelson H, Wong K (1991) Excitatory synaptic responses mediated by $GABA_A$ receptors in the hippocampus. Science 253:1420-1423.

Miller P (1960) Respiration in the desert locust. II. The control of the spiracles. J Exp Biol 37:237-263.

Miller P (1966) The regulation of breathing in insects. Adv Insect Physiol 3:279-354.

Miller P (1967) The derivation of the motor command to the spiracles of the locust. J Exp Biol 46:349-371.

Milner P (1974) A model for visual shape recognition. Psychol Rev. 816:521-35.

Mobbs P (1982) The brain of the honeybee *Apis mellifera*. 1. The connections and spatial organization of the mushroom bodies. Phil Trans R Soc Lond 298:309-354.

Moraczewski J, Czubaj A, Bakowska J (1977) Organization and ultrastructure of the nervous system in *Catenulida* (Turbellaria). Zoomorphologie 87:87-95.

Morales B, Labarca P, Bacigalupo J (1995a) A ciliary K+ conductance sensitive to charybdotoxin underlies inhibitory responses in toad olfactory receptor neurons. FEBS Lett 359:41-44.

Morales B, Ugarte G, Labarca P, Bacigalupo J (1995b) Odorant-activated k+-current inhibits toad olfactory neurons. Chemical Senses 20:146-147.

Mori K (1987) Membrane and synaptic properties of identified neurons in the olfactory bulb. Prog Neurobiol 29:274-320.

Mori K, Imamura K, Mataga N (1992) Differential specificities of single mitral cells in rabbit olfactory bulb for a homologous series of fatty acid odor molecules. J Neurophysiol 67:786-789.

Mori K, Yoshihara Y (1995) Molecular recognition and olfactory processing in the mammalian olfactory system. Prog Neurobiol 45:585-619.

Moruzzi G, Magoun H (1949) Brainstem reticular formation and activation of the encephalogram. Electroencephalogr Clin Neurophysiol 1:455-473.

Moulton D (1963) Electrical activity in the olfactory system of rabbits with indwelling electrodes. In: Zotterman Y (ed) Olfaction and Taste I. pp 71-84. Pergamon Press, Oxford.

Moulton D (1976) Spatial patterning of response to odors in the peripheral olfactory system. Physiol Rev 56:578-593.

Mozell M, Sheehe P, Hornung D, Kent P, Youngentob S, Murphy S (1987) Imposed and inherent mucosal activity patterns: Their composite representation of olfactory stimuli. J Gen Physiol 90:625-650.

Munk M, Roelfsema P, König P, Engel A, Singer W (1996) Role of reticular activation in the modulation of intracortical synchronization. Science 272(5259):225-6.

Murlis J, Elkington J, Cardé R (1992) Odor plumes and how insects use them. Ann Rev Entomol 37:505-532.

Murray A, Del Corso D, Tarassenko L (1991) Pulse-stream VLSI neural networks mixing analog and digital techniques. IEEE Trans Neural Networks 2:193-204.

Murthy V, Fetz E (1992) Coherent 25-Hz to 35-Hz oscillations in the sensorimotor cortex of awake behaving monkeys PNAS 89:5670-5674.

Murthy V, Fetz E (1996) Oscillatory activity in sensorimotor cortex of awake monkeys: Synchronization of local field potentials and relation to behavior. J Neurophysiol 76:3949-3967.

Murthy V, Fetz E (1996) Synchronization of neurons during local field potential oscillations in sensorimotor cortex of awake monkeys. J Neurophysiol 76:3968-3982.

Mustaparta (1971) Spatial distribution of receptor responses to stimulation with different odors. Acta Physiol Scand 82:154-166.

Nakamura T, Gold G (1987) A cyclic nucleotide-gated conductance in olfactory

receptor cilia. Nature 325:442:444.

Nef P, Heldman J, Lazard D, Jaye M, Hanukoglu I, Lancet D (1989) Olfactory-specific cytochrome P450. J Biol Chem 264:6780-6785.

Neuenschwander S, Singer W (1996) Long-range synchronization of oscillatory light responses in the cat retina and lateral geniculate nucleus. Nature 379:728-733.

Ngai J, Dowling M, Buck L, Axel R, Chess A (1993) The family of genes encoding odorant receptors in the channel catfish. Cell 72:657-666.

Nicolelis M, Baccala L, Lin R, Chapin J (1995) Sensorimotor encoding by synchronous neural ensemble activity at multiple levels of the somatosensory system. Science 268:1353-1358.

Nicolelis M, Fanselow E, Ghazanfar A (1997) Hebb's dream: The resurgence of cell assemblies. Neuron 19:219-221.

Nowycky M, Mori K, Shepherd G (1981) Blockade of synaptic inhibition reveals long-lasting synaptic excitation in isolated turtle olfactory bulb. J Neurophysiol 46:649-658.

O'Connell R, Mozell M (1969) Quantitative stimulation of frog olfactory receptors. J Neurophysiol 32:51-63.

O'Keefe J, Recce (1993) Phase relationship between hippocampal place units

and the EEG theta-rhythm. Hippocampus 3:317-330.

Onoda N (1992) Odor-induced fos-like immunoreactivity in the rat olfactory bulb. Neurosci Lett 137:57-160.

Oram M, Perrett D (1992) Time course of neural responses discriminating different views of the face and head. J Neurophysiol 68:70-84.

Orona E, Rainer E, Scott J (1984) Dendritic and axonal organization of mitral and tufted cells in the rat olfactory bulb. J Comp Neur 226:346-356.

Ottoson D (1959) Comparison of slow potentials evoked in the frog's nasal mucosa and olfactory bulb by natural stimulation. Acta Physiol Scand 47:149-159.

Ozaki M, Morisaki K, Idei W, Ozaki K, Tokunaga F (1995) A putative lipophilic stimulant carrier protein commonly found in the taste and olfactory systems. A unique member of the pheromone binding protein superfamily. Eur J Biochem 230:298-308.

Parmentier M, Libert F, Schurmans F, Schiffmann S, Lefort A, Eggerickx D, Ledent C, Mollereau C, Gerard C, Perret J, Grootgoid A, Vassart G (1992) Expression of members of the putative olfactory receptor gene family in mammalian germ cells. Nature 355:453-455.

Pelosi, P. (1994) Odorant-binding proteins. Crit Rev Biochem Mol Biol 29:199-228.

Pelosi P (1996) Perireceptor events in olfaction. J Neurobiol 30:3-19.

Pelosi P, Baldaccini N, Pisanelli A (1982) Identification of a specific olfactory receptor for 2-isobutyl-3-methoxypyrazine. Biochem J 201:245-248.

Pelosi P, Maida R (1995) Odorant-binding proteins in insects. Comp Biochem Physiol 111B:503-515.

Pes D, Dalmonte M, Ganni M, Pelosi P (1992) Isolation of 2 odorant-binding proteins from mouse nasal tissue. Comp Biochem B 103:1011-1017.

Pes D, Pelosi P (1995) Odorant-binding proteins of the mouse. Comp Biochem B 112:471-479.

Pevsner J, Reed R, Feinstein P, Snyder S (1988) Molecular cloning of odorant-binding protein: member of a ligand carrier family. Science 241:336-339.

Pevsner J, Sklar P, Snyder S (1986) Odorant-binding protein: localization to nasal glands and secretions. PNAS 83:4942-4946.

Pevsner J, Trifiletti R, Strittmatter S, Snyder S (1985) Isolation and characterization of an olfactory receptor protein for odorant pyrazines. PNAS 82:3050-3054.

Pinching A, Powell T (1971) The neuropil of the glomeruli of the olfactory bulb. J Cell Sci 9:347-377.

Price J, Powell T (1970) The mitral and short axon cells of the olfactory bulb. J Cell Sci 7:631-651.

Pryor W, Church D, Govindan C, Crank G (1982) Oxidation of thiols by nitric oxide and nitrogen dioxide: synthetic utility and toxological implications. J Org Chem 47:156-159.

Rall W, Shepherd G (1968) Theoretical reconstruction of field potentials and dendrodendritic synaptic interactions in olfactory bulb. J Neurophysiol 31:884-915.

Rama-Krishna N, Getchell M, Tate S, Margolis F, Getchell T (1992) Glutathione and g-glutamyl transpeptidase are differentially distributed in the olfactory mucosa of rats. Cell Tissue Res 270:475-484.

Raming K, Krieger J, Breer H (1990) Primary structure of a pheromone-binding protein from *Antheraea pernyi*: homologies with other ligand-carrying proteins. J Comp Physiol B 160:503-509.

Raming K, Krieger J, Strotmann J, Boekhoff I, Kubick S, Baumstark C, Breer H (1993) Cloning and expression of odorant receptors. Nature 361:353-356.

Recce M, O'Keefe J (1989) The tetrode: an improved technique for multi-unit extracellular recording. Soc Neurosci Abstr 15:1250.

Ressler K, Sullivan S, Buck L (1993) A zonal organization of odorant receptor

gene expression in the olfactory epithelium. Cell 73:597-609.

Ressler K, Sullivan S, Buck L (1994) Information coding in the olfactory system: evidence for a stereotyped and highly organized epitope map in the olfactory bulb. Cell 79:1245-1255.

Restrepo D, Boekhoff I, Breer (1993) Rapid kinetic measurements of second messenger formation in olfactory cilia from channel catfish. Am J Physiol Cell Physiol 264:C906-C911.

Restrepo D, Miyamoto T, Bryant B, Teeter J (1990) Odor stimuli trigger influx of calcium into olfactory neurons of the channel catfish. Science 249:1166-1168.

Restrepo D, Teeter J, Schild D (1996) Second messenger signaling in olfactory transduction. J Neurobiol 30:37-48.

Retzius, G (1892) Die endigungsweise des riechnerven. In: Biologisches Untersuchungen. Neue Folge. Retzius G (ed). Samson and Wallin, Stockholm, pp 25-28.

Reuter M (1990) From innovation to integration: Trends of the integrative systems in microturbellarians. In: The early brain. Gustafsson M, Reuter M (eds) pp 161-178. Abo: Abo Academy Press.

Reuter M, Palmberg I (1990) Synaptic and nonsynaptic release in *Stenostomum leucops*: A study of the nervous system and sensory receptors. In: The

early brain. Gustafsson M, Reuter M (eds) pp 121-136. Abo: Abo Academy Press.

Revial M, Duchamp A, Holley A, MacLeod P (1978) Frog olfaction: odor groups, acceptor distribution, and receptor categories. Chem Senses 3:23-33.

Richmond B, Optican L (1987) Temporal encoding of two-dimensional patterns by single units in primate inferior temporal cortex. II. Quantification of response waveform. J Neurophysiol 57:147-161.

Robertson R (1986) Neuronal circuits controlling flight in the locust: central generation of the rhythm. TINS 9:278-280.

Robertson R, Pearson K (1983) Interneurons in flight system of the locust: distribution, connections and resetting properties. J Comp Neurol 215:33-50.

Robertson R, Pearson K (1985) Neural circuits in the flight system of the locust. J Neurophysiol 53:110-128.

Rodriguez R, Haberly L (1989) Analysis of synaptic events in the opossum piriform cortex with improved current source density techniques. J Neurophysiol 61:702-718.

Roskams A, Bredt D, Dawson T, Ronnett G (1994) Nitric oxide mediates the formation of synaptic connections in developing and regenerating olfactory receptor neurons. Neuron 13:289-299.

Rougeul A, Bouyer J, Dedet L, Debray O (1979) Fast somato-parietal rhythms during combined focal attention and immobility in baboon and squirrel monkey. Electroenceph Clin Neurophysiol 46:310-319.

Ryba N, Tirindelli R (1997) A new multigene family of putative pheromone receptors. Neuron 19:371-379.

Rybczynski R, Reagan J, Lerver M (1989) A pheromone degrading aldehyde oxidase in the antennae of the moth *Manduca sexta*. J Neurosci 9:1341-1353.

Ryckebusch S, Bower J, Mead C (1989) Modeling small oscillating biological networks in analog VLSI. In D. S. Touretzky (ed.) Advances in Neural Information Processing Systems 1. Morgan Kauffman: San Mateo, CA pp 384-393.

Ryckebusch S, Laurent G (1993) Rhythmic patterns evoked in locust leg motor neurons by the muscarinic agonist pilocarpine. J Neurophysiol 69:1583-1595.

Ryckebusch S, Mead C (1989) An analog VLSI model for oscillatory biological neural circuits. In Journées d'Electronique 1989: Réseaux de neurones artificiels. Presses Polytechniques Romandes: Lausanne, Switzerland. pp 303-312.

Sahani M, Pezaris J, Andersen R (1998a) Extracellular recording from multiple neighboring cells: a maximum-likelihood solution to the spike-separation

problem. Computational Neuroscience: Trends in Research 1998. Bower J (ed.) Plenum Press, New York.

Sahani M, Pezaris J, Andersen R (1998b) On the separation of signals from neighboring cells in tetrode recordings. Advances in Neural Information Processing Systems 10, Jordan M, Kearns M, Solla S (eds.), MIT Press, Cambridge, MA.

Sahley C, Martin K, Gelperin A (1992) Odors can induce feeding motor-responses in the terrestrial mollusk *Limax maximus*. Behav Neuro 106:563-568.

Sallaz M, Jourdan R (1993) C-fos expression and 2-deoxyglucose uptake in the olfactory bulb of odour-stimulated awake rats. NeuroReport 4:55-58.

Sansom, C., North, A., and Sawyer, L. (1994) Structural analysis and classification of lipocalins and related proteins using a profile-search method. *Biochim. Biophys. Acta* 1208:247-255.

Sarpeshkar R, Watts L, Mead CA (1992) Refractory Neuron Circuits. Internal Memorandum, Physics of Computation Laboratory, California Institute of Technology.

Sass H (1978) Olfactory receptors on the antenna of male Periplaneta americana: Response constellations that include food odors. J Comp Physiol 128:227-233.

Sass H (1978) Physiological and morphological identification of olfactory receptors on the antenna of male *Periplaneta americana*. In: Olfaction and Taste VII. Starre H (ed) Information Retrieval, London p 194.

Satou M (1974) Electrical responses at various levels of the olfactory pathway in himé salmon, *Oncorhynchus nerka*. Jap J Physiol 24:389-402.

Satou M (1990) Synaptic organization, local neuronal circuitry, and functional segregation of the teleost olfactory bulb. Progress Neurobiol. 34:115-142.

Saucier D, Astic L (1986) Analysis of the topographical organization of olfactory epithelium projections in rat. Brain Res Bull 16:455-462.

Schmitt B, Ache B (1979) Olfaction: responses of a decapod crustacean are enhanced by flicking. Science 205:204-206.

Schoenfeld T, Clancy A, Forbes W, Macrides F (1994) The spatial organization of the peripheral olfactory system of the hamster. I. Receptor neuron projections to the main olfactory bulb. Brain Res Bull 34:183-210.

Schuman E, Madison D (1994) Nitric oxide and synaptic function. Ann Rev Neurosci 17:153-183.

Schürmann F(1974) Bemerkungen zur Funktion der Copora pedunculata im Gehirn der Insekten aus morphologischerSicht. Exp Brain Res 19:406-432.

Schütt A, Basar E (1994) Olfactory field potential oscillations in the isolated Helix brain: different odors induce different rhythmicities. Abst 39th Mtg Germ. EEG Soc.

Schwarting G, Crandall J (1991) Subsets of olfactory and vomeronasal sensory epithelial cells and axons revealed by monoclonal antibodies to carbohydrate antigens. Brain Res 547:239-248.

Schwartz A (1994) Direct cortical representation of drawing. Science 265:540-542.

Schwob J, Gottlieb D (1986) The primary olfactory projection has two chemically distinct zones. J Neurosci 6:3393-3404.

Scott J (1981) Electrophysiological identification of mitral and tufted cells and distributions of their axons in olfactory system of the rat. J Neurophysiol 46:918-931.

Scott J, Davis L, Shannon D, Kaplan C (1996) Relation of chemical structure to spatial distribution of sensory responses in rat olfactory epithelium. J Neurophysiol 75:2036-2049.

Scott J, Wellis D, Riggott M, Buonviso N (1993) Functional organization of the olfactory bulb. Microsc Res Tech 24:142-156.

Segura E, De Juan A (1966) Electroencephalographic studies in toads. Electroenceph Clin Neurophysiol 21:373-380.

Selzer R (1981) The processing of a complex food odor by antennal olfactory receptors of *Periplaneta americana*. J Comp Physiol 144:509-519.

Sengupta P, Chou J, Bargmann C (1994) Odr-10 encodes a 7 transmembrane domain olfactory receptor required for responses to the odorant diacetyl. Cell 84:899-909.

Shadlen M, Newsome W (1998) The variable discharge of cortical neurons: implications for connectivity, computation, and information coding. J Neurosci 18:3870-3896.

Shannon C (1948) Bell Syst Tech J 27:379.

Shepherd G (1972) Synaptic organization of the mammalian olfactory bulb. Physiol Rev 52:864-917.

Shepherd G (1979) The functional analysis of local circuits in the olfactory bulb. In: The Neurosciences: Fourth study program. Schmitt F, Worden F (eds) MIT Press, Cambridge MA, pp 129-144.

Shipley M, Ennis M (1996) Functional organization of the olfactory system. J Neurobiol 30:123-176.

Sicard G, Holley A (1984) Receptor cell responses to odorants: similarities and differences among odorants. Brain Res 292:283-296.

Sicard, G (1985) Olfactory discrimination of structurally related molecules: receptor cell responses to camphoraceous odorants. Brain Res 326:203-212.

Sieck M, Wenzel B (1969) Electrical activity of the olfactory bulb of the pigeon. Electroenceph Clin Neurophysiol 26:62-69.

Siklos L, Rickmann M, Joo F, Freeman W, Wolff J (1995) Chloride is preferentially accumulated in a subpopulation of dendrites and periglomerular cells of the main olfactory-bulb in adult rats. Neuroscience 64:165-172.

Simmers A, Bush B (1983) Motor programme switching in the ventilatory system of *Carcinus maenas*: The neuronal basis of bimodal scaphognathite beating. J Exp Biol 104:163-181.

Singer W, Gray C (1995) Visual feature integration and the temporal correlation hypothesis. Ann Rev Neurosci 18: 555-586.

Skeen L (1977) Odor-induced patterns of deoxyglucose consumption in the olfactory bulb of the tree shrew, *Tupaia Glis*. Brain Res 124:147-153.

Sompolinsky H, Kanter I (1986) Temporal association in asymmetric neural networks. Phys Rev Lett 57:2861-2864.

Stamler J, Simon D, Osborne J, Mullins M, Jaraki O, Michel T, Singel D, Loscalzo J (1992) S-Nitrosylation of proteins with nitric oxide: synthesis and characterization of biologically active compounds. PNAS 89:444-448.

Steinbrecht R, Ozaki M, Ziegelberger G (1992) Immunocytochemical localization of pheromone binding protein in moth antennae. Cell Tissue Res 270:287-302.

Steriade M, Amzica F, Contreras D (1996a) Synchronization of fast (30-40 Hz) spontaneous cortical rhythms during brain activation. J Neurosci 16(1):392-417.

Steriade M, Timofeev I, Durmuller N, Grenier F (1998) Dynamic properties of corticothalamic neurons and local cortical interneurons generating fast rhythmic (30-40 Hz) spike bursts. J Neurophys 79(1):483-490.

Stewart W, Kauer J, Shepherd G (1979) Functional organization of rat olfactory bulb, analyzed by the 2-deoxyglucose method. J Comp Neurol 185:715-734.

Stewart W, Pedersen P (1987) The spatial organization of olfactory nerve projections. Brain Res 411:248-258.

Stopfer M, Bhagavan S, Smith B, Laurent G (1997) Impaired odour discrimination on desynchronization of odour-encoding neural assemblies. Nature 390:70-74.

Stopfer M, Wehr M, MacLeod K, Laurent G (in press) Neural dynamics, oscillatory synchronization, and odour codes. In: Insect Olfaction. Hansson W (ed) to appear.

Strong S, Koberle R, van Steveninck R, Bialek W (1998) Entropy and information in neural spike trains. Phys Rev Lett 80:197-200.

Sullivan S, Adamson M, Ressler K, Kozak C, Buck L (1996) The chromosomal distribution of mouse odorant receptor genes. PNAS 93:884-888.

Sullivan S, Bohm S, Ressler K, Horowitz L, Buck LB (1995) Target-independent pattern specification in the olfactory epithelium. Neuron 15:779-789.

Sullivan S, Dryer L (1996) Information processing in mammalian olfactory system. J Neurobiol 30:20-36.

Sun X, Fonta C, Masson C (1993) Odor quality processing by bee antennal lobe interneurons. Chem Senses 18:355-377.

Takagi S, Shibuya, T (1960) The potential oscillations observed in the olfactory epithelium, nerve and bulb of the toad and frog. Jap J Physiol 10:499-508.

Tanabe T, Iino M, Takagi S (1975) Discrimination of odors in the olfactory bulb, pyriform-amygdaloid areas, and orbitofrontal cortex of the monkey. J Neurophysiol 38:1284-1296.

Tank D, Hopfield J (1987) Neural computation by concentrating information in time. PNAS 84:1896-1900.

Thesen A, Steen J, Dϕving K (1993) Behavior of dogs during olfactory tracking. J Exptl Biol 180: 247-251.

Theunissen F, Miller J (1995) Temporal encoding in nervous systems: a rigorous definition. J Comput Neurosci 2:149-162.

Theunissen F, Roddey J, Stufflebeam S, Clague H, Miller J (1996) Information theoretic analysis of dynamical encoding by four identified primary sensory interneurons in the cricket cercal system. J Neurophys 75:1345-1364.

Thommesen G (1978) The spatial distribution of odor-induced potentials in the olfactory bulb of char and trout (salmonidae). Acta Physiol. Scand. 102:414-426.

Thommesen G, Dϕving K (1976) Spatial distribution of the EOG in rat; a variation with odor quality. Acta Physiol Scand 99:270-280.

Thorpe S, Fize D, Marlot C (1996) Speed of processing in the human visual system. Nature 381:520-522.

Thorpe S, Gautrais J (1997) Rapid Visual Processing using Spike Asynchrony. NIPS Jordan M (ed) MIT Press, pp 901-907.

Thorpe S, Imbert M (1989) In: Connectionism in perspective. Pfeifer R et al. (eds) Amsterdam: Elsevier pp 63-92.

Troemel E, Chou J, Dwyer N, Colbert H, Bargmann C (1995) Divergent seven transmembrane receptors are candidate chemosensory receptors in *C. elegans*. Cell 83:207-218.

Trotier D, Dϕving K (1996a) Functional role of receptor neurons in encoding olfactory information. J Neurobiol 30:58-66.

Trotier D, Dϕving K (1996b) Direct influence of the sodium pump on the membrane potential of vomeronasal chemoreceptor neurons in frog. J Physiol (Lond) 490.3:611-621.

Trotier D, Dϕving K , Rosin J (1993) Voltage-dependent currents in microvillar receptor cells of the frog vomeronasal organ. Eur J Neurosci 5:995-1002.

Ueda H, Kaeriyama M, Mukasa K, Urano A, Kudo H, Shoji T, Tokumitsu Y, Yamauchi K, Kurihara K (1998) Lacustrine sockeye salmon return straight to their natal area from open water using both visual and olfactory cues. Chem Senses 23:207-212.

Vaadia E, Haalman I, Abeles M, Bergman H, Prut Y, Slovin H, Aertsen A (1995) Dynamics of neuronal interactions in monkey cortex in relation to behavioral events. Nature 373:515-521.

van de Grind W (1988) The possible structure and role of neuronal smart mechanisms in vision. Cognitive Systems 2:163-180.

van Vreeswijk C, Abbott L, Ermentrout B (1994) When Inhibition not excitation synchronizes neural firing. J Comput Neurosci 1:313-321.

Vassar R, Chao S, Sitcheran R, Nuñez J, Vosshall L, Axel R (1994) Topographic

organization of sensory projections to the olfactory bulb. Cell 79:981-991.

Vassar R, Ngai J, Axel R (1993) Spatial segregation of odorant receptor expression in the mammalian olfactory epithelium. Cell 74:309-318.

Verlander J, Huggins S (1977) Computer analysis of the electroencephalographic activity of the caiman olfactory bulb. Electroenceph Clin Neurophysiol 42:829-834.

Vogt R, Kohne A, Dubnau J, Prestwich G (1989) Expression of pheromone binding proteins during antennal development in the gypsy moth *Lymantria dispar*. J Neurosci 9:3332-3346.

Vogt R, Riddiford L (1981) Pheromone binding and inactivation by moth antennae. Nature 193:161-163.

von der Malsburg C (1981) The correlation theory of brain function. Internal report. Max Plank Institute for Biophysical Chemistry, Gottingen, West Germany.

von der Malsburg C, Schneider W (1986) A neural cocktail party processor. Biol Cybern 54:29-40.

Waldrop B, Christensen T, Hildebrand J (1987) GABA-mediated synaptic inhibition of projection neurons in the antennal lobes of the sphinx moth *Manduca sexta*. J Comp Physiol A 161:23-32.

Waldrow U (1977) CNS units in cockroach (*Periplaneta americana*): Specificity of response to pheromones and other odor stimuli. J Comp Physiol 116:1-17.

Wang X-J, Rinzel J (1993) Spindle rhythmicity in the reticularis thalami nucleus: synchronization among mutually inhibitory neurons. Neuroscience 53:899-904.

Watts L (1992) Designing Networks of Spiking Silicon Neurons and Synapses. Proceedings of Computation and Neural Systems Meeting CNS*92, Kluwer: San Francisco, CA.

Watts L (in press) Event-Driven Simulation of Networks of Spiking Neurons. Neural Information Processing Systems 1993.

Wehr M, Laurent G (1996) Odor encoding by temporal sequences of firing in oscillating neural assemblies. Nature 384:162-166.

Wehr M, Laurent G (1998) Relationship between afferent and central temporal patterns in the locust olfactory system. Submitted.

Wehr M, Pezariz J, Sahani M (1998) Simultaneous paired intracellular and tet-rode recordings for evaluating the performance of spike sorting algorithms. In preparation.

Weimann J (1992) Multiple task processing in neural networks: Numerous central pattern generators in the stomatogastric nervous system of the crab, *Cancer borealis*, PhD Thesis, Department of Biology, Brandeis University.

Weimann J, Meyrand P, Marder, E (1991) Neurons that form multiple pattern generators: identification and multiple activity patterns of gastric/pyloric neurons in the crab stomatogastric system. J Neurophysiol 65:111-122.

Welch, P (1967) The use of fast fourier transform for the estimation of power spectra: a method based on time averaging over short, modified periodograms. IEEE Trans Audio Electroacoust AU-15:70-73.

Wellis D, Scott J, Harrison T (1989) Discrimination among odorants by single neurons of the rat olfactory bulb. J Neurophysiol 61:1161-1177.

Wenzel B, Sieck M (1972) Olfactory perception and bulbar electrical activity in several avian species. Physiol Behav 9:287-293.

White J, Hamilton K, Neff S, Kauer J (1992) Emergent properties of odor information coding in a representational model of the salamander olfactory-bulb. J Neurosci 12:1772-1780.

Willis M, Arbas E (1991) Odor-modulated upwind flight of the sphinx moth, M*anduca sexta*. J Comp Physiol A 169:427-440.

Willis M, Butler M, Tolbert L (1995) Normal glomerular organization of the antennal lobes is not necessary for odor-modulated flight in female moths. J Comp Physiol A 176:205-216.

Wilson D (1966) Insect walking. Ann Rev Entomol 11:103-122.

Wilson D, Leon M (1987) Evidence of lateral synaptic interactions in the olfactory bulb output cell responses to odors. Brain Res 417:175-180.

Wilson D, Leon M (1988) Spatial pattern of olfactory bulb single unit responses to learned olfactory cues in young rats. J Neurophysiol 59:1770-1783.

Wilson M, Bower J (1992) Cortical oscillations and temporal interactions in a computer-simulation of piriform cortex. J Neurophysiol 67: (4) 981-995.

Wu J, Wu C, Guan L, Cohen A (1995) Local field potential in the antennal lobe of the *Antheraea* moth (*A. pernyi*): pheromone related oscillations? Soc Neurosci Abstr 21:134.

Yokoi M, Mori K, Nakanishi S (1995) Refinement of odor molecule tuning by dendrodendritic synaptic inhibition in the olfactory bulb. PNAS 92:3371-3375.

Zhainazarov A, Ache B, (1995) Odor-induced currents in *Xenopus* olfactory receptor cells measured with perforated-patch recording. J Neurophysiol 74:479-483.

Zhang Y, Chou J, Bradley J, Bargmann C, Zinn K (1997) The *Caenorhabditis elegans* 7-transmembrane protein Odr-10 functions as an odorant receptor in mammalian-cells. PNAS 94:12162-12167.

Zhao H, Dibello P, Carlson J, Firestein S (1995) Odorant receptors in tiger salamander. Soc Neurosci Abstr 21:130.